DEVELOPING ELECTROCHEMICAL METHODS FOR THE DETECTION OF BACTERIAL CELLS

by

BAVITHTHIRA SUGANTHAN

(Under the Direction of Ramaraja P. Ramasamy)

ABSTRACT

Bacteria are ubiquitous; some are pathogenic to plants, animals, or humans. Due to their potential to cause major disease outbreaks, the need for rapid and reliable methods of bacterial detection is highly significant to food safety, public health, and environmental safety. Conventional methods of bacteria detection usually take a few hours to days for identification and often need skilled experts and specialized equipment. On the other hand, biosensors can offer a simpler alternative to conventional methods with several advantages, including ease to use, low detection limits, high sensitivity, desirable selectivity, and faster detection, for real-time monitoring. This dissertation mainly focuses on the development of an electrochemical biosensor architecture based on bacteriophage and bacteriophage protein-based recognition molecules to detect specific bacteria that are highly significant to healthcare and food safety.

The first approach involves developing charge-directed, aligned immobilization of bacteriophage on a nanostructured electrode for selective detection of bacterial cells using

electrochemical impedance spectroscopy (EIS) as the detection technique. As a proof of concept, *Listeria monocytogenes* was used as a model target (analyte), and commercially available P100 LISTEX phage was used as a recognition molecule to develop a phage-based impedimetric biosensor architecture. The architecture showed high sensitivity towards *L. monocytogenes* in select food samples.

The second approach involves developing a phage-protein-based biosensor by immobilizing a genetically engineered phage protein onto a nanostructured electrode for selective detection of bacterial cells using the EIS technique. As proof of concept, *Campylobacter jejuni* was used as the model analyte, and the genetically engineered phage protein CC-FlaGrab served as the recognition (bioreceptor) molecule. This architecture showed high sensitivity and specificity toward *C. jejuni* in select samples.

These two architectures could be the foundation for developing more electrochemical biosensing architectures for bacterial cell detection using a combination of recognition molecules and nanostructured electrodes that could be integrated into lab-on-chip devices for commercial development.

INDEX WORDS: Bacteriophage, phage protein, electrochemical biosensor, food safety, impedance spectroscopy, *Listeria monocytogenes*, *Campylobacter jejuni*.

DEVELOPING ELECTROCHEMICAL METHODS FOR THE DETECTION OF BACTERIAL CELLS

by

BAVITHTHIRA SUGANTHAN

BS, WAYAMBA UNIVERSITY OF SRI LANKA, SRI LANKA, 2012

MS, UNIVERSITY OF KELANIYA, SRI LANKA, 2016

A Dissertation Submitted to the Graduate Faculty of The University of Georgia in Partial Fulfillment of the Requirements for the Degree

DOCTOR OF PHILOSOPHY

ATHENS, GEORGIA

2022

DEVELOPING ELECTROCHEMICAL METHODS FOR THE DETECTION OF BACTERIAL CELLS

by

BAVITHTHIRA SUGANTHAN

Major Professor:	Ramaraja P. Ramasamy
Committee:	William S. Kisaalita
	Mark A. Eiteman
	Jose I. Reyes de Corcuera
	Yajun Yan

Electronic Version Approved:

Ron Walcott
Vice Provost for Graduate Education and Dean of the Graduate School
The University of Georgia
December 2022

DEDICATION

I dedicate my dissertation to my loving dad, mom, husband, and daughter for their unconditional love and all the sacrifices.

ACKNOWLEDGMENTS

First, I would like to thank my major Professor, Dr. Ramaraja Ramasamy, for his continuous guidance, encouragement, and valuable suggestions. I want to thank him for his continued support during the hard times. He guided me throughout my Ph.D., and his constructive comments helped me to improve my research work and finish my dissertation on time.

I also like to thank my committee members Dr. William Kissalita, Dr. Mark Eiteman, Dr. Jose Reyes de Corcuera, and Dr. Yajun Yan, for their valuable advice, continuous encouragement, and suggestions. I greatly appreciate your guidance and feedback for keeping me on the right track to completing my Ph.D.

I express my sincere gratitude to Dr. Christine Szymanski and her lab members, Dr. Clay S Crippen and Ms. Ashley Rogers; Mr. Oliver Gregory; Dr. Michael Adams and his lab members, Dr. Chang-hao Wu and Dr. Dominik Haja; Dr. Jason Locklin and his lab member, Mr. Ryan Maynard; Dr. Yajun Yan and his lab member Dr. Jian Wang for guiding, helping and allowing me to use their reagents and equipment during my doctoral research.

I highly appreciate Dr. Francisco Diez-Gonzalez, Director Center for food safety, Dr. Nikki Shariat, Assistant Professor, Department of Population Health, and Dr. Christine Szymanski, Professor Department of Microbiology, for kindly providing the *Listeria monocytogenes* Scott A, *Salmonella enterica* subsp. *enterica* serotype Typhimurium 291RH, and *Escherichia coli* O157:H7, respectively.

I want to thank all the funding sources of my doctoral study, including The Center for Food Safety, The University of Georgia, and the Southern Company. I also want to thank the administrative staff of the Department of College of Engineering, Ms. Margaret Sapp, Ms. Victoria E Martine, and Ms. Karina Soranz, for their support over the years.

I like to thank our senior lab members, Dr. Yan Zhou, Dr. Narendran Sekar, Dr. Yi Fang, and our previous postdoc Dr. James Manuel for all the help and support you have provided. In addition, I would like to thank my previous and current lab mates, Ms. Alyssa Ghuman, Dr. Hamid Asadi, Mr. Or Zolti, Mr. Sanket Nagdeve, Ms. April Rains, Mr. Austin Duncan, and undergraduate students Ms. Dhara Patel, Mr. Thomas Sporer and Mr. Nichcholas Szaro for all your valuable help and moral and emotional support during my hard times. Also, I would like to thank all the summer interns for making our lab enjoyable.

In addition, I would like to thank all my friends in Athens Dr. Natasha Perumal, Dr. Zahra Nawaz, Ms. Samanthi Ranathunga, Dr. Shaima Nazaar, Dr. Prasangi Rajapaksha, Dr. Ishan Mohamed, Mr. Afaq Niyaz, Mr. Theekshana Jayalath, Ms. Keshini Weerasinghe and my friends in Riverbend south building Ms. Sneha Kandapal, Ms. Sarada Sripada, Ms. Hemshika Rajpurohit for your unconditional love and support. I also wanted to thank Ms. Mamtha Ramaraja for all your care and support. Completing the Ph.D. with a child was a challenging process. However, you helped me in various ways when I struggled to balance my studies and family. I am extremely thankful for all your help during my hard times.

I also express my heartfelt thanks to my beloved dad, mom, and brother for your blessings and moral and emotional support in completing my Ph.D. I will always remember the sacrifices you made for me from childhood to improve my studies. Thank you so much for everything. I would also like to thank my mother-in-law, brother-in-law, and sister-in-law

for their blessings and support in completing my Ph.D. This accomplishment would not be possible without your support.

I also like to express my appreciation to my loving husband, Dr. Suganthan Amirthagunanathan, for providing tremendous and continuous support as a pillar. Thank you for everything and for supporting me in completing this Ph.D. journey successfully. Finally, I thank my daughter, Ms. Aathira Suganthan. Thank you so much for keeping us motivated with your cute, loving, and innocent smile.

TABLE OF CONTENTS

Page

LIST OF TABLES

Page

LIST OF FIGURES

Page

CHAPTER 1

BACKGROUND

1.1 Microbial Electrochemical Systems

Microbial electrochemical systems (MES) use microorganisms to convert chemical energy derived from biomolecules into electrical energy. It is a promising, rapidly emerging sustainable technology that integrates electrochemistry, microbiology, and materials science to produce value-added chemicals and electricity or enables microbial-based detection systems [1, 2]. Microbial electrochemical systems could use live microorganisms or enzymes derived from the microorganisms as catalysts to carry out a bio-electrochemical reaction. MESs can be classified into Microbial Fuel Cells (MFC) and Microbial Electrolysis or Electrosynthesis Cells (MEC), depending on the reaction type and electron transfer route [3].

In MES, electrons generated by substrate oxidation move from the anode to the cathode. These electrons are then used to reduce an electron acceptor in the cathode chamber, resulting in the current generation [4]. In recent years MES have also been used for waste treatment by utilizing organic waste as biodegradable substrates. The electrical energy produced in MESs can be directly used for electricity generation (Microbial Fuel Cell, MFC) [5-7]. Contrarily electricity (electrons transport from anode to cathode) in MESs can be used for the production of H_2 and other valuable chemicals (Microbial Electrolysis Cell,

MEC) [8-10], synthesize natural compounds (microbial electrosynthesis) or remediate contaminants (microbial remediation cells) [11-14], or be used for desalination (microbial desalination cells) [15-17].

1.2 Microbial Fuel Cells

The restricted accessibility and environmental impacts of fossil fuels have increased the need for alternative energy sources. The yearly global energy demand is increasing rapidly. The annual energy consumption is currently calculated as 580 terajoules (TJ), which is predicted to increase to 740 million TJ in 2040 [18, 19]. In the meantime, intensive resource use for municipal, industrial, and agricultural purposes will keep the environment degrading, posing a threat from global warming and its effects. As a result, the development of renewable energy sources has become essential for a sustainable environment, particularly through reducing reliance on energy imports and diversifying the sources of energy production [20]. Energy can also be derived from the different types of wastewater and food waste using Microbial fuel cells.

Microbial fuel cells (MFC) are electrochemical devices that generate electricity by oxidizing organic substrates (Table 1.1) using microorganisms as biocatalysts in the anode chamber. (Figure 1.1) In MFC, electrons generated during intracellular metabolism from the anode to the cathode electrode are accepted by oxygen or another) electron acceptor, which results in the generation of electric current [4]. Even though current generation by bacteria was initially reported in 1911 by Potter [21], extensive work on MFC did not start until the early 1990s. Initially, transferring electrons to the electrodes outside the cells was thought to require electron shuttles and chemical mediators and was considered a major

drawback. In 1999, electron shuttles and chemical mediators were demonstrated as not essential for transferring electrons [22]. A group of microorganisms called exoelectrogens could transfer electrons outside the cell without these mediators, making MFC a viable option.

1.3 Extracellular Electron Transfer

Exoelectrogenicity is the capability of microorganisms to transmit electrons to electron acceptors located outside of their cellular membrane. In primitive bacteria, extracellular electron transfer activity plays an important role in the electron transport chain using insoluble iron-oxides (Fe(III) oxide) as electron acceptors. These microorganisms are called exoelectrogens, and they are also named electrogens, electroactive, and anode-respiring bacteria [23]. Exoelectrogens have been detected in gram-positive and gram-negative bacteria, including the Gamma, Delta, Beta, and Alpha Proteobacteria and species from the Firmicutes, Acidobacteria phyla, and a Hyperthermophile *Pyrococcus furiosus* [24-26]. In addition to bacteria, fungi and cyanobacteria have also demonstrated EET capabilities [27-29].

Microbial fuel cells (MFC) use the extracellular electron transfer (EET) ability of microorganisms to produce energy using organic substrates. These bacteria transfer their electrons to the electrode, employing it as an alternative electron sink to terminal electron acceptors. Outer membrane proteins, nanowires (conductive pili), and endogenous or exogenous electron shuttles are three major mechanisms microorganisms use to transfer electrons between the electrodes and the microorganisms (Figure 1.2).

In addition there are broad range of applications of extraacellular transfer in the field of biosensor development. Two main different types of electron transfer mechanisms such as direct and indirect electron transfer mechanisms are widely in amperometric enzyme based bosensors. Establishing a quick electron transfer from the biological component to the electrode is a crucial prerequisite for the creation of amperometric biosensors with high sensitivity and quick response characteristics [30-34].

1.3.1 Direct Electron Transfer

Direct electron transfer (DET), which necessitates physical contact between the electrode's surface and the redox centers of microorganisms [35], can be accomplished directly (mediated-less) by the electroactive species, such as cell-wall cytochromes, of the adherent organism [36-38]. Alternatively, a conductive layer is formed in outer membranes to conduct electrons [39]. *Shewanella oneidensis* MR-1, for instance, produced bacterial nanowires (pili) in its outer membrane that aid extracellular electron transfer. Another way of electron transport was the secretion of electroactive metabolite(s) in the extracellular matrix. For instance, quorum-sensing molecules generated by *Shewanella putrefaciens* into the extracellular matrix, known as microbial natural-electron mediators, have demonstrated the capacity to mediate electron transfer. The efficiency of the mitochondrial respiratory chain was found to be a key regulator of the electron transfer capacity. Inhibition of the respiratory chain, chemically with specific enzyme inhibitors or genetically by knocking out specific genes from respiratory chain complexes, reduces the electrochemical response [40]. Similarly, over-expressing the specific genes involved in the respiratory electron transport chain complexes increased the electrochemical response [41].

Further, the DET mechanism is widely used in amperometric biosensors / third-generation biosensors. The redox center of the enzyme and the electrode surface are directly connected electronically to create DET-based biosensors. DET-based biosensor platform has significant advantages over mediated electron transfer (MET). First, the lack of mediators and electroactive substrates/products enables a higher selectivity because the biosensor can run at a potential closer to the redox enzyme's E°, hence lowering the possibility of interfering reactions. Second, unspecific reactions may be aided by both soluble/immobilized mediators and electroactive substrates/products [33, 34, 42, 43]

1.3.2 Mediated Electron Transfer

In contrast to exoelectrogens, many bacteria are electrochemically inactive, which prevents them from transferring their electrons to the electrode surfaces without the aid of soluble chemical redox mediators [44, 45]. Thus, to facilitate the microbe-electrode interactions through a procedure known as mediated electron transfer (MET) [46, 47], artificial redox mediators (exogenous electron shuttles) are needed.

There are two types of mediated electron transfer processes; single and double-mediated electron transfer processes were used to transfer the electrons outside the cell. 2,6-dichlorophenolindophenol (DCIP) [48] has been used as a traveling electron mediator (a membrane permeable molecule) for a single mediated transfer process, where a mixture of menadione and hexacyanoferrate(III) (ferricyanide or FCN) [49, 50] was used as a double mediated electron transfer process. When compared to the reactions of the single mediator system, the double mediator systems resulted in faster electron transfer and increased sensitivity [33, 51].

MET mechanism is widely used in enzyme-based amperometric biosensor systems for species for which direct electron-transfer sensors are impractical and mediated electron-transfer sensors offer a useful detection method. Biologically active or synthetic charge carriers can be used as intermediaries to facilitate electrical communication between the redox enzymes and the electrodes. The term "electron transfer mediators" generally refers to these synthetic electron donors or acceptor compounds. The redox enzymes can be accepted in place of the natural oxidants or reductants in these organisms. The reversible electrochemistry of the mediators is anticipated to allow for quick interactions with the redox enzyme, oxidizing or reducing the enzyme's active site. The features of the mediator and the overall system affect the efficiency of electron transport. Two main advantages are associated with the use of mediated electron transfer process. It is possible to prevent the interference of undesirable species by using mediators at low oxidation potentials. Further, the enzyme electrode can become somewhat pH insensitive if the oxidation of the reduced mediator does not involve protons [30, 43, 52, 53].

1.4 Photosynthetic MFCs

Generating electricity from photosynthetic microorganisms such as cyanobacteria, green algae, or subcellular components have been explored as an environmentally friendly means to get renewable energy. When photosynthetic microorganisms or subcellular components are employed in an MES, it is called photo bioelectrochemical cells (PBEC) (Figure 1.3). For producing light-induced photocurrents, the PBEC uses cyanobacteria like *Anabaena variabilis, Spirulina platensis, Synechococcus elongatus* [54], *Synechocystis* sp. [55, 56], *Nostoc* sp. [57], and as well as green algae like *Chlamydomonas reinhardti* [58], *Chlorella*

vulgaris [59], and *Ulva lactuca* [59]. Thus, the use of photosynthetic MFC that uses microorganisms that can transform sunlight into chemical energy is gaining interest. The photosystem I and photosystem II light-harvesting complexes, which serve as the building blocks of photosynthesis, are found in these bacteria. Their use in MFC is sustainable in terms of producing bioenergy. However, not all photosynthetic MFC use the entire living microbial cell; some additionally utilize subcellular components in the photosynthesis process. Chloroplasts, thylakoid membranes, and extracted photosystems are only a few examples of the sub-cellular components employed in photosynthetic MFC. Even if considerably higher power densities were attained utilizing above mentioned isolated photosynthetic machineries, they are not viable for applications for the following reasons:

(1) The laborious and skillful isolation procedure

(2) Requirement of specific environmental conditions like temperature, pH, ionic concentration of the medium, etc.) to ensure the stability of the isolated unit

(3) Instability due to photodamage

(4) It cannot self-repair photodamage because it exists in an artificial environment where there is no natural counterpart

All the limitations can be solved using whole-cell photosynthetic bacteria in photosynthetic MFCs. The entire cell retains all its natural biological processes, which gives it greater stability when immobilized on electrode surfaces.

1.4.1 Cyanobacteria in MFCs

Cyanobacteria can act as a potential anode catalyst in photo-bioelectrochemical cells to generate electricity sustainably, economically, and environmentally friendly. Further,

cyanobacteria are more advantageous than other photosynthetic microbes in the following ways: (1) Cyanobacteria are considerably more stable and can endure extreme environmental circumstances, including light intensity, temperature, dryness, and CO_2 level, because they evolved 3.5 billion years ago and are currently present in all terrestrial and marine environments on earth; (2) Cyanobacteria execute oxygenic photosynthesis similarly to higher plants and algae since they are the prehistoric ancestors of chloroplasts; (3) The entire genomes of widely studied cyanobacteria such as *Synechococcus* and *Synechocystis* have been sequenced and are accessible for molecular and genetic manipulation.

Enhancing Exoelectrogenicity in Genetically Engineered Cyanobacteria

The cyanobacterial PBEC typically experiences a lower extracellular electron flux, regardless of the extracellular electron transport mode (direct or mediated), because the electrons must be switched from their natural routes [(overlapping photosynthetic (P-ETC) and respiratory electron transport chain (R-ETC)] to alternative pathways to reach the electrode. The most effective method to enhance PBEC performance would involve altering the electron harvesting pathways through the genetic modification of cyanobacterium. These microbes can be modified through genetic engineering to help enhance the current in PBEC. This was already addressed by our research group in 2016 by developing a genetically engineered cyanobacterium *Synechococcus elongatus* PCC 7942 to express outer membrane cytochrome S, a non-native redox protein (OmcS). OmcS is primarily in charge of reducing metal in exoelectrogens. In comparison to the equivalent wild-type cyanobacterium, the modified *S. elongatus* PCC 7942 displayed better

extracellular electron transfer ability, which led to a 9-fold higher photocurrent generation on the anode of a PBEC. As part of my doctoral research, I enhanced the exoelectrogenecity of the cyanobacteria using genetic modification, as described in appendix A.

Cyanobacteria produce excess electrons through a photosynthetic electron transport chain when exposed to high light intensities. However, these excess electrons are re-oxidized by the respiratory terminal oxidases (RTOs) in the respiratory electron transport chain (R-ETC) to protect the cyanobacteria from photodamage. [60]. We hypothesize that the power-generating ability of cyanobacteria could be increased by knocking out the genes responsible for the respiratory terminal oxidases (RTO), and rerouting the electrons outside of the cell to an anode [61] would be a promising approach to use these microorganisms in photo-bioelectrochemical cells for electric power generation based on light to electricity conversion. (Figure 1.4) In my research, the genes responsible for the various RTOs present in R-ETC in *Synechococcus elongatus* PCC7942 include bd-type quinol oxidase (*cydBA*), aa_3-type cytochrome oxidase (*coxBAC*) and cbb_3-type cytochrome oxidase (c*coNQ*) were knocked out individually (single mutants) and in combination (double mutants) to enhance the extracellular electron transfer ability. Successful construction of single and double mutants were confirmed with PCR. The ferricyanide reduction assay and conventional electrochemical experiments were used to investigate the extracellular transfer and photocurrent generation ability of mutants. The research work described in the appendix A reviews the photocurrent generation ability of single and double mutants. Results revealed that most double and single mutants generated more current density than wild-type.

1.5 Hyperthermophile in MFCs

Pyrococcus furiosus (*Pf*), a hyper-thermophile, can act as an anode biocatalyst in generating electricity in a high-temperature microbial fuel cell (MFC) using carbon-based organic substrates. The suitability of *Pf* as an anode biocatalyst for this application depends on its ability to transfer electrons extracellularly to a metallic electrode or a terminal electron acceptor outside the cell [25, 26]. In *Pf*, the membrane-bound hydrogenases (MBH) use reducing equivalents from oxidative fermentation to produce hydrogen, which is believed to be used by soluble hydrogenases (SHI and SHII) for nicotinamide cofactor regeneration. MBH and SHI/II enzyme complexes are believed to participate in extracellular electron transport by serving as intermediate sites in the electron transport pathways.

In my doctoral research (appendix B), we have genetically manipulated SH and MBH to investigate their contributions to extracellular electron transport. Herein, genetically engineered *Pf* strains were produced to over-express SHI (OESHI), over-express MbhJ-N (OEMbhJ-N), knock-out SHI/SHII (ΔSHI/II), or knock-out MbhL (ΔMbhL). Soluble ferric citrate and insoluble ferric oxide were used to investigate the ability of engineered *Pf* strains to reduce extracellular oxidants (Figure 1.5). In addition, *Pf* was used as the anode catalyst in a two-chamber microbial fuel cell setup to study its exo-electrogenic ability for electricity generation. The results revealed that exo-electrogenicity could be achieved in engineered strains, but likely at the expense of cell growth. In the presence of insoluble ferric oxide, the OESHI strain showed an enhancement of exo-electrogenicity by 108 % over the parent strain, while the ΔSHI/II showed a modest enhancement of exo-electrogenicity by 5 %. However, in the presence of soluble ferric citrate, the ΔMbhL strain

resulted in a 120 % increase in its exo-electrogenicity over the parent strain, and both OESHI and ΔSHI/II exhibited higher exo-electrogenicity than the parent strain by about 51 % and 16 % respectively. Overall experiments revealed that the ΔMbhL strain produced the highest exo-electrogenic ability among these *Pf* strains. In addition, ΔMbhL strain grown in sulfur-containing media yielded the highest current and power densities using the two chamber MFC, with values of ~750 mA m^{-2} and ~225 mW $m^{-2,}$ respectively at a cell voltage of 0.3 V. To the best of our knowledge this is the first research attempt to compare and report the electrical current generation ability of different strains of genetically engineered *Pf.*

1.6 MES for Chemical Production

A variant form of MES is known as microbial electrolyzers or microbial electrolysis cells (MEC). The concept of microbial electrolysis cells originated in 2005, with the key feature of using an external voltage on top of the MFC potential to enable hydrogen gas production at the cathode through the reduction of protons [62, 63]. MECproduce hydrogen with less than half the voltage or electrical energy required for traditional water electrolysis [8]. MEC effectively produce hydrogen from various organic materials, making them a viable technology for generating renewable and sustainable hydrogen gas from organic feedstocks. MEC exhibit large hydrogen yields and require only a little electrical energy input.

Further, MFC represents a promising technology for recovering energy from waste organics either as electrical power or for producing hydrogen (H_2), but also for producing hydrogen peroxide (H_2O_2) and many other compounds [64]. The cathode, which operates

at normal temperature, removes electrons from the substrates and changes them into hydrogen. Both biological and metal-based cathode catalysts are possible. Compared to MFC, the compositions of the microbial communities of MECs are not fully understood [8]. Both MFC and MEC promote the growth of exogenous bacteria. However, MFC usually has air cathodes and oxygen diffusion into the anode chamber. The MEC operates under fully anaerobic conditions, thus supporting the growth of obligately anaerobic bacteria such as the exoelectrogenic *Geobacter* spp. and non-electrogenic fermentative or methanogens. A common method for enriching bacterial communities in MEC is to perform MFC and convert anodes to MEC [62, 65]. This procedure ensures biofilm formation at the anode and selects an external electrogenic community for MEC operation. Alternatively, the effluent from the MFC/MEC containing exogenous bacteria can be used as inoculum or scraping the biofilm of the anode and transferred onto a new electrode [66, 67].

1.7 Microbially-Induced Corrosion

In MEC, the hydrogen evolution reaction (HER) produces hydrogen at the cathode. For a MEC to be commercially viable, the electrode material—or electrocatalyst—of choice is crucial [68]. A good catalyst should generally possess the following characteristics: High selectivity for the desired product, energy efficiency at an acceptable turnover rate, and stability in the reaction environment are all desirable characteristics. Researchers have studied biotic and abiotic catalysts to develop effective hydrogen-evolving cathodes. Examples of biotic systems include, for instance, the usage of HER-biocathodes made of microorganisms [8, 69, 70]. Other research has demonstrated that the enzymes secreted by

microorganisms under certain circumstances enhance hydrogen synthesis but also contribute to the corrosion of the metal electrode [71]. Corrosion in cathodes negatively impacts hydrogen production efficiency [72]. It is important to use anticorrosive metals. However, anticorrosive platinum-based alloy metals are expensive and are not economically feasible to use in the MEC. Using the aromatic corrosion inhibitors from the plant extracts on the cathode materials could be economically feasible and environmentally friendly to overcome corrosion-related problems in MFC. During my doctoral research, I studied how the redox behavior of plant-derived aromatic compounds changes at different environmental pH conditions. We have used seven different active compounds. The findings were discussed in detail in appendix C.

1.8 Application of MES to Biosensing

Diseases caused by pathogenic microorganisms are of major global concern, and overpopulation, climate change, and the emergence of antibiotic resistance bacterial infections only exacerbate the problem. The prevention of microbial diseases depends heavily on identifying pathogens, pollutants, and other significant hazardous biomolecules, such as toxins. Rapid and sensitive detection with selective microbe identification is crucial in clinical microbiology, microbial forensics, and food and environmental studies. Rapid detection and treatment, however, are hampered by the lack of effective diagnostic instruments. Traditional microbiological techniques, such as culture, plating techniques, microscopy, and serology, frequently used for detecting pathogens, are insufficient.

On the other hand, the culture and plating methods need complex stages such as pre-enrichment, selective plating, biochemical screening, and serological confirmation [73].

Such techniques are frequently time-consuming, laborious, and ineffective since they rely on microorganisms' capacity to multiply and form colonies [74]. Small bioanalytical tools and biosensors have demonstrated a significant capacity for rapid and accurate analysis, making them useful for the early detection of infections [75]. Label-free approaches, including microbial electrochemical systems (MES), have been used with biosensors to track cellular and biological activities. Using MES, non-invasive methods, one can directly monitor extracellular or intracellular activity [76, 77]. Living organisms in MESs receive their sustenance from biodegradable organic substrates. Under anaerobic conditions, electrons are released through the electron transport chain (ETC) and transported to a molecule other than oxygen due to the microbial-catalyzed oxidation of the degradable organic molecules [78]. Accepting the electrons causes the formation of an electrical current directly correlated with activity and the overall number of metabolically active live microbial cells in the presence of the proper electrode material(s). However, dead or inactive cells are not participating in the microbial electrochemical processes because they lack electrochemical activity [79, 80]. Eventually, it may be possible to discern between living and dead bacteria when monitoring cell viability and microbial reactions online. However, the right electrode materials with biocompatibility, electrical conductivity, and catalytic activity are required to build high-performance MES [81]. As a result, several different nanostructures were created, including those made of carbon-based materials like graphene or carbon nanotubes [single-walled (SWCNTs) or multi-walled carbon nanotubes (MWCNTs)] [82]. They support the bioactivity of the generated biofilm in addition to improving the electrochemical signals and the durability of the electrodes [79]. Major advancements in the operation of MESs can be made by optimizing the electrode materials

to improve the electron transfer at the microorganism-electrode interface because the construction of MESs necessitates the effective integration of microbiology with electrochemistry and material sciences [83]. With improved sensitivities, reduced costs, and portability for on-site analysis, biosensors have been suggested as replacements for the current analytical procedures. Due to their potential significance for applications in medicine, diagnostics, the environment, and biosecurity, biosensors have gained a lot of attention [84, 85]. Biosensors combine biological recognition elements with a physical transducer that transforms the biological reactions into quantifiable signals. Optical, mechanical, calorimetric, or electrochemical methods can all be used to detect these signals [86]. The most popular biosensing methods use electrochemical biosensors because of their excellent specificity, sensitivity, and usability. Additionally, using them enables the online detection of a wide range of analytes in complex matrices (e.g., blood, serum, urine, or food).

Designing and constructing biosensors is a multidisciplinary task requiring knowledge and skills in various fields, including molecular biology, synthetic biology, protein engineering, chemistry, nanotechnology, bioelectrochemistry, and materials science.

The development of enzymatic biosensors depends heavily on the efficient transmission of electrons between redox enzymes and electrocatalytic surfaces. All living systems heavily depend on reactions involving the transport of electrons between molecules at surfaces; therefore, understanding the electron transfer process is crucial for biosensor development. I have learned and developed the skills needed to construct biosensors by studying the extracellular electrogenic abilities of genetically engineered cyanobacteria (Appendix A) and *Pyroccoccus* (Appendix B). During this study, I have understood the concepts related

to the two main types of extracellular electron transfer processes (direct and mediated electron transfer process). In addition, I have learned how biological redox couples interact with each other through literature.

Further, while researching cyanobacteria and *Pyrococcus,* I learned about the different immobilization methods to immobilize bacterial cells on different electrode surfaces. I have used different carbon nanoparticles, and nanostructured electrode surfaces for those experiments due to their excellent electrical conductivity, biocompatibility, and electrocatalytic characteristics. Carbon nanostructures have demonstrated potential performance as electrode materials. With all the gathered experiences and knowledge, I was able to focus on the selection and optimization of the electrode materials and could fabricate the electrode surfaces for biosensing applications through chemical alternation so that biological molecules would interact with the electrode surface.

Table 1.1: Variety of substrates used in MFCs

Bacterial strains	**Substrate**	**Anode Electrode**	**Electrode surface (cm^2)**	**Power output (mW/m^2)**	**References**
Coculture: *Geobacter sulfurreducens* and *Escherichia coli*	Acetate	Heat- treated graphite fiber brushes	15	918 ± 27	[87]
Geobacter biofilm	Acetate	Modified graphite rod	5.81	100	[88]
Shewanella oneidensis	Lactate	Graphene Au modified carbon paper (CP/G/Au)	6	508	[89]
Shewanella oneidensis	Lactate	Carbon cloth	1	2630	[90]
Recombinant *Klebsiella pheumoniae – S. oneidensis* consortium	Glucose and Xylose	Carbon cloth	6.25	104.7 ± 10	[91]

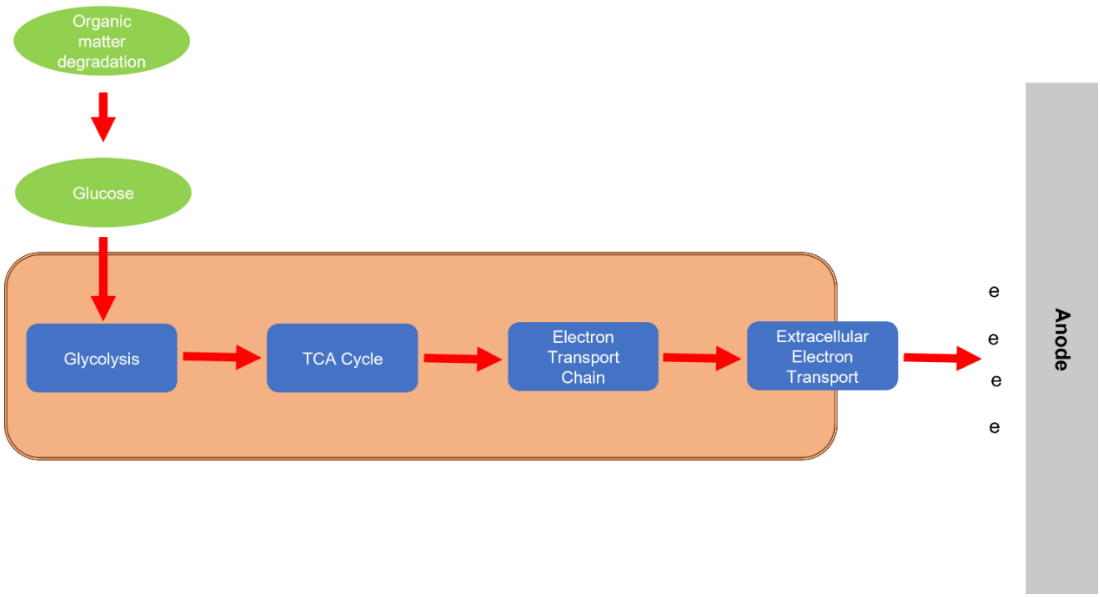

Figure 1.1: Interaction between microbe and electrode.

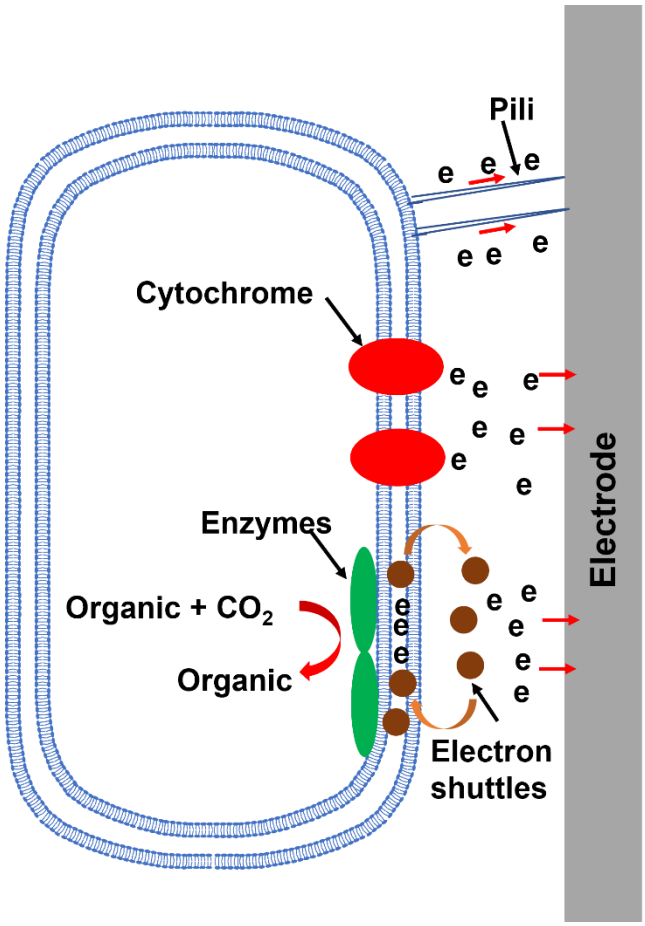

Figure 1.2: Three different electron transfer mechanisms from bacteria to the electrode. Direct electron transfer mediated by pilli /nano wires (a) and outer membrane cytochromes (b) Indirect electron transfer is mediated by electron shuttles.

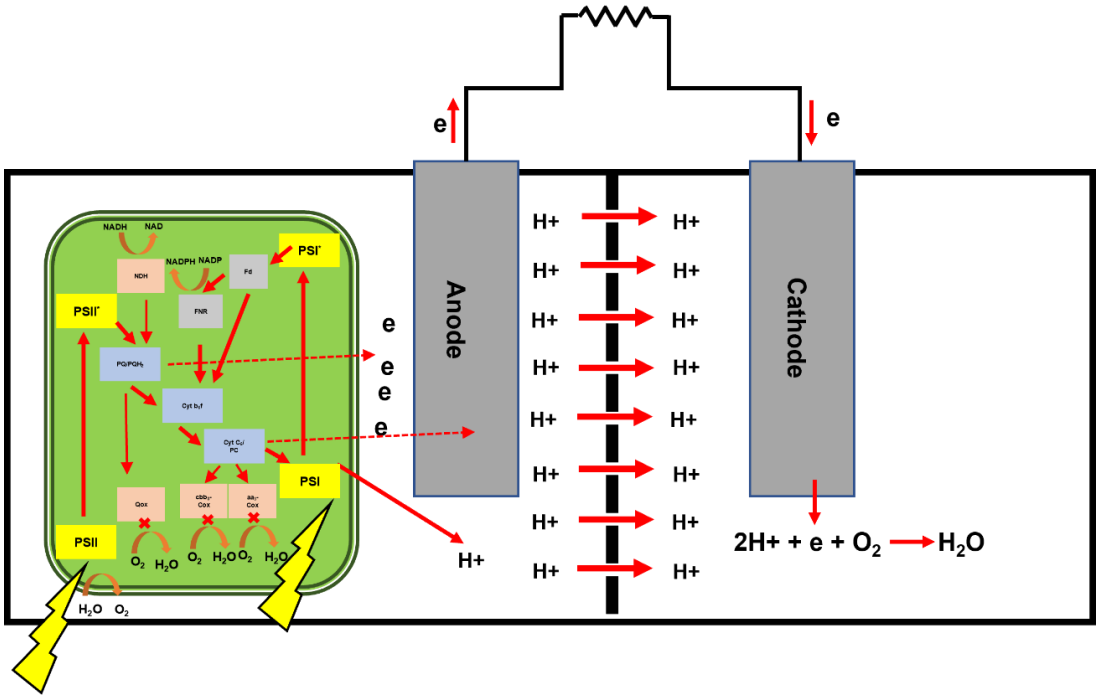

Figure 1.3: Photosynthetic microbial fuel cells (photo bio electrochemical cells).

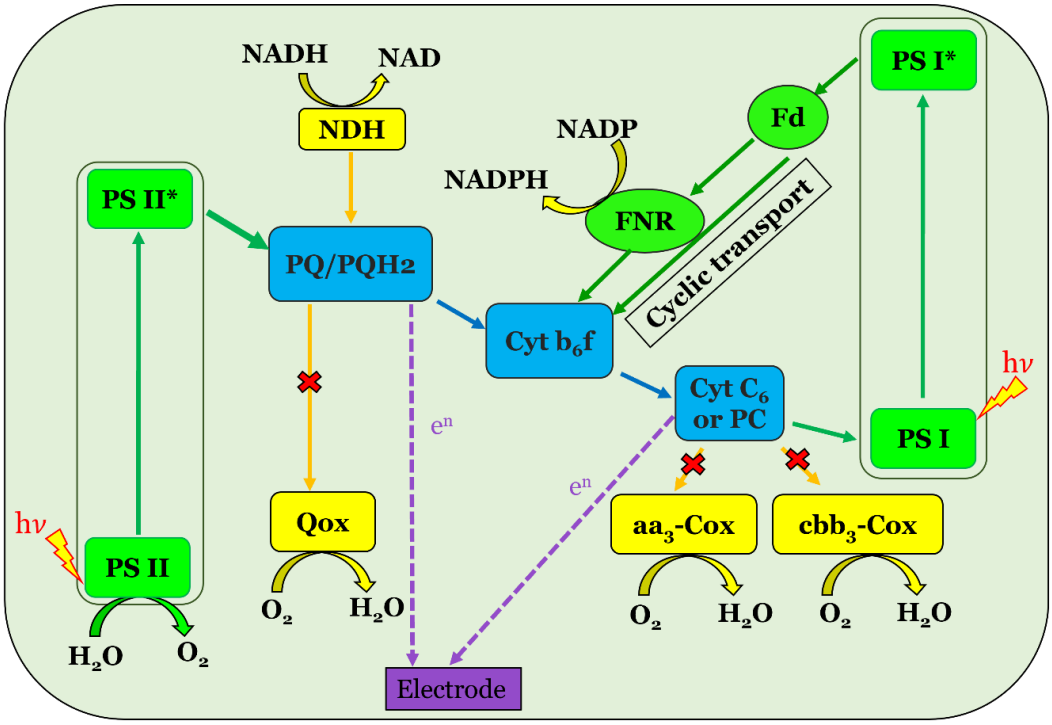

Figure 1.4: Schematic representation of enhancing the exoelectron transfer ability of the genetically engineered cyanobacteria.

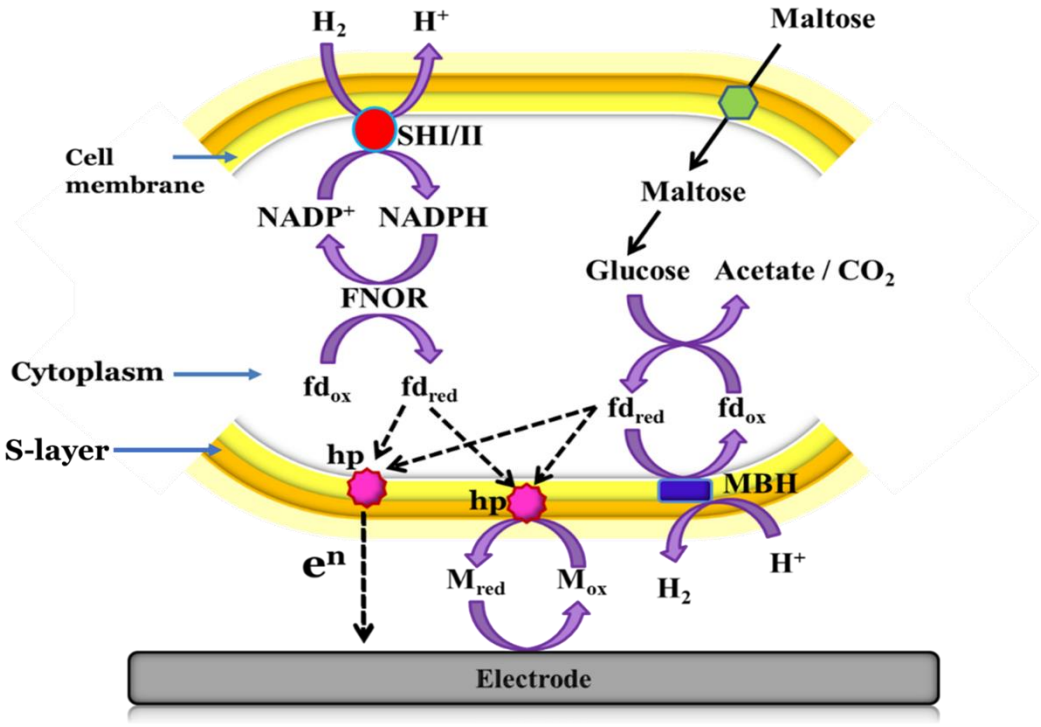

Figure 1.5: Schematic diagram of respiratory electron transport pathway and hypothetical extracellular electron transport pathway of *Pyrococcus furiosu*s.

CHAPTER 2

UTILIZATION OF MICROBIAL BIOELECTROCHEMICAL REACTIONS FOR BIOSENSING APPLICATIONS – LITERATURE REVIEW

2.1 State-of-the-art Methods for Bacterial Cell Detection

Bacteria are single-cell microorganisms present in various environments, including soil and water. Some bacteria survive in extreme temperature and pressure conditions. Humans and animals are the best reservoirs for microorganisms. Most microbes within the body are harmless, and a few are even beneficial. Only a small number of microbial specie are harmful and are responsible for diseases. Bacterial infections are a prominent cause of death in both industrialized and developing countries, claiming the lives of more than 6.7 million people each year [92, 93]. Millions of people are infected with these bacteria each year, with the most prevalent causes of infection being clinical, foodborne, airborne, and waterborne [1]. Clinical, food and environmental contamination are perennial concerns in healthcare, food safety, and environmental monitoring worldwide. These infections are expensive to treat, accounting for 8.7 % (33 billion US dollars) of annual healthcare costs in the United States [94, 95]. Bacterial infections can be divided into many categories, such as central nervous system infections, skin infections, respiratory tract infections, gastrointestinal (GI) tract infections, etc. According to CDC, most of these bacterial infections are related to GI tract infections and skin infections. Foodborne pathogens cause

GI infections, and skin infections are mainly caused by *Staphylococcus aureus* (“staph infections”).

Even though most staph infections are not harmful, some staph infections could be serious and lead to fatal conditions, including sepsis, pneumonia, and endocarditis. These staph infections caused by methicillin-resistant *Staphylococcus aureus* (MRSA), methicillin-susceptible *Staphylococcus aureus* (MSSA), vancomycin intermediate *Staphylococcus aureus* (VISA) and vancomycin-resistant *Staphylococcus aureus* (VRSA) [96]. Foodborne illnesses caused by pathogenic microorganisms are one of the significant public health concerns worldwide. The Centers for Disease Control and Prevention (CDC) estimates that 48 million Americans fall ill each year from eating contaminated foods. The CDC's national outbreak reporting system (NORS) reports that major foodborne pathogens such as *Escherichia coli, Listeria, Salmonella, vibrio*, Hepatitis A, Norovirus, and *Cyclospora* caused 20,854 major foodborne outbreaks from 1998 to 2017. Reported outbreaks caused 403,110 illnesses, 16,517 hospitalizations, and 392 deaths [97]. The discrepancies between the CDC estimate and NORS reported case shows the extent of unreported cases regards to foodborne illnesses.[98] Even though past reports identify norovirus as the most common cause of outbreaks and non-typhoidal *Salmonella* as the primary cause of bacterial contamination of food in the U.S. *Listeria monocytogenes* is not only responsible for the highest hospitalization rate but also the highest percentage of reported deaths in the U.S. Major foodborne outbreaks caused by some of the selected major etiological agents between 1998 to 2017 are provided in Table 2.1. Illnesses and complications caused by these major foodborne pathogens are provided in Table 2.2. Economic research services estimate that foodborne pathogens cost the U.S. economy $15.5 billion annually [99]. This

estimate is only the cost associated with medical care, time lost from work, and losses due to death. The inclusion of costs associated with recalls of the food products, loss of consumer interest, and other unaccounted costs could drive the economic losses due to foodborne pathogens much higher. Therefore, it is important to develop accurate and robust detection methods to isolate and enumerate pathogens present in the food sample as early as possible in the food supply chain. Even though predominant conventional detection methods such as standard microbiological and biochemical tests are highly reliable, inexpensive, sensitive, and allow both qualitative and quantitative assessment of pathogens, these methods require laboratory space and skilled labor, which are time-consuming. Standard microbiological test also requires pre-enrichment steps to concentrate on the bacterial cells. Initially, a non-selective medium is used to revive the cells from the food matrix, followed by a selective medium to identify the target pathogen. Finally, biochemical tests are used for further confirmation. This process typically requires 48 hours to several days, depending on the nature of the food sample and the type of target microorganisms. This longer testing time in traditional methods contributes to a significant time lag between the first outbreak of foodborne pathogens to its final identification and verification [100, 101]. In the food industry, this longer testing time contributes to a significant time lag between the first outbreak of foodborne pathogens and its final identification. This drawback contributes to an increase in foodborne illnesses and affects the economy due to the large recall of food products. Bacterial pathogens are responsible for a majority of food-borne illnesses and early diagnosis of food borne pathogens if of important to both the food and healthcare industries. The time between collecting a patient's sample and receiving diagnosis results through a health care diagnostic lab can often

surpass a week. While waiting for results, a broad spectrum of antibiotics is frequently prescribed, and the CDC states that over 30 % of patients are treated unnecessarily with antibiotics, leading to antibiotic resistance in humans. Therefore, rapid identification of these bacteria is important.

2.1.1 USDA/FDA Approved Detection Methods and Commercial Test Kits

Hundreds of commercial test kits validated by recognized independent organizations such as the Association of Official Agricultural Chemists (AOAC) are available to detect multiple foodborne pathogens. Most of the kits use one of the three major methods of detection. Immunological, molecular, and biosensors are the common methods used commercially to detect foodborne pathogens [102, 103]. Although some of the commercially available detection methods significantly reduce detection time compared to standard microbiological methods, they lack necessary sensitivity and selectivity for use diagnosis of pathogens in the food supply chain. This is due to the interference from the components of the food matrix with detection signal. Sensitivity and selectivity are important criteria for distinguishing true positives and negatives from those of the false signals. Therefore, these methods require samples to be enriched or suitably processed before analysis [104]. Even though the enrichment step helps improve the discrimination of live and dead cells, the revival of injured cells and dilution of the inhibitors present in the food sample is time-consuming and considered a major limitation in terms of rapid detection [105].

Immunoassays:

Immunoassays are based on the specific binding of an antibody to an antigen present in the target pathogen. This method is widely used in the food industry since it provides highly sensitive and specific measurements qualitatively or quantitatively depending on the type of immunological reaction. The sensitivity and specificity of immunoassays are mainly determined by the antibody used. Therefore the use of well-selected monoclonal antibodies would provide an added advantage [106]. Immune assays that are commonly used in the detection of foodborne pathogens are latex agglutination test (LAT), reverse passive latex agglutination test, enzyme-linked immunosorbent assay (ELISA), and Lateral flow assay (LFA).

Latex Agglutination Test (LAT)

In the latex agglutination test, a single colony of an antigen is usually mixed with latex beads coated with antibodies, and visible agglutination/ precipitation of the latex beads reveals the presence of the target antigen. No precipitation represents the absence of the target pathogen [107]. LAT is considered a rapid, simple, and inexpensive method. It is widely used in clinical samples to detect various bacterial pathogens. Some clinical applications include the detection of Campylobacter in stool samples and *Neisseria meningitidis* in cerebrospinal fluid [108, 109]. The reverse passive latex agglutination test allows the determination of the presence or absence of soluble antigens like bacterial toxins in the food sample [104]. The drawback of latex agglutination and reverse passive latex agglutination tests is that they only provide a qualitative measurement.

Lateral Flow Assay (LFA)

Lateral flow assay is a modified ELISA test. It employs a reagent pad where samples are deposited. When samples migrate due to capillary action, they encounter specific antibodies conjugated with color-emitting nano particles and are immobilized at the test line downstream. Presence of target antigen indicated by the presence of a test line and control line, while the absence of antigen would only result in a control line. LFA does not provide quantitative data and generally requires enriched samples. Also, false-positive results might occur due to the interference of materials present in the food matrix [110]. RapidChek *Salmonella*, FoodChek *E. coli* and RapidChek *E. coli*, Singlepath® *Campylobacter*, employs lateral flow assay to detect foodborne pathogens (Table 2.3, 2.4, and 2.7).

Enzyme-Linked Immunosorbent Assay (ELISA)

ELISA is the earliest and most commonly used method in the food and health industries to detect pathogens [103]. In commercially used sandwich ELISA assay, antibodies specific to target bacteria are immobilized on a solid matrix, and bacterial samples (antigens) are added and then incubated with the enzyme-conjugated antibody. This step is followed by adding a fluorescent, chemiluminescent or chromogenic enzyme substrate. The signal generated from enzyme activity is directly proportional to the number of bacterial cells. The detection limit of the ELISA ranges from 10^3-10^5 CFU/ mL for bacterial cells and a few ng/mL for toxins [103, 111, 112]. The necessity of pre-enrichment to avoid contamination in food samples is considered a major drawback of utilizing ELISA in the food industry [110]. TRANSIA™ plate *Staph* enterotoxins (A,B,C,D,E), TRANSIA™

plate *Staph* enterotoxins (A,B,C1,C2,C3,D,E), 3M Tecra *Staph. aureus* visual immunoassay for *Staphylococcus aureus*; TRANSIA plate *Salmonella* gold, 3M Tecra *Salmonella* Visual immunoassay for *Salmonella*; TRANSIA plate *Listeria* for *Listeria monocytogenes* and 3M Tecra *E. coli* for *E. coli* employs ELISA technique for detection (Table 2.3, 2.4, 2.5 and 2.6).

Molecular Methods:

Molecular methods were developed to detect the target pathogens by specifically detecting the unique DNA or RNA sequence of the target pathogen offering a high level of specificity. Polymerase chain reaction (PCR), reverse transcriptase PCR (RT-PCR), loop-mediated isothermal amplification (LAMP), quantitative PCR (qPCR), multiplex qPCR, and microarray are widely used molecular methods to detect foodborne pathogens.[113] PCR and qPCR dominate the commercially available detection kits. Although these tests require expensive equipment and consumables, they have become standard tools in most developed countries. PCR and qPCR have been used in diverse food matrices, with appropriate matrix and internal amplification controls, and in high-throughput applications.

Polymerase Chain Reaction (PCR)

PCR uses specific primers designed to amplify a unique region of the target pathogen genome. Amplifying the target sequence using specific primers indicates the presence of the target organism in the sample. Use of specific primers minimizes the occurrence of false positives, and the amplification process makes it more sensitive [114]. The limit of detection for conventional PCR is 10^2 – 10^4 CFU/ml. Assurance GDS or *E. coli*, Bax

system *E. coli* O157:H7; Bax system *L. monocytogenes*; Bax system *Salmonella* employs PCR technique for the detection (Table 2.3, 2.4, and 2.5).

Multiplex PCR (mPCR)

Multiplex PCR is a technique that allows the amplification of multiple gene targets to detect multiple organisms simultaneously. The basic principle is similar to conventional PCR. However, multiple pairs of primers are used in multiplex PCR, whereas single pairs of primers are used in conventional PCR. Nowadays, multiplex PCR can detect five or more pathogens simultaneously [115]. Both conventional PCR and multiplex PCR do not allow quantification. Both methods require a thermocycler, agarose gel electrophoresis unit, and the expertise to use them. They are also laborious and time-consuming, making them unsuitable for high throughput analysis and automated processes [116]. Another drawback of PCR is that it cannot discriminate between live and dead cells since DNA would also present in the dead cells. The sensitivity of PCR could be affected by the presence of inhibitors in the food matrix. So, pre-enrichment is necessary to minimize the presence of inhibitors.

Reverse Transcriptase PCR (RT-PCR)

Reverse transcriptase PCR (RT-PCR) is a technique that detects the presence of RNA from the target pathogen. In this process, RNA from the sample is transcribed to complementary (cDNA) using the reverse transcriptase enzyme, and cDNA is used for PCR using specific primers against target organisms. This method would discriminate the viable cells from the

dead cell since RNA rapidly degrades in the dead cells [117]. Commercially available Tadpole employs RT-PCR to detect *Campylobacter* (Table 2.7).

Loop-mediated Isothermal Amplification (LAMP)

Loop-mediated isothermal amplification (LAMP) is a single-tube technique used in food industries to amplify DNA. It is considered a rapid, simple, and cost-effective method since it does not require a costly thermal cycler. In contrast to conventional PCR, LAMP is carried at a constant temperature (60-65 ^{o}C), and this amplifies 10^9 copies of target DNA within an hour. In addition, LAMP could be combined with reverse transcription (Reverse Transcription loop-mediated isothermal amplification) step to allow the detection of RNA. This enables to discrimination of viable and non-viable cells [118-122]. 3M Molecular Detection Assay 2 uses LAMP to detect *Campylobacter* (Table 2.7).

Quantitative PCR (qPCR)

qPCR is a technique where fluorescent molecules are used to monitor the amplification in real time, enabling simultaneous detection and quantification of the bacterial cells. This method is more sensitive than conventional PCR since it requires a low copy number. The use of specific probes could allow more accurate detection with qPCR than conventional PCR that uses a pair of primers. However, qPCR could still be inhibited by the contamination of other substances in the food matrixes [122]. 10^2 – 10^4 CFU/ml is considered the limit of detection of the qPCR. With multiple specific probes, Multiplex qPCR can be used to detect multiple pathogens simultaneously [123]. This could be considered a rapid and effective alternative to identify the causative agents in a multi-

foodborne pathogen outbreak [124]. Utilization of sophisticated equipment, the requirement of skilled labor, and knowledge could be considered major limiting factors for using qPCR in the field. Bax System *E. coli* O157:H7 real-time for *E. coli*, ADIAFOOD Detection System, DuPont BAX® System and iQ-CheckTM for *Campylobacter* and Bax system for *S. aureus* use qPCR for the detection (Table 2.3 and 2.7).

Oligonucleotide DNA microarray

Oligonucleotide DNA microarray is widely used to detect foodborne pathogens, where hundreds of single-stranded DNA probes are coated on a glass slide or chips. Each oligonucleotide probe could bind to a specific part of a gene sequence and produce the probe-sample complex. The intensity of the fluorescence is proportional to the concentration of the labeled nucleic acid. This technique could be used to detect multiple pathogens simultaneously. Therefore, this could be used in the high throughput analysis, which could be automated. However, high cost is a limiting factor for the utilization of this technique in the food supply chain. [110, 125]. Gene sequence kits for *Listeria monocytogenes* and *Salmonella* and Gene-trak for *Staphylococcus aureus* use this technique for the detection (Table 2.4, 2.5, and 2.6).

Biosensors

Biosensors are analytical devices consisting of a bioreceptor, a transducer system, and a data processing unit. In a typical biosensor, bioreceptor molecules interact with the target analyte, and a transducer converts the interaction or binding event into a measurable signal (Figure 2.1a). Antigen, toxin, antibody, DNA, whole bacteriophage, or phage display

peptides/phage's receptor binding proteins could be bio-receptors (Figure 2.1b). Based on the transduction mechanism, biosensors are classified into optical, electrochemical, electronic, piezoelectric, pyroelectric, and gravimetric. Many researchers have widely used optical-based and electrochemical-based biosensors (Figure 2.2). Various spectroscopy techniques, including polarization, luminescence, fluorescence, surface-enhanced plasma resonance, refraction, and absorption, are used in optical biosensors. Electrochemical biosensors can be classified into amperometric, potentiometric, impedimetric, and conductometric based on observed parameters such as current, potential, impedance, and conductance. Electrochemical biosensors are advantageous for bacterial detection in food and health sectors because of their low cost, sensitivity, selectivity, simplicity, and ability to miniaturize [110, 122-124] easily.

Unlike other methods, biosensors are portable and easy to use in the field. The usage of biosensors is also simple and does not require any special expertise. Portability and ease of use with biosensors make them valuable in the field and at any point in supply chains. Biosensors are also easy to automate to handle many samples (multiplexed detection). The biosensor also detects pathogens in real-time and quantitatively, while other methods require longer detection and qualitative data. The specificity of the biosensor is considered one of the important criteria, and it highly depends on the type of biorecognition element (bioreceptor) used. Even though antibodies and enzymes pose high selectivity, they are susceptible to pH and temperature variations. This is a limitation to using this method in the food supply chain where field and food sample conditions cannot be altered easily to suit the testing methods. Even though DNA-based electrochemical biosensors are much more tolerable for a range of pH and temperature, they do not discriminate the live and

dead cells. Rapid B biosensor is capable of detecting *Salmonella* and as well as *E. coli* O157:H7 [107]. Immune-based assay flow cytometry technique was used in the Rapid B method. This product has been reported to detect the pathogen in real-time rapidly. In addition, buffers, conditioners, and other additives allow this method to use for the food sample with complex matrix without sample preparation. The product was also reported to discriminate the live and dead cells and quantify the viable cells. An impermeant membrane dye that only penetrates dead cells is used to discriminate between live and dead cells.

2.1.2 Criteria for Bacterial Cell Detection Methods

Even though many diagnostic methods have been developed throughout the years, most pose practical issues in diagnosing pathogens in the food supply and distribution chain. Many methods used in commercially available kits require laboratory equipment that is not portable for use in the field, and some require technical skills or expertise to execute the test. Even though the pre-enrichment step is essential in generating enough sample for positive detection and to increase the signal-to-noise ratio in the measurements, this step is the most time-consuming in the overall diagnosis (Figure 2.3). Using antibodies in some of these methods makes them relatively expensive but makes the test's stability into question. These methods are also difficult to automate to handle many samples. Any new rapid method should be as reliable and specific as current methods but also stable, inexpensive, and compatible with automation compared to current methods. Portability and the requirement of minimal expertise to handle biosensors make it a viable option for rapid testing.

Electrochemical biosensors could be easily miniaturized into smaller devices compatible at multiple points in the farm-to-shelf supply chain. Electrochemical biosensors also allow for automation to detect pathogens with many samples. This would be very useful in food processing plants and health sectors that handle large volumes and batches of food samples or clinal samples and would allow the detection to be incorporated into the production pipeline. The nucleic acid and antibody-based electrochemical biosensors have the same issues associated with molecular or immunoassay-based detection methods. Electrochemical biosensors based on phages or phage proteins are emerging as viable alternatives for nucleic acid and antibody-based biosensors. Bacteriophage-based electrochemical biosensors are very accurate and specific due to their high specificity toward the target organisms. Specificity and the stability of bacteriophages are preserved in a wide range of pH and temperature. This type of biosensor is also known to discriminate between live and dead bacterial cells, as the bacteriophage binding to the target bacteria depends on the presence of a functional receptor on the bacterial surface. Unlike other methods, some samples might not require enrichment due to their selectivity toward the target. Even for the most complex samples that require enrichment, bacteriophage-based biosensors could be coupled with microfluidic devices that used specific bacteriophages modified with magnetic particles that would isolate target organisms. This separation and isolation method could be quicker than conventional enrichment steps and also enable portable device development. They would also be easy to automate and employ in production pipelines. So, bacteriophage- or bacteriophage protein-based biosensors would be an ideal method for rapid detection as they provide portability, affordability, and compatibility with automation while not compromising reliability and specificity.

2.2 Phage as a Recognition Molecule for Biosensing Applications

Bacteriophages (phages) are obligate parasites that do not have their own metabolic machinery and use bacteria as hosts to multiply and produce more virions. Phages are ubiquitous and exist in the ratio of 10:1 in the environment with respect to bacteria [126]. Most phages specifically recognize their host (bacteria) to the strain level, with some exceptions, such as *Listeria* Phage A511. Even though interaction mechanisms between phage and bacteria remains an actively ongoing research area, studies show that phages heavily depend on their specific recognition factors, also known as receptor binding proteins (RBPs) or receptor binding phage protein (RBPPs), to recognize and attach to their specific sites on the bacterium and injects its genetic material (DNA/RNA) and take over host machinery to propagate new virions.[127, 128]. Phages could be classified as virulent (lytic phages) or temperate phages (lysogenic phages) based on their interaction with the host. Lytic phages attach to bacterial cells and take over the cell machinery of the bacterium to replicate their genetic material and make phage components. Then they lyse the cell and release new virions. Lysogenic phages will integrate their genome into the host genome and remain dormant.

Depending on the condition, lysogenic phages could induce lytic cycles [129, 130]. For better biosensor designing, understanding the bacteriophage infection process is important. The major steps of bacteriophage infection include adsorption, uptake, host takeover, maturation, and release. Phage attaches to the host during adsorption. Most phages use receptor-binding proteins on tail fiber attachment towards a specific receptor on the bacterial surface. This interaction is important for the specificity of a phage towards a specific host. The next step in infection is uptake, in which phages inject their genome into

bacterial cytoplasm. During host takeover, phage breaks down the host genome and takes over the bacterial replication, transcription, and translation machines. In this step, phage genome is replicated, and a large number of phage mRNAs and proteins are produced. In the maturation step, newly synthesized biomolecules are assembled into mature phage particles inside the cytoplasm of bacteria. In the last step, bacteria are lysed, and the daughter phages are released. In lysogenic phages, after the uptake step phage genome is incorporated into the bacterial genome and replicated with the replication of bacteria. When induction happens, the phage genome excises out of the bacterial genome and proceeds with the rest of the infection steps. The use of phages in detection manipulates the specificity of phage receptor binding proteins towards the specific receptors on specific bacterial species. So, using a phage with a specific RBP would bind only to the bacterial species with the compatible receptor while not binding to other types of bacteria and components of the food matrix. When a natural bacteriophage is used in the biosensor, upon adsorption, which is critical for detection, the rest of the infection process proceeds. This means that immobilized phage loses its genome, which means the sensor is not reusable. Eventually, the bacterial cell is lysed, and a large number of new bacteriophages are released with the proceeding of the infection cycle. Detection time should be rapid enough to avoid these steps of the infection cycle. Otherwise, the lysis of bacteria and competition from new bacteriophages for the bacteria would affect the accuracy and sensitivity of the detection signal. This could be addressed by using lysogenic bacteriophages or genetically modified not to proceed with the rest of the infection cycle. Alternatively, receptor-binding phage protein could be used in biosensor development which does not kill or lyse the bacterial cell.

Another factor we need to consider during phage-based biosensor development is the co-evolution of phage and its bacterial host. Bacterial host develops resistance to counter phages over time, and bacteria could develop resistance to different steps of phage infection. Bacteria are known to develop resistance by losing their receptor responsible for phage interaction or developing an extracellular capsule that would prevent access to the receptor from receptor-binding phage proteins. This would prevent phage at the adsorption step. Some bacteria also show uptake blocks to prevent the genome uptake of absorbed phages. Bacteria can also develop restriction enzymes and clustered regularly interspaced short palindromic repeats (CRISPR) to remove phage genome that has up taken into the cytoplasm. Restriction enzymes discriminate the modified DNA of bacterial genome from the unmodified DNA of phage genome and break down phage DNA. In the CRISPR immune system, bacteria insert short phage DNA segments in between repeat sequences and use that sequence in the future to recognize phage DNA sequences and chop with nucleases [131]. It is important to understand bacterial resistance when developing biosensors based on phages and phage proteins. Since impedimetric biosensors are based on the adsorption of receptor binding phage protein to a receptor on the bacterial surface receptor, any resistance to phage adsorption presence in the natural bacterial population would lead to false-negative and reduced sensitivity. So, understanding, identifying, and using the phages or phage proteins that have minimal resistance among the natural population of target bacterial species is critical. However, the duration of interaction between bacteria and phase during a biosensing test is not long enough for these bacterial resistances to fully develop or evolve.

2.2.1 Types of Phages for Biosensors:

Wildtype Phages

Bacteriophage-based biosensors are very accurate and specific due to their high specificity toward the target organisms [132-134]. Specificity and the stability of bacteriophages are preserved in a wide range of pH and temperature. This biosensor is also known to discriminate between live and dead bacterial cells, as the bacteriophage binding to the target bacteria depends on the presence of a functional receptor on the bacterial surface [135]. Unlike other methods, some samples might not require enrichment due to their selectivity toward the target.

Developing a biosensor to detect the bacteria using phage-based or receptor-binding phage protein-based biosensor is challenging since the analyte (whole bacterial cells) is larger than other small analytes like antigen/antibody. In addition, epitopes present on the surface of the bacteria might lead to a non-specific interaction with the surface of the transducer. Most target receptors, such as proteins and peptidoglycan, are on the cell membrane of bacteria. However, some bacterial target receptors, such as proteoglycan present in the flagella (Ex: *Campylobacter*). Bacteriophages or receptor-binding phage proteins are immobilized on the surface of the transducer, and they are required to be properly immobilized on the surface of the transducer to bind with the bacterial cells efficiently. The immobilization methods, such as physical adsorption[136, 137], chemical linkage [136, 138], and affinity interaction, were used to immobilize the bacteriophage. Physical immobilization of phages is carried out by incubating the transducer in a phage-containing solution. Phages could be immobilized onto the surfaces using van der Waals forces or

electrostatic interactions. Most of the phages carry a net negative charge on their structure. Therefore positively charged surface of the transducer could be used to immobilize the bacteriophage [139]. However, phages might leak due to the weak interactions between phages and surfaces, a major drawback of this method. The anchoring of phages on a biosensor detection architecture by chemical bonds is important for developing a consistent and stable detection system. Chemical linkage was used to immobilize the bacteriophage on the surface using covalent bonds. For example, T4 phages were covalently immobilized on gold surfaces using a self-assembled monolayer of dithiobis (succinimidyl propionate) (DTSP). Substances like bovine serum albumin were used on the surfaces to prevent non-specific binding.[136] However, the purity of the phage is considered an important criterion for chemical linkages. Phages are multiplied inside the bacterial cell to obtain high titers. Phages have to go through several purification steps to remove the contaminants such as bacterial protein, carbohydrates, and lipids to obtain pure phage preparation. These purification steps, such as ultra-high speed centrifugation [136], ultra-filtration [140], and size exclusion chromatography [141], could severely affect the immobilization of these phages onto an electrode.

Wild-type phages are biologically active and will lyse the host cell upon infection, leading to erroneous biosensor signals. Some phages show enzymatic activity towards their host bacterial surface receptor. P22 phage for *Salmonella enterica* and Sf6 phages targeting *Shigella flexnari* show endorhaminosidase activity towards the O-antigen on the surface of bacteria, which would result in detachment of bacteria after initial binding [142]. Such enzymatic activity would lead to inconsistent signals on a biosensor architecture and changes in detection efficiency. Phages bound on the sensor architecture are also

susceptible to drying. Intact phages can collapse on the sensor surface upon drying, making their tail fibers unavailable for binding with the host receptor [143].

Reporter Phages

Bacteriophages could be genetically engineered to increase the sensitivity and selectivity of the biosensor. Phages have been genetically engineered by adding a fluorescence tag to their genetic material. At the end of the lytic cycle, the fluorescence tag would be present in all progenies after cell lysis. At the end of the lytic cycle, these fluorescence-labeled phages will act as a probe for detection [144]. Food-borne pathogens such as *E. coli* [145], *Salmonella* [146], *Staphylococcus aureus* [147], and *Listeria monocytogenes* [148] have been successfully detected using reporter-phage-based techniques. This could increase the sensitivity and save time by eliminating the secondary enrichment step during the sample preparation before detection. The biggest advantage of reporter-based technology is distinguishing the live and dead cells since the phages cannot propagate inside the dead bacterial cell. However, virulence factors evolved on bacteria and bacterial defense mechanisms such as the presence of prophage[149], DNA restriction enzyme[150], presence of phage-specific inhibition genes [151], and antiviral immunity system [152] act as barriers for the phage to infect bacteria and are considered major drawbacks of utilizing reporter phage technology in bacterial detection [153].

Phage-Based Optical Biosensors

Phage-based biosensors using optical transducers have been widely investigated for food pathogen detection [132, 134, 154]. Based on the working principle, optical-based

biosensors could be divided into two: labeled and label-free. Techniques such as surface plasmon resonance (SPR), surface-enhanced Raman spectroscopy (SERS), fluorescence/ phosphorescence spectrometry, and bio/ chemiluminescence are mostly used for optical biosensing.

Surface Plasma Resonance (SPR) Sensors

SPR sensors measure the changes in the refractive index near the sensor's surface due to the interaction of the target analyte in solution and bio-receptors on the transducer surface. SPR system could be used to detect larger biomarkers such as bacteria. Bacteriophages have been successfully immobilized on the SPR sensor surface as probes to detect *S. aureus*, [155] *E. coli* O157:H7, and methicillin-resistant *Staphylococcus aureus* (MRSA) [156] (Table 2.11). Further, bacteriophage receptor binding proteins were also used as biorecognition probes on SPR architectures to detect food-borne pathogens such as *Campylobacter* [157] and *Salmonella*[143].

Bioluminescence Biosensors

The bioluminescence assay technique provides a quantitative diagnosis. In this method, light emission by the intercellular components is measured based on the bioluminescence reaction with the luciferase enzyme. Lytic phage is used as a recognition probe to detect the target bacteria and lyse the bacterial cells. The use of lytic phage provides sensitivity and makes the process simple. This method is also considered rapid since it eliminates the time-consuming conventional culture methods. Foodborne pathogens such as *E.coli* and *Salmonella* have been detected using ATP bioluminescence assay [158]. Adenylate kinase

could be used as an alternative cell marker to increase the sensitivity of the bioluminescence assay. However, and amount of adenylate kinase will depend on the type, growth stage of the bacterial cells, type of the phage, and the infection time [159]. The lack of specificity is considered a major drawback of this method.

Electrochemical Sensors

Amperometric and impedimetric-based biosensors are the two most commonly used electrochemical-based sensors used to detect pathogens.

Amperometric Electrochemical Biosensors

The amperometric technique is one of the electrochemical-based detection methods widely used for pathogen detection. One of the ways amperometry can be used for sensing is to detect ions in solution by measuring the changes in electric current. Once phage infects the bacteria, cell content such as enzymes will be released into the surrounding medium. A specific substrate is used to measure and quantify enzyme activity. Researchers have combined amperometry-based detection with the phage typing method to specifically detect foodborne pathogens such as *E. coli* K12, *Bacillus cereus*, and *E. coli* O157:H7 [160-162]. (Table 2.11).

Impedimetric Electrochemical Biosensors

The electrochemical impedance spectroscopy (EIS) technique has been widely used to monitor the changes in the interfacial impedance over a range of frequencies as a result of biomolecular interaction. In the process of bacterial detection using a phage as a

recognition element, changes in impedance occur due to the attachment of microorganisms to the phages present on the sensor surface. This method was used to detect *E. coli* using phage by our group [163]. Even though EIS is considered a label-free detection method compared to the amperometric technique, a lower detection limit is considered a major limitation of utilizing this method to detect foodborne pathogens. In addition, phage-based EIS sensor detection could be adversely affected by cell lysis. These two drawbacks could be overcome by utilizing the receptor-binding phage proteins on the transducer surfaces (Table 2.11).

2.3 Receptor Binding Proteins (RBPs) / Receptor Binding Phage Proteins (RBPPs) as Recognition Molecules for Biosensing Applications

Some of the limitations associated with bacteriophages for pathogen biosensing can be overcome by using RBP or RBPP as bioreceptors. The unique host recognition by phages comes from the RBPs located on the tail fibers, and the binding of these proteins triggers the injection of the phage genetic material into the host [164, 165]. These RBPs recognize unique proteins or carbohydrates on the bacterial surface [166]. Advancements in genome information, cloning, and molecular biology methods allow us to rapidly identify potential RBPs and produce them with high purity at a lower cost.

2.4 Whole Phage versus RBPPs / RBPs for Biosensing Applications

RBPPs are smaller in size than phages, allowing more RBPPs per unit surface area than phage particles, thus allowing more target bacteria binding per unit surface area and thereby increasing the sensitivity of the test. The possibility of having a large number of

RBPPs per unit surface would also allow the detection of multiple pathogens simultaneously using specific RBPPs, without compromising on sensitivity. Naturally occurring phages would proceed with the infection cycle and lyse the target bacterial cells. But in the case of RBPPs, only the attachment of the protein to the bacterial receptor takes place without proceeding into the infection process and makes RBPPs-based biosensors reusable. The use of the whole bacteriophage has a higher chance of developing bacterial resistance to phage than RBPPs. The purification process for bacterial phages is long and affects the phage filaments involved in bacterial binding, thereby reducing the sensitivity. Recombinant RBPPs are relatively easy to purify with high purity and minimal damage to the receptor-binding domain. Some phages have an enzymatic activity that separates phage particles from the bacterial host after initially binding. The use of phages with these activities would negatively affect the accuracy of the detection. Studies show RBPs exhibit improved stability against environmental factors such as pH and temperature and resistance against proteases [167]. RBPs could be added with tags at an appropriate position without altering their binding affinity, and those tags could be used to oriented RBPs on the biosensor electrode surface. These advantages offered by RBPs make them an attractive alternative to phage-based biosensors.

2.5 Interaction between *Campylobacter* Phage Protein FlaGrab (formerly Gp047/ Gp48) and *Campylobacter* Phage NCTC 12673 and *Campylobacter jejuni*

NCTC 12673 phage is a T4 type, *Campylobacter jejuni*-specific lytic phage that belongs to the member of the *Cp8virus* genus of the *Eucampyvirinae* subfamily of the *Myoviridae* family. T4-type phages consist of 2 parts: Head and Tail. The head consists of nucleic acid

and capsid protein. This phage contains 135 kbp double-stranded DNA chromosomes, 172 open reading frames (ORFs), and 3 tRNA genes. This phage has a long, contractile tail, with 26 icosahedral protein capsids [168-170]. *C .jejuni* is a microaerophilic gram-negative bacteria [171]. It causes bloody diarrhea, and chronic infection could lead to Guillain-Barre syndrome (GBS), an autoimmune disorder that causes the immune system to damage nerves. GBS causes muscle weakness, which could lead to paralysis in severe conditions [172]. After ingesting contaminated food or water, *C. jejuni* invades the gastrointestinal epithelial cells and causes inflammation, leading to diarrhea [173, 174]. The flagella of *C. jejuni* play a crucial role in colonizing the human gastrointestinal tract. Flagellar filaments are composed of eleven protofilaments that are composed of flagellin subunits. The flagellar filament is driven by a multi-subunit motor protein's proton motive force (PMF) [175]. Proper flagella formation and normal filament movement in *Campylobacter* require flagellar glycosylation [176, 177].

***Campylobacter* Phage NCTC 12673 Protein - FlaGrab (formerly Gp047 & Gp48)**

FlaGrab is a receptor-binding phage protein expressed by NCTC 12673 phage [178]. FlaGrab binds to pseudominic acid (Pse5Ac7Am) glycan displayed on flagellin subunits of *C. jejuni* flagella. Even though, we know the amino acid sequence of the protein, any structural features, conserved domains or critical amino acids involved in receptor binding have not been reported. This protein recognizes flagellin from almost all the strains of *C. jejuni* and *Campylobacter coli* (*C. coli*) [170]. The binding of FlaGrab to the flagella reduces bacterial motility. Homologs of FlaGrab are present in all the members of Eucampyvirinae, indicating its importance in the phage lifecycle [169, 179, 180].

Proteomic analysis and antibody recognition did not show the presence of FlaGrab on the phage virion, indicating the non-structural role of the protein [168, 181, 182]. The binding domain of FlaGrab is located in the c-terminal quarter of the protein (CC-FlaGrab), and CC-FlaGrab has been shown to detect both C. *jejuni* and *C. coli* [170]. FlaGrab inhibits the growth of the bacteria, and the growth-inhibiting activity was shown to be located in the C terminal quarter of the FlaGrab. Even though FlaGrab poses bacteriostatic properties, no bacteriolytic properties have been seen. RNA sequence analysis showed that binding of FlaGrab showed down-regulation of energy metabolism genes, especially those involved in the TCA cycle, carbon metabolism, and oxidative phosphorylation. FlaGrab has also been immobilized onto solid surfaces without altering its binding specificity towards *C. jejuni* and *C. coli* [157].

FlaGrab is a good bioreceptor for a biosensor to detect those pathogens as a receptor-binding phage protein (RBPP) that specifically binds to *C. jejuni* and *C. coli*. Unlike most RBPPs, which are a component of virion tail fibers, FlaGrab is a nonstructural secreted protein. The only way to employ it in a biosensor is by directly using the protein to develop into a biosensor. Flagrab is smaller than the whole phage, so it would allow more protein to be coated per unit surface area. Since the bacterial binding property is residing on C-terminal quarter of the protein (CC-FlaGrab), we could further reduce the size of the bioreceptor and thereby increase number of molecules per unit area and sensitivity of the biosensor. Even though CC-FlaGrab harbors bacteriostatic properties, it does not lyse the bacterial cells. This makes it a better alternative to the use of phages. The availability of a genetically engineered CC-FlaGrab with a GST tag would allow better purification and better orientating of the protein on a biosensor for productive interaction with the bacterial

receptor. Immobilization of protein could be targeted towards the GST tag, thereby minimizing the damage to critical amino acids involved in the interaction with the receptor. Since previous studies have shown that GST-tagged FlaGrab could be immobilized on the gold surface, we know that the protein is compatible with immobilization, and immobilization could be done without affecting the interaction with the target organism. We could also use the same immobilization technique in the development of biosensors. Since most of the *C. jejuni* and *C. coli* strains are detected by FlaGrab, it indicates most strains have the receptor for the protein and minimal resistance in the natural bacterial population. These properties make FlaGrab a better bioreceptor for a biosensor to selectively detect *C. jejuni*.

2.6 Immobilization Methods to Attach Phage and Phage Receptor-Binding Protein onto Nanostructured Electrodes

Immobilization of biomolecules is a process where biomolecules are attached to a solid support or within the solid support. Strategies for immobilizing various biomolecules, such as proteins, enzymes, antibodies, and nucleic acids, onto nanomaterial supports have been extensively studied and widely used in numerous biosensor applications. In enzyme-based biosensors, proper immobilization of enzymes is considered a crucial factor due to the instability of the freely moving enzyme. Immobilization of enzymes to solid support provides numerous advantages. Immobilization reduces the cost of operation since the free enzyme system requires additional processing and purification steps. Immobilized enzymes are more stable than free-form enzymes. Immobilization also allows a single batch of enzymes to be used repetitively. Removing the enzyme from the reaction solution

also allows the reaction to be controlled. Immobilization also helps in avoiding contamination of products with enzymes could be avoided by simply removing the enzyme from the system.

Four main types of immobilization techniques have been used to immobilize the enzymes on to electrode, including adsorption, entrapment, covalent coupling, and cross-linking. Enzyme-immobilization methods could be classified as physical and chemical, depending on the interaction mode between enzymes and support carriers. Physical methods include adsorption and entrapment, where covalent coupling and cross-linking are classified under chemical methods. The advantages and disadvantages of each immobilization method are summarized in Table 2.12.

Physical Adsorption

Physical adsorption of an enzyme is considered the simplest method. In physical adsorption, enzymes are adsorbed on the support matrix via weak van der Waals forces, electrostatic or hydrophobic, hydrophilic interactions, or hydrogen bonding. In this method, a concentrated solution of an enzyme is mixed and placed in contact with the solid support for a while under suitable conditions [183]. The main advantage of the adsorption method is the minimal use of reagents or activation steps. Even though there is evidence that this method could stabilize enzyme activity [184], in this type of adsorption method, enzymes tend to desorb or leach out with a change in pH, temperature, or ionic strength since the enzymes are not strongly attached. In addition, nonspecific adsorption of other proteins and substrates may lead to contamination and interferes with the signal [183, 185, 186]. Therefore, the adsorption-based immobilization method is usually carried out by

combining with other immobilization methods, such as cross-linking or entrapment in the form of a layer. So far, the adsorption-based enzyme immobilization method has not been used alone in practical biosensors [187].

Entrapment

Enzymes or proteins are susceptible to protease degradation, and they can easily aggregate under the influence of external factors. Entrapment/encapsulation is the best way to avoid any adverse influence on enzymes or proteins. Entrapment is a physical immobilization method where an enzyme is not directly attached to the support, but the enzyme is physically entrapped inside a porous polymeric matrix or a membrane by covalent or non-covalent bonds [188, 189]. Various membranes, such as collagens, nylon, gelatin, and polycarbonates, have been used for entrapment. These membranes serve as semipermeable materials where the enzymes are retained while allowing free diffusion of substrates and products. This method will decrease the leaching of the enzymes and improve the stability of the enzyme. In this method, the enzyme will initially be mixed with a monomer solution. Later, the monomer solution was polymerized by changing the experimental conditions or by a reaction process to entrap the enzymes. A disadvantage of the approach is the resistance to the mass transfer occurs as the extension of polymerization appears to increase the thickness of the gel matrix. Hence the substrate cannot penetrate deep into the gel matrix to enter the enzyme's active site.

Moreover, if the size of the pores of the support matrix is too large, the trapped enzyme could leak [186]. Further, the growth of microorganisms on the surface of the membrane causes the enzyme layer to be inhibited, causing the sensor to behave incorrectly [183].

The entrapment of enzymes could be achieved by chemical, electrochemical, and photopolymerization, the sol-gel process for the lattice type, and microencapsulation for the microcapsule type [186, 187].

Literature reported that different types of supports or carriers could overcome limitations associated with the entrapment. An efficient entrapment was achieved with alginate-gelatin-calcium hybrid carriers that prevented the leakages of enzymes and provided greater mechanical stability. Mesoporous silica and chitosan could also be used as a carrier to increase the adsorption capacity and prevent enzyme leaching [190, 191]. Nanostructured supports such as electrospun nanofibers and pristine materials have been widely used in the entrapment process in various applications, including biosensors [189, 192-195]. The amperometric biosensor was developed by entrapping the glucose oxidase in electrochemically coated nanofilms on porous platinum, which resulted in significant increases in catalysis level and increased the sensitivity of the biosensor [196]. In addition, sol-gels have been widely used as carriers to immobilize the proteins using the entrapment method in biosensors focusing on increasing sensitivity and decreasing response time. Sol gels are highly porous silica materials with specific properties such as thermal and mechanical stability, rigidity, and chemical inertness [187, 197, 198].

Electro polymerization is another method to physically immobilize enzymes into conductor polymers such as polyaniline and polypyrolle [199-204]. In the presence of an enzyme, the electrochemical potentiostatic and galvanostatic polymerization of the monomers produces a very sensitive and thin layer. This method could be used in commercially available electrode materials such as gold, carbon, and platinum and the possibility of

miniaturization. However, the exact amount of immobilized enzyme is difficult to determine and is considered a drawback of this method [205].

Covalent Bonding/Covalent Coupling

Enzyme immobilization by covalent binding is one of the most extensively used methods, where covalent bonds are formed between the functional groups present on the enzymes and support matrix. The enzyme's active position must not be involved in covalent bonding so that enzyme inhibitors can be added to the enzyme solution during covalent bonding treatment [183]. The functional group of proteins/enzymes suitable for covalent bonding involves the α and ε amino groups of the lysine and arginine; the thiol group of cysteine; the phenol ring of tyrosine, and the indol group of tryptophane, the imidazole group of histidine and hydroxyl group serine and threonine [206, 207]. Further, peptide-modified surfaces used to immobilize the enzymes resulted in higher specific enzyme activity, stability, and controlled protein orientation [208]. The enzyme binding to the support takes place in 2 steps. First, surface activation will occur via linker molecules such as glutaraldehyde [209] or carbodiimide as the bridge between the surface carrier and enzyme. Second, the enzyme will take two days to activate support through covalent bonding. In addition, several methods, such as reticulation and enzyme fixation by self-assembled monolayer, have been included to make the covalent binding more efficient and stable.

Reticulation is a process where enzyme molecules create an insoluble, rigid structure. The linker molecule called glutaraldehyde could also be used for reticulating enzyme molecules. The reticulation process offers some advantages. In the presence of an inert

protein like bovine serum album (BSA), the stability of the immobilized enzyme could be improved. In addition, it provides firmness for enzyme-enzyme and enzyme-protein couplings. However, the reticulation process might increase the response time of the biosensor since reticulation induces the formation of diffusion barriers [210].

Self-assembled monolayers (SAM) can also create monomolecular films of biomolecules on a wide range of substrates for oriented enzyme immobilization on biosensors [211-213]. This method could be preferably used on metallic electrodes such as gold, silver, and platinum for biosensing applications [213-215].

Covalent immobilization provides a strong binding between the enzyme and support matrix. Therefore, it helps to eliminate or minimize enzyme leakage. In addition, covalent coupling provides greater resistance to external conditions such as pH and temperature variations [186, 216]. However, enzyme denaturation might occur since enzymes undergo several chemical modifications for functionalization [186, 217, 218]. Even though the immobilization process increases the enzyme stability, enzyme activity might be decreased in affinity reaction, and it is also a time-consuming process. Low reproducibility is considered a major drawback of this method. Cross-linking enzyme immobilization is an irreversible process that creates intermolecular cross-linkages between the enzyme molecules through covalent bonds. In this process, the enzyme is not attached to the support in the reaction mixture. Therefore, it is not much preferred in enzyme immobilization. However, it is considered a useful method in combination with other immobilization methods, such as adsorption, to minimize enzyme leakages. Glutaraldehyde is extensively used for crosslinking processes due to its high efficiency, stability, and low cost. Aldehyde

groups at the two ends of glutaraldehyde react with the free amino groups of enzymes and form cross-linkages [219-226].

2.6.1 Nanostructured Electrodes

Development in nanotechnology facilitates the use of a variety of nanomaterials in different types of applications, including the development of biosensors. Nanostructured electrodes are widely used as electrochemical transducers as they provide high sensitivity by generating large interfacial surface areas for electrochemical interactions. The high surface area provided by nanomaterials also increases conductivity. Nanomaterials such as carbon nanotubes, carbon nanorods, graphene, metal or metal oxide nanoparticles, and quantum dots have been widely used in nanostructured electrodes as electrochemical transducers [227-229].

Carbon nanotubes (CNTs) have been widely used in transducers due to their unique structural and chemical properties in biosensing applications. CNTs are not only highly conductive but also highly stable. In addition, the highly porous surface of CNTs provides a large electroactive area for binding various biological molecules, which increases the biosensor's sensitivity [230-233]. The high surface-to-volume ratio of CNTs allows high molecule charge per geometric unit, which helps signal amplification. The chemical properties of CNTs could be changed permanently or reversibly through various surface functionalization. Functionalization is a process where molecules are attached to surfaces to impart the surfaces with specific applications like biosensors. The functionalization of CNTs could be classified into covalent and non-covalent functionalization. Non-covalent functionalization of CNTs is considered an alternative strategy to immobilize biomolecules

over covalent functionalization since they preserve their intrinsic, mechanical, and electronic properties. This non-covalent functionalization aids in enhancing the bio-affinity of CNTs and increasing the effective electrical communication between the bioreceptor and the transducer [234].

In addition to CNTs, metallic nanoparticles such as gold and silver have also been used in different biosensors due to their unique optical and electrochemical properties. These metallic nanoparticles (Ex: gold nanoparticles) are functionalized with thiols, disulfides, amines, and carboxyl functional groups and could further be linked to biomolecules such as proteins and nucleic acids for various applications. Due to their plasmonic properties, gold nanoparticles are mostly used as transducers in optical biosensors [229, 235, 236].

Metal oxide nanomaterials have been used in electrochemical biosensors, especially in amperometric enzymatic biosensors, due to their biocompatibility, semiconducting properties, sensitivity, selectivity, and low detection limit. In addition, the surface hydroxyl groups on metal oxide nanomaterials can be conducive to surface functionalization to link to enzymes reliably [237, 238].

2.7 Immobilization of RBPP, CC-FlaGrab on a Nanostructured electrode to detect *Campylobacter jejuni* and *Campylobacter coli*

Over the past years, different bio-probes such as an enzyme, antigens/antibodies, nucleic acid, and whole bacteriophages have been extensively used as bio-receptors on nanostructured electrodes to detect food-borne pathogens. However, using receptor-binding phage protein as a bioreceptor biomolecule in a biosensor is relatively new. RBPPs are considered potential bioreceptor since it possesses several advantages compared to

antibodies due to their specificity, binding affinity, and stability to various environmental conditions.

In this dissertation research, we have expressed the c-terminal quarter of Gp047 [CC-Gp047 -recently renamed CC-FlaGrab] [178] in *Escherichia coli* BL21 cells which is responsible for the interaction with the bacterial receptor, a flagellar glycan [239]. FlaGrab was genetically engineered to express with Glutathione S-transferase (GST) tag, an enzyme, to be purified with glutathione-based columns. Even though the amino acid sequence of this protein is known, very little is known about its structure of the protein. The bioinformatics analysis did not show the presence of any known domains in RBPP protein. Developing an immobilization technique for GST-CC-FlaGrab without affecting its physical, chemical, and mechanical properties is crucial for a successful biosensor design to detect *Campylobacter jejuni*.

An ideal method for immobilizing CC-FlaGrab is to immobilize it strong enough to minimize the leaching of the protein while preserving its interaction with the bacterial receptor glycan molecule. So, any immobilization technique should not affect the critical amino acid involved in interacting with the bacterial receptor. The immobilization method should also consider the correct orientation and conformation of the protein for productive interaction. If the immobilization method could target the GST tag for immobilization purposes instead of the CC-FlaGrab, the adverse effects on the structure of the RBPP and critical amino acid would be minimized. The method should also be compatible with the nanostructured probe to increase the surface area and sensitivity of the detection. It should also be a method that does not require a complete understanding of the structural information of the protein.

The use of physical adsorption for immobilization does not require information about the structure of CC-FlaGrab, and it is also simple and inexpensive. But random weak interaction between solid support and protein might involve critical amino acids for receptor binding, and protein might not be oriented in the correct direction and conformation to have a productive interaction with the receptor. Weak interactions between the protein and surface could be affected by the difference in pH and temperature associated with food samples, which might affect the detection's sensitivity. As a receptor-binding protein, access of CC-FlaGrab to the bacterial receptor is critical for functional interaction. Even though entrapment could allow free movement of substrates and products in enzyme immobilization, receptor access to the RBPP could be blocked due to the larger size of both receptor and RBPPs. So, entrapment would not be a good method to immobilize CC-FlaGrab. Other methods for attachment of CC-FlaGrab on the electrodes for *C. jejuni* detection are discussed below.

Approach 1: Immobilization of GST-CC-FlaGrab on a gold nanostructured electrode

The covalent bonding of CC-FlaGrab is ideal for minimizing the leaching of the protein and making it stable across changing pH and temperature encountered with food samples and field conditions. The caveat with covalent bonding without a better understanding of structure is that we could affect the critical amino acids involved in RBPP-receptor interaction or cause changes to conformation. It is also hard to orient all the RBPP to produce productive interaction with receptors with random covalent bond formation. The presence of the GST tag and its high affinity to glutathione with the self-assembly monolayer assembly could be used to address the issues mentioned above. We could form

a self-assembled monolayer of glutathione on a nanostructured electrode and use the affinity of the GST tag associated with the CC-FlaGrab to immobilize it to the electrode surface. Past studies have shown that gold electrodes could be used to generate glutathione self-assembled monolayer. A similar assembly was used to show the biding of CC-FlaGrab to *C. jejuni* using the plasmon resonance technique [157]. We could use a gold nanoparticle-based nanostructured gold electrode to increase the surface area and sensitivity of the detection. Bovine serum albumin (BSA) will be added to block the substrate surface to avoid the nonspecific attachment of bacteria to the substrate surface. This method would allow us to orient the RBPP to produce productive interaction with the receptor. It also preserves the critical amino acids involved in the interaction and conformation of the protein. In addition, literature shows that this method does not interfere with the binding with the bacteria [240]. Even though GST-glutathione interaction is stable across a big range of pH, extreme pH might be affected by the stability of this interaction (Figure 2.4).

Approach 2:Immobilization of GST-CC-FlaGrab on a carbon nanostructured electrode

We could also use a crosslinker to immobilize CC-FlaGrab to the nanostructured carbon electrode. We could use a glassy carbon electrode with functionalized multi-walled carbon nanotubes (MWCNTs) and use 1-pyrenebutanoic acid succinimidyl ester (PBSE) as a crosslinker and attach the GST-CCGp047 through the linker to the surface. Since PBSE reacts with the N-terminal amine group, it allows us to orient the protein in a way that would allow productive interaction with the receptor. Since the GST tag is at the N terminal, the chemical reaction with the crosslinker would have minimal impact on the

conformation or critical amino acids of the CC-FlaGrab. Since the protein is linked through a covalent bond to the linker, the chance of leaching out is minimized, and the protein would be stable at pH and temperature changes. PBSE has been widely used in numerous biosensor applications with many types of proteins [241, 242]. (Figure 2.5)

Best Approach to immobilize GST-CC-FlaGrab on a nanostructured electrode to detect C. jejuni and C. coli

The covalent bonds methods proposed above could immobilize CC-FlaGrab in an orientation that would result in productive interaction with glycan receptors on *C. jejuni* and *C. coli* and would not affect any critical amino acids involved in the interaction. Even though the interaction between glutathione and GST tag is strong, that is not as strong as the covalent bonding between PBSE crosslinker and N-terminal GST tag of CC-FlaGrab. So, the covalent bonding with the crosslinker (PBSE) method would result in minimal leaching of RBPPs. So, we believe that the covalent bonding using the crosslinker (PBSE) method would be the best option for the immobilization of FlaGrab to a nanostructured electrode and immobilization of GST-CC-FlaGrab onto glutathione self-assembled monolayer as a viable alternative.

Table 2.1: Reported multistate bacterial pathogen outbreaks in the US (1998-2017) [243, 244]

	E. coli	***L. monocytogenes***	***Salmonella spp.***	***Campylobacter***	***S. aureus***	***Shigella***	***Vibrio***	***Bacillus***
Total outbreaks	615	78	2,711	499	695	189	178	673
Illnesses	13,730	940	72,412	8602	10983	7,703	1,856	9062
Hospitalizations	2,256	686	8,554	374	583	310	74	133
Deaths	39	140	100	1	6	2	3	5
% of hospitalizations among illnesses	16.4	72.9	11.8	4.4	5.3	4.0	4.0	1.5
% of deaths among illnesses	0.28	14.90	0.14	0.01	0.05	0.02	0.16	0.05

Table 2.2: Summary of major bacterial illnesses in the US [244, 245]

Etiology	**Infective dose (number of cells to start an infection)**	**Name of the disease**	**Life-threatening complications**
Escherichia coli	<10	Hemorrhagic colitis	Hemolytic uremic syndrome
Listeria monocytogenes	<1000	Listeriosis	Stillbirth, miscarriage, and life-threatening infection to newborn
Salmonella spp	15-20	Salmonellosis	
Campylobacter jejuni	400-500	Campylobacteriosis	Guillain-Barre syndrome, muscle weakness, and paralysis
Staphylococcus aureus	10^3-10^8	Food poisoning	
Shigella	<10	Shigellosis	
Vibrio parahaemolyticus	>1 million	Gastroenteritis	
Bacillus cereus	$>10^6$/g	Food poisoning	

Table 2.3: Main characteristics of selected commercially available test kits to detect *E. coli*

Method	Manufacturer	Technique	Testing method/Comments	Limit of detection	Reference
TRANSIA AG EIA EHEC	BioControl	Enzyme Immunoassay	Antibodies specific for EHEC antigens	NR	[246]
Assurance GDS for *E. coli* O157:H7	BioControl	Immunomagnetic Separation (IMS), PCR	Primers and antibody-coated magnetic beads	NR	[247]
Bax System *E. coli* O157:H7 real time	DuPont™	Real Time PCR	Primers	10^4 CFU/mL	[248]
Bax System *E. coli* O157:H7	DuPont™	PCR	Primers	10^5 CFU/mL	[249]
FoodChek *E. coli* O157:H7 test kit	FoodCheck Systems Inc.	Lateral flow immunoassay	antibody-coated super-paramagnetic nanoparticles in a lateral flow immunoassay format.	NR	[250]
Rapid B	Vivione Biosciences	Immunoassay + Flowcytometry	Capture by the specific antibody	NR	[251]
Reveal for *E. coli* O157:H7	Neogen®	Antibody enrichment and detection through membrane migration	Antibodies	1 CFU/25 g	[252]
3M Tecra *E. coli* O157:H7 visual	3M	Enrichment + ELISA	Antibodies	NR	[253]

NR = Not reported

Table 2.4: Main characteristics of selected commercially available test kits to detect *Listeria monocytogenes*

Method	Manufacturer	Technique	Testing method/Comments	Limit of detection	Reference
Assurance GDS for *L. monocytogenes*	BioControl	PCR, Immunomagnetic Separation (IMS)	Primers and antibody-coated magnetic beads	NR	[254]
Bax System *L. monocytogens* 24E	DuPont™	PCR	Target specific primers	10^4 CFU/mL	[255]
Bax System *L. monocytogenes*	DuPont™	Real-Time PCR	Target specific primers	NR	[256]
GeneQuence	Neogen®	DNA-hybridization microwell test	DNA probe-colorimetric detection	NR	[257]
TRANSIA PLATE *L. monocytogens*	BioControl	Sandwich ELISA	*Listeria*-specific antibody	NR	[258]
Reveal 2.0 for *Listeria*	Neogen®	Antibody enrichment and detection through membrane migration (Lateral flow)	Anti-*Listeria* antibodies are used to bind *Listeria* antigens in the sample. These complexes travel through the nitrocellulose membrane until they reach a zone that can be detected.	1-5 CFU/25 g of food	[259]

NR = Not reported

Table 2.5: Main characteristics of selected commercially available test kits to detect *Salmonella*

Method	Manufacturer	Technique	Testing method/Comments	Limit of detection	Reference
Bax System *Salmonella*	DuPont™	PCR	Target specific primers	10^5 CFU/mL	[252]
GeneQuence	Neogen®	DNA-hybridization microwell test	DNA probe-colorimetric detection	1-5 CFU/25 g of food	[260]
RapidChek Select *Salmonella*	NR	Lateral flow Immunoassay	Antibodies Color development of on the strip	NR	[261]
Reveal 2.0	Neogen®	Antibody enrichment and detection through membrane migration	Antibodies	10^6 CFU/mL	[262]
TRANSIA PLATE *Salmonella* gold	BioControl	Sandwich ELISA	Antibodies	NR	[263]
3M Tecra *Salmonella* visual immunoassay	3M	ELISA	Antibody	NR	[264]

NR = Not reported

Table 2.6: Main characteristics of selected commercially available test kits to detect *Staphylococcus aureus* and enterotoxins

Method	Manufacturer	Target	Technique	Testing method/Comments	Limit of detection	Reference
Bax System *Staphylococcus aureus*	DuPont™	*S. aureus*	Real-time PCR	Target specific primers	1-10 CFU/g of food	[265]
TRANSIA plate *Staphylococcal* Enterotoxins ID	BioControl	*Staphylococcal* enterotoxin A,B,C,D, and E	Sandwich ELISA	Antibodies	20-60 pg/mL	[266]
TRANSIA plate *Staphlococcal* Enterotoxins Plus	BioControl	*Staphylococcal* enterotoxin A,B,C1,C2,C3, D, and E	Sandwich ELISA	Antibodies	0.25 ng enterotoxins/ g of food	[267]
3M Tecra *Staph. aureus* visual immunoassay	3M	*S. aureus*	ELISA	Antibody	1-5 CFU/3g of food	[268]

Table 2.7: Main characteristics of selected commercially available test kits to detect *Campylobacter*

Method	Manufacturer	Technique	Testing method/Comments	Limit of detection	Reference
ANSR for Campylobacter	Neogen®	RT-PCR	Primer and fluorescent probe	1CFU/analytical unit	[269]
Bruker MALDI Biotyper Method	Bruker	MALDI-TOF mass spectrometry		NR	[270]
DuPont BAX® System Real-Time PCR for *Campylobacter jejuni*, and *Campylobacter lari*	DuPont™	Real-time PCR	Target specific primers	10^4 CFU/mL, after enrichment	[271]
iQ-Check *Campylobacter* Real-Time PCR	Bio-Rad	Real-Time PCR	Fluorescent probes and primers	NR	[272]
Singlepath® *Campylobacter*	Singlepath®	Lateral flow immunoassay	Gold-labelled antibodies - color development of on the strip	NR	[273]
Tadpole *Campylobacter jejuni* Real-Time PCR Identification kit	Tadpole™	RT-PCR	Primers and Taqman probe	NR	[253]
Veriflow *Campylobacter*	Veriflow®	combines PCR with chromatography	Primers and gold-protein conjugates for visual detection on nitrocellulose	NR	[274]
VIDAS® *Campylobacter* (CAM)	VIDAS®	ELFA (Enzyme-Linked Fluorescent Assay)	Antibodies	NR	[275]

3M Molecular Detection Assay 2	3M	Loop-Mediated Isothermal Amplification (LAMP)	Isothermal DNA amplification (6 primers and Bst DNA polymerase) and bioluminescence detection	1-5 CFU/ sample	[276]

NR = Not Reported

Table 2.8: Main characteristics of selected commercially available test kits to detect *Mycobacterium tuberculosis* [277]

Assay		Technique	Testing method/ Comments	Limit of Detection
T-SPOT®.TB test		ELISpot Immunoassay	Indirect measure the number of IFN-γ spot-forming cells (SFC) on ex vivo stimulation with specific antigens	1 TB-specific T cell in 250,000 PBMCs
QuantiFERON®–TB Gold In-Tube test (QFT-GIT)		Interferon-γ release assays (IGRA)-Immunoassay	Indirect ELISA-based assay that measure IFNγ secreted by MTB-specific T cells on ex vivo stimulation with specific antigens	NR
Amplified-MTD test (Gen-Probe)		Nucleic Acid detection	Transcription- mediated amplification, hybridization protection assay for Mycobacterial 16S rRNA	1 CFU per test
COBAS MTB test (Roche)		Nucleic Acid detection	Primers and probes targeting 16S rRNA gene and esx genes frrom sputum and bronchoalveolar lavage (BAL) samples	*M. tuberculosis*= 7.6-8.8 CFU/ml; *M. bovis BCG*=0.9-1 CFU/ml

NR = Not Reported

Table 2.9: Main characteristics of selected commercially available test kits to detect *Staphylococcus aureus/* MRSA [277]

Assay	Technique	Testing method/ Comments	Limit of Detection
Xpert MRSA/SA SSTI (Cepheid)	Real-time PCR	Detects DNA of Staphylococcal protein A (spa), the gene for MecA-mediated oxacillin resistance (mecA), and SCCmec inserted in the SA chromosomal attB site	*S. aureus*= 50-123 CFU/swab; MRSA= 82/242 CFU/swab
Staphylococcus QuickFISH BC (AdvanDx, Inc.)	Fluorescence In Situ Hybridization (FISH) using protein-nucleic acid (PNA) probes	Uses PNA probes hybridizing to S. aureus-specific rRNA sequences and of other Staphylococcus species isolated from blood	105 CFU/mL
BD Max MRSA Assay (BD)	Real-time PCR using probes	Direct detection of Methicillin-resistant Staphylococcus aureus (MRSA) DNA from nasal swabs	273 to 645 CFU/swab

NR = Not Reported

Table 2.10: Main characteristics of selected commercially available test kits to detect other common bacterial pathogens [277]

Bacterial Pathogen	Assay	Technique	Testing Method/ Comments	Limit of Detection
Group A *Streptococcus*	GASDirect Test (Gen-Probe)	Hybridization protection assay	Use probes for the qualitative detection of Group A Streptococcal rRNAs from throat swabs	NR
Bacillus anthracis	JBAIDS anthrax detection kit (Idaho Technology Inc.)	Real-time PCR	Primers target DNA sequences on the pXO 1 and the pXO2 plasmids from Bacillus anthracis	1,000 CFU/mL of whole blood
Yersinia pestis	JBAIDS Plague Detection Kit (BioFire Diagnostics, Inc.)	Real-time PCR	Primers and hydrolysis probes to detect *Y. pestis* DNA from whole blood/ sputum	50 CFU/mL for whole blood; 670 CFU/mL for sputum
Mycoplasma pneumoniae	Illumigene Mycoplasma Direct DNA Amplification Assay (Meridian	Loop-mediated isothermal DNA amplification (LAMP)	Targets an intracellular protease-like gene of the *Mycoplasma pneumoniae* DNA in human throat swabs	*M. pneumoniae* M129= 200CFU/ml; *M. pneumoniae* FH= 2350 CFU/ml

	Bioscience, Inc.)			
Coxiella burnetii	JBAIDS Q Fever Detection Kit (Idaho Technology, Inc.)	Real-time PCR	Detect target DNA sequence from *C. burnetii* in serum	10 median tissue culture infectious dose (TCID50)/mL
Bordetella pertussis	AmpliVue Bordetella Assay (Quidel Corporation)	Isothermal helicase-dependent amplification (HDA)	Qualitative detection of *B. pertussis* nucleic acids isolated from nasopharyngeal swab	Strain A639=3.93 CFU/assay
Chlamydia trachomatis, Neisseria gonorrhoeae and Trichomonas vaginalis	CTGCTV2 (BD)	Real-time PCR	Detection of specific bacterial DNA in vaginal swab specimens, and male and female urine specimens	*C. trachomatis*= 1.25-5 Elementary Bodies (EB)/mL ; *N. gonorrhoeae*= 15-60 Cells/mL; *T. vaginalis*= 1.88-7.5 TV/mL
Chlamydia trachomatis, Neisseria gonorrhoeae, Trichomonas vaginalis and Mycoplasma genitalium	Alinity m STI Assay (Abbott Molecular, Inc.)	Real-time PCR	Detection of *C. trachomatis, T. vaginalis and M. genitalium* rRNA sequences and *N. gonorrhea* genomic DNA sequences	*C. trachomatis*=17.0 Elementary Bodies (EB)/mL; *N. gonorrhea*= 7.5 Colony Forming Units (CFU)/mL; *T. vaginalis*= 0.1 TV/mL; *M. genitalium*= 165 Genome Equivalents (GE)/mL
Chlamydia trachomatis,	APTIMA Assay	Transcription-mediated	Targeting 23s rRNA	7.25 inclusion forming unit (IFU)/swab;

Neisseria gonorrhoeae, Trichomonas vaginalis and Mycoplasma genitalium	for *Chlamydia trachomatis* (Gen-Probe)	amplification and hybridization protection assay		5 IFU/mL urine
Enterococcus	Xpert® vanA Assay (Cepheid)	Real-time PCR	Detect the vanA gene that is frequently associated with vancomycin-resistant enterococci (VRE) obtained from rectal swab specimens	37 CFU/swab
Escherichia coli, Pseudomonas aeroginosa	*E. coli/P. aeruginosa* PNA FISH (AdvanDx Inc.)	Peptide nucleic acid fluorescence in situ hybridization assay	FISH technique using fluorescein-labeled peptide nucleic acid probes targeting rRNA	NR
Francisella tularensis	JBAIDS Tularemia Detection Kit (Idaho Technology, Inc.)	Real-time PCR using hydrolysis probes	Oligonucleotide primers and a fluorescent-labeled target assay probe that specifically detects *F. tularensis* DNA from blood and sputum	NR

NR = Not Reported

Table 2.11: List of Phage-based biosensors to detect food-borne pathogens

Method	Transducer	Bioreceptor	Target food-borne pathogen	Limit of detection	References
Optical based sensor	Surface plasma resonance	T4 Phage	*E. coli* O157:H7	10^3CFU/mL	[156]
	Surface plasma resonance	BP14 Phage	MRSA	10^3CFU/mL	[156]
	Surface plasma resonance	Lytic phage (phage 12600)	*S. aureus*	10^4CFU/mL	[278]
	Bioluminescence	*E. coli* phage	*E. coli*	10^3CFU/mL	[158]
	Bioluminescence	Felix phage or Newport phage	*Salmonella newport*	10^3CFU/mL	[158]
	Bioluminescence	phage SJ2	*Salmonella enteritidis*	10^3CFU/mL	[159]
Electrochemical based biosensor	Amperometric	B1-7064 Phage	*Bacillus cereus*	10 CFU/mL	[279]
	Amperometric combined with pre-filtration	Phage lamba	*E. coli* K12	100 CFU/mL	[162]
	Impedimetric	T4 Phage	*E. coli*	10^4CFU/mL	[280, 281]
	Impedimetric	T2 Phage	*E. coli* B	10^3CFU/mL	[234]
	Impedimetric	SATA-8505	MRSA	1.23×10^2 CFU/ml	[282]

Table 2.12: Benefits and drawbacks of various enzyme immobilization methods [197, 283]

Method	Advantages	Disadvantages
Adsorption	✓ Simple ✓ Inexpensive ✓ Low enzyme loading is required ✓ Mild procedure ✓ Non -destructive technique ✓ Loss of enzyme activity is negligible	✓ Enzyme leakage takes place ✓ Insensitive ✓ Enzyme linkages are highly dependent on pH, temperature, and solvent
Entrapment	✓ Universal for any enzyme ✓ Mild procedure ✓ Low enzyme loading	✓ Large diffusional barriers ✓ Loss of enzyme activity by leakage ✓ Some enzyme loss
Covalent bonding	✓ High stability ✓ Absence of diffusion barriers ✓ Leakage of the enzyme is very unlikely ✓ Ideal for commercialization ✓ Low response time	✓ Expensive ✓ Low reproducibility ✓ Loss of enzyme activity is significant ✓ High enzyme loading ✓ Complicated and time-consuming process
Cross-linking	✓ Inexpensive ✓ Simple procedure ✓ Widely used in physiologically adsorbed enzymes or Proteins	✓ High enzyme loading ✓ Higher enzyme activity loss ✓ Relatively low enzyme activity

(a)

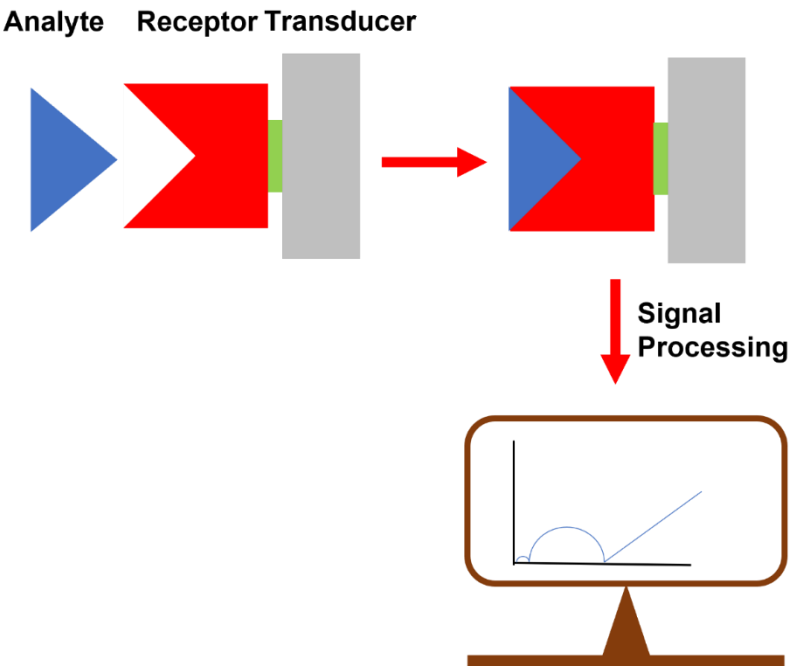

(b)

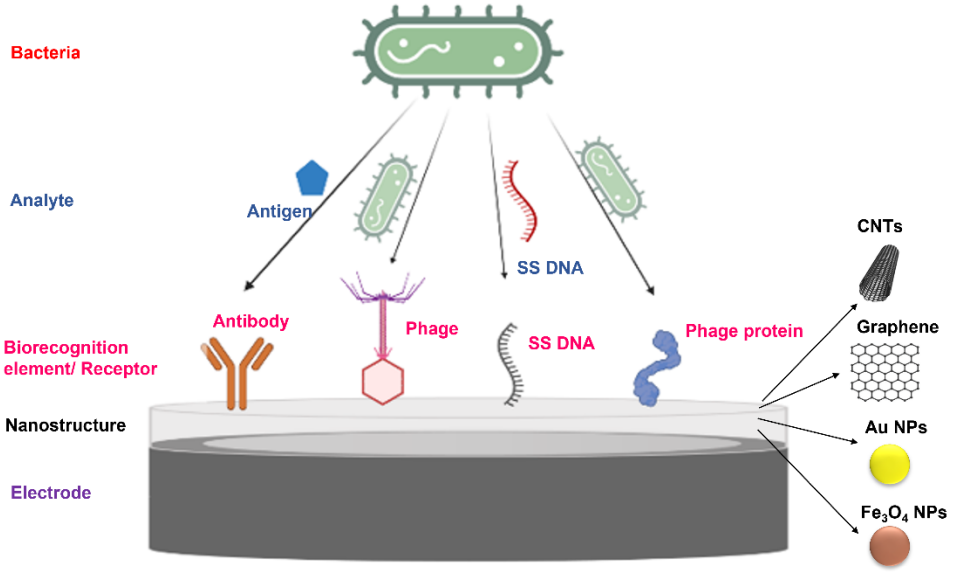

Figure 2.1: Main components of a biosensor. Schematic diagram of the biosensor (a) Structure of the biosensor for bacterial detection (b).

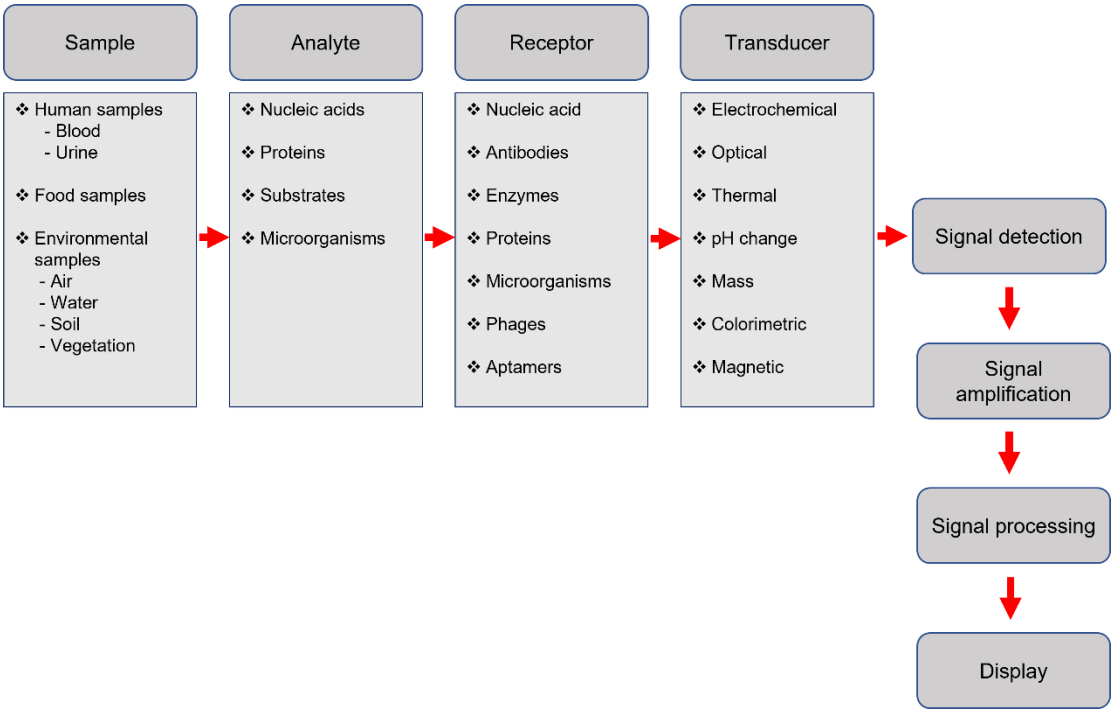

Figure 2.2: Different types of biosensors

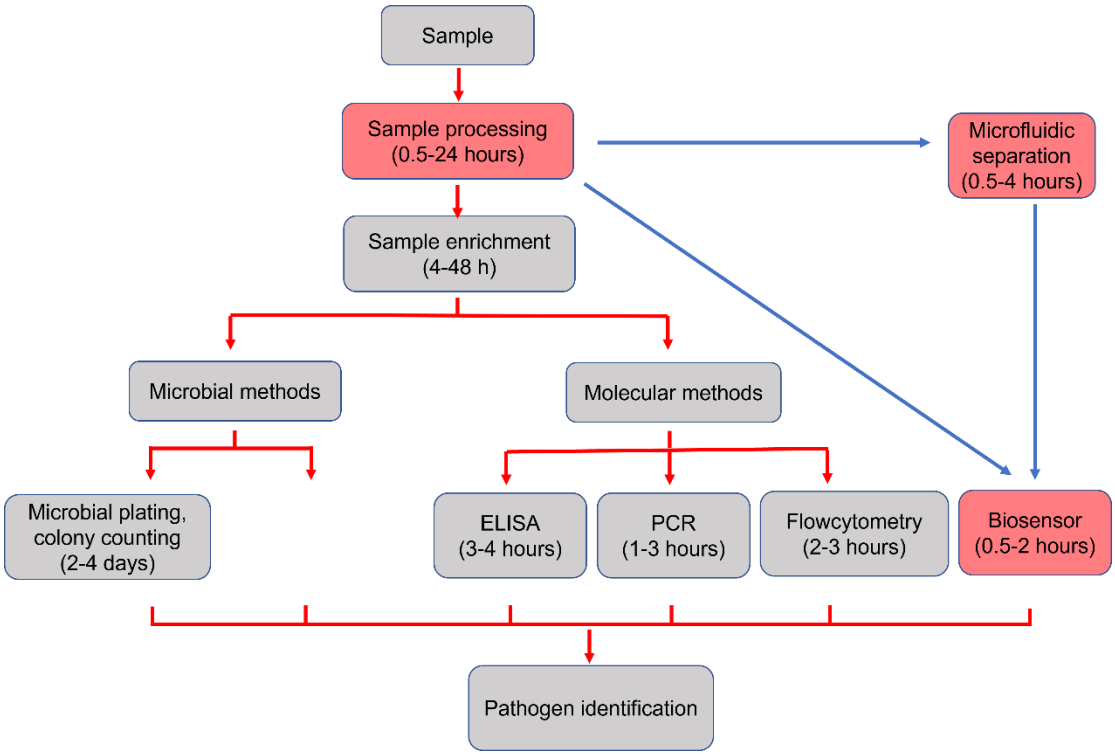

Figure 2.3: Schematic representation of the methods used for the bacterial detection

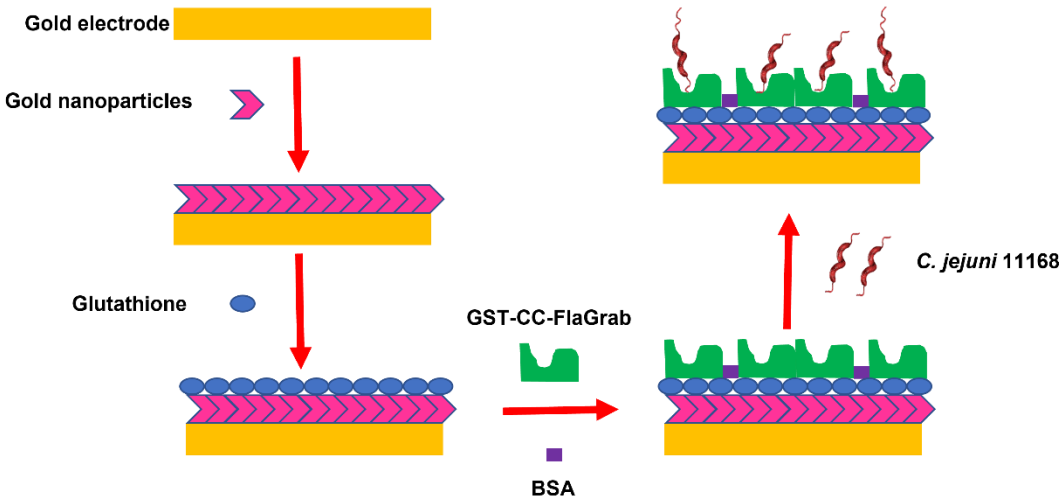

Figure 2.4: Immobilization of GST-CC-FlaGrab on a gold nanostructured electrode

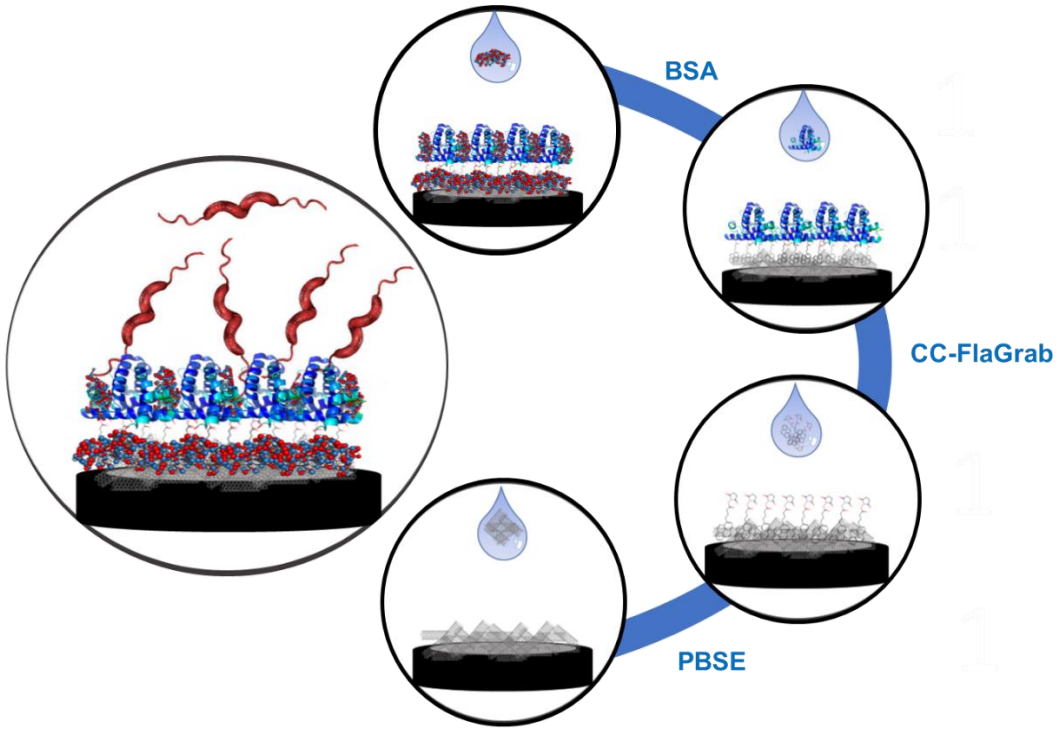

Figure 2.5: Immobilization of GST-CC-FlaGrab on a carbon nanostructured electrode

CHAPTER 3

P100 PHAGE AS A BIORECEPTOR TO DETECT *LISTERIA MONOCYTOGENES* BACTERIAL CELLS

This chapter contains text from the following publication:

Or Zolti*, Bavithithira Suganthan*, Ryan Maynard, Hamid Asadi, Jason Locklin, and Ramaraja P. Ramasamy

*Equal Contribution

Journal of The Electrochemical Society 169 (6), 2022

Abstract

Electrochemical biosensors are good alternatives to molecular detection methods due to their ease of use, high specificity, sensitivity, and low cost. Bacteriophages can serve as excellent biorecognition elements in biosensors due to their robust stability in a range of environmental conditions and their ability to distinguish between live and dead bacterial cells. Here, as a proof of concept for a electrochemical biosensor we report a potentially disruptive rapid diagnostic method based on electrochemical biosensing principles that use bacteriophages as bioreceptors for selective identification and quantification of *Listeria monocytogenes L. monocytogenes* is a common foodborne pathogen that has been responsible for many foodborne illness outbreaks in recent years. *Listeria* contamination in food products is identified only through molecular tests conducted in diagnostic laboratories. No established phage-based diagnostic methods for *L. monocytogenes* during food production or processing are used. The impedimetric biosensing architecture for *L. monocytogenes* detection was developed by immobilizing P100 bacteriophage onto quarternized polyethylenimine-modified carbon nanotubes using an in-house developed molecular tethering method. The resulting sensor showed high selectivity and sensitivity toward *L. monocytogenes* with a limit of detection of 8.4 CFU/mL. Initial results demonstrate that the biosensing architecture is highly reliable in its selectivity towards its target analyte, *L. monocytogenes*.

Key words: Biosensors, Food Safety, *Listeria monocytogenes*, Bacteriophage, Electrochemistry, Carbon nanotubes.

3.1. Introduction

Foodborne pathogens are becoming increasingly problematic worldwide due to increased hospitalization, mortality, and food-related financial cost. Among foodborne pathogens, *Salmonella* spp., *Escherichia coli* O157:H7, and *L. monocytogenes* are very commonly found in fresh produce, eggs, deli meats, ready to eat food products, soil, foliage, water, mud, and silage [284-286]. The FoodNet surveillance reports show that *L. monocytogenes* is the highest cause of hospitalization, at 93 % of confirmed infection cases, and death at 17 % of these cases, according to studies conducted over ten years between 2006 to 2015 [287]. *L. monocytogenes* can multiply at temperatures as low as 4 ^{o}C and survive in freezing temperatures as low as -18 ^{o}C. *L. monocytogenes* causes a severe illness called listeriosis that is life-threatening, especially for pregnant women, newborns, babies, the elderly, and immunocompromised patients. Therefore, it is essential to develop accurate and robust detection methods for the bacteria present in the food samples as early as possible in food production and supply [288].

The prevailing gold standard for foodborne pathogens detection is culture-based methods. Samples are taken at specific control points during the manufacturing and distribution process, cultivated on a nutrient-filled medium, plated, and tested with visual, biochemical, and immunological means before and after enrichment. Although very accurate, this method is not ideal due to the long processing time, sample transportation, robustness, and expensive skilled labor and equipment [289-293]. To overcome these shortcomings, the industry needs a faster and cost-efficient detection method with similar or even better sensitivity to comply with modern food and safety standards [294-296]. These concerns have encouraged researchers to improve current methods and develop new analytical

methods. The target sensitivity standard is currently coming from PCR testing, with an average limit of detection (LOD) of 100 CFU/mL depending on the buffer and the gene used for amplification [297, 298]. Electrochemical biosensing has emerged as a viable method for this application with its simple signal generation instrument, fast detection time, and very high sensitivity. Its simplicity allows anyone with basic training to operate such a sensor and still obtain reliable results. Their quick detection time makes electrochemical biosensors compatible with food industry demands, and high sensitivity enables the user to adhere to regulatory agency guidelines without risking mass recalls [299]. An electrochemical biosensor consists of an electrochemical transducer (electrode) with a bio-recognition element immobilized on its surface. Commonly used biorecognition elements are DNA/RNA, oligonucleotides, aptamers, enzymes, antibodies, or bacteriophages. Bacteriophages possess certain advantages over other types of bio-recognition elements due to their robust stability in non-ideal environmental conditions such as temperature, pH, and humidity and their ability to distinguish between live and dead bacterial cells. Bacteriophages are relatively inexpensive, easy to handle, ubiquitous in nature, and can be prepared and maintained using simple procedures [300]. The literature reported the use of phage peptides, enzymes, and proteins to detect *L. monocytogenes*. Still, the whole phage was not used to detect *L. monocytogenes* electrochemically [301-305]. The low number of publications involving the use of bacteriophage as a biorecognition element suggests they have not yet been fully explored, increasing the interest in exploring it further.

The orientation of the phage upon immobilization on the transducer's surface significantly increases its effectivity in capturing its target bacteria [306]. Bacteriophage P100 belongs to the *Caudovirales* order and the *Herelleviridae* family with a negatively-charged capsid

and a positively-charged contractile tail that consists of the capturing protein [307, 308]. Due to this structured dipole, by creating a positively charged surface, it is possible to control the orientation of the P100 phage and ensure that its capsid proteins are positioned to capture the target bacteria. This orientated immobilization method has already been demonstrated in our previous work using the myoviridae family of bacteriophages on polyethylenimine functionalized carbon nanotubes (PEI-CNT) electrodes for the capture of *E. coli* and *Staphylococcus aureus* cells [282, 306, 309, 310]. To increase the transducer's surface positive charge for the orientation of phage during immobilization, a quarternization of the amine groups in the PEI molecules could be used, as it has been reported to possess a good yield [311, 312]. The quarternized amines possess a high positive charge and can improve phage orientation on the carbon nanotube electrode for bacterial cell capture.

This paper presents our work on developing an electrochemical biosensor to detect *L. monocytogenes* using P100 phage as the biorecognition molecule. The biosensor architecture was made of a nanostructured carbon nanotube-based electrode, on which P100 phages were immobilized as recognition molecules (bioreceptors). The carbon nanotubes were functionalized with quarternized polyethylenimine-modified CNT (q-CNT) to aid in a charge-directed oriented immobilization of phages on the electrode to enable selection detection of *L. monocytogenes*.

3.2. Experimental

3.2.1. Materials

Acid-treated multiwalled carbon nanotubes (COOH-functionalized multiwalled CNTs) with an outer diameter of 30-50 nm and length of 10-20 μm were purchased from Cheap Tubes Inc., 0.05-micron type N gamma alumina powder (alumina polishing powder) was purchased from Electron Microscopy Sciences. Polyethylenimine, potassium bromide (KBr), 1-pyrenebutanoic acid succinimidyl ester (PBSE), bovine serum albumin (BSA), and glutaraldehyde (all five from Sigma-Aldrich), disodium phosphate (Na_2HPO_4) (Research Products International Corp), sodium chloride (NaCl) (EMD chemicals), magnesium sulfate heptahydrate [($MgSO_4.7H_2O$ (J.T. Baker)], thionyl chloride ($SOCl_2$) and iodomethane (CH_3I) (both from Alfa Aesar), potassium phosphate dibasic (KH_2PO_4) and potassium chloride (both from BDH), tris base, typtone, and ethanol (all three from Fisher scientific), yeast extract and agar powder (both from Becton Dickinson and Company), methylene chloride (DCM) (VWR) were purchased and used as received.

Phosphate-buffered saline (PBS, 10X) (100 mL) was prepared by mixing 0.2 g of KCl, 8 g of NaCl, 0.245 g of KH_2PO_4, and 1.4 g of Na_2HPO_4. PBS (1X) (pH 7.4) was prepared by diluting the 10X PBS buffer. Luria Bertani (LB) (100 mL) (pH 7.0) was prepared by mixing 1 g of tryptone, 0.5 g of yeast extract, and 1 g of NaCl. SM buffer (pH 7.5) was prepared by mixing 100 mM NaCl, 8 mM $MgSO_4$. $7H_2O$, 50 mM Tris base, and 0.01 % Gelatin. Standard Brain Heart Infusion (BHI) media was prepared according to the instructions on the bottle. Milli-Q water (resistivity =18 MΩ.cm) was used to prepare all the media and chemicals. All buffers and media are sterilized before use. Electrodes were purchased from

CH Instruments, Inc. Glassy carbon (part number CHI104), screen printed electrode (Zensor), platinum wire (part number CHI115), and Ag/AgCl (part number CHI111) were used as working, counter, and reference electrodes

3.2.2. Methods

Microbiological Methods

Listeria monocytogenes Scott A, a pathogenic strain, was used as the target analyte, whereas *Salmonella enterica* subsp. *Enterica* serovar Typhimurium 291RH (ser. Typhimurium-291RH) and *Escherichia coli* O157:H7 (*E. coli* O157:H7) were used as the non-target analytes. Listex P100 bacteriophage (P100 Phage) was purchased from Micreos Food Safety B.V. *L. monocytogenes* Scott A was grown by inoculating a single colony in 3 mL of BHI media and incubated at 37 ^{o}C for 24 hours at 200 rpm. A 500 µL aliquot of the overnight culture was inoculated in 50 mL of fresh BHI medium and incubated at 37 ^{o}C for about 5 hours in an incubator shaker until it reached the mid-log phase. In this study, ser. Typhimurium-291RH and *E. coli* O157:H7 are used as the non-target analyte and grown by the same method, with the use of LB media for *E. coli* O157:H7 strain as the only difference made. One milliliter of the mid-log phase bacterial culture was centrifuged at 5000 rpm for 8 min. The supernatant was removed and washed twice with 1X PBS buffer to remove any media residue, and finally, the pellet was resuspended in 1X PBS buffer. Then, dilution series was prepared. Enumeration of bacteria was performed by plate-count techniques and expressed in CFU/mL. Plaque assay was carried out with P100 phage and *L. monocytogenes* to measure the phage titer and was expressed in PFU/mL. A soft agar

overlay technique was carried out to evaluate the specificity of the P100 phage. The soft agar overlay technique was carried out with the target (*L. monocytogenes*) and non-target bacteria (ser. Typhimurium-291RH and *E. coli* O157:H7) with the presence and absence of P100 phage.

Quaternization of PEI-f-CNT

The first step was to convert the commercially available COOH-functionalized multi-walled CNTs into PEI-CNT using the procedure described in our previous work [306]. For this, 2 mg of COOH-functionalized CNTs were dispersed in 1 mL of dimethylformamide and sonicated for 5 minutes. 6 mL of $SOCl_2$ was added to the suspension to acylate the carboxylic acid, and the $SOCl_2$ acylated the carboxylic group. The suspension was refluxed for 24 hours with constant stirring under 120 ^oC. The suspension was centrifuged at 10000 rpm for 8 minutes following the reflux to form a pellet. The pellet was washed with anhydrous tetrahydrofuran (THF) and dried at room temperature under vacuum for 2 hours. 5 mL dimethylformamide (DMF) was used to resuspend the pellet and then stirred in an N_2 environment at 90 ^oC. 100 mg of PEI was then added and reacted for three days. It was then centrifuged at 10000 rpm for 8 minutes, washed with methanol, and dried at a temperature of 70 ^oC. The second step was to quarternize the amine groups in the PEI functional group. Iodomethane was used to quarternize the PEI functional group, as schematically shown in Figure 3.1 (a). For this purpose, 8 mg of PEI-CNT powder was added to a 5 mL round bottom flask. 2 mL of methylene chloride was added to the flask using a micropipette. 20 wt% of iodomethane was pipetted into the flask, sealed by a septum, and vented using a 23G needle. The heterogeneous mixture was then stirred at

room temperature for three days before the solvent and excess reactant was evaporated with gentle heating over one hour. The quarternized product (q-CNT) was analyzed using a Nicolet 6700 FT-IR spectrometer to verify the quarternization of the amine groups and the surface potential of the different modification steps (e.g., COOH-CNT, PEI-CNT, q-CNT, and the P100 phage), all samples were suspended in deionized water and were measured using by ZetaSizer (Malvern) to confirm the increase in positive charge. The q-CNT dispersion was made by suspending the product in deionized water at a 1 mg/mL ratio and sonicated for an hour using an ultrasonic homogenizer (Omni International, SONICRAPTOR 250).

Electrode Preparation

A glassy carbon electrode was polished with alumina polishing powder on a polishing pad, followed by sonication in deionized water in a sonication bath for 5 minutes, and dried in an oven for 1 hour at 70 ^{o}C. Once the electrode dried, 16 µL of the q-CNT solution was drop cast onto a glassy carbon electrode and then dried in an oven at 70 ^{o}C, as shown in Figure 3.2 (a). Before phage attachment, the q-CNT-modified electrode was activated using 1-pyrenebutanoic acid succinimidyl ester (PBSE) as a molecular tethering agent. The PBSE molecular structure is shown in Figure S1 in the supplementary material. The modified GCE was placed in an ice container, and four microliters of 10 mM PBSE solution (in DMF) were drop-cast onto it and reacted for 15 minutes. Excess PBSE was rinsed using DMF, and finally, the electrode was washed twice with 1X PBS prior to phage attachment. An electric field-induced phage immobilization method [282, 309, 310] was developed and demonstrated previously in our group to attach phages to the modified GCE electrode.

P100 phages contain negatively charged capsids and positively charged tail fibers. The strong positive charge on the q-CNT and electric field-induced immobilization created an oriented phage layer chemically anchored to the surface by applying a potential 0.5 V between the working and counter electrodes for 2 hours [306]. After immobilization, the electrode was rinsed twice with SM buffer and washed with 1X PBS buffer. Following the wash, 6 µL of 0.01 % BSA solution was deposited on the electrode to block areas that might not have been completely modified for 30 minutes. The signal measured with and without the surface blocking agent is shown in the supplementary information Figures S2-S4. Finally, the electrode was incubated in 1X PBS for 15 minutes before using in electrochemical experiments.

Electrochemical Impedance Measurements

The bacterial solution (50µL) was drop cast on the working electrode and incubated for 8 minutes before the measurement. The impedimetric characterization was carried out using the CHI-920C model potentiostat (CH Instruments Inc., Austin, TX). The electrochemical system was a standard 3-electrode cell using a glassy carbon working electrode (GCE) (CH Instruments Inc., Austin, TX), Ag/AgCl reference electrode. The counter electrode was a Pt wire. Electrochemical impedance spectroscopy (EIS) measurements were done in 5 mM $[Fe(CN)_6]^{4-}/[Fe(CN)_6]^{3-}$ as redox couple, with a frequency range of 1 Hz to 100 kHz with an AC amplitude of 5 mV. The resulting measurement is presented as ΔR_{CT} (ohm) or ΔR_{CT} (%) where:

$$\Delta R_{CT}\ (\%) = \frac{R_{CT,measured} - R_{CT,baseline}}{R_{CT,baseline}} \times 100\ \% \quad (1)$$

$$\Delta R_{CT}\ (ohm)\ =\ (R_{CT,measured}\ -\ R_{CT,baseline}) \quad (2)$$

All measurements were done at room temperature under standard conditions.

Electrode Preparation for Scanning Electron Microscope (SEM) Images

Morphological characterization of the prepared electrode after exposure to the target and non-target bacterial cells was done with an SEM scanning electron microscope (SEM, FEI Teneo, FEI Co.). A screen-printed electrode was modified with P100 phage, as described before. Target and non-target bacteria were incubated for 8 minutes on the electrode, followed by fixing them to the electrode with 3 % glutaraldehyde solution overnight. Once fixed, the electrodes were dehydrated using increasing concentrations of ethanol for 10-20 min each (50, 60, 70, 80, 90, and 100 %). The electrodes were then sputter-coated (Leica sputter coater) in 10 nm thickness of Au-Pd for SEM imaging.

3.3. Results and Discussion

Quaternization of PEI-CNT

An FTIR absorption spectra were obtained and analyzed for the peaks corresponding to the desired functional groups after each step of the CNT modification process, shown in Figure 1 (a). The spectra for COOH modified, PEI modified, and quarternized CNT is shown in Figure 3.1 (b). The bands pointing to the successful PEI modification on the CNT were confirmed by the formation of a C-N stretching band at wavelengths: 1020 cm^{-1}, 1170 cm^{-1}, and 1620 cm^{-1}. A second confirmation was obtained from the C=O stretching band at 1700 cm^{-1}, which became more pronounced as the modification process advanced. The quaternization of CNT following the second step of the modification was confirmed by the

band that appeared at 2040 cm^{-1}, as shown in Figure 3.1 (b), which points to the formation of quaternary ammonium ion [313].

The modified q-CNT were analyzed for their surface charges using zeta potential measurements for a secondary confirmation of the quaternization process, resulting in a high positive charge. As shown in Table 3.1, the zeta potential in 1X PBS (pH 7.4) results show a positive charge after PEI modification due to the oxygen electronegativity that created a localized positive charge at the succinimidyl functional group. After quarternization, the zeta potential of the CNT increased an additional 46 %, which corresponds to the transformation of the amine groups on the PEI-CNT, confirming the successful quarternization step of PEI-CNT and the formation of quaternary amines. The negative zeta potential from the P100 phage suggests that a positive electric potential should be used for charge-directed immobilization on the q-CNTs, as demonstrated by us in previous work [282, 309, 310].

Impedimetric Response of Biosensor

The phage-modified electrode architecture was optimized for its phage and carbon nanotube loading. Immobilization procedures were also optimized to allow the biosensor to accurately detect *L. monocytogenes*. The biosensor was tested using electrochemical impedance spectroscopy using 5 mM $[Fe(CN)_6]^{4-}/[Fe(CN)_6]^{3-}$ as a redox couple. The Nyquist plots in Figure 3.2 (b) show the electrochemical impedance responses of the modified electrode biosensor before and after phage immobilization on the CNT-modified electrode. A significant increase in the charge transfer resistance (R_{CT}), as observed by the magnitude of the semicircle, can be observed upon immobilization of the phage. This is

expected as an insulating layer of phage covers the conductive forest of the CNT interface on the electrode, which significantly decreases the charge transfer kinetics. The addition of BSA molecules as surface blockers (using 0.01 % BSA solution) further increased the R_{CT}. The BSA surface blockers aid in minimizing the non-specific binding of components other than the P100 phage on the electrode to reduce the R_{CT} value from non-target pathogens. The R_{CT} also noticeably increased upon introducing the target pathogen *L. monocytogenes* on the surface, even at low concentrations (10^2 CFU/mL).

Detection of L. monocytogenes

The impedimetric biosensing response of the phage-modified electrode was tested at different concentrations of the *L. monocytogenes* in the sample ranging from 1 CFU/mL to 10^8 CFU/mL; the results are shown in Figure 3 (a). For comparison, the R_{CT} response of the biosensor in the absence of *L. monocytogenes* was also obtained. The responses originated from the same starting point in the high-frequency region; however, at increasing concentrations of bacteria, the magnitude of the semicircle increased with the bacteria (analyte) concentration. The Nyquist response was fitted with a Randles equivalent circuit [shown as an inset in Figure 3 (a)] as reported before, to determine the values of the constant phase element (CPE1), the diffusional resistance element (the Warburg impedance, W1), the ionic solution's ohmic (R_{ohm}) resistance, and the electrode's charge transfer (R_{CT}) resistance. A calibration curve between charge transfer resistance and the analyte concentration was generated from the R_{CT} data and plotted in Figure 3 (b). The calibration curve shows a near-linear range of reliable detection between 10^0 and 10^5 CFU/mL, beyond which the signal reaches a plateau, as seen in the inset.

Limit of detection was calculated using three different methods based on triplicates measurements. The limit of detection was estimated using the following expressions (Regression analysis)[314]:

$$SD = SE \times \sqrt{n} \quad (3)$$

$$LOD = 3.3 \times \left(\frac{SD}{s}\right) \quad (4)$$

Where *SD* is the standard deviation of the intercept, *SE* is the standard error of the intercept, *n* is the number of points used for the linear fit, and s is the slope of the linear fit. The LOD of the phage-modified biosensor for *L. monocytogenes* was calculated to be 8.4 CFU/mL. It is about two orders of magnitude lower than molecular-based methods and exceeds the commonly used standards of detection limits [315]. LOD was calculated based on the three sigma (3σ) method as a second method. According to Figure 3.3c, the value for the 3σ was 40.581(1σ was 13.527). So, values less than or equal to 40.581 was considered noise. Therefore, according to Figure 3.3b, the lowest concentration of *L. monocytogenes* that could detect without noise was 10 CFU/ mL. As a third method, LOD was calculated based on the lowest concentration of the *L. monocytogenes* was able to detect by our developed sensor. According to Figure 3.3b, the concentration of the *L. monocytogenes* used for the experiment was 10 CFU/mL. Therefore, LOD was 10 CFU/mL [157].

In all three methods, the LOD for our phage based biosensor was 10 CFU/mL or very closer to 10 CFU/mL.

Role of Phage as Biorecognition Element:

The role of the P100 phage as the biorecognition element for detecting the target *L. monocytogenes* is evident from the differences in the impedimetric signals arising from the phage-immobilized electrode when compared to an electrode that does not contain phage as seen in Figure 3.4 (a). The R_{CT} measured by the biosensor is significantly higher when phage is present on the surface. The numerical values as the distance from the measured baseline are shown in Figure 3.4 (b), with the absolute measured R_{CT} values displayed above the bars. This is expected as the phage plays a key role in capturing and attaching *L. monocytogenes* cells onto the electrode, which increases the interfacial impedance, resulting in a higher charge transfer resistance value. In comparison, the electrodes with no phage have a far less selective attachment of *L. monocytogenes* cells onto the electrode resulting in a lower interfacial impedance value. It can also be noticed that the difference is more pronounced at higher concentrations of bacteria. The results indicate that the phage plays a key role in aiding the selective attachment of *L. monocytogenes* to the electrode and as a signal enhancer for quantitative detection.

Specificity of the Biosensor:

The specificity of the P100 phage was evaluated using non-target bacterial analytes. SEM images of a modified electrode after exposure to *L. monocytogenes*, ser. Typhimurium-291RH, or *E. coli* O157:H7 were taken. In addition, a soft agar overlay technique was used with the same bacteria in the presence of the P100 phage. An SEM image of the electrode after exposure to *L. monocytogenes* is shown in Figure 3.5 (a); the yellow arrows point to the bacterial cells captured by the P100 phage attached to the surface. Figure 3.5 (b) shows

a plate clear of bacterial colonies after exposure to the phage. The yellow arrow indicates that the other side of the petri dish is visible through the semi-transparent media. s 3.5 (c) and (e) show the electrode surface after exposure to ser. Typhimurium-291RH and *E. coli* O157:H7, respectively. As expected, no bacterial cells were visible on the electrode surface. The specificity was confirmed by the soft agar overlay with either bacteria, as seen in s 3.5 (d) and (f). Both plates were covered entirely with colonies and formed a non-transparent layer, and no plaques appeared. The spherical structures in Figure 3.5 (a), Figure 3.5 (c), and Figure 3.5 (e) show the BSA molecules on the electrode surface.

The EIS measurements revealed similar results with respect to the specificity of the P100 phage towards *L. monocytogenes* detection, as shown in

Figure **3.6** (a). For phage-modified electrodes, the Nyquist plots show only a small variation in the ΔR_{CT} (%) from their baseline value for the non-target pathogens (ser. Typhimurium-291RH 7 %, *E. coli* O157:H7 17 %). In contrast, a significant variation (43 %) in ΔR_{CT} (%) was observed for *L. monocytogenes*. Moreover, in the absence of phage, the electrode exhibited the lowest R_{CT} change from the baseline for *L. monocytogenes* (10 %) compared to non-target pathogens (ser. Typhimurium-291RH 19 %, *E. coli* O157:H7 36 %) as seen in

Figure **3.6** (b), which contributes to the non-target R_{CT} signal. The results demonstrate that phage provides the specificity needed for *L. monocytogenes* detection. However, the specificity could be improved by minimizing the non-specific attachment of non-target pathogens on the electrode surface by exploring other surface-blocking molecules or the inclusion of biocide to deter non-target bacterial cells. The scale and intensity of those experiments are beyond the scope of this work.

Stability Studies

The electrochemical stability of the biosensor was evaluated after electrode preparation. Phage immobilized eight different electrodes were stored at 4 ^{o}C in 1X PBS solution for one hour, day, week, and two weeks. After each period, a detection experiment with 100 CFU/mL of *L. monocytogenes* was performed. Each period was tested in duplicates, and the measurement error was calculated for each one. The R_{CT} value was measured, and the ΔR_{CT} *(%)* was calculated with respect to the response after one hour. Figure 3.7 shows that the biosensor's responses were stable after 24 hours, with only a 10 % drop in signal and an error margin of ± 2 %. After a week, the reduction in the signal was 30 % with respect to the response obtained an hour after preparation, but the response was stable with an error of ±1 %. The low error value suggests that the sensor performance is repeatable after one week. After two weeks, the reduction in the signal was 70 %, and the error increased to ±7 %. It is clear that after two weeks, there is a degradation of the phage's activity and that the signals are very low; the high error suggests that they are also less accurate beyond two weeks.

3.4. Conclusions

An ultra-sensitive and selective sensor for *L. monocytogenes* was developed and tested The sensor could selectively detect the target bacteria with a LOD of 8.4 CFU/mL. This value is below the current commonly used PCR standards, although demonstrated only in laboratory buffer samples. The biorecognition element, P100 phage, exhibits desirable selectivity towards *L. monocytogenes*, although more work should be done on non-selective binding between the electrode and other non-target analytes. This is the scope of

future work where suitable surface-blocking agents will be employed to minimize non-specific binding and the accuracy of *L. monocytogenes* detection by the sensor architecture. The novel quaternization of the PEI-CNT has made their surface much more suitable for oriented phage deposition, which was critical in achieving high selectivity and sensitivity. The biosensor was shown to be stable for up to a week after phage attachment with a signal that is 70 % of the one achieved one hour after preparation. The biosensor, under optimal conditions, gave a linear response from 10 to 10^4 CFU/mL, with good reproducibility and stability. These characteristics make it a promising method for industrial and private food monitoring detection of foodborne pathogens. Our future work would involve testing the biosensor with food samples to investigate and quantify the performance of the sensing architecture in simulated food samples.

3.5. Acknowledgments

L. monocytogenes Scott A *strain*, *E. coli* O157:H7, and ser. Typhimurium-291RH were kindly provided by Dr. Francisco Diez-Gonzalez (University of Georgia, Griffin), Dr. Christine Szymanski, and Dr. Nikki Shariat (University of Georgia, Athens), respectively. Funding for this work was provided by The Center for Food Safety, The University of Georgia.

Table 3.1: Surface charge measurements of the phage and the different stages of CNT modification

	Zeta potential
COOH-CNT	$-31.3 \pm 0.4\ [mV]$
PEI-CNT	$31.7 \pm 0.8\ [mV]$
q-CNT	$46.3 \pm 0.8\ [mV]$
P100 Phage	$-9.7 \pm 0.7\ [mV]$

.

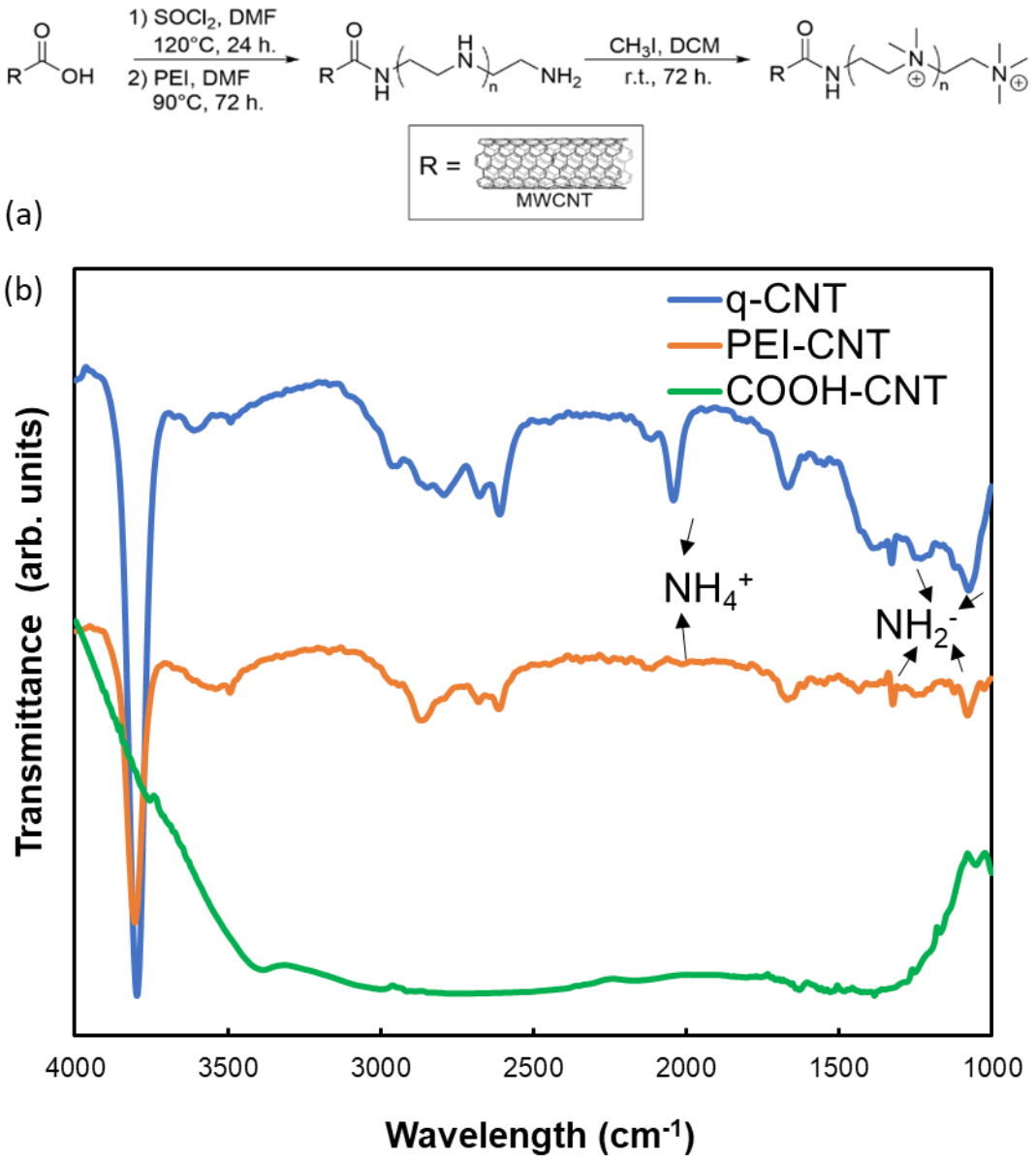

Figure 3.1: (a) Quaternization of CNT for phage immobilization and (b) FTIR spectrum of CNT after different steps during modification.

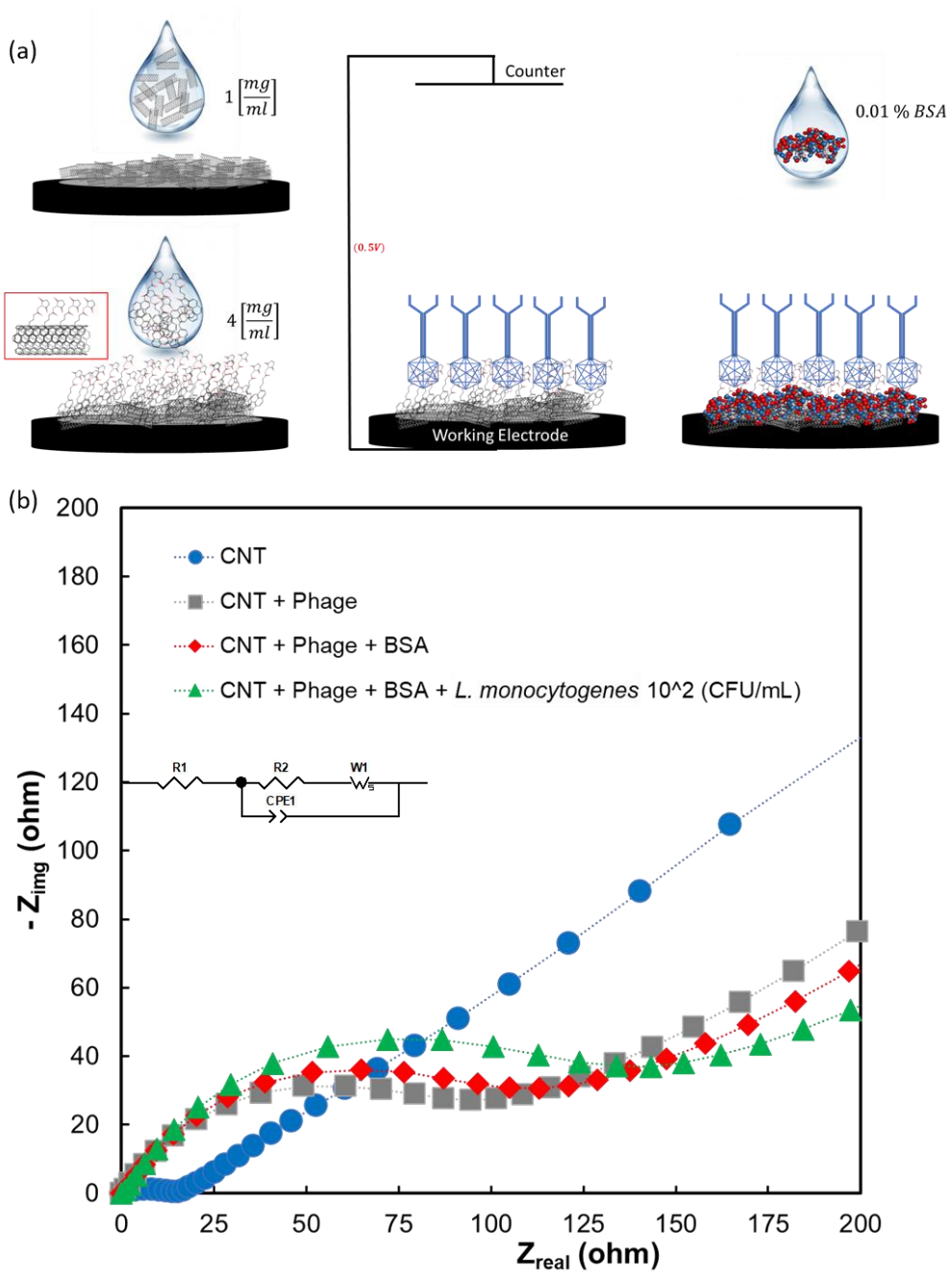

Figure 3.2: (a) Electrode preparation steps including drop-cast deposition of q-CNT on the electrode followed by PBSE crosslinker deposition and electric-field induced P100 phage immobilization and finally deposition of 0.01 % BSA as a surface blocking agent and (b) Nyquist plot of the electrode after each step of the electrode preparation process.

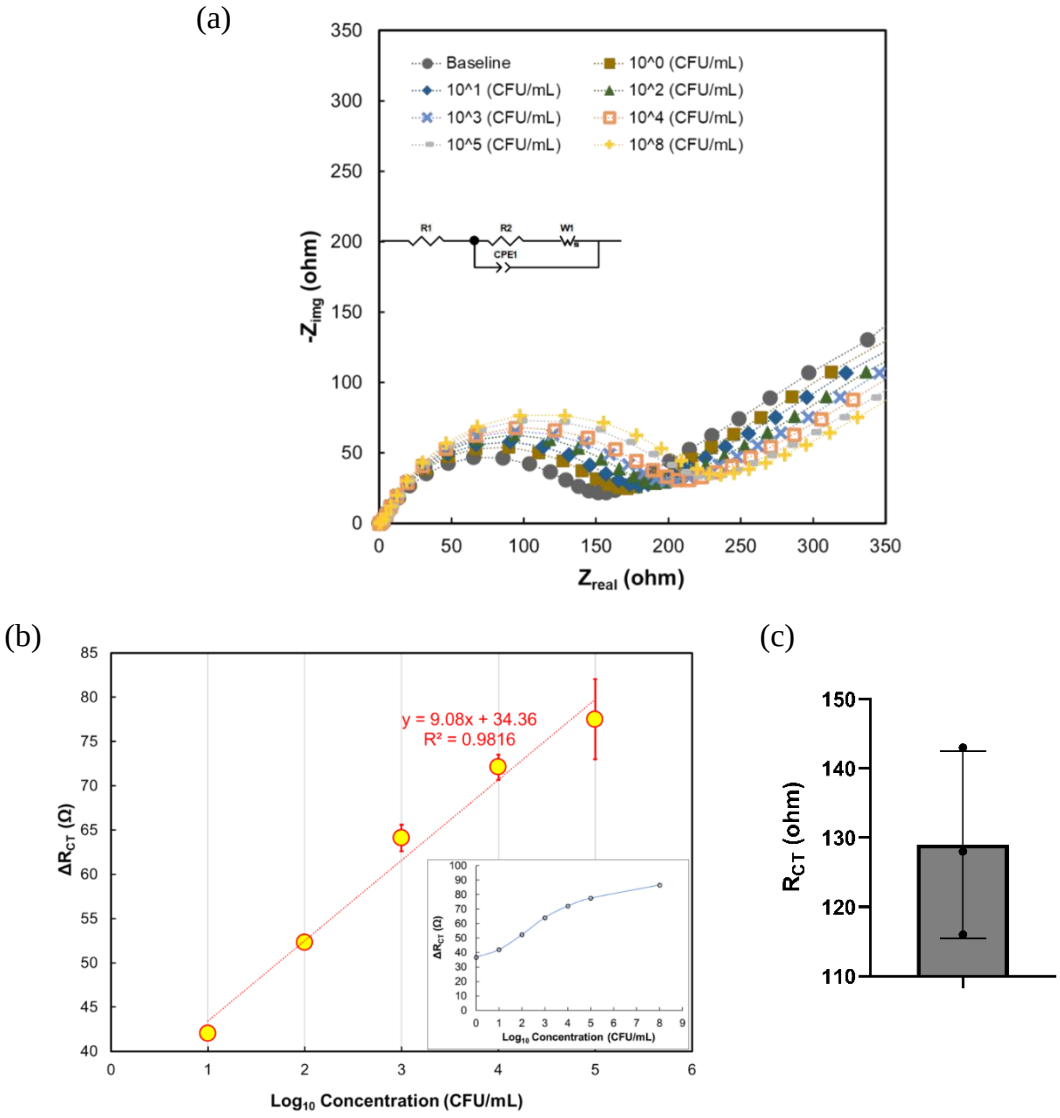

Figure 3.3: (a) Nyquist plots show biosensor's impedance response to varying concentrations of the target analyte, *L. monocytogenes*. The equivalent electrical circuit used for fitting the Nyquist data is given in the inset. (b) Calibration curve showing a linear relationship between the differential charge transfer resistance ΔR_{CT} (ohm) and the logarithmic of bacterial concentration. The full concentration range of the calibration curve is given in the inset. (c) Bar chart shows the R_{CT} values of the baseline of the replicates. In this Bar chart 1 SD is 13.157.

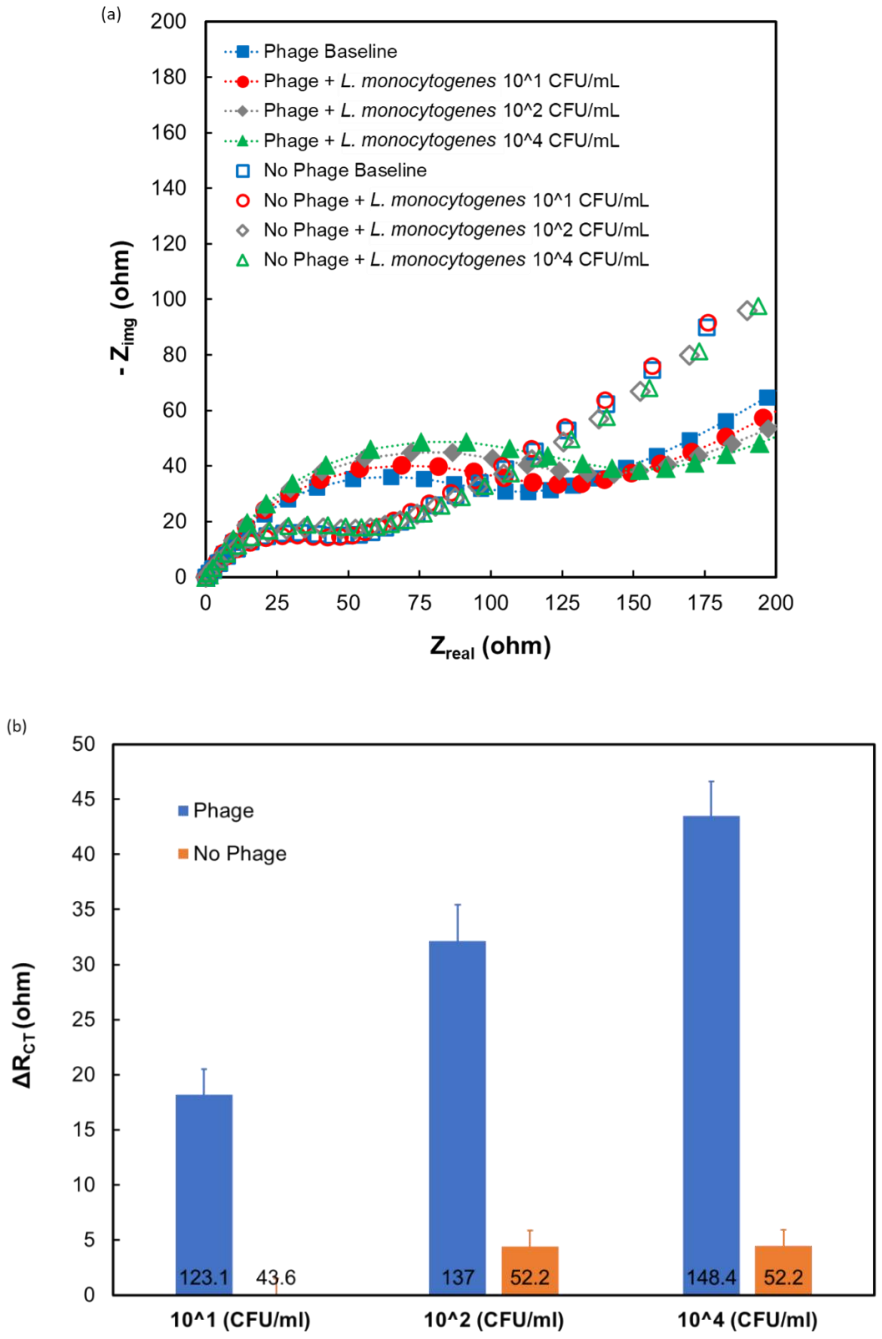

Figure 3.4: Impedance response of the biosensor to target *L. monocytogenes*: (a) Nyquist plot of the impedimetric response to *L. monocytogenes* with (full shapes) and without (hollow shapes) P100 phage and (b) ΔR_{CT} (ohm) values with and without phage expressed as the difference from baseline impedance values with no bacteria.

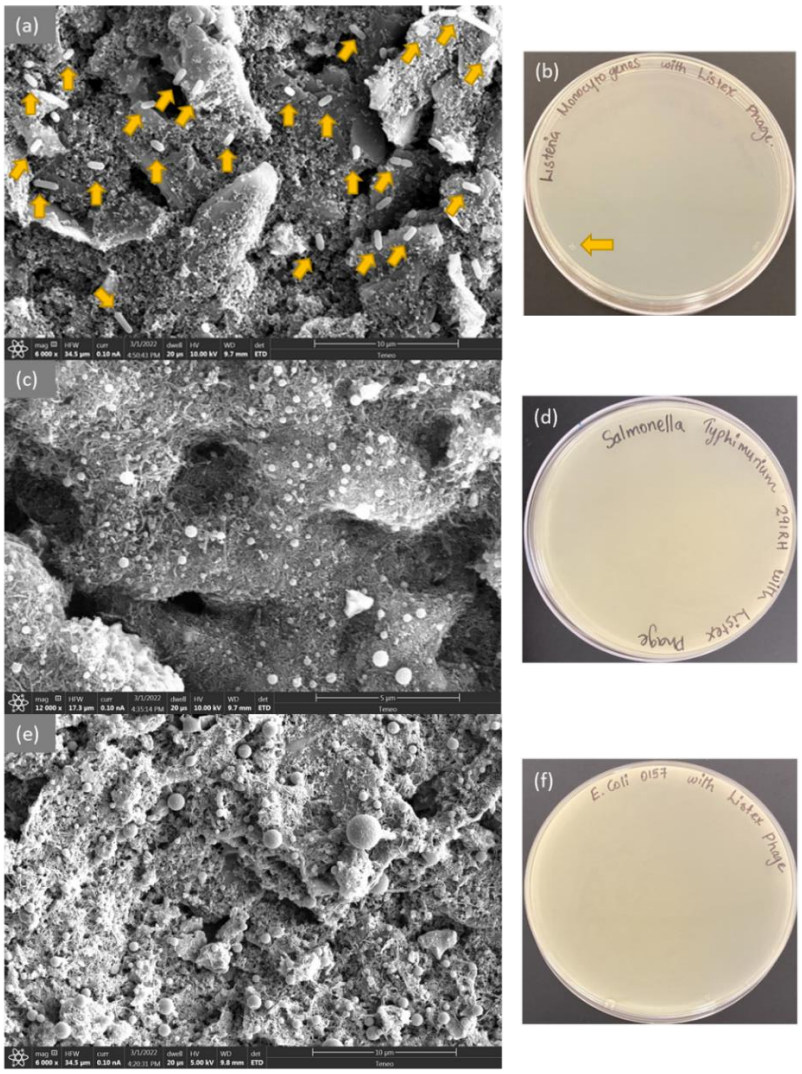

Figure 3.5: P100 phage selectivity in SEM and phage assay studies with target and non-target bacteria. (a) SEM image of a modified electrode after exposure to *L. monocytogenes*. The arrows mark the bacterial cells; (b) phage assay on a plate with *L. monocytogenes*, arrow marks the visible mark on the other side of the media; (c) SEM image of a modified electrode after exposure to *E. coli* O157:H7; (d) phage assay on a plate with *E. coli* O157:H7 with P100 phage; (e) SEM image of a modified electrode after exposure to ser. Typhimurium-291RH; and (f) phage assay on a plate with ser. Typhimurium-291RH with P100 phage.

(a)

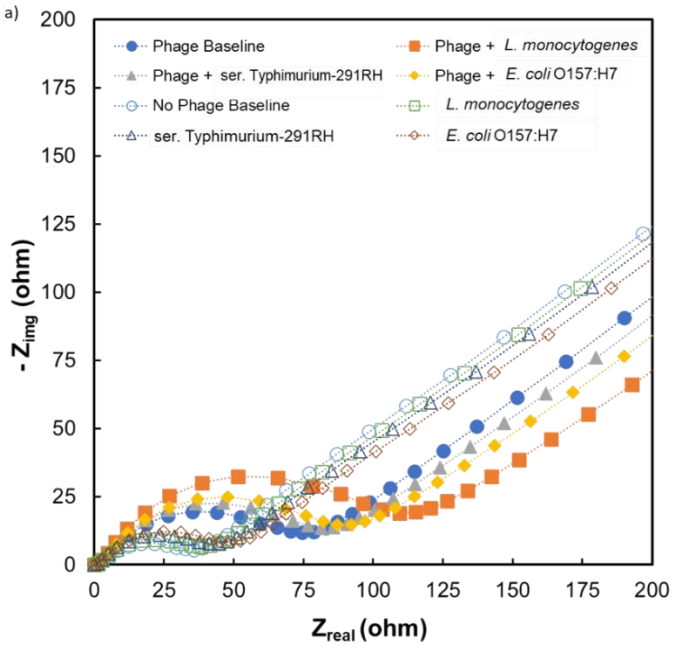

(b)

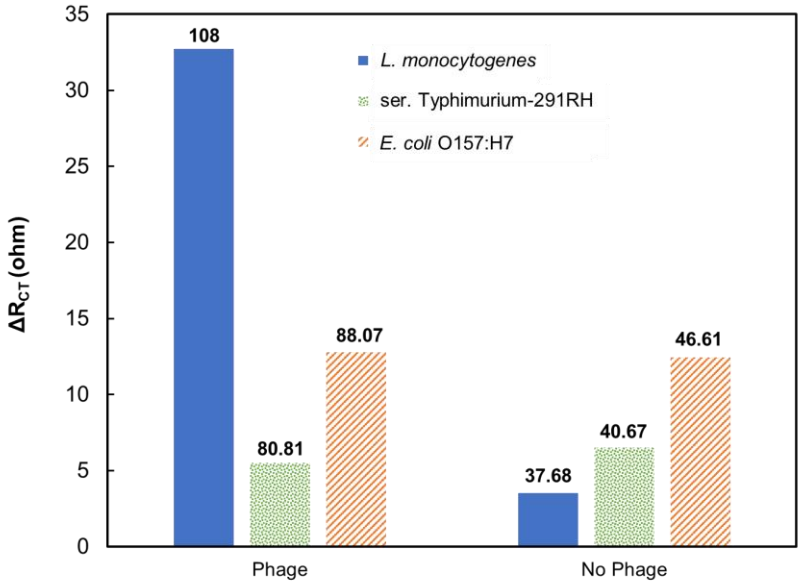

Figure 3.6: Response to target and non-target pathogens with and without phage. (a) Nyquist plot of the impedimetric response to target and non-target bacteria with (full shapes) and without (hollow shapes) P100 phage; (b) ΔR_{CT} (ohm) values of the response as the difference from baseline values with and without P100 phage. The absolute values of R_{CT} values are shown on top of each bar graph.

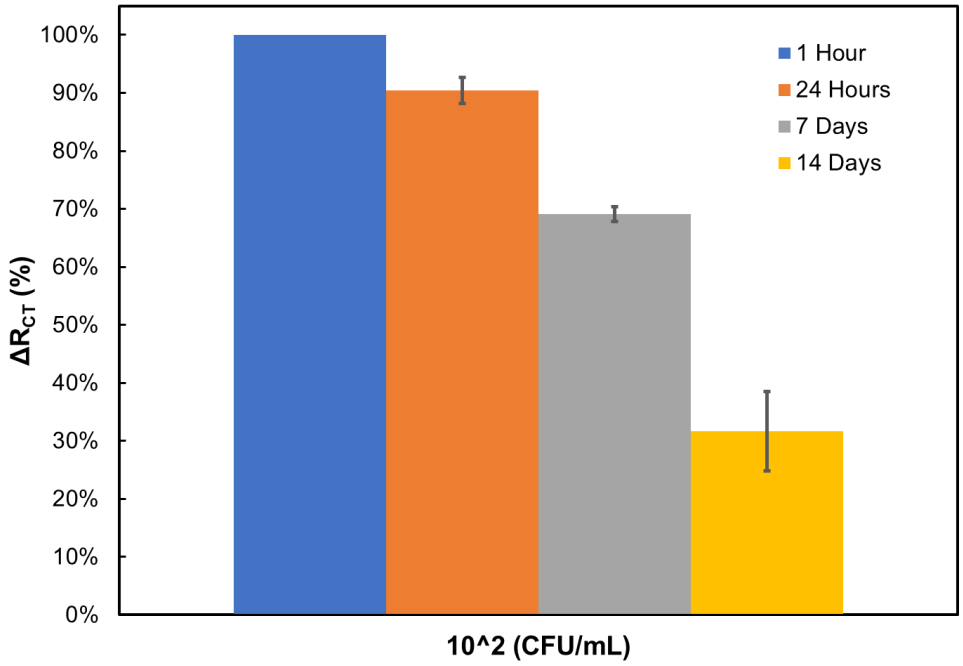

Figure 3.7: ΔR_{CT} (%) values as difference from baseline value taken within the first hour of making the electrode

CHAPTER 4

PHAGE PROTEIN-BASED BIOSENSOR ARCHITECTURE TO DETECT *CAMPYLOBACTER JEJUNI* BACTERIAL CELLS

Bavithithira Suganthan, Ashley Rogers, Clay S Crippen, Hamid Asadi, Or Zolti, Christine M Szymanski, and Ramaraja P. Ramasamy. To be submitted to Biosensors and Bioelectronics.

Abstract

Phage-protein-based electrochemical biosensors provide several advantages for diagnosing bacterial cells due to their high specificity and rapid response. This study is aimed to develop a phage protein-based impedimetric electrochemical biosensor architecture for detecting bacterial cells at concentrations of 100 CFU/mL with high specificity. As a proof of concept, we report a novel impedimetric phage protein-based biosensor to detect *Campylobacter jejuni* using a genetically engineered receptor-binding phage protein, FlaGrab, as a bioreceptor. *C. jejuni* is a common food pathogen found in poultry that can cause severe life-threatening illnesses in humans. The electrochemical impedance spectroscopy (EIS) technique was used to measure resistance changes of the sensor upon interaction with *C. jejuni*. The sensitivity of the phage protein immobilized electrode was evaluated using suspensions of different concentrations of *C. jejuni* NCTC 11168 (10^2 -10^9 CFU/mL). The selectivity of the biosensor towards *C. jejuni* NCTC 11168 was analyzed using non-target bacterial cells such as *Salmonella enterica* subsp. *enterica* serotype Typhimurium 291RH and *Listeria monocytogenes* Scott A. Impedance measurements were taken at different concentrations of *C. jejuni* NCTC 11168. The change transfer resistance of the biosensor increased with the increasing concentration of *C. jejuni* NCTC 11168 cells. The detection limit was determined to be ~100 CFU/mL. Further, the detection was highly selective toward *C. jejuni* NCTC 11168 as no signal was observed for ser. Typhimurium-291 RH and *L. monocytogenes* Scott A. The proposed biosensor exhibited a low limit of detection and high specificity. Furthermore, the phage protein-based biosensors developed

in this work would be ideal for rapid diagnostic applications in food, clinical and environmental monitoring.

Keywords: Biosensor, *Campylobacter jejuni*, Food safety, Impedance, Protein

4.1. Introduction

Campylobacter jejuni, microaerophilic gram-negative bacteria, is a common food pathogen found in poultry that can cause severe life-threatening illnesses in humans [171]. It causes bloody diarrhea, and chronic infection could lead to Guillain-Barre syndrome (GBS), an autoimmune disorder that causes the immune system to damage nerves. The flagella of *Campylobacter jejuni* play a crucial role in colonizing the human gastrointestinal tract. Flagellar filaments are composed of eleven protofilaments formed out of flagellin subunits. The flagellar filament is driven by the proton motive force (PMF) generated by a multi-subunit motor protein [175]. Proper flagella formation and normal filament movement in *Campylobacter* require flagellar glycosylation [176, 177]. FlaGrab is a receptor-binding phage protein expressed by NCTC 12673 phage [178]. FlaGrab binds to pseudominic acid (Pse5Ac7Am) glycan displayed on flagellin subunits of *C. jejuni* flagella. Even though we know the amino acid sequence of the protein and its structural features, conserved domains or critical amino acids involved in receptor binding have not been reported yet. This protein recognizes flagellin from almost all the strains of *C. jejuni* and *Campylobacter coli* (*C. coli*) [170]. The binding of FlaGrab to the flagella reduces bacterial motility. Proteomic analysis and antibody recognition did not show the presence of FlaGrab on the phage virion, indicating the non-structural role of the protein [168, 181, 182]. The binding domain of FlaGrab is located in the c-terminal quarter of the protein (CC-FlaGrab), and CC-FlaGrab has been shown to detect both C. *jejuni* and *C. coli* [170]. Unlike most RBPPs, which are components of virion tail fibers, FlaGrab is a nonstructural secreted protein.

The only way to employ it in a biosensor is by directly using the protein to develop into a biosensor. Flagrab is smaller than the whole phage, so it would allow more protein to be coated per unit surface area. Since the bacterial binding property resides on the C-terminal quarter of the protein (CC-FlaGrab), we could further reduce the bioreceptor's size and thereby increase the number of molecules per unit area and sensitivity of the biosensor. Even though CC-FlaGrab harbors bacteriostatic properties, it does not lyse the bacterial cells, making it a better alternative to phages. The availability of a genetically engineered CC-FlaGrab with a GST tag would allow better purification and better orientating of the protein on biosensors for productive interaction with the bacterial receptor. Immobilization of protein could be targeted towards the GST tag, thereby minimizing the damage to critical amino acids involved in the interaction with the receptor. Since there are previous studies that have shown that GST-tagged FlaGrab could be immobilized on the gold surface, we know that the protein is compatible with immobilization, and immobilization could be done without affecting the interaction with the target organism. Since most of the *C. jejuni* and *C. coli* strains are detected by FlaGrab, it indicates most strains have the protein receptor and indicate minimal resistance in the natural bacterial population. These properties make FlaGrab a better bioreceptor for a biosensor [157].

This paper describes our work on developing an impedimetric biosensor architecture to detect *C. jejuni* using RBPP as the biorecognition molecule. The biosensor architecture was made of a multi-walled nanostructured carbon nano tubes-based glassy carbon electrode. We have used 1-pyrenebutanoic acid, succinimidyl ester (PBSE), as a molecular linker to immobilize the RBPP on the electrode. The response of the biosensor was measured based on the monitoring of the change in the charge-transfer resistance resulting

in the binding of the *C. jejuni* to the RBPP. We also have used *Listeria monocytogenes* Scott A (*L. monocytogenes*) and *Salmonella enterica* subsp. *Enterica* serovar Typhimurium 291RH (ser. Typhimurium-291RH).

4.2. Experimental

4.2.1. Materials

Multiwalled carbon nanotubes (CNTs) with an outer diameter of 20-30 nm and length of 10 – 30 µm were purchased from Cheap Tubes Inc. Silica polishing powder (0.05-micron type N gamma silica powder) was purchased from Electron Microscopy Sciences. Working electrode [Glassy carbon electrode (part number CHI104)], reference electrode [Ag/AgCl (part number CHI111)], and counter electrode [platinum wire (part number CHI115)] were purchased from CH Instruments, Inc. BL21(DE3) Competent *E.coli* cells were purchased from New England Biolabs. The GST column for protein purification (GSTrapTM HP) was purchased from GE Healthcare. Mueller Hinton agar (MH) and brain heart infusion (BHI) (both from Hardy Diagnostics CRITERION^{TM}), 1-pyrenebutanoic acid succinimidyl ester (PBSE), bovine serum albumin (BSA) (both from Sigma-Aldrich), disodium phosphate (Na_2HPO_4) (Research Products International Corp), sodium chloride (NaCl) (EMD chemicals), magnesium sulfate heptahydrate ($MgSO_4.7H_2O$ (J.T. Baker), potassium phosphate dibasic (KH_2PO_4) and potassium chloride (both from BDH), tris base, tryptone, ethanol and glutathione (all four from Fisher scientific), yeast extract and agar powder (both from Becton Dickinson and Company), were purchased and used as received. Phosphate-buffered saline (PBS, 1X) (1 L) was prepared by mixing 8 g of NaCl, 1 440 g

of Na_2HPO_4, 270 mg of KH_2PO_4, and 200 mg of KCl. BHI media was prepared according to the instructions on the chemical bottle. Luria Bertani (LB) (1 L) (pH 7.0) was prepared by mixing tryptone (10 g), yeast extract (5 g), and NaCl (10 g). Milli-Q water (resistivity =18 MΩ.cm) was used to prepare all the media, buffer, and chemicals. All buffers and media are sterilized before use.

4.2.2. Methods

Bacterial Growth Conditions

A microaerophilic *C. jejuni* NTCT 11168 (was used as the target analyte, whereas *Listeria monocytogenes* Scott A and *Salmonella enterica* subsp. *Enterica* serovar Typhimurium 291RH (ser. Typhimurium-291RH) were used as non-target analytes. *C. jejuni* (NTCT 11168) was grown on BHI agar at 37°C under microaerobic conditions (85 % N_2, 10 % CO_2, 5 % O_2). A single colony of ser. Typhimurium-291RH and Scott A were inoculated in 3 mL of BHI liquid media separately and incubated at 37 oC overnight, at 200 rpm. A 500 µL aliquot of the overnight culture was inoculated into 50 mL of fresh liquid BHI medium and incubated at 37 ^oC in an incubator shaker until it reached the mid-log phase. The spread plate technique was used to enumerate the bacteria and express them in CFU/mL.

Extraction, Purification, and Confirmation of the FlaGrab:

CC-FlaGrab was expressed in *E. coli* BL21 using the IPTG induction method as GST-fused proteins and purified using the FPLC system as described previously, except that proteins

were eluted in 10 mM reduced L-glutathione in 1xPBS [169] [316]. A 12.5 % Sodium dodecyl-sulfate polyacrylamide (SDS-PAGE) gel electrophoresis was carried out to confirm the size of the extracted protein. Samples were run at 110V for 10 minutes and then 165V for 65 minutes.

Measuring the Concentration of the Protein

TM BCA Protein Assay Kit (Thermo Scientific) was used to measure the concentration of the protein. Twenty-five microliters of each standard or unknown sample were pipetted into a microplate well (working range = 20–2000 µg/mL). 200 µL of the working reagent was added to each well and mixed the plate thoroughly on a plate shaker for 30 seconds. The plate was covered and incubated at 37°C for 30 minutes. Finally, the plate was cooled down, and the absorbance was taken at 562 nm using a plate reader.

Growth Clearance Assay

A bacterial growth clearance assay was carried out using the previous overlay method with some modifications [182]. Briefly, BHI broth was used to harvest overnight bacterial cultures, and the OD600 was adjusted to 0.35. A 5-mL aliquot of this suspension was added to an empty petri dish and incubated for 4 hours at 37 °C without shaking. Later, 200 µL of the suspension (OD600 of 0.5) was combined with 5 mL of sterile 0.6 % molten agar at 55°C. Then, the suspension was applied to the surface of an MH plate that had been preheated to 37 °C and contained 1.5 % agar. Then, 10 µL UV-sterilized CC-FlaGrab solution (0.38-3.79 mg/mL in 10 mM reduced L-glutathione in 1xPBS) was spotted onto the agar surface and allowed to absorb into the agar completely. Then the plate was inverted

and incubated at 37 °C under microaerobic conditions. After 18 to 24 hours, growth-clearing zones were noticed.

Preparation of CNT Dispersion and Fabrication Protein Immobilized Electrode

The homogenous CNT dispersion was prepared by adding 1 mg of MWCNTs to 1 ml DMF and ultrasonicated for an hour at 40W using an ultrasonic homogenizer (Omni International, SONICRAPTOR 250).

A glassy carbon electrode (GCE) was polished using the 0.05 μm alumina powder on a polishing pad for 5 minutes and then sonicated for 5 minutes in a bath sonicator to remove adhered polishing powder. Later. The electrode was rinsed with DI water, kept in the oven at 70 °C for 45 minutes until it was completely dry, and allowed to cool down at room temperature. Once it cooled down, 1.5 μL of the CNT dispersion was drop cast on the GCE electrode surface and allowed to dry for 15 minutes at room temperature, and then it was dried at 70 °C for 5 minutes in the oven. Once the electrode dried, it was transferred to an ice bucket and allowed to cool down before immobilizing the protein on the electrode. PBSE, a molecular tethering molecule, was used to immobilize the protein onto the CNT-modified electrode. For this process, the CNT-modified electrode was rinsed with DMF, then 4.5 μL of 10 mM PBSE was drop cast on the electrode and incubated for 15 minutes, then excess PBSE was rinsed with DMF and followed by 1X PBS (pH 7.4). In the next step, 5 μL of CC-FlaGrab protein (in 1X PBS buffer) (0.38-3.79 mg/mL) was drop cast on the electrode surface and incubated for 24 hours at 4 °C to immobilize the protein on the electrode surface. Later it was rinsed with 1X PBS buffer to remove any unbound protein. In the next step, 0.1 % BSA solution in 1 X PBS was dropped on the electrode surface and

incubated for 30 minutes to block any unmodified surfaces of the electrode. Lastly, the electrode was thoroughly washed and incubated for 15 minutes with 1X PBS buffer.

Electrochemical Impedance Measurements

Fifty microliters of *C. jejuni* were dropped cast on the modified glassy carbon electrode and incubated for 12 minutes under microaerobic conditions (85 % N_2, 10 % CO_2, 5 % O_2). Then the electrode was washed with 1X PBS and used for an electrochemical experiment. The impedimetric characterization was carried out using the CHI-920C model potentiostat (CH Instruments Inc., Austin, TX). The electrochemical system consists of 3 electrodes; glassy carbon (GC) working electrode (CH Instruments Inc., Austin, TX), Ag/AgCl reference electrode, and the Pt wire as a counter electrode. Electrochemical impedance spectroscopy (EIS) measurements were carried out in 5mM $[Fe(CN)_6]^{4-}/[Fe(CN)_6]^{3-}$ as redox couple, with a frequency range of 1Hz to 10 kHz with an amplitude of 5mV. The resulting measurement will be presented as $\%R_{CT}$ where:

$$\%R_{CT} = \frac{R_{CT,\ measured} - R_{CT,\ baseline}}{R_{CT,\ baseline}} \times 100\%$$

Sensitivity of the Biosensor

For sensitivity measurement, different concentrations of *C. jejuni* (from 10^2 CFU/mL to 10^8 CFU/mL) were prepared and tested with an RBPP immobilized biosensor. Before impedimetric electrochemical impedance measurements, 50 µL of solution *C. jejuni* was incubated with RBPP immobilized electrode for 12 minutes in a microaerophilic

environment. Finally, the electrode was washed with 1X PBS buffer, and impedimetric measurements were taken.

Specificity of the biosensor

The specificity study of the CC-FlaGrab protein was evaluated with the target and non-target pathogens; *L. monocytogenes* and ser. Typhimurium-291RH presence and absence of the CC-FlaGrab protein. The same concentration of (10^7 CFU/mL) of both target and non-target pathogens were used.

Stability of the biosensor

The stability of the biosensor was evaluated after fabricating the electrode with CC-FlaGrab. RBPP immobilized electrodes were stored at 4 ^oC in 1X PBS solution for one day, one week, and two weeks and were tested using 100 CFU/mL of *C. jejuni* after each period. R_{CT} was measured, and % R_{CT} was calculated from the experimental data in relation to the response one hour later. The measurement error was computed for every period that was tested in duplicates.

4.3. Results and Discussion

Confirmation of the Size, Concentration and Activity of the Protein

The SDS- PAGE gel image in Figure 4.1abc show that the total protein size is 62 kD, including a 26 kD size GST tag. The protein concentration was 0.962 mg/mL after purifying with a 50 kDa column. Further, the agar growth clearance assay showed that the

phage protein did not allow the *C. jejuni* 11168 to multiply, confirming that the extracted protein is in the active stage (Figure 4.2).

Fabrication and Working Principle of the Biosensor

Figure 4.3 shows a schematic representation of the suggested method for immobilizing phage protein and the *C. jejuni* detection. The basal substrate, GCE, was modified by drop-casting with a thin layer of MWCNTs. Carbon nanotubes (CNTs) have been widely used in transducers due to their unique structural and chemical properties in biosensing applications. CNTs are not only highly conductive but also highly stable. In addition, the highly porous surface of CNTs provides a large electroactive area for binding various biological molecules, which lead to an increase in the sensitivity of the biosensor [230-233]. The high surface-to-volume ratio of CNTs allows high molecule charge per geometric unit, which helps signal amplification. In addition, it acts as the architecture for immobilizing the biorecognition element, phage protein. An ideal method for immobilizing CC-FlaGrab is to immobilize it strong enough to minimize the leaching of the protein while preserving its interaction with the bacterial receptor glycan molecule. So, any immobilization technique should not affect the critical amino acid involved in interacting with the bacterial receptor. The immobilization method should also consider the correct orientation and conformation of the protein for productive interaction. Potentially if the immobilization method could specifically target the GST tag for immobilization purposes instead of the CC-FlaGrab, the adverse effects on the structure of the RBPP and critical amino acid would be minimized. The method should not only be compatible with the nanostructured probe to increase the surface area and sensitivity of the

detection but also be a method that does not require a complete understanding of the structural information of the protein.

PBSE has been successfully used in numerous biosensor applications with many types of proteins. In this work, PBSE was used to immobilize phage protein onto the MWCNT-modified electrode covalently [233, 234, 282, 306, 317-321]. PBSE acts as a crosslinker and attaches CC-FlaGrab (formerly GST-CCGp047) through the linker to the surface of the MWCNTs. The aromatic pyrenyl moiety of the PBSE forms an irreversible Π-Π stacking and strongly attaches to the surface of the MWCNT. Since PBSE reacts with the N terminal amine group, it allows us to orient the protein in a way that would allow productive interaction with the receptor. Since the GST tag is at the N terminal, the chemical reaction with the crosslinker would have minimal impact on the conformation or critical amino acids of the CC-FlaGrab. Since the protein is linked through a covalent bond to the linker, the chance of leaching out is minimized, and the protein would be stable at pH and temperature changes.

Further, the bacterial binding property resides on the protein's C-terminal quarter (CC-FlaGrab). In addition, CC-FlaGrab binds to pseudominic acid (Pse5Ac7Am) glycan displayed on flagellin subunits of *C. jejuni*. Once the protein immobilization was complete, the C. jejuni was drop casted on the electrode, and different concentrations of *C. jejuni* were incubated with the immobilized electrode. At last, *C. jejuni* detection was accomplished by EIS by comparing the difference between R_{CT} before and after the target *C. jejuni* and the phage protein were immobilized.

Electrochemical Characterization and Detection of the *C. jejuni*

Sensitivity of the Biosensor

Figure 4.4 displays the results of testing the impedimetric biosensing response of the phage-modified electrode at various concentrations of *C. jejuni* in the sample, ranging from 10^2 CFU/mL to 10^9 CFU/mL. Results showed that the magnitude of the semicircle (impedimetric responses) increased when the concentrations of *C. jejuni* increased. Further, the R_{CT} data were used to create a calibration curve between charge transfer resistance and analyte concentration, which was then shown in Figure 4.4 (b). As seen in the inset, the calibration curve demonstrates a nearly linear range of reliable detection between 10^2 and 10^7 CFU/mL, beyond which the signal reaches a plateau. The following formulae were used to estimate the limit of detection and quantification based on triplicates measurements. Where n is the number of points used for the linear fit, s is the slope of the fit, and SD and SE are the intercept's standard deviation and standard error, respectively [322].

$$SD = SE \times \sqrt{n} \quad (1)$$

Experimental results reveal that the LOD of the phage protein-modified biosensor for *C. jejuni* is 10^2 CFU/mL, which is well below the standard.

Specificity of the Biosensor

Figures 4.5 a and b show the Nyquist plots of target and non-target bacterial cells in the presence and absence of CC-FlaGrab, respectively. The results demonstrate that the phage protein-modified electrode is nonresponsive to non-target bacterial cells (*L. monocytogenes* Scott A and ser. Typhimurium-291RH). In contrast, a significant variation

was observed for *C. jejuni* 11168. Further, in the absence of phage protein, the electrode showed very low R_{CT} change from the baseline for *C. jejuni* 11168 compared to non-target pathogen *L. monocytogenes* Scott A (Figure 4.6 a and b). Thus, the phage protein-based biosensor is specific only to target bacterial cells.

Further, SEM images confirm that *C. jejuni* selectively attached to the fabricated biosensor architecture, whereas none of the *L. monocytogenes* 11168 and ser. Typhimurium-291RH cells (non-target) attached to the biosensor architecture (Figure 4.7). These two data reveal that the developed phage protein (CC-FlaGrab) based protein architecture is specific towards the target bacterial cell.

Stability of the Biosensor

Figure 4.8 demonstrates that the biosensor responses had decreased by 29 % with 5 % error margin after three days of preparation. After a week, the signal had decreased by 34 % compared to the response obtained in one day (24 hours), with a stable error of 5 %. However, the sensor performance reduced to 10 % after 2 weeks of electrode preparation, which clearly shows that CC-FlaGrab protein's activity degrades after 2 weeks and that the signals are quite weak.

4.4. Conclusion

We have developed a highly specific novel biosensor to detect *C. jejuni*. The sensor was developed by immobilizing a phage protein on a MWCNT modified glassy carbon electrode using a crosslinker. The immobilized bioreceptor phage protein was highly reactive and stable when reacted with the target analyte. The proposed biosensor exhibited

a low detection limit of 10^2 CFU/mL, which is well below the standard. The biosensor responded linearly from 10^2 to 10^7 CFU/mL under ideal circumstances, with good reproducibility and stability. These features make it a promising tool for detecting bacterial cells in food, clinical and environmental monitoring. Simulated sample experiments should be carried out to study and evaluate the performance of this developed sensor.

4.5. Acknowledgment

The authors thank Dr. Francisco Diez-Gonzalez (The University of Georgia, Griffin) and Dr. Nikki Shariat (The University of Georgia, Athens) for kindly providing *L. monocytogenes* Scott A strain and ser. Typhimurium-291RH respectively.

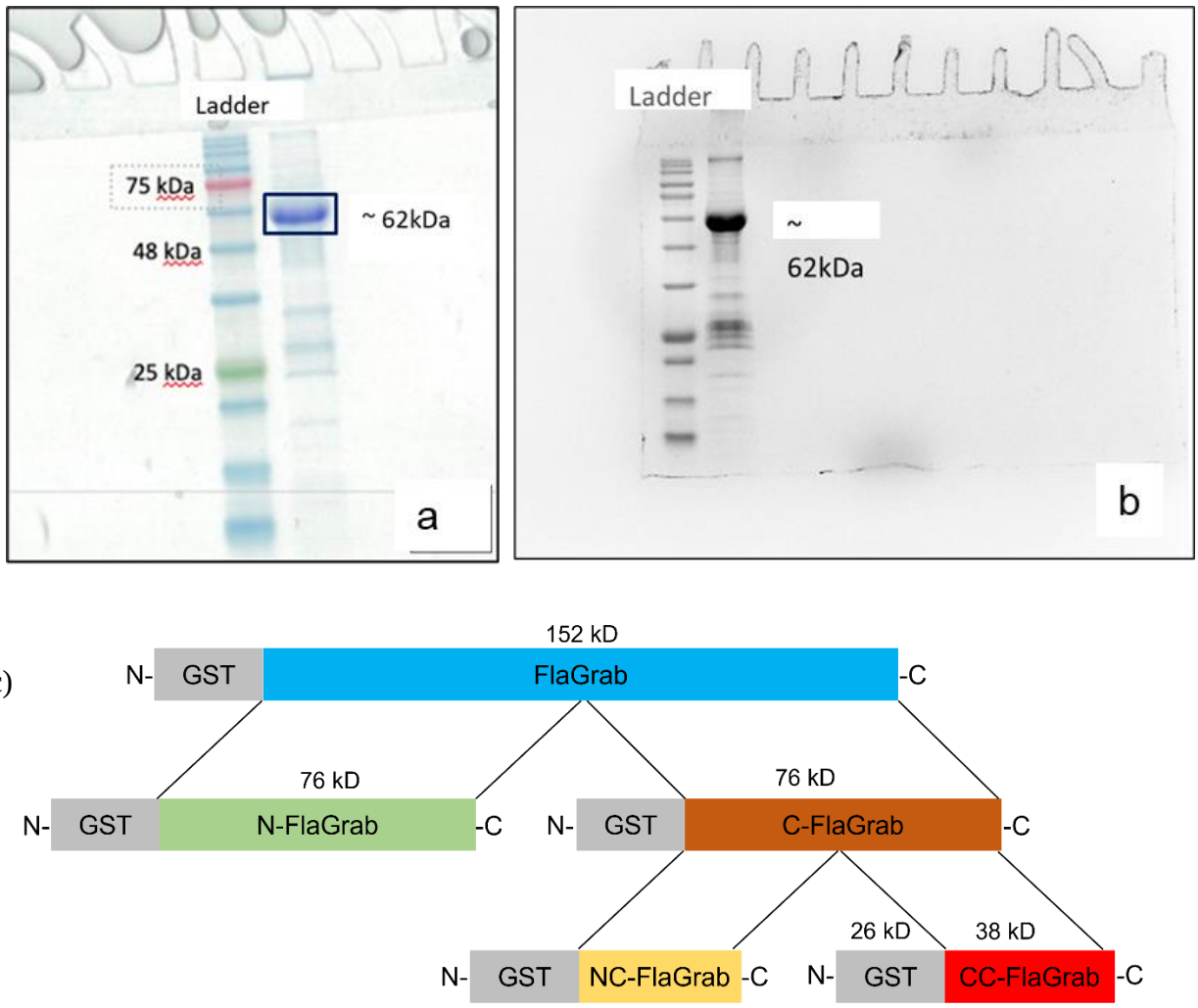

Figure 4.1: SDS-PAGE before (a) and after (b) concentrating the purified CC-FlaGrab phage protein (c) Schematic diagram of the phage protein (CC-FlaGrab)

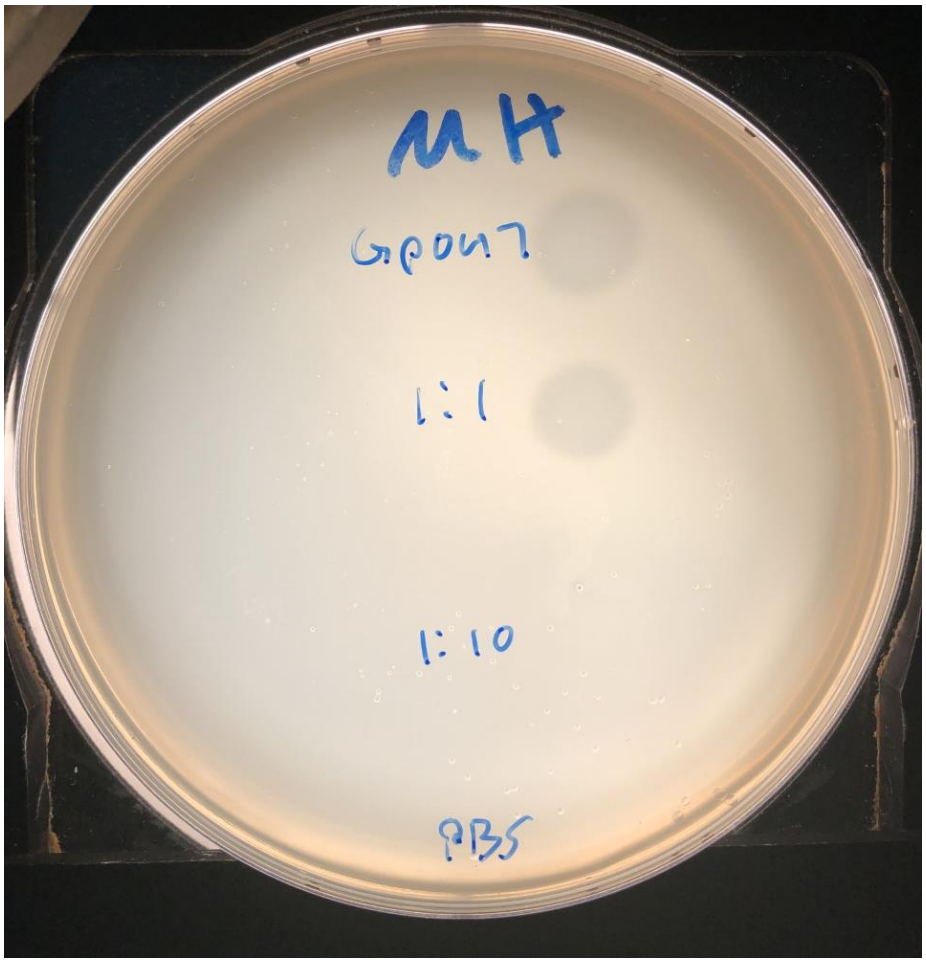

Figure 4.2: Agar plate growth clearance assay in the presence of undiluted CC-FlaGrab protein (CC-FlaGrab protein is labeled as Gp047 in the image) and diluted CC-FlaGrab protein in the buffer in two different ratios (1:10 and 1:1 ratio).

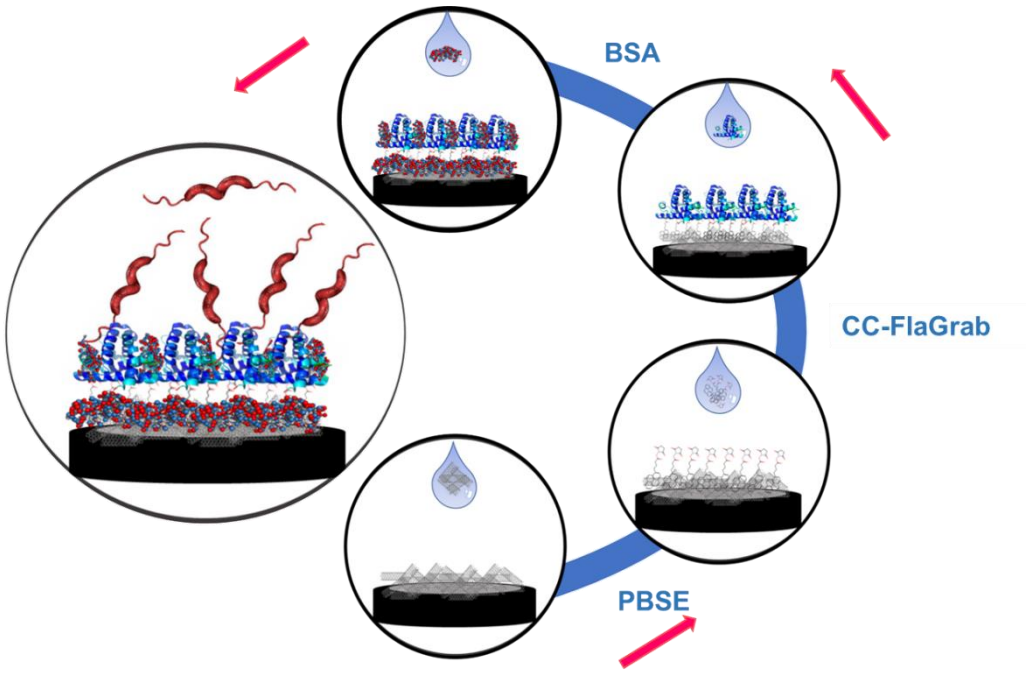

Figure 4.3 Electrode preparation process, including addition of MWCNTs, adding the cross linker PBSE, drop casting the phage protein CC-FlaGrab and finally addition of 0.1 % BSA as a blocking agent

(a)

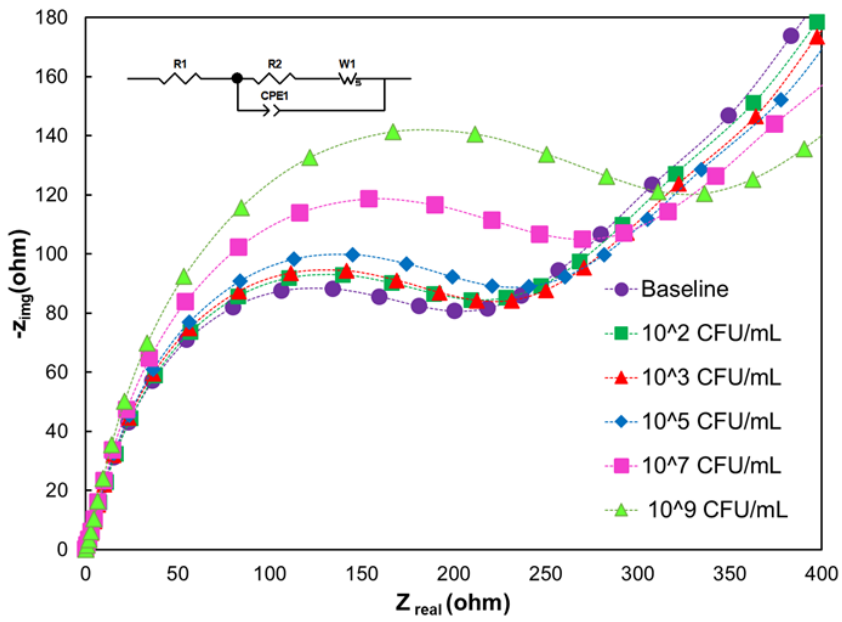

(b)

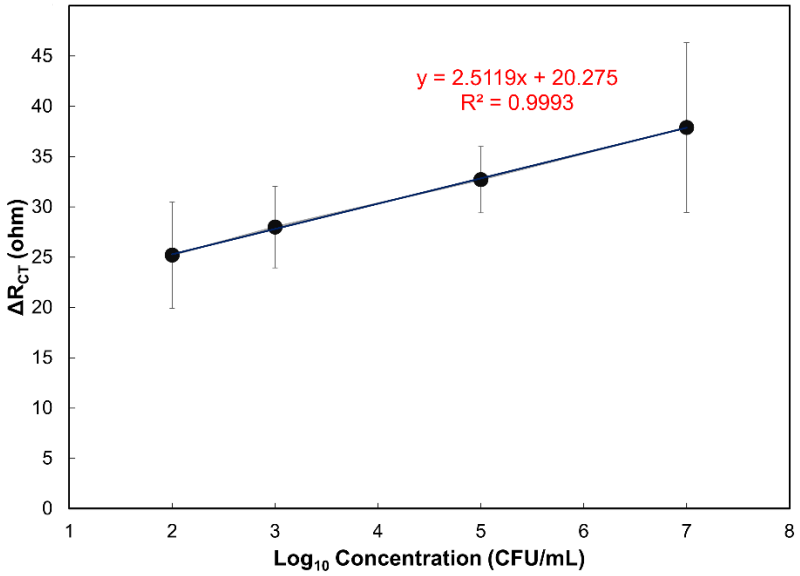

Figure 4.4: (a) Nyquist plots show impedance response to varying concentrations of the target analyte *C. jejuni* 11168. The equivalent electrical circuit used for fitting the Nyquist data is shown in the inset. (b) Calibration curve showing a linear relationship between the differential charge transfer resistance ΔR_{CT} (ohm) and the logarithmic of *C. jejuni* 11168 concentrations.

(a)

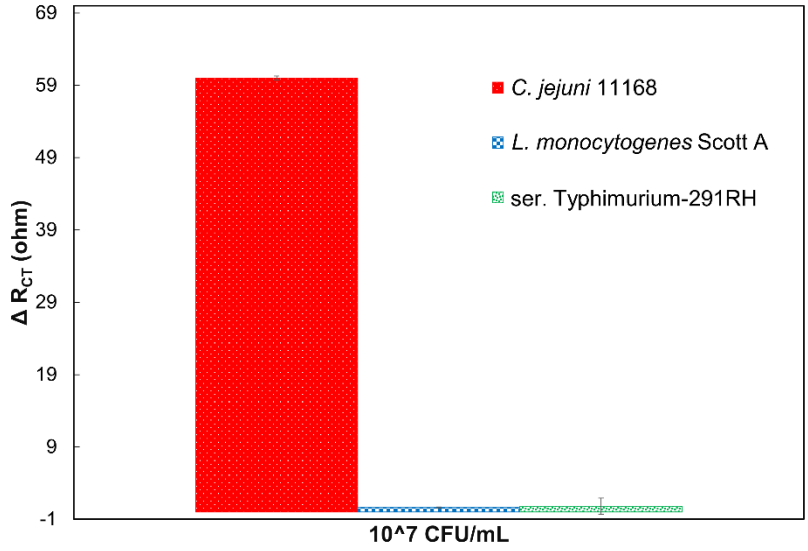

(b)

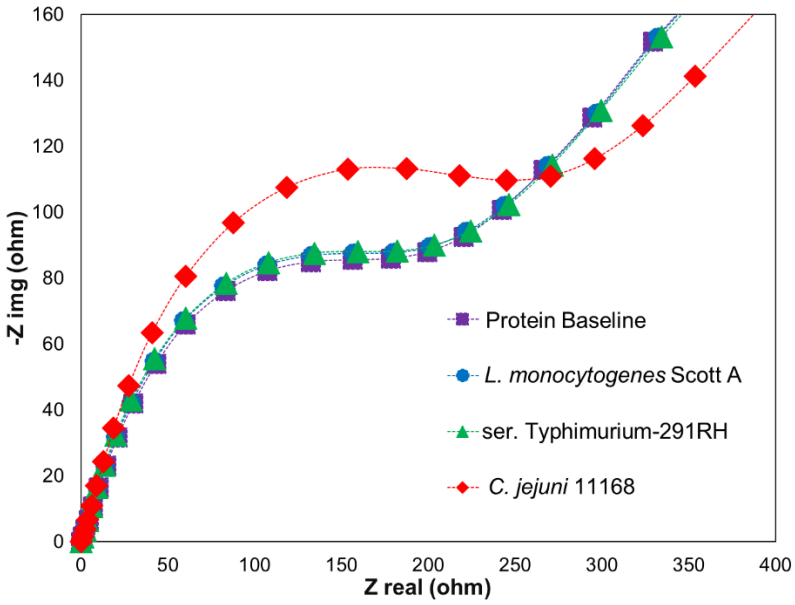

Figure 4.5: Response to target and non-target pathogens in the presence of phage protein. (a) Nyquist plot of the impedimetric response to target and non-target bacterial cells in the presence of CC-FlaGrab protein (b) ΔR_{CT} (ohm) values of the response as the difference from baseline values with CC-FlaGrab protein.

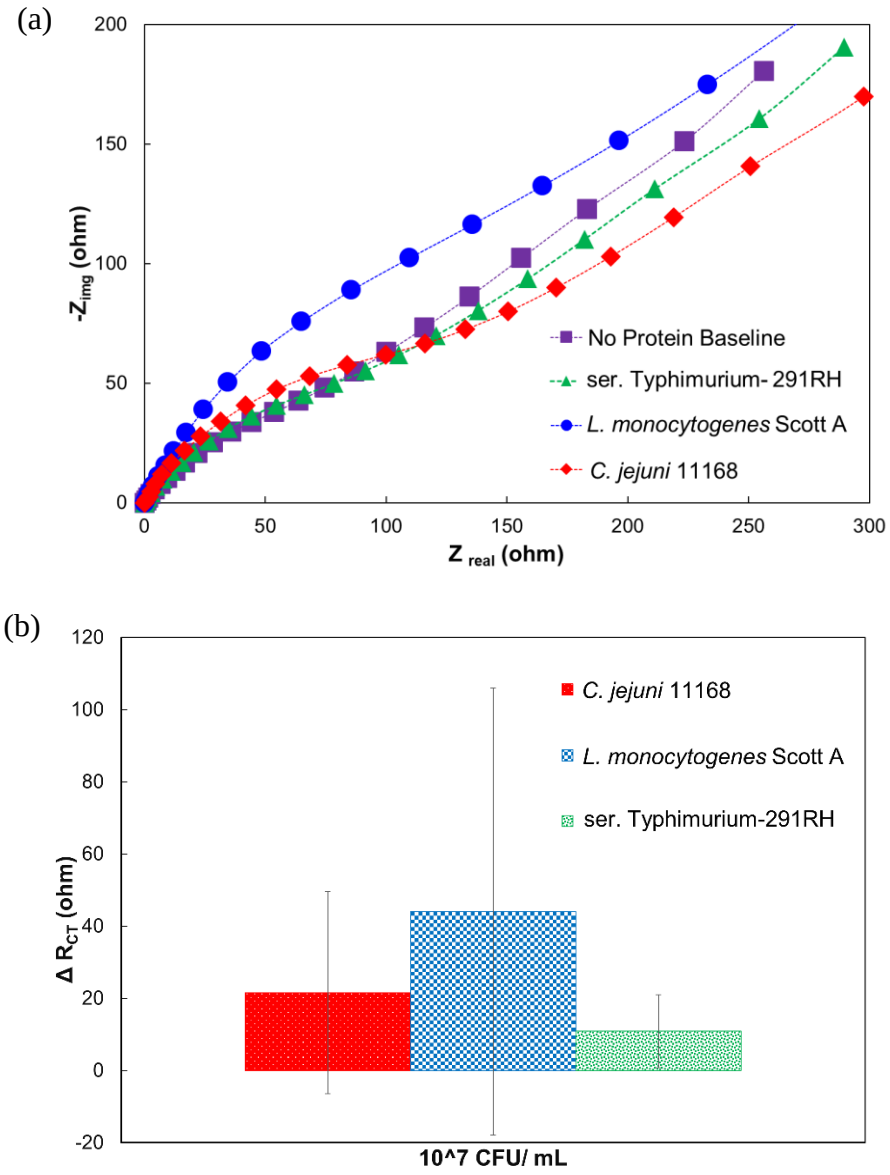

Figure 4.6: Response to target and non-target pathogens in the absence of phage protein. (a) Nyquist plot of the impedimetric response to target and non-target bacterial cells in the absence of CC-FlaGrab protein (b) ΔR_{CT} (ohm) values of the response as the difference from baseline values when CC-FlaGrab is absent.

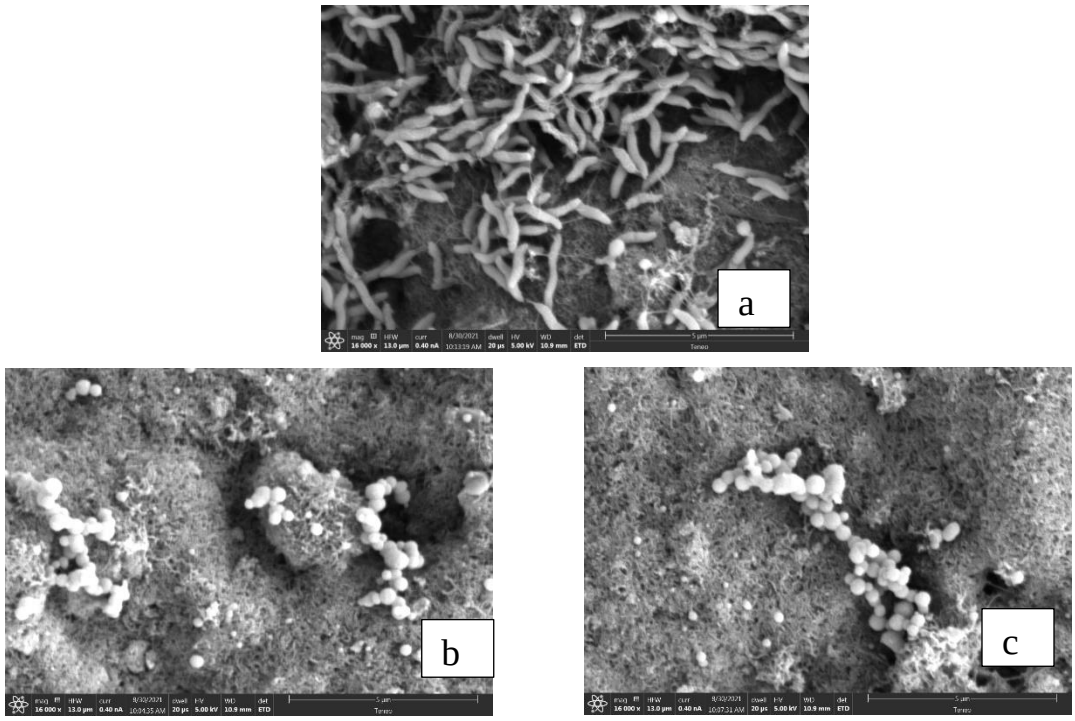

Figure 4.7: Phage protein CC-FlaGrab specificity in SEM with target and non-target bacteria. Phage protein modified electrode after exposure to *C. jejuni* 11168 (a), *L. monocytogenes* Scott A (b), and ser. Typhimurium-291 RH (c).

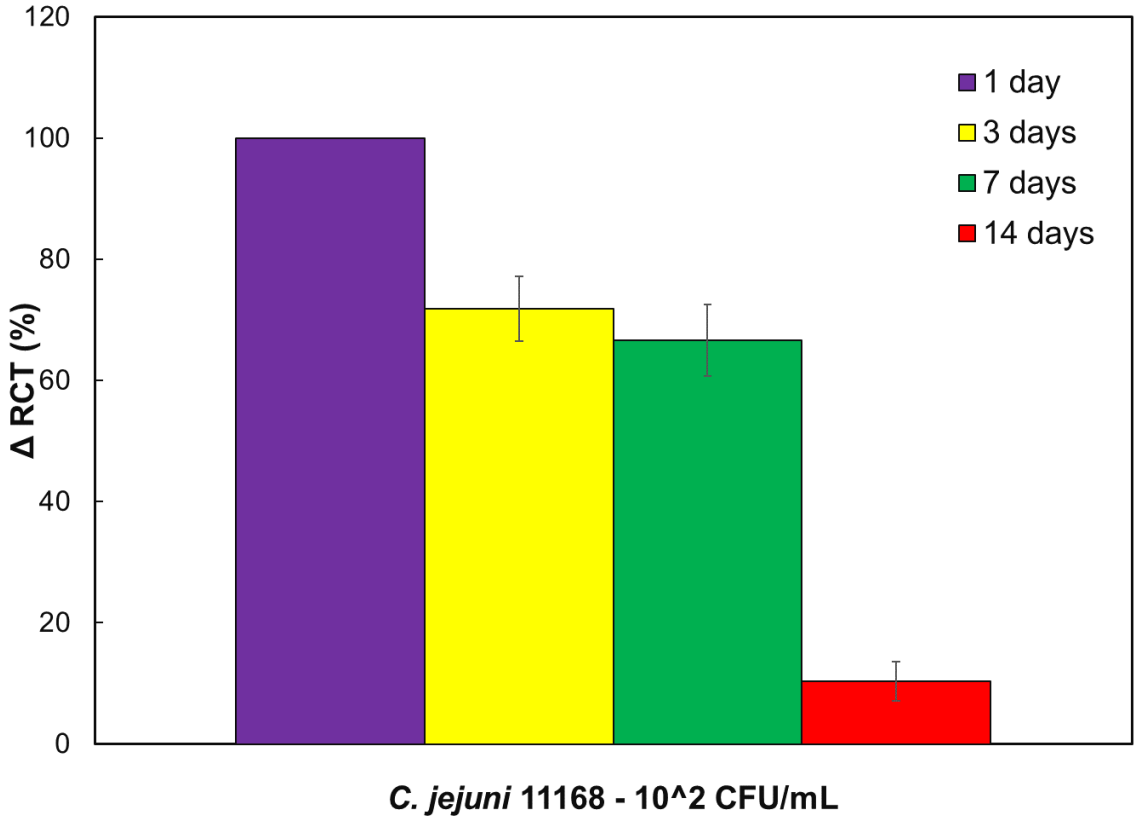

Figure 4.8: ΔR_{CT} (%) values from baseline value taken within a day of making the electrode

CHAPTER 5

EVALUATION OF THE DEVELOPED ARCHITECTURES TO DETECT THE BACTERIAL CELLS IN SIMULATED SAMPLES

Bavithithira Suganthan, Or Zolti, Ashley Rogers, Clay S Crippen, Ryan Maynard, Christine M Szymanski, Jason Locklin, and Ramaraja P. Ramasamy. To be submitted to Biosensors and Bioelectronics.

Abstract

The detection and identification of bacterial pathogens are crucial in medicine, food safety, public health, and environmental monitoring and intervention. Traditional culture-based detection methods and molecular testing are time-consuming, expensive, and require specialized tools and experienced operators. At the point of interest, there is an increasing requirement for the quick and accurate detection of bacteria in complicated samples. Here, we have developed two potentially quick diagnostic platforms based on electrochemical biosensing principles that identify and quantify the target bacterial cells using bacteriophages and receptor-binding proteins. Initial results revealed that developed phage and phage protein-based biosensing architectures could specifically identify the target bacterial cells present in the complex environment with high sensitivity and selectivity.

Keywords: Phage, Phage protein, Biosensor, *Listeria monocytogenes*, *Campylobacter jejuni*

5.1. Introduction

Bacterial infections are a prominent cause of death in both industrialized and developing countries, claiming the lives of more than 6.7 million people each year [92, 93]. Millions of people are infected with these bacteria each year, with the most prevalent causes of infection being clinical, food-borne, airborne, and waterborne. Even though predominant conventional detection methods are highly reliable, they are time-consuming. Identification processes typically require 24 hours to several days, depending on the nature of the clinical or food sample and the type of target bacteria [100, 101, 323]. There is an increasing demand for rapid and sensitive detection of bacteria in complicated samples. However, direct detection of bacterial cells in food and clinal samples is challenging due to the interferences in the food matrix and the cellular components in the clinal samples. These challenges cause false positive and false negative results since the interference from cellular components and clinical sample matrices affect the developed architectures' sensitivity and selectivity.

Biosensors, specifically phage and phage protein-based electrochemical biosensors, are good alternatives for bacterial cell detection due to their high specificity, sensitivity, and ability to provide rapid responses [306, 324-326]. Phage-based biosensors are very accurate and specific due to their high specificity toward the target organisms. Specificity and the stability of bacteriophages are preserved in a wide range of pH and temperature. This biosensor is also known to discriminate between live and dead bacterial cells as the phage binding to the target bacteria depends on functional receptors on the bacterial surface. In addition to phage-based biosensors, phage protein-based biosensors play a major role in detecting bacterial species. Phage proteins or receptor binding-based proteins (RBPPs) are

phage-associated proteins that recognize unique proteins or carbohydrates on the bacterial surface [157, 178, 239, 327, 328]. RBPPs are much smaller than phages, increasing the test's sensitivity by allowing more target microorganisms to bind per unit surface area. It will also allow multiple organism detection without comprising sensitivity. RBPPs are more stable in environmental conditions such as pH and temperature and are resistant to proteases [167]. In this study, we validate the robustness and reliability of the developed phage and phage protein-based impedimetric biosensor architectures with the spiked chicken broth and cecal samples obtained from chicken.

5.2. Experimental

5.2.1. Materials

A protease inhibitor cocktail was purchased from Thermo Scientific™ Halt™ (100X), and pasteurized chicken broth was purchased in a local grocery store. All the other chemicals and substances needed to develop a phage-based biosensor to detect *L. monocytogenes* were purchased and developed using the procedure described in our previous work (hapter3). Further, the cultures *L. monocytogenes* Scott A, *Escherichia coli* O157:H7, *Salmonella enterica* subsp. *Enterica* serovar Typhimurium 291RH (ser. Typhimurium-291RH) were also cultured as described in our previous work (Chapter 3). Similarly, all the other necessary materials needed to develop phage protein biosensors to develop *C. jejuni* 11168 were purchased according to the information provided in Chapter 4. In addition, *C. jejuni* 11168 was cultured as described in our previous work in chapter 4. Electrochemical experiments were carried out using the electrochemical impedance

spectroscopy (EIS) technique using the CHI-920C potentiostat (CH Instruments Inc., Austin, TX). EIS measurements were carried out with a frequency range of 1 Hz to 100 kHz and an AC amplitude of 5 mV using 5 mM $[Fe(CN)_6]^{4-}/[Fe(CN)_6]^{3-}$ redox couple. All the EIS experiments were carried out in a sterile environment at room temperature.

5.2.2. Methods

Validating the Sensitivity of the Developed Phage-based Biosensor Architecture with a Chicken Broth Sample

Commercially available pasteurized chicken broth was used as a simulated sample for the experiment. Chicken broth was diluted 10^4 times with PBS before experiments [329-335]. Different concentrations of *Listeria monocytogenes* Scott A (10^2 CFU/mL to 10^6 CFU/mL) were prepared in a diluted chicken broth sample. In the next step electrochemical experiment was carried out using the impedimetric spectroscopy technique. As a first step phage modified electrode was incubated with 50 µL of the chicken broth and incubated for eight minutes, washed with PBS buffer, and EIS measurement was taken as described in the materials and method section. This reading was considered the baseline reading. In the next step, the electrode was rewashed with PBS buffer, and 50 µL of different concentrations of *L. monocytogenes* were dropped cast and incubated for 8 minutes, and EIS measurements were taken ΔR_{CT} was calculated as shown in equation 1.

$$\Delta R_{CT}\ (ohm) = (R_{CT,measured} - R_{CT,baseline}) \quad (1)$$

Validating the Specificity of the Developed Phage-based Biosensor Architecture with a Chicken Broth Sample

A known concentration (10^3 CFU/mL) of *L. monocytogenes* Scott A was used as a target analyte, whereas the same concentrations of *E. coli* O157:H7 and ser. and Typhimurium-291 were used as non-target analytes. All three cultures were prepared in a diluted chicken broth. Finally, the EIS measurements were taken for the three cultures described earlier in the materials and method section, and ΔR_{CT} was calculated as shown in equation 1.

Validating the Sensitivity of the Receptor Binding Phage Protein-based Biosensor Platform with a Chicken Cecal Sample

The chicken cecal sample was used as a simulated sample for the experiment. The cecal samples were obtained from the Southern Poultry Research Group, Georgia, and were surgically removed. In the next step, cecal contents were extracted aseptically and resuspended in equal-weight sterile PBS. In the initial step, 100 µL of the cecal sample was diluted with 900 µL PBS buffer. Then 10 µL of the protease inhibitor cocktail (100X) was added to the diluted cecal sample, mixed, and incubated at 37 °C for 30 minutes [336]. After incubation, the content was further diluted 100 times [336-340], and the diluted cecal sample was used to prepare different concentrations of *C. jejuni* 11168 (10^2, 10^3, 10^5, $10^{7,}$ and 10^9 CFU/mL). In the next step electrochemical experiment was carried out using the EIS technique. As a first step, receptor binding phage protein-modified electrode was incubated with 50 µL of the diluted cecal sample and incubated for 8 minutes, washed with PBS buffer, and EIS measurement was taken as described in the materials and method section. This reading was considered the baseline reading. In the next step, the electrode

was rewashed with PBS buffer, and 50 µL of different concentrations of *C. jejuni* 11168 were drop cast and incubated for 8 minutes, and EIS measurements were taken ΔR_{CT} was calculated as shown in equation 1.

Validating the Specificity of the Receptor Binding Phage Protein-based Biosensor Architecture with a Chicken Cecal Sample

A known concentration (10^5 CFU/mL) of *C. jejuni* 11168 was used as a target analyte, whereas the same concentrations of *L. monocytogenes* Scott A and ser. Typhimurium-291RH were used as non-target analytes. All three cultures were prepared in a diluted cecal sample. Finally, the EIS measurements were taken for the three cultures described earlier materials and methods section, and ΔR_{CT} was calculated as shown in equation 1.

5.3. Results and Discussion

Sensitivity of the Developed Phage-based Biosensor Platform with a Chicken Broth Sample

The phage-immobilized electrode was tested with chicken broth samples to determine whether the phage-based biosensor could accurately detect and quantify *L. monocytogenes* Scott A in simulated samples. Following analysis, it was shown that components of chicken broth, such as proteins and fatty acids, minerals, nucleotides, free amino acids, and organic acids, adhere to the electrode surface and greatly contribute to the R_{CT}, which could obstruct the detection of bacteria [341]. Therefore, several optimization procedures were carried out. Finally, lower background and higher R_{CT} variations were observed by diluting

the chicken broth 10^4 times with PBS buffer before the experiment. In addition, the diluted chicken broth was used as an additional blocking agent before the impedimetric detection experiments. Chicken broth contains a large number of proteins and fatty acids. Collagen, gelatin, and actin are the main proteins in chicken broth. The isoelectric point of these proteins is 4.7, 4.7, and 5.5, respectively [341-344]. The pH of the chicken broth is 6-7. Therefore, the net charge of these proteins is negative. These negatively charged proteins have a high tendency to interact with the surface of the electrode since the surface of the glassy carbon electrode was modified with highly positively charged quarternized polyethylenimine-modified carbon nanotubes. Therefore, these proteins can interact with the surface of the electrode not covered by P100 bacteriophages. Using the diluted chicken broth as a blocking agent prior to experiments could minimize the non-specific adsorption of the proteins onto the electrode.

The Nyquist plots shown in Figure 5.1 were obtained by testing simulated sample equivalents using chicken broth. The results demonstrate that ΔR_{CT} values increased with the increasing concentrations of *L. monocytogenes* Scott A in chicken broth. In this study, ΔR_{CT} could be defined as $\Delta R_{CT} = Ri - R0$, where Ri is the RCT value after incubation of a diluted chicken broth sample containing *L. monocytogenes* Scott A cells, and R0 is the R_{CT} value after blocking the electrode surface with diluted chicken broth, but before bacterial cell detection [345]. A linear correlation was observed between the concentration of 10^2 and 10^6 CFU/mL *L. monocytogenes* Scott A and the ΔR_{CT}. The LOD of *L. monocytogenes* Scott A is 10^2 CFU/ml of diluted chicken broth sample, equivalent to commercially available highly sensitive techniques, including real-time PCR. These findings showed that the phage-immobilized electrode could detect *L. monocytogenes*

Scott A cells in chicken broth with high sensitivity. Table 5.1 in the literature provides a list of biosensors for detecting *L. monocytogenes*. Compared to previously developed biosensors, our suggested biosensor offers a limit of detection and detection time that is equivalent to or even better.

Specificity of the Developed Phage-based Biosensor Architecture with a Chicken Broth Sample

E. coli O157:H7 and ser. Typhimurium-291RH were used as negative control to evaluate the specificity of the developed biosensor. Chicken broth samples were prepared with the known concentrations of the control bacterial strains (10^3 CFU/mL) using the same method as the *L. monocytogenes* Scott A samples. According to Figures 5.2 ac, even though *L. monocytogenes* Scott A showed a clear shift in the R_{CT} (52.89 %), both *E. coli* O157:H7 (18.44 %) and ser. Typhimurium-291RH (33.23 %) also gave signals for the phage-modified electrode. However, the electrode showed the lowest R_{CT} change from the baseline for *L. monocytogenes* in the absence of phage (9.12 %) compared to non-target pathogens, ser. Typhimurium-291RH (26.82 %), *E. coli* O157:H7 18.44 %), as shown in Figures 5.2 bc, contribute to the non-target R_{CT} signal. According to the findings, phage offers the specificity required for *L. monocytogenes* identification. However, the specificity could be increased by reducing the non-specific attachment of non-target pathogens on the electrode surface. It is necessary to investigate additional surface-blocking molecules or to include a biocide to repel non-target bacterial cells. In addition, the research concerning the simultaneous detection of several bacteria strains in one sample with this method is still

lacking, which is more practical for addressing bacterial infection issues in different fields, including water monitoring, the food industry, and clinical diagnosis.

Validating the Sensitivity of the Developed Phage Protein-based Biosensor Architecture with the Chicken Cecal Sample

The phage protein immobilized electrode was tested with chicken cecal samples containing *C. jejuni* 11168 to evaluate the applicability of the phage protein-based biosensor. The ceca, a pair of blind-ended sacs that open off the large intestine, make up the largest portion of the chicken GIT. The cecum is the primary location for bacterial fermentation and pathogen colonization because of its larger and more diversified microbial population and longer digestion time (12–24 h). Cecal samples of chickens are similar to fecal samples of other animals, so the highest concentration of bacteria would be present in those samples. Literature studies report that the phyla Firmicutes, Bacteroidetes, and Proteobacteria are dominant in the chicken cecal microbiota [338-340, 346-354]. Even though the cecal samples contain many bacterial cells, it does not contain *C. jejuni* 11168. But the samples contain *C. jejuni* 81-176, which does not react with the CC-FlaGrab protein we used to modify the electrode. In addition to microbiota, cecal samples contain large amounts of proteases like serine and metalloproteases [336, 355, 356]. Therefore cecal samples were treated with a commercially available protease inhibitor cocktail before using the cecal samples in the detection experiments since these proteases have a high chance of degrading the phage proteins used for immobilization purposes.

Further, cecal samples contain acetate, propionate, and butyrate produced through fermentation [352, 357]. To minimize the background effect (non-specific adsorption of chicken cecal components onto the electrode surface), the cecal samples were diluted 10^2 times, and the diluted cecal sample was first incubated with the developed biosensor for 10 min and rinsed with the PBS buffer [336-340, 358]. After rinsing the EIS measurement, the result served as the baseline for the rest of the measurements. In the next step, known concentrations of *C. jejuni* 11168 (10^2, 10^3, 10^5, 10^7 to 10^9 CFU/mL) were spiked to dilute the cecal samples and those samples used for the sensitivity experiments. Figure 5.3a shows that R_{CT} values increased as the concentration of *C. jejuni* 11168 increased. For this set of studies, the increment in R_{CT} could be defined as $\Delta R_{CT} = R_i - R_0$, where R_i is the R_{CT} value after incubation of *C. jejuni* 11168 cells, and R_0 is the R_{CT} value after blocking with diluted cecal samples that do not contain, any target *C. jejuni* 11168 cells.

Figure 5.3c shows a linear correlation between ΔR_{CT} and the bacterial concentration between 10^2 and 10^9 CFU/mL. The LOD of *C. jejuni* 11168 is 10^2 CFU/ml of diluted cecal sample, equivalent to commercially available highly sensitive techniques, including real-time PCR. These findings showed that the phage protein immobilized electrode could detect *C. jejuni* 11168 cells in the cecal sample with high sensitivity. Table 5.2 in the literature provides a list of biosensors for detecting *C. jejuni* 11168. Compared to previously developed biosensors, our suggested biosensor offers a limit of detection and detection time that is equivalent to or even better. Furthermore, we believe that further optimizations are needed to increase the sensitivity and minimize the error.

Validating the Specificity of the Developed Phage Protein-based Biosensor Architecture with the Chicken Cecal Sample

L. monocytogenes Scott A and ser Typhimurium-291RH were used as negative controls to evaluate the specificity of the developed biosensor. Known concentrations (10^5 CFU/mL) of *C. jejuni* 11168, *L. monocytogenes* Scott A, and ser Typhimurium-291RH cells were separately spiked to the diluted cecal samples and used for specificity studies. No obvious R_{CT} values were observed for both *L. monocytogenes* Scott A (4.8 %) or ser Typhimurium-291RH (6.37 %) cells, as shown in Figure 5.4c. However, a large variance in R_{CT} (%) was observed for *C. jejuni* 11168 (98.36 %), demonstrating the high specificity of the phage protein-based biosensor and the eliminable physical adhesion of bacterial cells onto the electrode surface. According to the findings, the proposed biosensor offers great potential to be used as a sensitive and reliable *C. jejuni* 11168 detection method in food, clinical and environmental diagnostics.

5.4. Conclusion

Highly selective and sensitive impedimetric biosensors were fabricated to detect *L. monocytogenes Scott A* and *C. jejuni* 11168 in simulated samples by immobilizing *Listeria*-specific phage and *C. jejuni* 11168 specific phage protein. The sensors were fabricated by immobilizing a phage protein on an MWCNT- modified glassy carbon using a molecular linker PBSE. EIS technique was utilized for direct impedimetric detection and quantification of target cells. The simulated samples were diluted with PBS buffer to minimize the background effect on the electrode matrix. In simulated samples, the phage-based biosensor exhibited higher sensitivity towards the target L. monocytogenes Scott A.

On the other hand, the immobilized phage protein showed high specificity and reactivity towards the target *C. jejuni* 11168 in the simulated samples. Both proposed sensors could detect the target bacteria *L. monocytogenes* Scott A and *C. jejuni* 11168 with a LOD of 10^2 CFU/mL. The developed biosensor showed promising characteristics as a quick detection tool for point-of-care diagnostics applications, including high specificity and good precision in simulated samples. All results indicate that the biosensor proposed in this study can be used for quantitative measurement of target bacteria and has great potential in detecting target bacteria in food, environmental and clinical diagnosis.

Table 5.1: Established biosensors used for the detection of *Listeria monocytogenes*

Detection technique	**Bio-recognition event**	**Sample type**	**Analysis time**	**Detection range/ limit**	**References**
Piezoelectric biosensors	Antigen-antibody	Milk	<1 h	10^2 CFU/mL	[359]
Amperometric biosensors	Antigen-antibody	Milk	-	10^2 to 10^6 CFU/mL	[360]
Impedimetric biosensors	Antigen-antibody	Filtered tomato extract	-	4 CFU/mL	[361]
Impedimetric biosensors	Magnetic nanoparticles-antibody-urease	Spiked lettuce	-	300 cells	[362]
Impedimetric biosensors	Modified magnetic nanoparticles-antibody-urease	Spiked lettuce	1 h	1.6×10^2 CFU/mL	[363]
Impedimetric biosensors	Immunomagnetic nanoparticles-urease -screen-printed electrode	Spiked lettuce	<3 h	1.6×10^3 CFU/mL	[364]

Table 5.2: Established biosensors used for the detection of *Campylobacter jejuni*

Detection technique	**Bio-recognition event**	**Sample type**	**Analysis time**	**Detection range/ limit (CFU/mL)**	**References**
Optical biosensors - SPR	Antibody	Apple juice	<1h	1.1×10^5	[365]
Optical biosensors - SPR	Antibody	Milk	25 minutes	10^2 -10^9	[366]
Electrochemical -Amperometric	Antibody, phosphatase	Turkey carcass wash,	2.5 h	10^2 -10^7 LOD=2 x 10^4	[367]
Electrochemical -Amperometric	Antibody	Milk	<1.5 h	$1*10^3$ -$5*10^5$ LOD = $4*10^2$	[368]

(a)

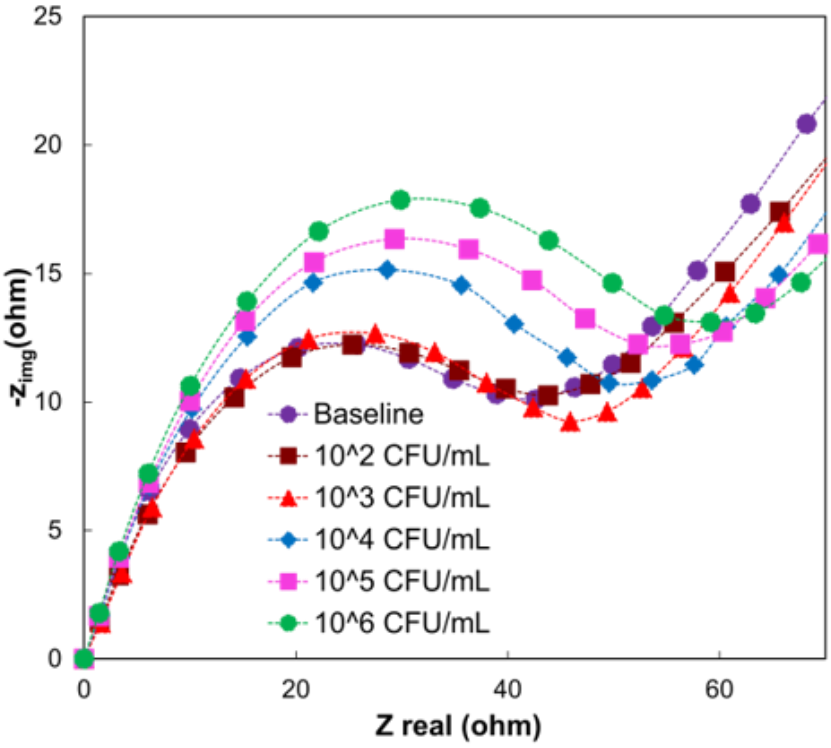
25
20
15
10
5
0
-Zimg(ohm)
0
20
40
60
Z real (ohm)
Baseline
10^2 CFU/mL
10^3 CFU/mL
10^4 CFU/mL
10^5 CFU/mL
10^6 CFU/mL

(b)

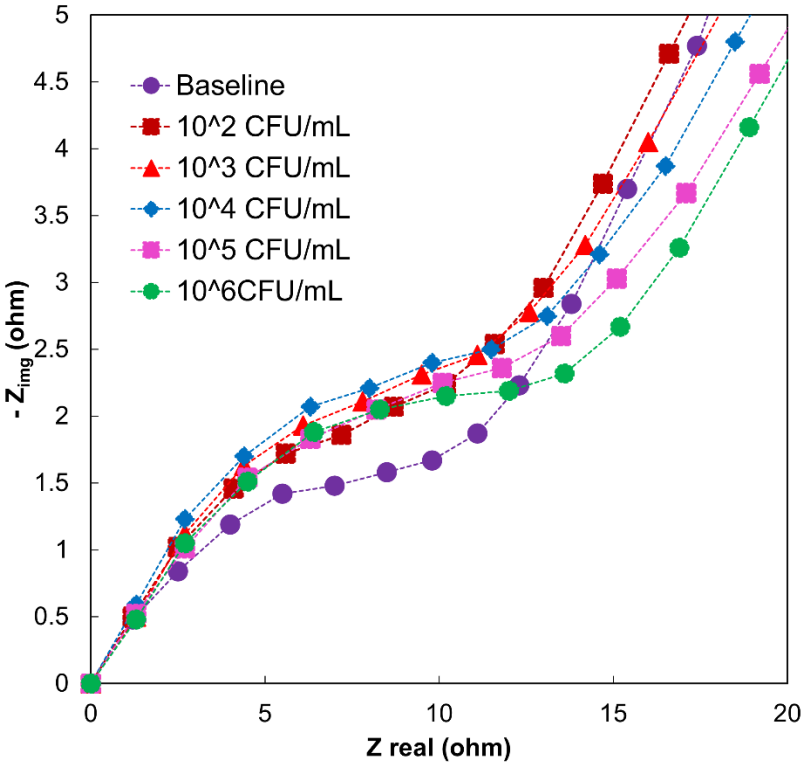
5
4.5
4
3.5
3
2.5
2
1.5
1
0.5
0
- Zimg (ohm)
0
5
10
15
20
Z real (ohm)
Baseline
10^2 CFU/mL
10^3 CFU/mL
10^4 CFU/mL
10^5 CFU/mL
10^6CFU/mL

(c)

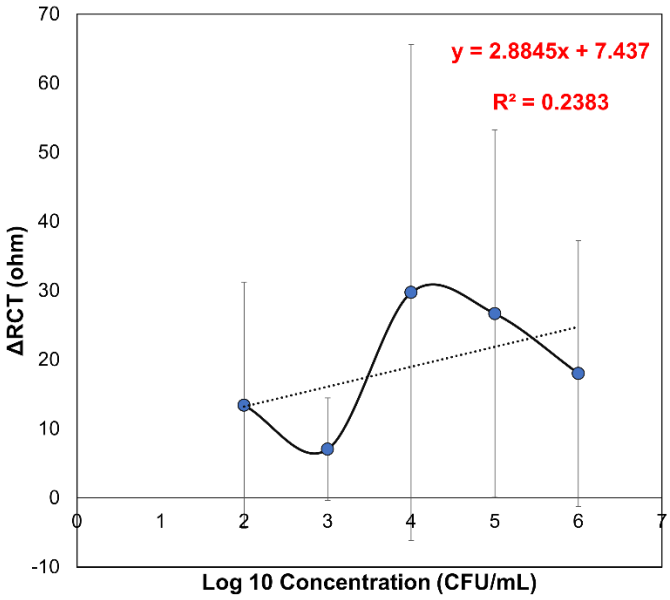

(d)

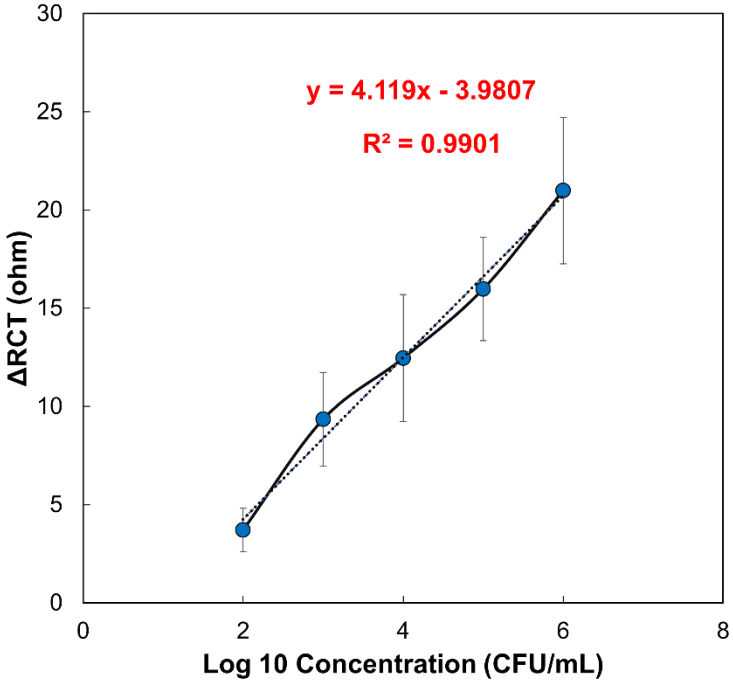

Figure 5.1: Response to different concentrations of target pathogen in chicken broth in the presence and absence of phage (a) Nyquist plots show impedance response to varying concentrations of the target analyte *L. monocytogenes* Scott A in chicken broth in the

presence of phage (b) Nyquist plots show impedance response to varying concentrations of the target analyte *L. monocytogenes* Scott A in chicken broth in the absence of phage (c) Calibration curve showing a linear relationship between the differential charge transfer resistance ΔR_{CT} (ohm) and the logarithmic of *L. monocytogenes* Scott A concentration in the phage modified electrode (d) Calibration curve showing a non-linear relationship between the differential charge transfer resistance ΔR_{CT} (ohm) and the logarithmic of *L. monocytogenes* Scott A concentration in the absence of phage on the electrode.

(a)

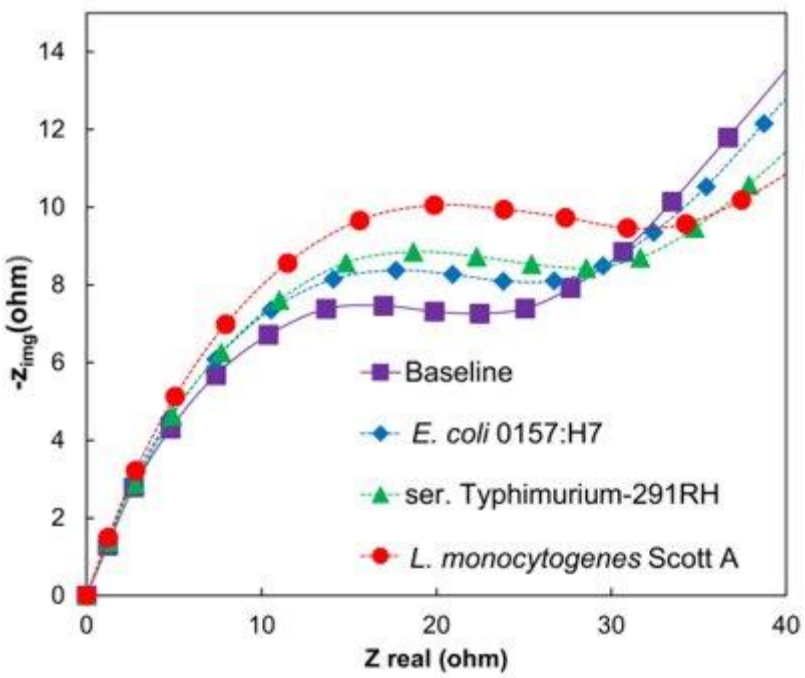
14
12
10
8
6
4
2
0
0
10
20
30
40
-z_img(ohm)
Z real (ohm)
Baseline
E. coli 0157:H7
ser. Typhimurium-291RH
L. monocytogenes Scott A

(b)

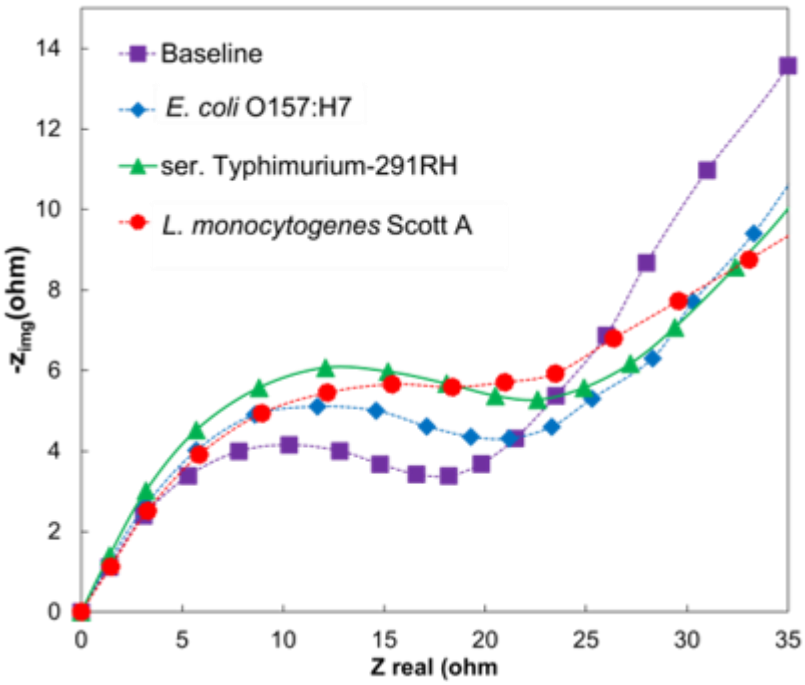
14
12
10
8
6
4
2
0
0
5
10
15
20
25
30
35
-z_img(ohm)
Z real (ohm
Baseline
E. coli O157:H7
ser. Typhimurium-291RH
L. monocytogenes Scott A

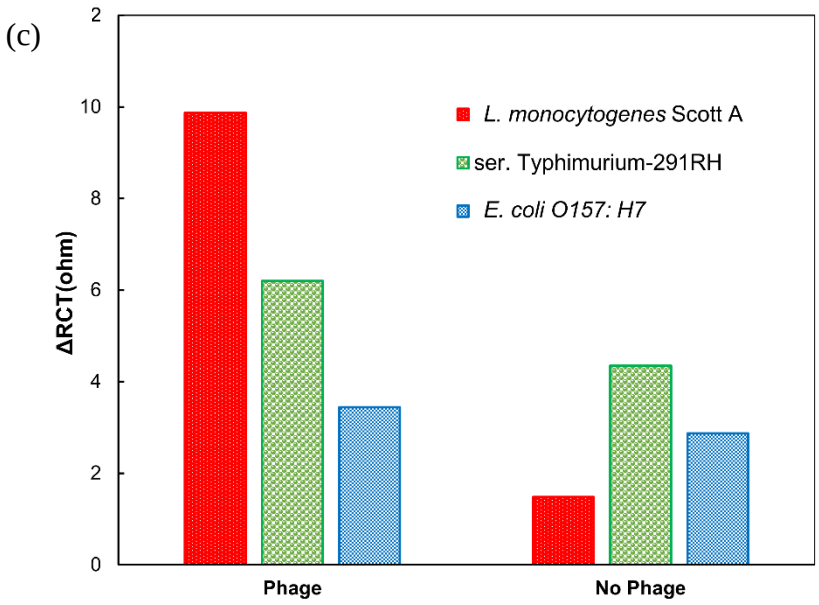

Figure 5.2: Response to target and non-target pathogens in chicken broth in the presence and absence of phage (a) Nyquist plot of the impedimetric response to target and non-target bacterial cells in the presence of phage (b) Nyquist plot of the impedimetric response to target and non-target bacterial cells in the absence of phage (c) ΔR_{CT} (ohm) values of the response as the difference from baseline values with phage and no phage.

(a)

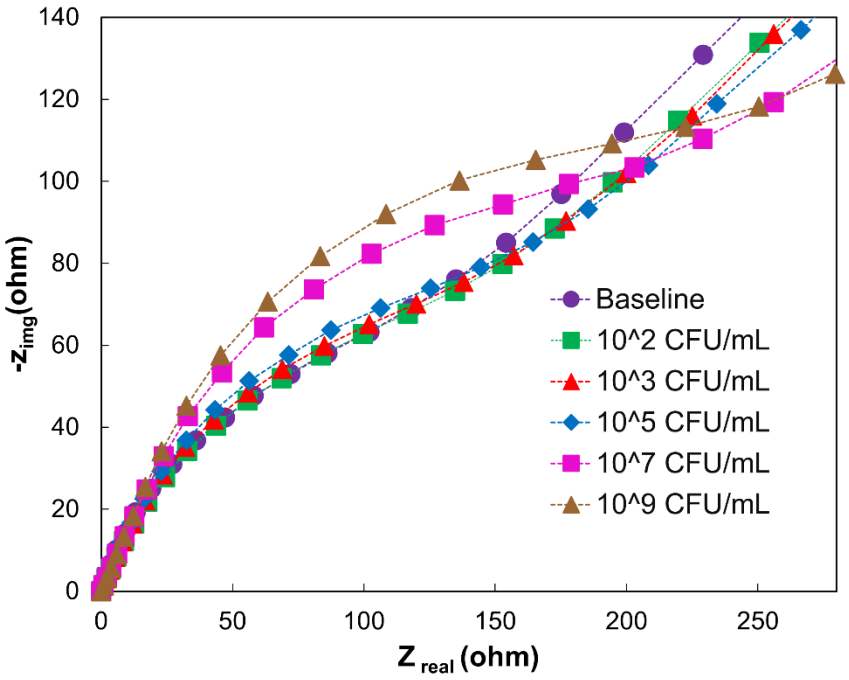
140
120
100
80
60
40
20
0
0
50
100
150
200
250
-Z img (ohm)
Z real (ohm)
Baseline
10^2 CFU/mL
10^3 CFU/mL
10^5 CFU/mL
10^7 CFU/mL
10^9 CFU/mL

(b)

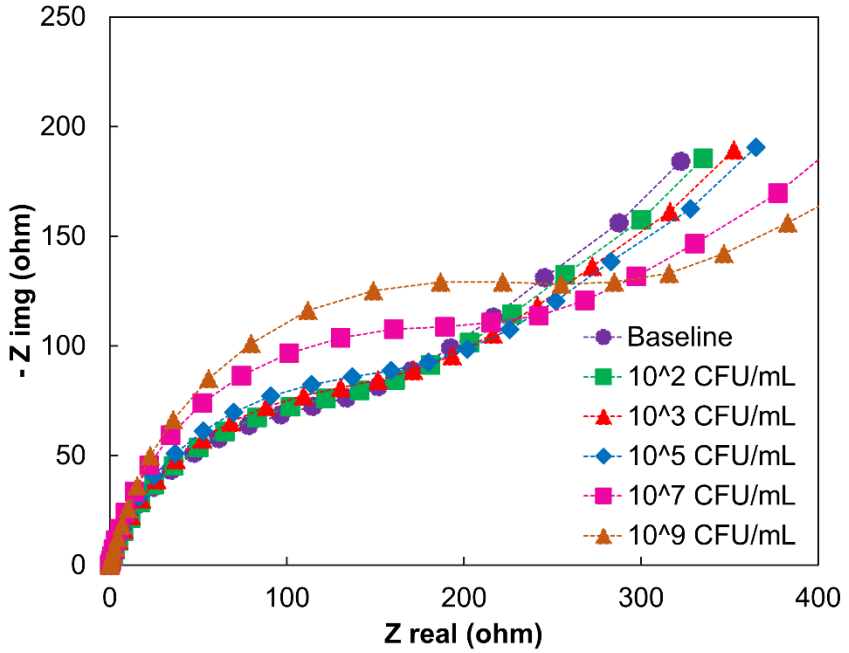
250
200
150
100
50
0
0
100
200
300
400
- Z img (ohm)
Z real (ohm)
Baseline
10^2 CFU/mL
10^3 CFU/mL
10^5 CFU/mL
10^7 CFU/mL
10^9 CFU/mL

(c)

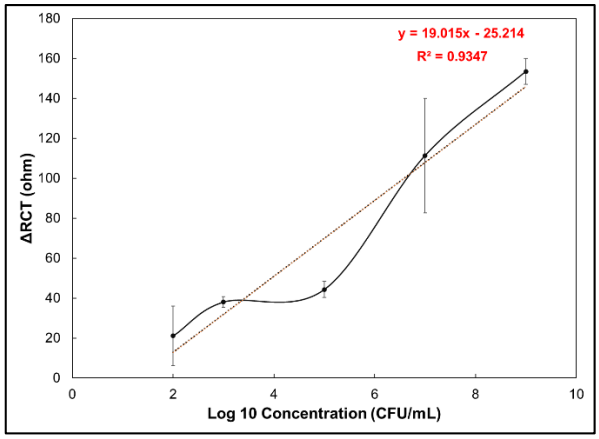

(d)

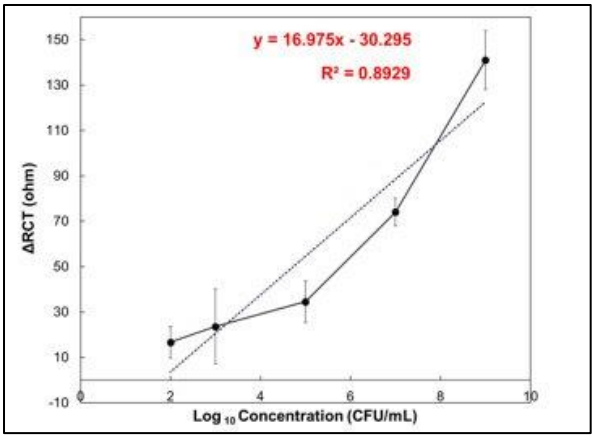

Figure 5.3: Response to different concentrations of target pathogen in the chicken cecal sample in the presence and absence of phage protein (a) Nyquist plots show impedance response to varying concentrations of the target analyte *C. jejuni* 11168 in the chicken cecal sample in the presence of phage protein (b) Nyquist plots show impedance response to varying concentrations of the target analyte *C. jejuni* 11168 in the chicken cecal sample in the absence of phage protein (c) Calibration curve showing a linear relationship between the differential charge transfer resistance ΔR_{CT} (ohm) and the logarithmic of concentration *C. jejuni* 11168 in the presence of phage protein on the electrode. (d) Calibration curve showing a linear relationship between the differential charge transfer resistance ΔR_{CT}

(ohm) and the logarithmic concentration *C. jejuni* 11168 in the absence of phage protein on the electrode.

(a)

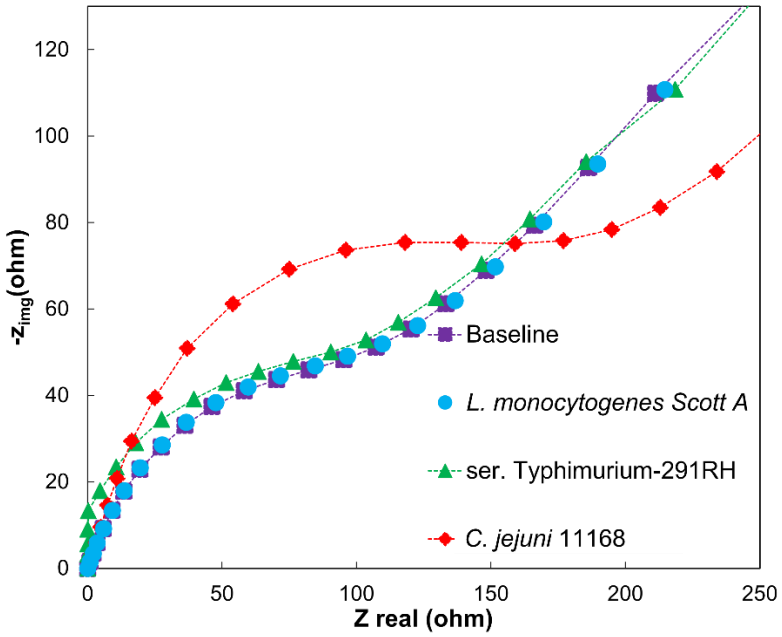
120
100
80
60
40
20
0
-z_img(ohm)
0
50
100
150
200
250
Z real (ohm)
Baseline
L. monocytogenes Scott A
ser. Typhimurium-291RH
C. jejuni 11168

(b)

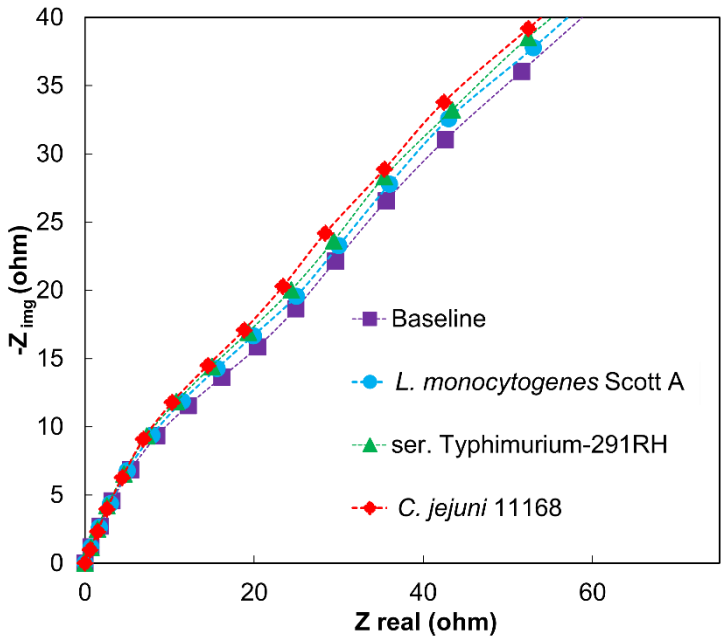
40
35
30
25
20
15
10
5
0
-Z img (ohm)
0
20
40
60
Z real (ohm)
Baseline
L. monocytogenes Scott A
ser. Typhimurium-291RH
C. jejuni 11168

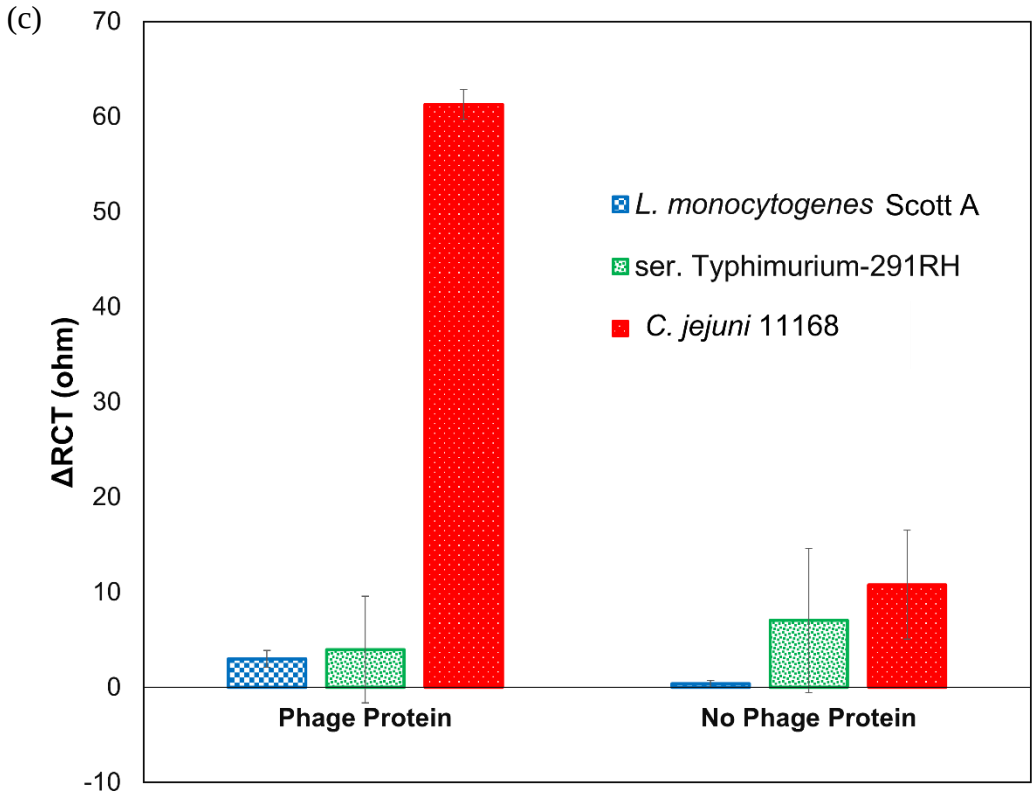

Figure 5.4: Response to target and non-target pathogens in the presence and absence of phage protein (a) Nyquist plot of the impedimetric response to target and non-target bacterial cells in the presence of phage protein (a) Nyquist plot of the impedimetric response to target and non-target bacterial cells in the absence of phage protein (c) ΔR_{CT} (ohm) values of the response as the difference from baseline values with phage protein and no phage protein.

CHAPTER 6

CONCLUSIONS AND FUTURE DIRECTIONS

Identifying bacterial pathogens on time is crucial in clinical, food safety, and environmental monitoring and interventions. Worldwide, bacterial infections frequently lead to morbidity and mortality. Despite the availability of medications, many illnesses frequently go undetected or are discovered with unacceptable delays. Current bacterial detection techniques rely on lab-based approaches such as cell culture, microscopic examination, and biochemical testing. Even though predominant conventional detection methods are highly reliable, they are time-consuming and expensive and demand specialized tools and experienced operators. The identification process typically requires 24 hours to several days, depending on the nature of the clinical or food sample and the type of target bacteria. This longer testing time creates major issues in the food and health sectors. Therefore, rapid identification of these bacteria is important. This dissertation is focused on developing sensor-based electrochemical methods to detect these bacterial cells in a short time. Biosensors are advantageous as they offer rapid responses toward their specific target analyte. Electrochemical biosensors are especially advantageous in terms of simplicity, sensitivity, and fast responses. Phage-based or phage protein-based biosensors are emerging as viable alternatives for nucleic acid and antibody-based biosensors. Bacteriophages are considered highly specific molecules for bacterial detection. In

addition, most phages use receptor-binding proteins on tail fiber attachment towards a specific receptor on the bacterial surface. This interaction is important for the specificity of a phage towards a specific host.

We developed phage-based and phage protein-based impedimetric biosensor architectures to detect bacterial cells. Further, these two architectures could detect any bacterial cells present in clinical, food, and environmental samples with high selectivity and sensitivity within a short duration. As proof of concept, the Listeria monocytogenes Scott A was used as a model analyte for the phage-based impedimetric biosensor architecture, and the P100 LISTEX phage was used as a bioreceptor molecule. The carbon nanotubes were functionalized with quarternized polyethyleneimine (q-CNT) to aid in a charge-directed oriented immobilization of phages on the electrode to detect *L. monocytogenes* Scott A. q-CNT was used to enhance the charge of the carbon nanotubes to facilitate the charge–directed orientation of the phages on the electrode. Further, a 0.01 % bovine serum albumin (BSA) blocking agent was used to block the surfaces in the electrode to avoid non-specific binding. Results revealed that the developed phage-based biosensor, under optimal conditions, gave a linear response from 10 to 10^4 CFU/mL, with good reproducibility. The sensor showed a detection limit of 8.4 CFU/mL in PBS buffer and 100 CFU/mL in a chicken broth sample. The biosensor exhibits good specificity for *L. monocytogenes* Scott A, but more work needs to be done on non-selective binding between the electrode and non-target analytes. The novelty of this work is the utilization of highly positively charged q-CNT in the immobilization of phages. Increased charge results from this method would allow more charged bioreceptor molecules and, thereby, the detection's sensitivity. So far, no one has reported the utilization of q-CNT for any biosensor immobilization process. In

addition, I believe a highly charged CNT architecture could be used to immobilize any charged bioreceptor molecules on a transducer surface. So, this concept could be used in various applications with charged bioreceptors. Our study is the first to develop an impedimetric phage-based biosensor to detect *L. monocytogenes.* This method would rapidly detect *L. monocytogenes* at 10^2 CFU/mL, which is on par with the industrial norm. Further, no one has reported using the food samples directly on the phage-based impedimetric biosensor to detect *L. monocytogenes*.

As a proof of concept for a phage protein-based impedimetric electrochemical sensor architecture, *C. jejuni* was used as a model analyte, and *Campylobacter* phage NCTC 12673 protein called CC-FlaGrab (formerly Gp047 & Gp48) was used as a bioreceptor molecule. The sensor was developed by immobilizing the phage protein on an MWCNT-modified glassy carbon electrode using a crosslinker 1-pyrenebutanoic acid succinimidyl ester (PBSE) to covalently attach the GST tag associated with the protein to the electrode surface. This process would allow us to orient protein correctly and use a strong chemical bond to minimize the leaching without significantly altering protein properties. Further, a 0.1 % bovine serum albumin (BSA) blocking agent was used to block the surfaces in the electrode to avoid non-specific binding. Results revealed that the developed novel impedimetric biosensor to detect *C. jejuni* using a phage protein exhibited high specificity with a low limit of detection of 10^2 CFU/mL, which is well below the standard. The biosensor responded linearly from 10^2 to 10^7 CFU/mL under ideal circumstances, with good reproducibility and stability.

Further, the sensor also showed a detection limit of 10^2 CFU/mL in a cecal sample. The biosensor exhibits good specificity for *C. jejuni*, but more work needs to be done to increase

the electrode's sensitivity. Furthermore, the phage protein-based biosensors developed in this work would be ideal for rapid diagnostic applications.

This is the first reported impedimetric phage-based detection method to detect *C. jejuni* in simulated samples. Even though the *Campylobacter* phage protein-based detection method for *C. jejuni* using a surface plasma resonance (SPR) sensor system has been reported, the requirement of sophisticated SPR equipment makes that approach expensive. Our impedimetric-based biosensor architecture to detect bacterial cells would be user-friendly and cost-effective compared to SPR-based methods.

The following path could be taken for future research on these topics based on the scope of the research discussed in this dissertation.

01. Phage offers the specificity required for the target we used for identification. However, the specificity could be increased by reducing the non-specific attachment of non-target pathogens on the electrode surface. It is necessary to investigate additional surface-blocking molecules or to include a biocide to repel non-target bacterial cells. In addition, further research needs to be carried out on more simulated samples.

02. The developed phage-protein-based biosensor provides an extraordinary specificity against the target bacteria we have used, even in a complex simulated sample. However, further research needs to be carried out to increase the sensitivity of the phage protein-based biosensor. Investigating with a higher concentration of phage protein than the concentration used in this study is necessary. Further, research must be carried out with very low concentrations (< 100 CFU/mL) of the target bacteria to achieve a lower detection limit than 100 CFU/mL. In addition, further research needs to be carried out in more simulated samples.

03. Developed phage and phage protein-based architectures to detect bacterial cells in a glassy carbon electrode. However, these two architectures should be converted to a screen-printed electrode setup to make the system portable. Further, the screen-printed electrode could be combined with a microfluidic device and create a Lab-on-a-chip architecture, which helps to minimize the pretreatment process needed for the food/clinic or environmental samples before feeding into the electrochemical system. In addition, the Lab-on-a-chip setup makes the detection process easy to use and portable and eliminates the need for specially trained personnel or any need for additional expensive equipment.

We developed phage and phage protein-based architectures to detect bacterial cells. We believe these architectures could detect any bacterial cells present in clinical, food, and environmental samples with high selectivity and sensitivity within a short time. Table 6.1 summarizes the availability of possible bacteriophages and phage-based proteins to be used using the proposed biosensor setup to detect all the other bacterial cells.

Table 6.1: Currently available phages/phage particles to be used as a bioreceptor in a biosensor

Target bacteria	Serotypes/ Strains	Name of phage product	Nature of phage product		Efficacy	Source of phage	The commercial product (Company)	Reference
			Whole phage	Phage component				
Staphylococcus aureus	Sa9	vB_SauS-phiIPLA35	Yes	-	100%	Dairy environment	-	[369]
Staphylococcus aureus (MRSA and MSSA)	46106	Phage Sb-1	Yes	-	100%	Eliava Institute	-	[370]
Staphylococcus aureus (MRSA and MSSA)	MRSA (N315, COL, Mu50) ATCC 6538	Phage K and Phage 92	Yes	-	100%	ATCC	Bacteriophages K and 92 (ATCC)	[371]
Staphylococcus aureus (MRSA)	MRSA USA300	Phage SATA-8505	Yes		100 %	ATCC	SATA-8505 (ATCC)	[282]
Staphylococcus aureus (VRSA)	-	Phage SATA-8505	Yes	-	100%	ATCC	SATA-8505 (ATCC)	[372]
Staphylococcus aureus (MRSA)	NRS382	Endolysins 80α, LysK, lysostaphin or WMY	-	Yes	100%	Recombinant protein	-	[373]

Listeria monocytogenes	WSLC 1001	Phage P100	Yes	-	100%	Dairy plant sewage effluent	PhageGuard Listex™ (Micreos Food Safety)	[374]
Listeria monocytogenes	-	Cocktail of 6 phages: LIST-36, LMSP-25, LMTA-34, LMTA-57, LMTA-94, LMTA-148	Yes	-	-	-	ListShield™ (Intralytix, Inc)	[375]
Escherichia coli	O157:H7 STEC	Coliphages DT1 and DT6	Yes	-	100%	Feces	-	[376]
Escherichia coli	BL21	T7 bacteriophage	Yes	-	99.9%	-	-	[377]
Escherichia coli	STEC and EHEC	CA911, CA933P, MFA933P and MFA45D	Yes	-	100%	Minced meat, pork sausage & bovine feces	-	[377]
Escherichia coli	O157:H7	ECML-4, ECML-117 and ECML-134	Yes	-	-	Fresh and salt water environments	EcoShield™ (Intralytix, Inc)	[378]

Escherichia coli	O157:H7	Cocktail of Phages pp01,e11/2 and e4/1c	Yes	-	-	Bovine farmyard slurry samples and Tokyo Institute of Technology	-	[379]
Escherichia coli biofilms	11303	T4 bacteriophage	Yes	-	100%	LGC Standards, Middlesex, UK	11303-B4 (ATCC)	[380]
Escherichia coli	K-12	Tail protein J from phage lambda	-	Yes	-	Recombinant protein	-	[381]
Escherichia coli	K1 strain A192PP	Capsule depolymerizing enzyme endosialidase E (endoE)	-	Yes	-	Recombinant protein	-	[382]
Lactobacillus brevis	8840 (NCIMB culture collection)	Myophage SA-C12	Yes	-		100 %	Fresh silage	[383]
Yersinia enterocolitica	O:3 strain 6471/76 and O:9 strain Ruokola/71	fHe-Yen3-01 (Podoviridae) fHe-Yen9-01, fHe-Yen9-02, fHe-	Yes	-	100%	Sewage	-	[384]

		Yen9-03 (Myoviridae)						
Salmonella enterica subsp.	Enterica serovar Typhimurium ATCC 14,028	BFSE16, BFSE18, PaDTA1, PaDTA9,PaDTA10 and PaDTA11	Yes	-	100%	Chicken feces, poultry exudates, and swine feces	-	[385]
Salmonella	Serovars Heidelberg, Enteritidis, and Typhimurium	Cocktail of two phages Fo1a and S16	Yes	-	-	-	PhageGuard S™ (PhageGuard)	[386]
Salmonella enterica subsp.	Serovar Typhimurium	Det7 phage tail protein (Det7T)	-	Yes	-	-	-	[328]
Salmonella enterica subsp.	Serovar Typhimurium	Long tail fiber (LTF) from phage S16	-	Yes	-	-	-	[387]
Salmonella enterica subsp.	serovar Typhimurium	Tail spike receptor binding protein from phage P22	-	Yes	-	Recombinant protein	-	[387]
Pseudomonas aeruginosa	-	ϕR18 and ΦS12-1	Yes	-	100%	Sewage	-	[388]

Pseudomonas aeruginosa biofilms	-	phage M4	Yes	-	99.90%	Health Protection Agency, Colindale, United Kingdom	-	[389]
Pseudomonas aeruginosa (Multi-drug resistant)	-	PA Phage cocktail (Pyophage #051007)	Yes	-	100%	Eliava Institute	-	[390]
Pseudomonas aeruginosa (Multi-drug resistant)	PAR50	PA-PP	-	Yes	-	Diabetic foot ulcers	-	[391]
Pseudomonas aeruginosa	PAO1, Br667, PA14	LoGT-008 endolysin (Artilysin)	-	Yes	-	Recombinant protein	-	[392]
Vibrio cholerae	AC 53, AC2846, and AC4653	Phages ICP1, ICP2, and ICP3	Yes	-	100%	Human feces	-	[393]
Klebsiella pneumoniae	B5055	Phage Kpn5	Yes	-	100%	Sewage	-	[394]
Campylobacter spp.	-	Type III phages NCTC 12672,	Yes	-	99%	Lohmann Animal	-	[395]

		12673, 12674, and 12678				Health, GmbH.		
Campylobacter jejuni	HPC5 GIIC8	Phage CP34	Yes	-	-	Retail Chicken	-	[396]
Campylobacter jejuni	GIIC8	Phage CP8	Yes	-	-	Retail Chicken	-	[396]
Campylobacter jejuni	2140CD1	Cocktail of 3 phages: phiCcoIBB35, phiCcoIBB37 and phiCcoIBB12	Yes	-	-	Free Range Chickens	-	[396]
C. jejuni and C. coli	*C. jejuni* NCTC11168 *and C. coli RM2228*	Receptor binding protein Gp047 of phage NCTC12673	-	Yes	-	Recombinant protein	-	[239]
Bacillus cereus	ATCC27348, ATCC21768, ATCC13061	BCP1-1 and BCP8-2	Yes	-	100%	Fermented food products	-	[397]

Bacillus anthracis and Bacillus cereus	-	PlyG lysin from γ phage	-	Yes	-	Recombinant protein	-	[398]
Bacillus anthracis	-	PlyPH lysin	-	Yes	-	-	-	[399]
Streptococcus pyogenes	-	PlyC (formerly C1) lysin	-	Yes	-	-	-	[400]
Streptococcus pyogenes	-	PlyPy lysin	-	Yes	-	Recombinant protein	-	[401]
Streptococcus pneumoniae	-	Pal lysin	-	Yes	-	Recombinant protein	-	[402]

REFERENCES

1. Butler, J.E., N.D. Young, and D.R. Lovley, *Evolution of electron transfer out of the cell: comparative genomics of six Geobacter genomes.* BMC genomics, 2010. **11**(1): p. 1-12.
2. Villano, M., et al., *Electrochemically assisted methane production in a biofilm reactor.* Journal of Power Sources, 2011. **196**(22): p. 9467-9472.
3. ElMekawy, A., et al., *Food and agricultural wastes as substrates for bioelectrochemical system (BES): the synchronized recovery of sustainable energy and waste treatment.* Food Research International, 2015. **73**: p. 213-225.
4. Logan, B.E., et al., *Microbial fuel cells: methodology and technology.* Environmental science & technology, 2006. **40**(17): p. 5181-5192.
5. Fornero, J.J., M. Rosenbaum, and L.T. Angenent, *Electric power generation from municipal, food, and animal wastewaters using microbial fuel cells.* Electroanalysis: An International Journal Devoted to Fundamental and Practical Aspects of Electroanalysis, 2010. **22**(7-8): p. 832-843.
6. Liu, H., S. Cheng, and B.E. Logan, *Production of electricity from acetate or butyrate using a single-chamber microbial fuel cell.* Environmental science & technology, 2005. **39**(2): p. 658-662.

7. Ren, Z., T.E. Ward, and J.M. Regan, *Electricity production from cellulose in a microbial fuel cell using a defined binary culture.* Environmental science & technology, 2007. **41**(13): p. 4781-4786.

8. Logan, B.E., et al., *Microbial electrolysis cells for high yield hydrogen gas production from organic matter.* Environmental science & technology, 2008. **42**(23): p. 8630-8640.

9. Liu, H., et al., *Microbial electrolysis: novel technology for hydrogen production from biomass.* Biofuels, 2010. **1**(1): p. 129-142.

10. Cheng, S., et al., *Direct biological conversion of electrical current into methane by electromethanogenesis.* Environmental science & technology, 2009. **43**(10): p. 3953-3958.

11. Aulenta, F., et al., *Trichloroethene dechlorination and H2 evolution are alternative biological pathways of electric charge utilization by a dechlorinating culture in a bioelectrochemical system.* Environmental science & technology, 2008. **42**(16): p. 6185-6190.

12. Gregory, K.B. and D.R. Lovley, *Remediation and recovery of uranium from contaminated subsurface environments with electrodes.* Environmental science & technology, 2005. **39**(22): p. 8943-8947.

13. Butler, C.S., et al., *Bioelectrochemical perchlorate reduction in a microbial fuel cell.* Environmental science & technology, 2010. **44**(12): p. 4685-4691.

14. Lovley, D.R. and K.P. Nevin, *A shift in the current: new applications and concepts for microbe-electrode electron exchange.* Current opinion in biotechnology, 2011. **22**(3): p. 441-448.

15. Mehanna, M., et al., *Microbial electrodialysis cell for simultaneous water desalination and hydrogen gas production.* Environmental science & technology, 2010. **44**(24): p. 9578-9583.

16. Jacobson, K.S., D.M. Drew, and Z. He, *Use of a liter-scale microbial desalination cell as a platform to study bioelectrochemical desalination with salt solution or artificial seawater.* Environmental science & technology, 2011. **45**(10): p. 4652-4657.

17. Luo, H., P.E. Jenkins, and Z. Ren, *Concurrent desalination and hydrogen generation using microbial electrolysis and desalination cells.* Environmental science & technology, 2011. **45**(1): p. 340-344.

18. Chae, K.-J., et al., *A solar-powered microbial electrolysis cell with a platinum catalyst-free cathode to produce hydrogen.* Environmental science & technology, 2009. **43**(24): p. 9525-9530.

19. *THE WORLD COUNTS*. September, 18 2022]; Available from: https://www.theworldcounts.com/challenges/climate-change/energy/global-energy-consumption.

20. Resch, G., et al., *Potentials and prospects for renewable energies at global scale.* Energy policy, 2008. **36**(11): p. 4048-4056.

21. Potter, M.C., *Electrical effects accompanying the decomposition of organic compounds.* Proceedings of the Royal Society of London. Series B, Containing Papers of a Biological Character, 1911. **84**(571): p. 260-276.

22. Kim, B.H., et al., *Mediator-less biofuel cell*. 1999, Google Patents.

23. Beegle, J. and A. Borole, *Chapter 11–Exoelectrogens for Microbial Fuel Cells*.* MFC, ed. PP Kundu and K. Dutta, Elsevier, 2018: p. 193-230.

24. Logan, B.E., *Exoelectrogenic bacteria that power microbial fuel cells.* Nature Reviews Microbiology, 2009. **7**(5): p. 375-381.

25. Sekar, N., et al., *Electricity generation by Pyrococcus furiosus in microbial fuel cells operated at 90 C.* Biotechnology and Bioengineering, 2017. **114**(7): p. 1419-1427.

26. Sekar, N., et al., *Exploring extracellular electron transfer in hyperthermophiles for electrochemical energy conversion.* ECS Transactions, 2016. **72**(30): p. 1.

27. Berk, R.S. and J.H. Canfield, *Bioelectrochemical energy conversion.* Applied microbiology, 1964. **12**(1): p. 10-12.

28. Gorby, Y.A., et al., *Electrically conductive bacterial nanowires produced by Shewanella oneidensis strain MR-1 and other microorganisms.* Proceedings of the National Academy of Sciences, 2006. **103**(30): p. 11358-11363.

29. Prasad, D., et al., *Direct electron transfer with yeast cells and construction of a mediatorless microbial fuel cell.* Biosensors and Bioelectronics, 2007. **22**(11): p. 2604-2610.

30. Habermüller, K., M. Mosbach, and W. Schuhmann, *Electron-transfer mechanisms in amperometric biosensors.* Fresenius' journal of analytical chemistry, 2000. **366**(6): p. 560-568.

31. Schachinger, F., et al., *Amperometric biosensors based on direct electron transfer enzymes.* Molecules, 2021. **26**(15): p. 4525.

32. Harnisch, F. and D. Holtmann, *Bioelectrosynthesis*. Vol. 490. 2019: Springer.

33. Hassan, R.Y., F. Febbraio, and S. Andreescu, *Microbial electrochemical systems: Principles, construction and biosensing applications.* Sensors, 2021. **21**(4): p. 1279.

34. Ikeda, T. and K. Kano, *Bioelectrocatalysis-based application of quinoproteins and quinoprotein-containing bacterial cells in biosensors and biofuel cells.* Biochimica et Biophysica Acta (BBA)-Proteins and Proteomics, 2003. **1647**(1-2): p. 121-126.

35. Shi, L., et al., *Extracellular electron transfer mechanisms between microorganisms and minerals.* Nature Reviews Microbiology, 2016. **14**(10): p. 651-662.

36. Carmona-Martinez, A.A., et al., *Cyclic voltammetric analysis of the electron transfer of Shewanella oneidensis MR-1 and nanofilament and cytochrome knock-out mutants.* Bioelectrochemistry, 2011. **81**(2): p. 74-80.

37. Xu, S., et al., *Multiheme cytochrome mediated redox conduction through Shewanella oneidensis MR-1 cells.* Journal of the American Chemical Society, 2018. **140**(32): p. 10085-10089.

38. Subramanian, P., et al., *Ultrastructure of Shewanella oneidensis MR-1 nanowires revealed by electron cryotomography.* Proceedings of the National Academy of Sciences, 2018. **115**(14): p. E3246-E3255.

39. Myers, C.R. and J.M. Myers, *Localization of cytochromes to the outer membrane of anaerobically grown Shewanella putrefaciens MR-1.* Journal of bacteriology, 1992. **174**(11): p. 3429-3438.

40. Malvankar, N.S. and D.R. Lovley, *Microbial nanowires for bioenergy applications.* Current Opinion in Biotechnology, 2014. **27**: p. 88-95.

41. Reguera, G., et al., *Extracellular electron transfer via microbial nanowires.* Nature, 2005. **435**(7045): p. 1098-1101.

42. Freire, R.S., et al., *Direct electron transfer: an approach for electrochemical biosensors with higher selectivity and sensitivity.* Journal of the Brazilian chemical society, 2003. **14**: p. 230-243.

43. Bollella, P. and E. Katz, *Enzyme-based biosensors: Tackling electron transfer issues.* Sensors, 2020. **20**(12): p. 3517.

44. Hernandez, C.A. and J.F. Osma, *Microbial electrochemical systems: deriving future trends from historical perspectives and characterization strategies.* Frontiers in Environmental Science, 2020. **8**: p. 44.

45. Pankratova, G. and L. Gorton, *Electrochemical communication between living cells and conductive surfaces.* Current Opinion in Electrochemistry, 2017. **5**(1): p. 193-202.

46. Wu, Y., et al., *Exogenous electron shuttle-mediated extracellular electron transfer of Shewanella putrefaciens 200: electrochemical parameters and thermodynamics.* Environmental Science & Technology, 2014. **48**(16): p. 9306-9314.

47. Schmitz, S. and M.A. Rosenbaum, *Boosting mediated electron transfer in bioelectrochemical systems with tailored defined microbial cocultures.* Biotechnology and bioengineering, 2018. **115**(9): p. 2183-2193.

48. Kwon, J., et al., *Rapid and Sensitive Detection of Aspergillus niger Using a Single-Mediator System Combined with Redox Cycling.* Analytical chemistry, 2018. **90**(22): p. 13491-13497.

49. Rawson, F.J., A.J. Downard, and K.H. Baronian, *Electrochemical detection of intracellular and cell membrane redox systems in Saccharomyces cerevisiae.* Scientific reports, 2014. **4**(1): p. 1-9.

50. Zhao, J., et al., *The different behaviors of three oxidative mediators in probing the redox activities of the yeast Saccharomyces cerevisiae.* Analytica chimica acta, 2007. **597**(1): p. 67-74.

51. Pirbadian, S., et al., *Shewanella oneidensis MR-1 nanowires are outer membrane and periplasmic extensions of the extracellular electron transport components.* Proceedings of the National Academy of Sciences, 2014. **111**(35): p. 12883-12888.

52. Elliott, J.R., et al., *Using simulations to guide the design of amperometric electrochemical sensors based on mediated electron transfer.* ChemElectroChem, 2020. **7**(13): p. 2797-2815.

53. Silveira, C.M. and M.G. Almeida, *Small electron-transfer proteins as mediators in enzymatic electrochemical biosensors.* Analytical and bioanalytical chemistry, 2013. **405**(11): p. 3619-3635.

54. Yagishita, T., T. Horigome, and K. Tanaka, *Effects of light, CO2 and inhibitors on the current output of biofuel cells containing the photosynthetic organism Synechococcus sp.* Journal of Chemical Technology & Biotechnology, 1993. **56**(4): p. 393-399.

55. Bombelli, P., et al., *Quantitative analysis of the factors limiting solar power transduction by Synechocystis sp. PCC 6803 in biological photovoltaic devices.* Energy & Environmental Science, 2011. **4**(11): p. 4690-4698.

56. Zou, Y., et al., *Photosynthetic microbial fuel cells with positive light response.* Biotechnology and bioengineering, 2009. **104**(5): p. 939-946.

57. Sekar, N., Y. Umasankar, and R.P. Ramasamy, *Photocurrent generation by immobilized cyanobacteria via direct electron transport in photo-bioelectrochemical cells.* Physical Chemistry Chemical Physics, 2014. **16**(17): p. 7862-7871.

58. Rosenbaum, M., U. Schröder, and F. Scholz, *Utilizing the green alga Chlamydomonas reinhardtii for microbial electricity generation: a living solar cell.* Applied microbiology and biotechnology, 2005. **68**(6): p. 753-756.

59. Velasquez-Orta, S.B., T.P. Curtis, and B.E. Logan, *Energy from algae using microbial fuel cells.* Biotechnology and bioengineering, 2009. **103**(6): p. 1068-1076.

60. Lea-Smith, D.J., et al., *Thylakoid terminal oxidases are essential for the cyanobacterium Synechocystis sp. PCC 6803 to survive rapidly changing light intensities.* Plant physiology, 2013. **162**(1): p. 484-495.

61. Sekar, N., et al., *Enhanced photo-bioelectrochemical energy conversion by genetically engineered cyanobacteria.* Biotechnology and bioengineering, 2016. **113**(3): p. 675-679.

62. Liu, H., S. Grot, and B.E. Logan, *Electrochemically assisted microbial production of hydrogen from acetate.* Environmental science & technology, 2005. **39**(11): p. 4317-4320.

63. Rozendal, R.A., et al., *Principle and perspectives of hydrogen production through biocatalyzed electrolysis.* International journal of hydrogen energy, 2006. **31**(12): p. 1632-1640.

64. Rozendal, R.A., et al., *Efficient hydrogen peroxide generation from organic matter in a bioelectrochemical system.* Electrochemistry Communications, 2009. **11**(9): p. 1752-1755.

65. Call, D. and B.E. Logan, *Hydrogen production in a single chamber microbial electrolysis cell lacking a membrane.* Environmental science & technology, 2008. **42**(9): p. 3401-3406.

66. Cheng, S. and B.E. Logan, *Sustainable and efficient biohydrogen production via electrohydrogenesis.* Proceedings of the National Academy of Sciences, 2007. **104**(47): p. 18871-18873.

67. Rozendal, R.A., et al., *Performance of single chamber biocatalyzed electrolysis with different types of ion exchange membranes.* Water research, 2007. **41**(9): p. 1984-1994.

68. Rozendal, R.A., et al., *Towards practical implementation of bioelectrochemical wastewater treatment.* Trends in biotechnology, 2008. **26**(8): p. 450-459.

69. Cheng, S. and B.E. Logan, *Evaluation of catalysts and membranes for high yield biohydrogen production via electrohydrogenesis in microbial electrolysis cells (MECs).* Water science and technology, 2008. **58**(4): p. 853-857.

70. Rozendal, R.A., et al., *Hydrogen production with a microbial biocathode.* Environmental science & technology, 2008. **42**(2): p. 629-634.

71. Mehanna, M., et al., *New hypotheses for hydrogenase implication in the corrosion of mild steel.* Electrochimica Acta, 2008. **54**(1): p. 140-147.

72. Brown, R.K., et al., *Combining hydrogen evolution and corrosion data-a case study on the economic viability of selected metal cathodes in microbial electrolysis cells.* Journal of Power Sources, 2017. **356**: p. 473-483.

73. Franco-Duarte, R., et al., *Advances in chemical and biological methods to identify microorganisms—from past to present.* Microorganisms, 2019. **7**(5): p. 130.

74. Rajapaksha, P., et al., *A review of methods for the detection of pathogenic microorganisms.* Analyst, 2019. **144**(2): p. 396-411.

75. Hassan, R.Y., et al., *Nanomaterials-based microbial sensor for direct electrochemical detection of Streptomyces Spp.* Sensors and Actuators B: Chemical, 2014. **203**: p. 848-853.

76. Hassan, R.Y. and U. Bilitewski, *Direct electrochemical determination of Candida albicans activity.* Biosensors and Bioelectronics, 2013. **49**: p. 192-198.

77. Hassan, R.Y., et al., *Carbon nanotube-based electrochemical biosensors for determination of Candida albicans's quorum sensing molecule.* Sensors and Actuators B: Chemical, 2017. **244**: p. 565-570.

78. Khater, D.Z., et al., *Development of bioelectrochemical system for monitoring the biodegradation performance of activated sludge.* Applied biochemistry and biotechnology, 2015. **175**(7): p. 3519-3530.

79. Mahmoud, R.H., et al., *Assisting the biofilm formation of exoelectrogens using nanostructured microbial fuel cells.* Journal of Electroanalytical Chemistry, 2018. **824**: p. 128-135.

80. Gao, G., et al., *A double-mediator based whole cell electrochemical biosensor for acute biotoxicity assessment of wastewater.* Talanta, 2017. **167**: p. 208-216.

81. Karube, I., T. Matsunaga, and S. Suzuki, *Microbioassay of nystatin with a yeast electrode.* Analytica chimica acta, 1979. **109**(1): p. 39-44.

82. Brownson, D.A., D.K. Kampouris, and C.E. Banks, *Graphene electrochemistry: fundamental concepts through to prominent applications.* Chemical Society Reviews, 2012. **41**(21): p. 6944-6976.

83. Qi, X., et al., *An electroactive biofilm-based biosensor for water safety: Pollutants detection and early-warning.* Biosensors and Bioelectronics, 2021. **173**: p. 112822.

84. Hassan, R.Y., et al., *A new disposable biosensor platform: carbon nanotube/poly (o-toluidine) nanocomposite for direct biosensing of urea.* Journal of Solid State Electrochemistry, 2018. **22**(6): p. 1817-1823.

85. Mustafa, F., R.Y. Hassan, and S. Andreescu, *Multifunctional nanotechnology-enabled sensors for rapid capture and detection of pathogens.* Sensors, 2017. **17**(9): p. 2121.

86. Hussein, H.A., et al., *Point-of-care diagnostics of COVID-19: from current work to future perspectives.* Sensors, 2020. **20**(15): p. 4289.

87. Qu, Y., et al., *Use of a coculture to enable current production by Geobacter sulfurreducens.* Applied and environmental microbiology, 2012. **78**(9): p. 3484-3487.

88. Commault, A.S., G. Lear, and R.J. Weld, *Maintenance of Geobacter-dominated biofilms in microbial fuel cells treating synthetic wastewater.* Bioelectrochemistry, 2015. **106**: p. 150-158.

89. Zhao, C.-e., et al., *Graphene/Au composites as an anode modifier for improving electricity generation in Shewanella-inoculated microbial fuel cells.* Analytical Methods, 2015. **7**(11): p. 4640-4644.

90. Lin, T., et al., *Engineered Shewanella oneidensis-reduced graphene oxide biohybrid with enhanced biosynthesis and transport of flavins enabled a highest bioelectricity output in microbial fuel cells.* Nano Energy, 2018. **50**: p. 639-648.

91. An, X., et al., *Engineering microbial consortia for high-performance cellulosic hydrolyzates-fed microbial fuel cells. Front Microbiol 5: 10*. 2019.

92. Fleischmann, C., et al., *Assessment of global incidence and mortality of hospital-treated sepsis. Current estimates and limitations.* American journal of respiratory and critical care medicine, 2016. **193**(3): p. 259-272.

93. DeAntonio, R., et al., *Epidemiology of community-acquired pneumonia and implications for vaccination of children living in developing and newly industrialized countries: A systematic literature review.* Human vaccines & immunotherapeutics, 2016. **12**(9): p. 2422-2440.

94. Torio, C.M. and B.J. Moore, *National inpatient hospital costs: the most expensive conditions by payer, 2013: statistical brief# 204.* 2016.

95. Ho, C.-S., et al., *Rapid identification of pathogenic bacteria using Raman spectroscopy and deep learning.* Nature communications, 2019. **10**(1): p. 1-8.

96. *Staphylococcus aureus in Healthcare Settings*. 2011 January 17, 2011 [cited 2022 Sep, 15 2022]; Available from: https://www.cdc.gov/hai/organisms/staph.html.

97. prevention, C.f.d.c.a. *National Outbreak Reporting System (NORS)*. 2019 [cited 2022 Oct 3,2022]; Available from: https://www.cdc.gov/nors/.

98. Scallan, E., et al., *Foodborne illness acquired in the United States—major pathogens.* Emerging infectious diseases, 2011. **17**(1): p. 7.

99. Hoffmann, S., *Cost estimates of foodborne illnesses.* 2014.

100. Feng, P., *Advanced techniques in food microbiology.* Food Microbiology: Fundamentals and Frontiers, pp. Doyle, MP, Beuchat, LR and Montville, TJ, Eds., ASM Press, Washington, DC, 2001.

101. Morin, K.H., *Food-borne illnesses: A continuing concern.* MCN: The American Journal of Maternal/Child Nursing, 2013. **38**(2): p. 120.

102. Hoorfar, J., *Rapid detection, characterization, and enumeration of foodborne pathogens.* Apmis, 2011. **119**: p. 1-24.

103. Mandal, P., et al., *Methods for rapid detection of foodborne pathogens: an overview.* Am. J. Food Technol, 2011. **6**(2): p. 87-102.

104. Feng, P., *Impact of molecular biology on the detection of foodborne pathogens.* Molecular biotechnology, 1997. **7**(3): p. 267.

105. FOOD, D. and D. ADMINISTRATION, *Bacteriological analytical manual*. 1995: AOAC International.

106. Notermans, S. and K. Wernars, *Immunological methods for detection of foodborne pathogens and their toxins.* International journal of food microbiology, 1991. **12**(1): p. 91-102.

107. Valderrama, W.B., et al., *Commercially available rapid methods for detection of selected food-borne pathogens.* Critical reviews in food science and nutrition, 2016. **56**(9): p. 1519-1531.

108. Landgraf, I.M., M.d.G.A. Alkmin, and M.d.F.P. Vieira, *Bacterial antigen detection in cerebrospinal fluid by the latex agglutination test.* Revista do Instituto de Medicina Tropical de São Paulo, 1995. **37**: p. 257-260.

109. Robinson, R.K., *Encyclopedia of food microbiology*. 2014: Academic press.

110. Goodridge, L., et al., *Strengths and shortcomings of advanced detection technologies*, in *Rapid Detection, Characterization, and Enumeration of Foodborne Pathogens*. 2011, American Society of Microbiology. p. 15-45.

111. Kumar, B.K., et al., *Development of monoclonal antibody based sandwich ELISA for the rapid detection of pathogenic Vibrio parahaemolyticus in seafood.* International journal of food microbiology, 2011. **145**(1): p. 244-249.

112. Sewell, A., et al., *The development of an efficient and rapid enzyme linked fluorescent assay method for the detection of Listeria spp. from foods.* International journal of food microbiology, 2003. **81**(2): p. 123-129.

113. Zeng, D., et al., *Advances and challenges in viability detection of foodborne pathogens.* Frontiers in microbiology, 2016. **7**: p. 1833.

114. Velusamy, V., et al., *An overview of foodborne pathogen detection: In the perspective of biosensors*. Biotechnology advances, 2010. **28**(2): p. 232-254.

115. Chen, J., et al., *Development and evaluation of a multiplex PCR for simultaneous detection of five foodborne pathogens.* Journal of applied microbiology, 2012. **112**(4): p. 823-830.

116. Zhou, B., et al., *Simultaneous detection of six food-borne pathogens by multiplex PCR with a GeXP analyzer*. Food control, 2013. **32**(1): p. 198-204.

117. Sheridan, G., et al., *Detection of mRNA by Reverse Transcription-PCR as an Indicator of Viability in Escherichia coliCells.* Appl. Environ. Microbiol., 1998. **64**(4): p. 1313-1318.

118. Yang, Q., K.J. Domesle, and B. Ge, *Loop-mediated isothermal amplification for Salmonella detection in food and feed: current applications and future directions.* Foodborne pathogens and disease, 2018. **15**(6): p. 309-331.

119. Mori, Y., et al., *Detection of loop-mediated isothermal amplification reaction by turbidity derived from magnesium pyrophosphate formation.* Biochemical and biophysical research communications, 2001. **289**(1): p. 150-154.

120. Malorny, B., et al., *Diagnostic real-time PCR for detection of Salmonella in food.* Appl. Environ. Microbiol., 2004. **70**(12): p. 7046-7052.

121. Ueda, S. and Y. Kuwabara, *The rapid detection of Salmonella from food samples by loop-mediated isothermal amplification (LAMP).* Biocontrol science, 2009. **14**(2): p. 73-76.

122. Bavisetty, S.C.B., et al., *Rapid pathogen detection tools in seafood safety.* Current Opinion in Food Science, 2018. **20**: p. 92-99.

123. Fukushima, H., et al., *Simultaneous screening of 24 target genes of foodborne pathogens in 35 foodborne outbreaks using multiplex real-time SYBR green PCR analysis.* International journal of microbiology, 2010. **2010**.

124. Liu, Y., et al., *Detection of 12 common food-borne bacterial pathogens by TaqMan real-time PCR using a single set of reaction conditions.* Frontiers in microbiology, 2019. **10**: p. 222.

125. Law, J.W.-F., et al., *Rapid methods for the detection of foodborne bacterial pathogens: principles, applications, advantages and limitations.* Frontiers in microbiology, 2015. **5**: p. 770.

126. Stern, A. and R. Sorek, *The phage-host arms race: shaping the evolution of microbes.* Bioessays, 2011. **33**(1): p. 43-51.

127. Singh, A., S. Poshtiban, and S. Evoy, *Recent advances in bacteriophage based biosensors for food-borne pathogen detection.* Sensors, 2013. **13**(2): p. 1763-1786.

128. Fernandes, S. and C. São-José, *Enzymes and mechanisms employed by tailed bacteriophages to breach the bacterial cell barriers.* Viruses, 2018. **10**(8): p. 396.

129. Janczuk, M., J. Niedziółka-Jönsson, and K. Szot-Karpińska, *Bacteriophages in electrochemistry: A review.* Journal of Electroanalytical Chemistry, 2016. **779**: p. 207-219.

130. Nicastro, J., et al., *Bacteriophage Applications-Historical Perspective and Future Potential*. 2016: Springer.

131. Hyman, P. and S.T. Abedon, *Bacteriophage host range and bacterial resistance*, in *Advances in applied microbiology*. 2010, Elsevier. p. 217-248.

132. Aliakbar Ahovan, Z., et al., *Bacteriophage based biosensors: trends, outcomes and challenges.* Nanomaterials, 2020. **10**(3): p. 501.

133. Farooq, U., et al., *Principle and development of phage-based biosensors.* Biosens. Environ. Monit, 2019.

134. Al-Hindi, R.R., et al., *Bacteriophage-Based Biosensors: A Platform for Detection of Foodborne Bacterial Pathogens from Food and Environment.* Biosensors, 2022. **12**(10): p. 905.

135. Jones, H.J., C.G. Shield, and B.M. Swift, *The Application of Bacteriophage Diagnostics for Bacterial Pathogens in the Agricultural Supply Chain: From Farm-to-Fork.* PHAGE, 2020. **1**(4): p. 176-188.

136. Singh, A., et al., *Immobilization of bacteriophages on gold surfaces for the specific capture of pathogens.* Biosensors and Bioelectronics, 2009. **24**(12): p. 3645-3651.

137. Nanduri, V., et al., *Phage as a molecular recognition element in biosensors immobilized by physical adsorption.* Biosensors and Bioelectronics, 2007. **22**(6): p. 986-992.

138. Ahn, S., et al., *Virus-based surface patterning of biological molecules, probes, and inorganic materials.* Colloids and Surfaces B: Biointerfaces, 2014. **122**: p. 851-856.

139. Cademartiri, R., et al., *Immobilization of bacteriophages on modified silica particles.* Biomaterials, 2010. **31**(7): p. 1904-1910.

140. Boratyński, J., et al., *Preparation of endotoxin-free bacteriophages.* Cell Mol Biol Lett, 2004. **9**(2): p. 253-9.

141. Naidoo, R., et al., *Surface-immobilization of chromatographically purified bacteriophages for the optimized capture of bacteria.* Bacteriophage, 2012. **2**(1): p. 15-24.

142. Lindberg, A., et al., *Interaction between bacteriophage Sf6 and Shigella flexner.* Journal of Virology, 1978. **27**(1): p. 38-44.

143. Singh, A., et al., *Bacteriophage tailspike proteins as molecular probes for sensitive and selective bacterial detection.* Biosensors and Bioelectronics, 2010. **26**(1): p. 131-138.

144. Lu, T.K., J. Bowers, and M.S. Koeris, *Advancing bacteriophage-based microbial diagnostics with synthetic biology.* Trends in biotechnology, 2013. **31**(6): p. 325-327.

145. Waddell, T.E. and C. Poppe, *Construction of mini-Tn 10luxABcam/Ptac-ATS and its use for developing a bacteriophage that transduces bioluminescence to Escherichia coli O157: H7.* FEMS microbiology letters, 2000. **182**(2): p. 285-289.

146. Kuhn, J., et al., *Detection of bacteria using foreign DNA: the development of a bacteriophage reagent for Salmonella.* International journal of food microbiology, 2002. **74**(3): p. 229-238.

147. Pagotto, F., M. Griffiths, and L. Brovko. *Phage-mediated detection of Staphylococcus aureus and Escherichia coli O157: H7 using bioluminescence*. in *Symposium on bacteriological quality of raw milk, Wolfpassing (Austria), 13-15 Mar 1996*. 1996. International Dairy Federation.

148. Loessner, M.J., et al., *Construction of luciferase reporter bacteriophage A511:: luxAB for rapid and sensitive detection of viable Listeria cells.* Appl. Environ. Microbiol., 1996. **62**(4): p. 1133-1140.

149. Harvey, D., et al., *Lysogenic phage in Salmonella enterica serovar Heidelberg (Salmonella Heidelberg): implications for organism tracing.* FEMS microbiology letters, 1993. **108**(3): p. 291-295.

150. Kim, J.-W., et al., *A novel restriction-modification system is responsible for temperature-dependent phage resistance in Listeria monocytogenes ECII.* Appl. Environ. Microbiol., 2012. **78**(6): p. 1995-2004.

151. Chopin, M.-C., A. Chopin, and E. Bidnenko, *Phage abortive infection in lactococci: variations on a theme.* Current opinion in microbiology, 2005. **8**(4): p. 473-479.

152. Barrangou, R. and P. Horvath, *CRISPR: new horizons in phage resistance and strain identification.* Annual review of food science and technology, 2012. **3**: p. 143-162.

153. Oechslin, F., *Resistance development to bacteriophages occurring during bacteriophage therapy.* Viruses, 2018. **10**(7): p. 351.

154. Senturk, E., et al., *Biosensors: a novel approach to detect food-borne pathogens.* Appl. Microbiol. Open Access, 2018. **4**: p. 1-8.

155. Balasubramanian, S., et al., *Lytic phage as a specific and selective probe for detection of Staphylococcus aureus—a surface plasmon resonance spectroscopic study.* Biosensors and Bioelectronics, 2007. **22**(6): p. 948-955.

156. Tawil, N., et al., *Surface plasmon resonance detection of E. coli and methicillin-resistant S. aureus using bacteriophages.* Biosensors and Bioelectronics, 2012. **37**(1): p. 24-29.

157. Singh, A., et al., *Specific detection of Campylobacter jejuni using the bacteriophage NCTC 12673 receptor binding protein as a probe.* Analyst, 2011. **136**(22): p. 4780-4786.

158. Blasco, R., et al., *Specific assays for bacteria using phage mediated release of adenylate kinase.* Journal of applied microbiology, 1998. **84**(4): p. 661-666.

159. Wu, Y., L. Brovko, and M. Griffiths, *Influence of phage population on the phage-mediated bioluminescent adenylate kinase (AK) assay for detection of bacteria.* Letters in applied microbiology, 2001. **33**(4): p. 311-315.

160. Dhull, N., et al., *Label-free amperometric biosensor for Escherichia coli O157: H7 detection.* Applied Surface Science, 2019. **495**: p. 143548.

161. Lojou, E. and P. Bianco, *Application of the electrochemical concepts and techniques to amperometric biosensor devices.* Journal of Electroceramics, 2006. **16**(1): p. 79-91.

162. Neufeld, T., et al., *Combined phage typing and amperometric detection of released enzymatic activity for the specific identification and quantification of bacteria.* Analytical chemistry, 2003. **75**(3): p. 580-585.

163. Guthy, C., et al., *Large-scale arrays of nanomechanical sensors for biomolecular fingerprinting.* Sensors and Actuators B: Chemical, 2013. **187**: p. 111-117.

164. Leiman, P.G. and M.M. Shneider, *Contractile tail machines of bacteriophages*, in *Viral Molecular Machines*. 2012, Springer. p. 93-114.

165. Casjens, S.R. and I.J. Molineux, *Short noncontractile tail machines: adsorption and DNA delivery by podoviruses,* in *Viral Molecular Machines*. 2012, Springer. p. 143-179.

166. Golshahi, L., et al., *In vitro lung delivery of bacteriophages KS4-M and ΦKZ using dry powder inhalers for treatment of Burkholderia cepacia complex and Pseudomonas aeruginosa infections in cystic fibrosis.* Journal of applied microbiology, 2011. **110**(1): p. 106-117.

167. Waseh, S., et al., *Orally administered P22 phage tailspike protein reduces Salmonella colonization in chickens: prospects of a novel therapy against bacterial infections.* PLoS One, 2010. **5**(11).

168. Kropinski, A.M., et al., *Genome and proteome of Campylobacter jejuni bacteriophage NCTC 12673.* Appl. Environ. Microbiol., 2011. **77**(23): p. 8265-8271.

169. Javed, M.A., et al., *A suggested classification for two groups of Campylobacter myoviruses.* Archives of virology, 2014. **159**(1): p. 181-190.

170. Javed, M.A., et al., *Bacteriophage receptor binding protein based assays for the simultaneous detection of Campylobacter jejuni and Campylobacter coli.* PLoS One, 2013. **8**(7).

171. Sacher, J.C., *Insights into the role of the flagellar glycosylation system in Campylobacter jejuni phage-host interactions.* 2018.

172. Prevention, C.f.D.C.a. *Campylobacter (Campylobacteriosis).* April, 13 2020; Available from: https://www.cdc.gov/campylobacter/guillain-barre.html.

173. Johnson, T.J., J.M. Shank, and J.G. Johnson, *Current and potential treatments for reducing Campylobacter colonization in animal hosts and disease in humans.* Frontiers in microbiology, 2017. **8**: p. 487.

174. Backert, S. and D. Hofreuter, *Molecular methods to investigate adhesion, transmigration, invasion and intracellular survival of the foodborne pathogen Campylobacter jejuni.* Journal of microbiological methods, 2013. **95**(1): p. 8-23.

175. Beeby, M., et al., *Diverse high-torque bacterial flagellar motors assemble wider stator rings using a conserved protein scaffold.* Proceedings of the National Academy of Sciences, 2016. **113**(13): p. E1917-E1926.

176. Gao, B., et al., *Novel components of the flagellar system in epsilonproteobacteria.* MBio, 2014. **5**(3): p. e01349-14.

177. Logan, S.M., *Flagellar glycosylation–a new component of the motility repertoire?* Microbiology, 2006. **152**(5): p. 1249-1262.

178. Sacher, J.C., et al., *Binding of phage-encoded FlaGrab to motile Campylobacter jejuni flagella inhibits growth, downregulates energy metabolism, and requires specific flagellar glycans.* Frontiers in microbiology, 2020. **11**: p. 397.

179. Janež, N., et al., *Identification and characterisation of new Campylobacter group III phages of animal origin.* FEMS microbiology letters, 2014. **359**(1): p. 64-71.

180. O'Sullivan, L., et al., *Comparative genomics of Cp8viruses with special reference to Campylobacter phage vB_CjeM_los1, isolated from a slaughterhouse in Ireland.* Archives of virology, 2018. **163**(8): p. 2139-2154.

181. Javed, M.A., et al., *A receptor-binding protein of C ampylobacter jejuni bacteriophage NCTC 12673 recognizes flagellin glycosylated with acetamidino-modified pseudaminic acid.* Molecular microbiology, 2015. **95**(1): p. 101-115.

182. Javed, M.A., et al., *A flagellar glycan-specific protein encoded by campylobacter phages inhibits host cell growth.* Viruses, 2015. **7**(12): p. 6661-6674.

183. Cabral, J., J. Kennedy, and R. Taylor, *Protein immobilization: Fundamentals and applications.* Ed. RF Taylor, Marcell Dekker Inc., New York, pág, 1991: p. 73-138.

184. Zoungrana, T., G.H. Findenegg, and W. Norde, *Structure, stability, and activity of adsorbed enzymes.* Journal of colloid and interface science, 1997. **190**(2): p. 437-448.

185. Nguyen, H.H., et al., *Immobilized enzymes in biosensor applications.* Materials, 2019. **12**(1): p. 121.

186. Nguyen, H.H. and M. Kim, *An overview of techniques in enzyme immobilization.* Applied Science and Convergence Technology, 2017. **26**(6): p. 157-163.

187. Reyes-De-Corcuera, J.I., H.E. Olstad, and R. García-Torres, *Stability and stabilization of enzyme biosensors: The key to successful application and commercialization.* Annual review of food science and technology, 2018. **9**: p. 293-322.

188. Singh, B. and B. Singh, *Biotechnology expanding horizons*. 2007: Kalyani publishers.

189. Datta, S., L.R. Christena, and Y.R.S. Rajaram, *Enzyme immobilization: an overview on techniques and support materials.* 3 Biotech, 2013. **3**(1): p. 1-9.

190. Castillo, R.R., D. Lozano, and M. Vallet-Regí, *Mesoporous silica nanoparticles as carriers for therapeutic biomolecules.* Pharmaceutics, 2020. **12**(5): p. 432.

191. Cai, D., et al., *Chitosan-capped enzyme-responsive hollow mesoporous silica nanoplatforms for colon-specific drug delivery.* Nanoscale Research Letters, 2020. **15**(1): p. 1-13.

192. Kim, J., H. Jia, and P. Wang, *Challenges in biocatalysis for enzyme-based biofuel cells.* Biotechnology advances, 2006. **24**(3): p. 296-308.

193. Dai, D. and L. Xia, *Effect of lipase immobilization on resolution of (R, S)-2-octanol in nonaqueous media using modified ultrastable-Y molecular sieve as support.* Applied biochemistry and biotechnology, 2006. **134**(1): p. 39-50.

194. Wang, Z.-G., et al., *Enzyme immobilization on electrospun polymer nanofibers: an overview.* Journal of Molecular Catalysis B: Enzymatic, 2009. **56**(4): p. 189-195.

195. Wen, H., et al., *Carbon fiber microelectrodes modified with carbon nanotubes as a new support for immobilization of glucose oxidase.* Microchimica Acta, 2011. **175**(3-4): p. 283-289.

196. De Corcuera, J.R., R. Cavalieri, and J. Powers, *Improved platinization conditions produce a 60-fold increase in sensitivity of amperometric biosensors using glucose oxidase immobilized in poly-o-phenylenediamine.* Journal of Electroanalytical Chemistry, 2005. **575**(2): p. 229-241.

197. Guisan, J.M., *Immobilization of enzymes and cells*. Vol. 22. 2006: Springer.

198. Homaei, A.A., et al., *Enzyme immobilization: an update.* Journal of chemical biology, 2013. **6**(4): p. 185-205.

199. Ramanavičius, A., A. Ramanavičienė, and A. Malinauskas, *Electrochemical sensors based on conducting polymer—polypyrrole.* Electrochimica acta, 2006. **51**(27): p. 6025-6037.

200. Geetha, S., et al., *Biosensing and drug delivery by polypyrrole.* Analytica Chimica Acta, 2006. **568**(1-2): p. 119-125.

201. Sen, T., S. Mishra, and N.G. Shimpi, *Synthesis and sensing applications of polyaniline nanocomposites: a review.* RSC advances, 2016. **6**(48): p. 42196-42222.

202. Mazeiko, V., et al., *Gold nanoparticle and conducting polymer-polyaniline-based nanocomposites for glucose biosensor design.* Sensors and Actuators B: Chemical, 2013. **189**: p. 187-193.

203. Lai, J., et al., *Polyaniline-based glucose biosensor: A review.* Journal of Electroanalytical Chemistry, 2016. **782**: p. 138-153.

204. Shoaie, N., et al., *Electrochemical sensors and biosensors based on the use of polyaniline and its nanocomposites: A review on recent advances.* Microchimica Acta, 2019. **186**(7): p. 1-29.

205. Wallace, G., M. Smyth, and H. Zhao, *Conducting electroactive polymer-based biosensors.* TrAC Trends in Analytical Chemistry, 1999. **18**(4): p. 245-251.

206. Novick, S.J. and J.D. Rozzell, *Immobilization of enzymes by covalent attachment*, in *Microbial enzymes and biotransformations*. 2005, Springer. p. 247-271.

207. D'souza, S., *Immobilized enzymes in bioprocess.* Current Science, 1999: p. 69-79.

208. Fu, J., J. Reinhold, and N.W. Woodbury, *Peptide-modified surfaces for enzyme immobilization.* PLoS One, 2011. **6**(4).

209. Betancor, L., et al., *Glutaraldehyde in protein immobilization*, in *Immobilization of enzymes and cells*. 2006, Springer. p. 57-64.

210. Nunes, G.S. and J.-L. Marty, *Immobilization of enzymes on electrodes*, in *Immobilization of Enzymes and Cells*. 2006, Springer. p. 239-250.

211. Ferretti, S., et al., *Self-assembled monolayers: a versatile tool for the formulation of bio-surfaces.* TrAC Trends in Analytical Chemistry, 2000. **19**(9): p. 530-540.

212. Samanta, D. and A. Sarkar, *Immobilization of bio-macromolecules on self-assembled monolayers: methods and sensor applications.* Chemical Society Reviews, 2011. **40**(5): p. 2567-2592.

213. Mandler, D. and S. Kraus-Ophir, *Self-assembled monolayers (SAMs) for electrochemical sensing.* Journal of Solid State Electrochemistry, 2011. **15**(7): p. 1535-1558.

214. Wink, T., et al., *Self-assembled monolayers for biosensors.* Analyst, 1997. **122**(4): p. 43R-50R.

215. Chen, D. and J. Li, *Interfacial design and functionization on metal electrodes through self-assembled monolayers.* Surface Science Reports, 2006. **61**(11): p. 445-463.

216. Taylor, R.F. and J.S. Schultz, *Handbook of chemical and biological sensors*. 1996: CRC Press.

217. Bilal, M., et al., *Multi-point enzyme immobilization, surface chemistry, and novel platforms: a paradigm shift in biocatalyst design.* Critical reviews in biotechnology, 2019. **39**(2): p. 202-219.

218. Hwang, E.T. and M.B. Gu, *Enzyme stabilization by nano/microsized hybrid materials.* Engineering in Life Sciences, 2013. **13**(1): p. 49-61.

219. Pal, K., A.T. Paulson, and D. Rousseau, *Biopolymers in controlled-release delivery systems*, in *Modern biopolymer science*. 2009, Elsevier. p. 519-557.

220. Migneault, I., et al., *Glutaraldehyde: behavior in aqueous solution, reaction with proteins, and application to enzyme crosslinking.* Biotechniques, 2004. **37**(5): p. 790-802.

221. Ma, B., et al., *Crosslinking strategies for preparation of extracellular matrix-derived cardiovascular scaffolds.* Regenerative biomaterials, 2014. **1**(1): p. 81-89.

222. Cheung, D.T. and M.E. Nimni, *Mechanism of crosslinking of proteins by glutaraldehyde I: reaction with model compounds.* Connective tissue research, 1982. **10**(2): p. 187-199.

223. Cheung, D.T., et al., *Mechanism of crosslinking of proteins by glutaraldehyde III. Reaction with collagen in tissues.* Connective Tissue Research, 1985. **13**(2): p. 109-115.

224. Barbosa, O., et al., *Glutaraldehyde in bio-catalysts design: A useful crosslinker and a versatile tool in enzyme immobilization.* Rsc Advances, 2014. **4**(4): p. 1583-1600.

225. Olde Damink, L., et al., *Glutaraldehyde as a crosslinking agent for collagen-based biomaterials.* Journal of materials science: materials in medicine, 1995. **6**(8): p. 460-472.

226. Ipek, Y., *Electrochemical behaviour of cross-linker glutaraldehyde as a receptor for carbaryl biosensor.* JOURNAL OF THE INDIAN CHEMICAL SOCIETY, 2020. **97**(11 A): p. 2218-2223.

227. Holzinger, M., A. Le Goff, and S. Cosnier, *Nanomaterials for biosensing applications: a review.* Frontiers in chemistry, 2014. **2**: p. 63.

228. Zhou, Y., Y. Umasankar, and R.P. Ramasamy, *Laccase-TiO2 nanoconjugates as catalysts for oxygen reduction reaction in biocathodes.* Journal of The Electrochemical Society, 2015. **162**(14): p. H911-H917.

229. Guo, X., *Surface plasmon resonance based biosensor technique: a review.* Journal of biophotonics, 2012. **5**(7): p. 483-501.

230. Ajayan, P., et al., *Opening carbon nanotubes with oxygen and implications for filling.* Nature, 1993. **362**(6420): p. 522-525.

231. Balasubramanian, K. and M. Burghard, *Chemically functionalized carbon nanotubes.* small, 2005. **1**(2): p. 180-192.

232. Zhao, Q., Z. Gan, and Q. Zhuang, *Electrochemical sensors based on carbon nanotubes.* Electroanalysis: An International Journal Devoted to Fundamental and Practical Aspects of Electroanalysis, 2002. **14**(23): p. 1609-1613.

233. Lawal, A.T., *Synthesis and utilization of carbon nanotubes for fabrication of electrochemical biosensors.* Materials Research Bulletin, 2016. **73**: p. 308-350.

234. Zhou, Y., Y. Fang, and R.P. Ramasamy, *Non-covalent functionalization of carbon nanotubes for electrochemical biosensor development.* Sensors, 2019. **19**(2): p. 392.

235. Li, S., et al., *Hydrogen peroxide biosensor based on gold nanoparticles/thionine/gold nanoparticles/multi-walled carbon nanotubes–chitosans composite film-modified electrode.* Applied Surface Science, 2012. **258**(7): p. 2802-2807.

236. Qiu, H., et al., *Adsorption of laccase on the surface of nanoporous gold and the direct electron transfer between them.* The Journal of Physical Chemistry C, 2008. **112**(38): p. 14781-14785.

237. Solanki, P.R., et al., *Nanostructured metal oxide-based biosensors.* NPG Asia Materials, 2011. **3**(1): p. 17-24.

238. Ansari, A.A., et al., *Nanostructured metal oxides based enzymatic electrochemical biosensors.* Biosensors, 2010: p. 302.

239. Javed, M.A., et al., *Bacteriophage receptor binding protein based assays for the simultaneous detection of Campylobacter jejuni and Campylobacter coli.* PLoS One, 2013. **8**(7): p. e69770.

240. Szymanski, C.M., et al., *Specific detection of Campylobacter jejuni using the bacteriophage NCTC 12673 receptor binding protein as a probe.* 2011.

241. Atalah, J., et al., *Improved stability of multicopper oxidase–carbon nanotube conjugates using a thermophilic laccase.* Catalysis Science & Technology, 2018. **8**(5): p. 1272-1276.

242. Ramasamy, R.P., et al., *High electrocatalytic activity of tethered multicopper oxidase–carbon nanotube conjugates.* Chemical Communications, 2010. **46**(33): p. 6045-6047.

243. Centers for Disease Control and Prevention. *MMWR Reports on Foodborne Illnesses and Outbreaks*. 2022 [cited 2022; Available from: https://www.cdc.gov/foodsafety/outbreaks/lists/mmwr-reports.html.

244. Centers for Disease Control and Prevention. *FoodNet Fast*. [cited 2022; Available from: https://wwwn.cdc.gov/FoodNetFast/PathogenSurveillance/AnnualSummary.

245. U.S. Food & Drug Administration. *CFSAN Education Resource Library*. 2021; Available from: https://www.fda.gov/food/resources-you-food/cfsan-education-resource-library.

246. Millipore Sigma. *TRANSIA™ AG EHEC*. [cited 2022 November 20, 2022]; Available from: https://www.sigmaaldrich.com/US/en/product/sial/4000bc.

247. Millipore Sigma. *Assurance® GDS E.coli O157:H7 Tq*. [cited 2022 November 20, 2022]; Available from: https://www.sigmaaldrich.com/deepweb/assets/sigmaaldrich/product/documents/652/346/gds-ecoli-dfu-ds5772en-ms.pdf.

248. DuPont. *DuPont™ BAX® System Real-Time PCR Assay E. coli O157:H7*. [cited 2022 November, 20 2022]; Available from: http://tools.thermofisher.com/content/sfs/manuals/RealTime%20Ecoli%20D14203648.pdf.

249. Hygiena. *BAX® System Real-Time PCR Assay E. coli O157:H7 Exact*. [cited 2022 November 20, 2022]; Available from: https://www.hygiena.com/wp-content/uploads/2021/04/BAX-Q7-Assay-Kit-Insert-Ecoli-Exact-EN.pdf.

250. FoodChek. *FoodChek™-E. coli O157 for the Detection of E. coli O157*. [cited 2022 November 20, 2022]; Available from: https://www.foodcheksystems.com/infosheets/FCEC/FoodChek-E%20coli%20O157%20FCEC-002%20Package%20Insert%20(version%20June%202013).pdf.

251. Miller, M., et al., *Vivione Bioscience RAPID-B® E. coli O157 Test Kit and non-O157 STEC Test Kit Evaluation.* Journal of AOAC International, 2015. **98**(2): p. 371-378.

252. Neogen. *Reveal® for E. coli O157:H7*. [cited 2022 November 20, 2022]; Available from: https://www.neogen.com/categories/microbiology/reveal-e-coli-o157-h7/#:~:text=The%20Reveal%C2%AE%20for%20E,hours%20for%2025%20g%20samples.

253. Jiang, Y., et al., *Validation of the TadpoleTM Campylobacter jejuni Real-Time PCR Identification Kit.* Journal of AOAC International, 2019. **102**(3): p. 842-854.

254. Millipore Sigma. *Molecular Detection for Rapid Food Pathogen Testing and Identification*. 2022; Available from: https://www.sigmaaldrich.com/US/en/technical-documents/technical-article/microbiological-testing/pathogen-and-spoilage-testing/assurance-gds-genetic-detection.

255. Wallace, F.M., et al., *DuPont Qualicon BAX® System Assay for Genus Listeria 24E.* Journal of AOAC International, 2011. **94**(3): p. 863-871.

256. DuPont. *DuPont™ BAX® System Real-Time PCR Assay L. monocytogenes*. 2014 [cited 2022 November 20, 2022]; Available from: http://tools.thermofisher.com/content/sfs/manuals/RT%20Lmonocytogenes%20D15134303.pdf.

257. Neogen. *Neogen's new 24-hour Listeria protocol receives AOAC approval*. 2006; Available from: https://www.neogen.com/neocenter/press-releases/neogens-new-24-hour-listeria-protocol-receives-aoac-approval/.

258. BioControl. *TRANSIA® PLATE Listeria*. [cited 2022 November 20, 2022]; Available from: https://jornades.uab.cat/workshopmrama/sites/jornades.uab.cat.workshopmrama/files/TRANSIA_PLATE_pathogenic_bacteria.pdf.

259. Neogen. *Reveal® 2.0 for Listeria*. [cited 2022 November 20, 2022]; Available from: https://www.neogen.com/categories/microbiology/reveal-2-listeria/.

260. Neogen. *Neogen's 24-hour GeneQuence® Salmonella Test receives AOAC status*. Available from: https://www.neogen.com/neocenter/press-releases/neogens-24-hour-genequence-salmonella-test-receives-aoac-status/.

261. Romer labs. *RapidChek SELECT™ Salmonella Test Kit*. [cited 2022 November 20, 2022]; Available from: https://www.foodriskmanagement.com/wp-content/uploads/2016/10/RapidChek-Select-Salmonella-Package-Insert_Origina_001.pdf.

262. Neogen. *Reveal® 2.0 for Salmonella*. [cited 2022 November 20, 2022]; Available from: https://www.neogen.com/categories/microbiology/reveal-2-salmonella/.

263. Millipore Sigma. *TRANSIA™ PLATE Salmonella Gold*. [cited 2022 November 20, 2022]; Available from: https://www.sigmaaldrich.com/US/en/product/sial/sa0180bc.

264. 3M. *3MTM TecraTM Salmonella Visual Immunoassay (VIA)*. [cited 2022 November 20, 2022]; Available from: https://multimedia.3m.com/mws/media/562804O/tecra-sal-via-protocol-high-microbial-load-aoac-oma-998-09.pdf.

265. Hygiena. *BAX® System Real-Time PCR Assay Staphylococcus aureus* [cited 2022 November 20, 2022]; Available from: ps://www.hygiena.com/wp-content/uploads/2020/09/BAX-Q7-Assay-Kit-Insert-Staphlococcus-Aureus-RT-English.pdf.

266. Millipore Sigma. *TRANSIA® PLATE Staphylococcal Enterotoxins*. Available from: https://www.sigmaaldrich.com/US/en/technical-documents/technical-article/microbiological-testing/pathogen-and-spoilage-testing/transia-plate-staphylococcal-enterotoxins.

267. Millipore Sigma. *TRANSIA™ PLATE Staph. Enterotoxins*. [cited 2022 November 20, 2022]; Available from: https://www.sigmaaldrich.com/US/en/product/sial/st0796bc.

268. 3M. *3M™ Tecra™ Pathogen and Toxin Visual Immunoassay (VIA) Tests*. [cited 2022 November 20, 2022]; Available from: https://multimedia.3m.com/mws/media/768188O/3m-tecra-pathogen-and-toxin-visual-immunoassay-via-tests.pdf.

269. Neogen. *ANSR® for Campylobacter*. [cited 2022 November 20, 2022]; Available from: https://www.neogen.com/categories/microbiology/ansr-campylobacter/#:~:text=ANSR%C2%AE%20for%20Campylobacter%20provides,rinse%20samples%20and%20carcass%20swabs.

270. Bruker. *MALDI Biotyper® for Food Microbiology*. [cited 2022 November 20, 2022]; Available from: https://www.bruker.com/en/applications/microbiology-and-diagnostics/food-beverage-microbiology/maldi-biotyper-for-food-microbiology.html.

271. Hygiena. *BAX® System Real-Time PCR Assay for Campylobacter jejuni / coli / lari, Hygiena™, Qualicon Diagnostics LLC*. [cited 2022 November 20, 2022]; Available from: https://us.vwr.com/store/product/16700730/bax-system-real-time-pcr-assay-for-i-campylobacter-jejuni-coli-lari-i-hygienatm-qualicon-diagnostics-llc.

272. Bio-Rad. *iQ-Check Campylobacter PCR Detection Kit* [cited 2022 November 20, 2022]; Available from: https://www.bio-rad.com/en-us/product/iq-check-campylobacter-pcr-detection-kit?ID=31c700d4-6655-4dc0-af7a-3876264dd8e6.

273. Millipore Sigma. *Singlepath® Campylobacter*. [cited 2022 November 20, 2022]; Available from: https://www.sigmaaldrich.com/US/en/product/mm/104143.

274. amsl scientific. [cited 2022 November 20, 2022]; Available from: https://www.amsl.com.au/campylobacter-veramsllow/.

275. bioMerieux Inc. [cited 2022 November 20, 2022]; Available from: https://www.biomerieux-usa.com/sites/subsidiary_us/files/doc/vidas_cam_vi-5.pdf.

276. 3M. *3M™ Molecular Detection Assay 2 - Campylobacter MDA2CAM96, 96 tests, 1 ea*. 2022 [cited 2022 November 27, 2022]; Available from: https://www.3m.com/3M/en_US/p/d/v000525618/.

277. U.S. Food & Drug Administration. *Nucleic Acid Based Tests*. 2022 [cited 2022; Available from: https://www.fda.gov/medical-devices/in-vitro-diagnostics/nucleic-acid-based-tests.

278. Lakshmanan, R.S., et al., *Phage immobilized magnetoelastic sensor for the detection of Salmonella typhimurium.* Journal of microbiological methods, 2007. **71**(1): p. 55-60.

279. Kretzer, J.W., et al., *Use of high-affinity cell wall-binding domains of bacteriophage endolysins for immobilization and separation of bacterial cells.* Appl. Environ. Microbiol., 2007. **73**(6): p. 1992-2000.

280. Lee, S., et al., *Isolation, characterization of bacteriophages specific to Microlunatus phosphovorus and their application for rapid host detection.* Letters in applied microbiology, 2006. **42**(3): p. 259-264.

281. Shabani, A., et al., *Bacteriophage-modified microarrays for the direct impedimetric detection of bacteria.* Analytical chemistry, 2008. **80**(24): p. 9475-9482.

282. Patel, D., Y. Zhou, and R.P. Ramasamy, *A bacteriophage-based electrochemical biosensor for detection of methicillin-resistant staphylococcus aureus.* Journal of The Electrochemical Society, 2021. **168**(5): p. 057523.

283. Basso, A. and S. Serban, *Industrial applications of immobilized enzymes—A review.* Molecular Catalysis, 2019. **479**: p. 110607.

284. Ramires, T., et al., *First report of Escherichia coli O157: H7 in ready-to-eat sushi.* Journal of Applied Microbiology, 2020. **128**(1): p. 301-309.

285. Ford, L., et al., *Seven Salmonella Typhimurium outbreaks in Australia linked by trace-back and whole genome sequencing.* Foodborne pathogens and disease, 2018. **15**(5): p. 285-292.

286. Desai, A.N., et al., *Changing epidemiology of Listeria monocytogenes outbreaks, sporadic cases, and recalls globally: A review of ProMED reports from 1996 to 2018.* International Journal of Infectious Diseases, 2019. **84**: p. 48-53.

287. *FoodNet, Foodborne Diseases Active Surveillance Network (FoodNet): FoodNet Surveillance Reports for 1996-2020 (Final Reports)*. 2021.

288. *Georgia Department of Public Health, Listeria Fact Sheet*. 2002.

289. Hedberg, C.W., *Foodborne illness acquired in the United States.* Emerging infectious diseases, 2011. **17**(7): p. 1338.

290. LeDuc, P., et al., *Beyond disease, how biomedical engineering can improve global health.* Science Translational Medicine, 2014. **6**(266): p. 266fs48-266fs48.

291. Priyanka, B., R.K. Patil, and S. Dwarakanath, *A review on detection methods used for foodborne pathogens.* The Indian journal of medical research, 2016. **144**(3): p. 327.

292. Feng, P., *Impact of molecular biology on the detection of foodborne pathogens.* Molecular biotechnology, 1997. **7**(3): p. 267-278.

293. Foddai, A.C. and I.R. Grant, *Methods for detection of viable foodborne pathogens: Current state-of-art and future prospects.* Applied Microbiology and Biotechnology, 2020. **104**(10): p. 4281-4288.

294. Lam, H.-M., et al., *Food supply and food safety issues in China.* The Lancet, 2013. **381**(9882): p. 2044-2053.

295. Chin, C.D., V. Linder, and S.K. Sia, *Lab-on-a-chip devices for global health: Past studies and future opportunities.* Lab on a Chip, 2007. **7**(1): p. 41-57.

296. Bunney, J., et al., *The use of electrochemical biosensors in food analysis.* Current Research in Nutrition and Food Science Journal, 2017. **5**(3): p. 183-195.

297. Jin, D., et al., *Rapid molecular identification of Listeria species by use of real-time PCR and high-resolution melting analysis.* FEMS microbiology letters, 2012. **330**(1): p. 72-80.

298. Aznar, R. and B. Alarcón, *PCR detection of Listeria monocytogenes: a study of multiple factors affecting sensitivity.* Journal of Applied Microbiology, 2003. **95**(5): p. 958-966.

299. Silva, N.F., et al., *Emerging electrochemical biosensing approaches for detection of Listeria monocytogenes in food samples: An overview.* Trends in Food Science & Technology, 2020. **99**: p. 621-633.

300. Kutter, E. and A. Sulakvelidze, *Bacteriophages: biology and applications*. 2004: Crc press.

301. Chen, I.-H., et al. *Isolation of highly selective phage-displayed oligopeptide probes for detection of listeria monocytogenes in ready-to-eat food*. in *Sensing for Agriculture and Food Quality and Safety X*. 2018. SPIE.

302. Carnazza, S., et al., *Recombinant phage probes for Listeria monocytogenes.* Journal of Physics: Condensed Matter, 2007. **19**(39): p. 395011.

303. Nanduri, V., et al., *SPR biosensor for the detection of L. monocytogenes using phage-displayed antibody.* Biosensors and Bioelectronics, 2007. **23**(2): p. 248-252.

304. Tolba, M., et al., *A bacteriophage endolysin-based electrochemical impedance biosensor for the rapid detection of Listeria cells.* Analyst, 2012. **137**(24): p. 5749-5756.

305. Singh, S., et al., *An insight in bacteriophage based biosensors with focus on their detection methods and recent advancements.* Environmental Technology & Innovation, 2020. **20**: p. 101081.

306. Zhou, Y., et al., *Charge-directed immobilization of bacteriophage on nanostructured electrode for whole-cell electrochemical biosensors.* Analytical Chemistry, 2017. **89**(11): p. 5734-5741.

307. Schoch, C.L., et al., *NCBI Taxonomy: a comprehensive update on curation, resources and tools.* Database, 2020. **2020**.

308. Baltimore, D., *Expression of animal virus genomes.* Bacteriological reviews, 1971. **35**(3): p. 235-241.

309. Zhou, Y. and R.P. Ramasamy, *Isolation and separation of Listeria monocytogenes using bacteriophage P100-modified magnetic particles.* Colloids and Surfaces B: Biointerfaces, 2019. **175**: p. 421-427.

310. Ghuman, A., Y. Zhou, and R.P. Ramasamy. *Selective Isolation and Concentration of Foodborne Bacterial Pathogens in a Microfluidic Device*. in *ECS Meeting Abstracts*. 2019. IOP Publishing.

311. Sommer, H.Z., H.I. Lipp, and L.L. Jackson, *Alkylation of amines. General exhaustive alkylation method for the synthesis of quaternary ammonium compounds.* The Journal of Organic Chemistry, 1971. **36**(6): p. 824-828.

312. Chen, F.C. and N.L. Benoiton, *A new method of quaternizing amines and its use in amino acid and peptide chemistry.* Canadian Journal of Chemistry, 1976. **54**(20): p. 3310-3311.

313. Socrates, G., *Infrared and Raman characteristic group frequencies: tables and charts*. 2004: John Wiley & Sons.

314. Shrivastava, A. and V.B. Gupta, *Methods for the determination of limit of detection and limit of quantitation of the analytical methods.* Chron. Young Sci, 2011. **2**(1): p. 21-25.

315. Agency, H.P., *Health Protection Agency. Guidelines for assessing the microbiological safety of ready-to-eat foods placed on the market.* 2009.

316. Kropinski, A.M., et al., *Genome and proteome of Campylobacter jejuni bacteriophage NCTC 12673.* Applied and environmental microbiology, 2011. **77**(23): p. 8265-8271.

317. Fang, Y., et al., *Detection of methyl salicylate using bi-enzyme electrochemical sensor consisting salicylate hydroxylase and tyrosinase.* Biosensors and Bioelectronics, 2016. **85**: p. 603-610.

318. Fang, Y., Y. Umasankar, and R.P. Ramasamy, *A novel bi-enzyme electrochemical biosensor for selective and sensitive determination of methyl salicylate.* Biosensors and Bioelectronics, 2016. **81**: p. 39-45.

319. Parimi, N.S., et al., *Kinetic and mechanistic parameters of laccase catalyzed direct electrochemical oxygen reduction reaction.* Acs Catalysis, 2012. **2**(1): p. 38-44.

320. Fang, Y. and R.P. Ramasamy, *Detection of p-ethylphenol, a major plant volatile organic compound, by tyrosinase-based electrochemical biosensor.* ECS Journal of Solid State Science and Technology, 2016. **5**(8): p. M3054.

321. Zolti, O., et al., *Electrochemical Biosensor for Rapid Detection of Listeria monocytogenes.* Journal of The Electrochemical Society, 2022. **169**(6): p. 067510.

322. Shrivastava, A. and V. Gupta, *Chron.* Young Sci, 2011. **2**: p. 21.

323. Datta, P., et al., *Evaluation of various methods for the detection of meticillin-resistant Staphylococcus aureus strains and susceptibility patterns.* Journal of Medical Microbiology, 2011. **60**(11): p. 1613-1616.

324. Ivnitski, D., et al., *Biosensors for detection of pathogenic bacteria.* Biosensors and Bioelectronics, 1999. **14**(7): p. 599-624.

325. Ahmed, A., et al., *Biosensors for whole-cell bacterial detection.* Clinical microbiology reviews, 2014. **27**(3): p. 631-646.

326. Ivnitski, D., et al., *Application of electrochemical biosensors for detection of food pathogenic bacteria.* Electroanalysis: An International Journal Devoted to Fundamental and Practical Aspects of Electroanalysis, 2000. **12**(5): p. 317-325.

327. Dunne, M. and M.J. Loessner, *Modified bacteriophage tail fiber proteins for labeling, immobilization, capture, and detection of bacteria*, in *Foodborne Bacterial Pathogens*. 2019, Springer. p. 67-86.

328. Hyeon, S.H., W.K. Lim, and H.J. Shin, *Novel surface plasmon resonance biosensor that uses full-length Det7 phage tail protein for rapid and selective detection of Salmonella enterica serovar Typhimurium.* Biotechnology and Applied Biochemistry, 2021. **68**(1): p. 5-12.

329. Zhang, J., et al., *An on-site, highly specific immunosensor for Escherichia coli detection in field milk samples from mastitis-affected dairy cattle.* Biosensors and Bioelectronics, 2020. **165**: p. 112366.

330. Haasnoot, W., et al., *Fast biosensor immunoassays for the detection of cows' milk in the milk of ewes and goats.* Journal of Dairy Research, 2004. **71**(3): p. 322-329.

331. Wei, D., et al., *Development of a surface plasmon resonance biosensor for the identification of Campylobacter jejuni.* Journal of Microbiological Methods, 2007. **69**(1): p. 78-85.

332. Ding, S., et al., *A fluorescent biosensor based on quantum dot–labeled streptavidin and poly-l-lysine for the rapid detection of Salmonella in milk.* Journal of Dairy Science, 2022. **105**(4): p. 2895-2907.

333. Poshtiban, S., et al., *Phage receptor binding protein-based magnetic enrichment method as an aid for real time PCR detection of foodborne bacteria.* Analyst, 2013. **138**(19): p. 5619-5626.

334. Kiruthika, R., et al., *Isolation and Identification of Chicken Feather Degrading Organisms from Soil Sample.* International Journal of Progressive Research in Science and Engineering, 2021. **2**(7): p. 124-132.

335. Sheikhzadeh, E., et al., *Label-free impedimetric biosensor for Salmonella Typhimurium detection based on poly [pyrrole-co-3-carboxyl-pyrrole] copolymer supported aptamer.* Biosensors and bioelectronics, 2016. **80**: p. 194-200.

336. Alemka, A., et al., *N-glycosylation of Campylobacter jejuni surface proteins promotes bacterial fitness.* Infection and immunity, 2013. **81**(5): p. 1674-1682.

337. Lund, M., et al., *Detection of Campylobacter spp. in ChickenFecal Samples by Real-TimePCR.* Journal of clinical microbiology, 2004. **42**(11): p. 5125-5132.

338. Baurhoo, B., et al., *Cecal populations of lactobacilli and bifidobacteria and Escherichia coli populations after in vivo Escherichia coli challenge in birds fed diets with purified lignin or mannanoligosaccharides.* Poultry Science, 2007. **86**(12): p. 2509-2516.

339. Salanitro, J., I. Fairchilds, and Y. Zgornicki, *Isolation, culture characteristics, and identification of anaerobic bacteria from the chicken cecum.* Applied microbiology, 1974. **27**(4): p. 678-687.

340. Marteau, P., et al., *Comparative study of bacterial groups within the human cecal and fecal microbiota.* Applied and environmental microbiology, 2001. **67**(10): p. 4939-4942.

341. Qi, J., et al., *Identification and characterization of the proteins in broth of stewed traditional Chinese yellow-feathered chickens.* Poultry science, 2018. **97**(5): p. 1852-1860.

342. Hitchcock, D.I., *The isoelectric point of gelatin at 40 C.* The Journal of General Physiology, 1924. **6**(4): p. 457-462.

343. Chi, S. and T. Chen, *Selected chemical and physical characteristics of chicken broth from broiler deboning by-products.* Journal of food processing and preservation, 1993. **17**(6): p. 407-420.

344. León-López, A., et al., *Hydrolysed collagen from sheepskins as a source of functional peptides with antioxidant activity.* International Journal of Molecular Sciences, 2019. **20**(16): p. 3931.

345. Han, L., et al., *A label-free electrochemical impedance cytosensor based on specific peptide-fused phage selected from landscape phage library.* Scientific reports, 2016. **6**(1): p. 1-10.

346. Musgrove, M., et al., *Detection of Campylobacter spp. in ceca and crops with and without enrichment.* Poultry Science, 2001. **80**(6): p. 825-828.

347. Corrier, D., et al., *Presence of Salmonella in the crop and ceca of broiler chickens before and after preslaughter feed withdrawal.* Poultry science, 1999. **78**(1): p. 45-49.

348. Saengkerdsub, S., et al., *Identification and quantification of methanogenic archaea in adult chicken ceca.* Applied and Environmental Microbiology, 2007. **73**(1): p. 353-356.

349. Pineda-Quiroga, C., et al., *Microbial and functional profile of the ceca from laying hens affected by feeding prebiotics, probiotics, and synbiotics.* Microorganisms, 2019. **7**(5): p. 123.

350. Gong, J., et al., *Diversity and phylogenetic analysis of bacteria in the mucosa of chicken ceca and comparison with bacteria in the cecal lumen.* FEMS microbiology letters, 2002. **208**(1): p. 1-7.

351. Rudi, K., et al., *Direct real-time PCR quantification of Campylobacter jejuni in chicken fecal and cecal samples by integrated cell concentration and DNA purification.* Applied and Environmental Microbiology, 2004. **70**(2): p. 790-797.

352. Asare, P.T., et al., *In vitro Modeling of Chicken Cecal Microbiota Ecology and Metabolism Using the PolyFermS Platform.* Frontiers in microbiology, 2021. **12**.

353. Pillai, S.D., et al., *A rapid method for screening for Salmonella typhimurium in a chicken cecal microbial consortium using gene amplification.* Avian Diseases, 1994: p. 598-604.

354. Salanitro, J., I. Blake, and P. Muirhead, *Studies on the cecal microflora of commercial broiler chickens.* Applied microbiology, 1974. **28**(3): p. 439-447.

355. Gibson, S., et al., *Significance of microflora in proteolysis in the colon.* Applied and Environmental Microbiology, 1989. **55**(3): p. 679-683.

356. Carroll, I.M., et al., *Fecal protease activity is associated with compositional alterations in the intestinal microbiota.* PLoS One, 2013. **8**(10): p. e78017.

357. Smith, B.J., et al., *Changes in the gut microbiome and fermentation products concurrent with enhanced longevity in acarbose-treated mice.* BMC microbiology, 2019. **19**(1): p. 1-16.

358. Santovito, E., et al., *A sensor-based system for rapid on-site testing of microbial contamination in meat samples and carcasses.* Journal of Applied Microbiology, 2022. **132**(2): p. 1210-1220.

359. Sharma, H. and R. Mutharasan, *Rapid and sensitive immunodetection of Listeria monocytogenes in milk using a novel piezoelectric cantilever sensor.* Biosensors and Bioelectronics, 2013. **45**: p. 158-162.

360. Cheng, C., et al., *Rapid detection of Listeria monocytogenes in milk by self-assembled electrochemical immunosensor.* Sensors and Actuators B: Chemical, 2014. **190**: p. 900-906.

361. Radhakrishnan, R., et al., *Detection of Listeria monocytogenes by electrochemical impedance spectroscopy.* Electroanalysis, 2013. **25**(9): p. 2231-2237.

362. Chen, Q., et al., *A sensitive impedance biosensor based on immunomagnetic separation and urease catalysis for rapid detection of Listeria monocytogenes using an immobilization-free interdigitated array microelectrode.* Biosensors and Bioelectronics, 2015. **74**: p. 504-511.

363. Chen, Q., et al., *Fast and sensitive detection of foodborne pathogen using electrochemical impedance analysis, urease catalysis and microfluidics.* Biosensors and Bioelectronics, 2016. **86**: p. 770-776.

364. Wang, D., et al., *Efficient separation and quantitative detection of Listeria monocytogenes based on screen-printed interdigitated electrode, urease and magnetic nanoparticles.* Food control, 2017. **73**: p. 555-561.

365. Taylor, A.D., et al., *Quantitative and simultaneous detection of four foodborne bacterial pathogens with a multi-channel SPR sensor.* Biosensors and Bioelectronics, 2006. **22**(5): p. 752-758.

366. Sista, S., et al. *Sensitive Surface Plasmon Resonance Biosensor for the Near-Real Time Detection of Campylobacter Jejuni*. in *ECS Meeting Abstracts*. 2006. IOP Publishing.

367. Che, Y., Y. Li, and M. Slavik, *Detection of Campylobacter jejuni in poultry samples using an enzyme-linked immunoassay coupled with an enzyme electrode.* Biosensors and Bioelectronics, 2001. **16**(9-12): p. 791-797.

368. Viswanathan, S., C. Rani, and J.-a.A. Ho, *Electrochemical immunosensor for multiplexed detection of food-borne pathogens using nanocrystal bioconjugates and MWCNT screen-printed electrode.* Talanta, 2012. **94**: p. 315-319.

369. Obeso, J.M., et al., *Use of logistic regression for prediction of the fate of Staphylococcus aureus in pasteurized milk in the presence of two lytic phages.* Applied and Environmental Microbiology, 2010. **76**(18): p. 6038-6046.

370. Leszczyński, P., et al., *Successful eradication of methicillin-resistantstaphylococcus aureus (MRSA) intestinal carrier status in a healthcare worker—Case report.* Folia microbiologica, 2006. **51**(3): p. 236-238.

371. Lungren, M.P., et al., *Bacteriophage K for reduction of Staphylococcus aureus biofilm on central venous catheter material.* Bacteriophage, 2013. **3**(4): p. e26825.

372. Pincus, N.B., et al., *Strain specific phage treatment for Staphylococcus aureus infection is influenced by host immunity and site of infection.* PloS one, 2015. **10**(4): p. e0124280.

373. Schmelcher, M., et al., *Evolutionarily distinct bacteriophage endolysins featuring conserved peptidoglycan cleavage sites protect mice from MRSA infection.* Journal of Antimicrobial Chemotherapy, 2015. **70**(5): p. 1453-1465.

374. Carlton, R., et al., *Bacteriophage P100 for control of Listeria monocytogenes in foods: genome sequence, bioinformatic analyses, oral toxicity study, and application.* Regulatory Toxicology and Pharmacology, 2005. **43**(3): p. 301-312.

375. Carter, C.D., et al., *Bacteriophage cocktail significantly reduces Escherichia coli O157: H7 contamination of lettuce and beef, but does not protect against recontamination.* Bacteriophage, 2012. **2**(3): p. 178-185.

376. Tomat, D., et al., *Phage biocontrol of enteropathogenic and shiga toxin-producing Escherichia coli in meat products.* Frontiers in cellular and infection microbiology, 2013. **3**: p. 20.

377. Vonasek, E.L., et al., *Incorporating phage therapy into WPI dip coatings for applications on fresh whole and cut fruit and vegetable surfaces.* Journal of food science, 2018. **83**(7): p. 1871-1879.

378. Ferguson, S., et al., *Lytic bacteriophages reduce Escherichia coli O157: H7 on fresh cut lettuce introduced through cross-contamination.* Bacteriophage, 2013. **3**(1): p. e24323.

379. O'flynn, G., et al., *Evaluation of a cocktail of three bacteriophages for biocontrol of Escherichia coli O157: H7.* Applied and Environmental Microbiology, 2004. **70**(6): p. 3417-3424.

380. KUSMIATUN, A., I. RUSMANA, and S. BUDIARTI, *Characterization of bacteriophage specific to bacillus pumilus from Ciapus River in Bogor, West Java, Indonesia.* HAYATI Journal of Biosciences, 2015. **22**(1): p. 27-33.

381. Shin, H.J. and W.K. Lim, *Rapid label-free detection of E. coli using a novel SPR biosensor containing a fragment of tail protein from phage lambda.* Preparative Biochemistry and Biotechnology, 2018. **48**(6): p. 498-505.

382. Mushtaq, N., et al., *Treatment of experimental Escherichia coli infection with recombinant bacteriophage-derived capsule depolymerase.* Journal of Antimicrobial Chemotherapy, 2005. **56**(1): p. 160-165.

383. Augustine, J. and S.G. Bhat, *Biocontrol of Salmonella Enteritidis in spiked chicken cuts by lytic bacteriophages ΦSP-1 and ΦSP-3.* Journal of basic microbiology, 2015. **55**(4): p. 500-503.

384. Jun, J.W., et al., *Bacteriophages reduce Yersinia enterocolitica contamination of food and kitchenware.* International journal of food microbiology, 2018. **271**: p. 33-47.

385. Gouvêa, D.M., et al., *Absorbent food pads containing bacteriophages for potential antimicrobial use in refrigerated food products.* LWT-Food Science and Technology, 2016. **67**: p. 159-166.

386. *Phage Guard*. [cited 2022 October 8th 2022]; 10/08/2019:[Available from: https://sds.chemtel.net/webclients/cheneybrothers/10105498SDS.pdf.

387. Denyes, J.M., et al., *Modified bacteriophage S16 long tail fiber proteins for rapid and specific immobilization and detection of Salmonella cells.* Applied and Environmental microbiology, 2017. **83**(12): p. e00277-17.

388. Yen, M., L.S. Cairns, and A. Camilli, *A cocktail of three virulent bacteriophages prevents Vibrio cholerae infection in animal models.* Nature communications, 2017. **8**(1): p. 1-7.

389. Olszak, T., et al., *In vitro and in vivo antibacterial activity of environmental bacteriophages against Pseudomonas aeruginosa strains from cystic fibrosis patients.* Applied microbiology and biotechnology, 2015. **99**(14): p. 6021-6033.

390. Letkiewicz, S., et al., *Eradication of Enterococcus faecalis by phage therapy in chronic bacterial prostatitis—case report.* Folia Microbiologica, 2009. **54**(5): p. 457-461.

391. Al-Wrafy, F., et al., *Identification and characterization of phage protein and its activity against two strains of multidrug-resistant Pseudomonas aeruginosa.* Scientific reports, 2019. **9**(1): p. 1-14.

392. Briers, Y., et al., *Engineered endolysin-based "Artilysins" to combat multidrug-resistant gram-negative pathogens.* MBio, 2014. **5**(4): p. e01379-14.

393. Augustine, J., M.V. Gopalakrishnan, and S.G. Bhat, *Application of ΦSP-1 and ΦSP-3 as a therapeutic strategy against Salmonella Enteritidis infection using Caenorhabditis elegans as model organism.* FEMS Microbiology Letters, 2014. **356**(1): p. 113-117.

394. Wei, C., et al., *Developing a bacteriophage cocktail for biocontrol of potato bacterial wilt.* Virologica sinica, 2017. **32**(6): p. 476-484.

395. Lau, G.L., et al., *Characteristics of a phage effective for colibacillosis control in poultry.* Journal of the Science of Food and Agriculture, 2012. **92**(13): p. 2657-2663.

396. Ushanov, L., et al., *Application of Campylobacter jejuni phages: challenges and perspectives.* Animals, 2020. **10**(2): p. 279.

397. Lone, A., et al., *Development of prototypes of bioactive packaging materials based on immobilized bacteriophages for control of growth of bacterial pathogens in foods.* International Journal of Food Microbiology, 2016. **217**: p. 49-58.

398. Schuch, R., D. Nelson, and V.A. Fischetti, *A bacteriolytic agent that detects and kills Bacillus anthracis.* Nature, 2002. **418**(6900): p. 884-889.

399. Yoong, P., et al., *PlyPH, a bacteriolytic enzyme with a broad pH range of activity and lytic action against Bacillus anthracis.* Journal of Bacteriology, 2006. **188**(7): p. 2711-2714.

400. Nelson, D., L. Loomis, and V.A. Fischetti, *Prevention and elimination of upper respiratory colonization of mice by group A streptococci by using a bacteriophage lytic enzyme.* Proceedings of the National Academy of Sciences, 2001. **98**(7): p. 4107-4112.

401. Lood, R., et al., *A highly active and negatively charged Streptococcus pyogenes lysin with a rare D-alanyl-L-alanine endopeptidase activity protects mice against streptococcal bacteremia.* Antimicrobial agents and chemotherapy, 2014. **58**(6): p. 3073-3084.

402. Loeffler, J.M., D. Nelson, and V.A. Fischetti, *Rapid killing of Streptococcus pneumoniae with a bacteriophage cell wall hydrolase.* Science, 2001. **294**(5549): p. 2170-2172.

403. Bradley, R.W., et al., *Terminal oxidase mutants of the cyanobacterium Synechocystis sp. PCC 6803 show increased electrogenic activity in biological*

photo-voltaic systems. Physical Chemistry Chemical Physics, 2013. **15**(32): p. 13611-13618.

404. Burgstaller, H., *Respiratory terminal oxidases of the cyanobacterium Synechococcus sp. strain PCC7942 (p. 101).* Vienna: University of Vienna, 2012.

405. Sekar, N., et al., *Role of respiratory terminal oxidases in the extracellular electron transfer ability of cyanobacteria.* Biotechnology and bioengineering, 2018. **115**(5): p. 1361-1366.

406. Berry, S., et al., *Electron transport routes in whole cells of Synechocystis sp. strain PCC 6803: the role of the cytochrome bd-type oxidase.* Biochemistry, 2002. **41**(10): p. 3422-3429.

407. Hart, S., et al., *Terminal oxidases of cyanobacteria.* Biochemical Society Transactions, 2005. **33**(4): p. 832-835.

408. Heidelberg, J.F., et al., *Genome sequence of the dissimilatory metal ion-reducing bacterium Shewanella oneidensis.* Nat Biotechnol, 2002. **20**(11): p. 1118-23.

409. Weber, K.A., L.A. Achenbach, and J.D. Coates, *Microorganisms pumping iron: anaerobic microbial iron oxidation and reduction.* Nature Reviews Microbiology, 2006. **4**(10): p. 752-764.

410. Sekar, N., et al., *Electricity generation by Pyrococcus furiosus in microbial fuel cells operated at 90° C.* Biotechnology and bioengineering, 2017. **114**(7): p. 1419-1427.

411. Fiala, G. and K.O. Stetter, *Pyrococcus furiosus sp. nov. represents a novel genus of marine heterotrophic archaebacteria growing optimally at 100 C.* Archives of Microbiology, 1986. **145**(1): p. 56-61.

412. Lee, H.-S., et al., *Transcriptional and biochemical analysis of starch metabolism in the hyperthermophilic archaeon Pyrococcus furiosus.* Journal of bacteriology, 2006. **188**(6): p. 2115-2125.

413. Schut, G.J., et al., *Mutational analyses of the enzymes involved in the metabolism of hydrogen by the hyperthermophilic archaeon Pyrococcus furiosus.* Frontiers in microbiology, 2012. **3**: p. 163.

414. McTernan, P.M., et al., *Intact functional fourteen-subunit respiratory membrane-bound [NiFe]-hydrogenase complex of the hyperthermophilic archaeon Pyrococcus furiosus.* Journal of Biological Chemistry, 2014. **289**(28): p. 19364-19372.

415. Schut, G.J., et al., *The modular respiratory complexes involved in hydrogen and sulfur metabolism by heterotrophic hyperthermophilic archaea and their evolutionary implications.* FEMS microbiology reviews, 2013. **37**(2): p. 182-203.

416. Nguyen, D.M., et al., *Two functionally distinct NADP+-dependent ferredoxin oxidoreductases maintain the primary redox balance of Pyrococcus furiosus.* Journal of Biological Chemistry, 2017. **292**(35): p. 14603-14616.

417. Adams, M.W., et al., *Key role for sulfur in peptide metabolism and in regulation of three hydrogenases in the hyperthermophilic archaeonPyrococcus furiosus.* Journal of Bacteriology, 2001. **183**(2): p. 716-724.

418. Lovley, D.R., *Organic matter mineralization with the reduction of ferric iron: a review*. Geomicrobiology Journal, 1987. **5**(3-4): p. 375-399.

419. Lovley, D.R., *Dissimilatory metal reduction.* Annual review of microbiology, 1993. **47**(1): p. 263-290.

420. Bretschger, O., et al., *Current production and metal oxide reduction by Shewanella oneidensis MR-1 wild type and mutants.* Appl Environ Microbiol, 2007. **73**(21): p. 7003-12.

421. Newton, G.J., et al., *Analyses of current-generating mechanisms of Shewanella loihica PV-4 and Shewanella oneidensis MR-1 in microbial fuel cells.* Appl. Environ. Microbiol., 2009. **75**(24): p. 7674-7681.

422. Jorge, A.B. and R. Hazael, *Use of Shewanella oneidensis for energy conversion in microbial fuel cells.* Macromolecular Chemistry and Physics, 2016. **217**(13): p. 1431-1438.

423. Bond, D.R. and D.R. Lovley, *Electricity production by Geobacter sulfurreducens attached to electrodes.* Appl Environ Microbiol, 2003. **69**(3): p. 1548-55.

424. Lovley, D.R., et al., *Geobacter metallireducens gen. nov. sp. nov., a microorganism capable of coupling the complete oxidation of organic compounds to the reduction of iron and other metals.* Arch Microbiol, 1993. **159**(4): p. 336-44.

425. Holmes, D.E., D.R. Bond, and D.R. Lovley, *Electron transfer by Desulfobulbus propionicus to Fe(III) and graphite electrodes.* Appl Environ Microbiol, 2004. **70**(2): p. 1234-7.

426. Alves, A.S., et al., *Exploration of the 'cytochromome' of Desulfuromonas acetoxidans, a marine bacterium capable of powering microbial fuel cells.* Metallomics, 2011. **3**(4): p. 349-353.

427. Yilmazel, Y.D., et al., *Electrical current generation in microbial electrolysis cells by hyperthermophilic archaea Ferroglobus placidus and Geoglobus ahangari.* Bioelectrochemistry, 2018. **119**: p. 142-149.

428. Du, Z., H. Li, and T. Gu, *A state of the art review on microbial fuel cells: a promising technology for wastewater treatment and bioenergy.* Biotechnology advances, 2007. **25**(5): p. 464-482.

429. Mathis, B., et al., *Electricity generation by thermophilic microorganisms from marine sediment.* Applied microbiology and biotechnology, 2008. **78**(1): p. 147-155.

430. Ha, P.T., et al., *Treatment of alcohol distillery wastewater using a Bacteroidetes-dominant thermophilic microbial fuel cell.* Environmental science & technology, 2012. **46**(5): p. 3022-3030.

431. Fu, Q., et al., *Bioelectrochemical analysis of a hyperthermophilic microbial fuel cell generating electricity at temperatures above 80 C.* Bioscience, biotechnology, and biochemistry, 2015. **79**(7): p. 1200-1206.

432. Allaoui, M., O. Rahim, and L. Sekhri, *Electrochemical Study on Corrosion Inhibition of Iron in Acidic Medium by Moringa Oleifera Extract.* Oriental Journal of Chemistry, 2017. **33**(2): p. 637-646.

433. Ashassi-Sorkhabi, H., D. Seifzadeh, and M. Hosseini, *EN, EIS and polarization studies to evaluate the inhibition effect of 3H-phenothiazin-3-one, 7-dimethylamin on mild steel corrosion in 1 M HCl solution.* Corrosion Science, 2008. **50**(12): p. 3363-3370.

434. Elayyachy, M., A. El Idrissi, and B. Hammouti, *New thio-compounds as corrosion inhibitor for steel in 1 M HCl.* Corrosion Science, 2006. **48**(9): p. 2470-2479.

435. Emregül, K.C. and M. Hayvali, *Studies on the effect of a newly synthesized Schiff base compound from phenazone and vanillin on the corrosion of steel in 2 M HCl.* Corrosion science, 2006. **48**(4): p. 797-812.

436. Quraishi, M. and D. Jamal, *Inhibition of mild steel corrosion in the presence of fatty acid triazoles.* Journal of applied electrochemistry, 2002. **32**(4): p. 425-430.

437. Noor, E.A., *The inhibition of mild steel corrosion in phosphoric acid solutions by some N-heterocyclic compounds in the salt form.* Corrosion Science, 2005. **47**(1): p. 33-55.

438. Popova, A. and M. Christov, *Evaluation of impedance measurements on mild steel corrosion in acid media in the presence of heterocyclic compounds.* Corrosion Science, 2006. **48**(10): p. 3208-3221.

439. Talati, J. and D. Gandhi, *N-heterocyclic compounds as corrosion inhibitors for aluminium-copper alloy in hydrochloric acid.* Corrosion Science, 1983. **23**(12): p. 1315-1332.

440. Halambek, J., K. Berković, and J. Vorkapić-Furač, *The influence of Lavandula angustifolia L. oil on corrosion of Al-3Mg alloy.* Corrosion Science, 2010. **52**(12): p. 3978-3983.

441. Okafor, P.C., et al., *Green approaches to corrosion mitigation.* International Journal of Corrosion, 2012. **2012**.

442. Abdel-Gaber, A., et al., *Inhibitive action of some plant extracts on the corrosion of steel in acidic media.* Corrosion science, 2006. **48**(9): p. 2765-2779.

443. Oguzie, E.E., *Evaluation of the inhibitive effect of some plant extracts on the acid corrosion of mild steel.* Corrosion science, 2008. **50**(11): p. 2993-2998.

444. Mo, S., H.-Q. Luo, and N.-B. Li, *Plant extracts as "green" corrosion inhibitors for steel in sulphuric acid.* Chemical papers, 2016. **70**(9): p. 1131-1143.

445. Bouklah, M., et al., *Thiophene derivatives as effective inhibitors for the corrosion of steel in 0.5 m H 2 SO 4.* Journal of Applied Electrochemistry, 2005. **35**(11): p. 1095-1101.

446. Fouda, A., A. Al-Sarawy, and E. El-Katori, *Pyrazolone derivatives as corrosion inhibitors for C-steel in hydrochloric acid solution.* Desalination, 2006. **201**(1-3): p. 1-13.

447. Shyamala, M. and A. Arulanantham, *Eclipta alba as corrosion pickling inhibitor on mild steel in hydrochloric acid.* 材料科学技术 (英文版), 2009(2009 年 05): p. 633-636.

448. Raja, P.B. and M.G. Sethuraman, *Natural products as corrosion inhibitor for metals in corrosive media—a review.* materials letters, 2008. **62**(1): p. 113-116.

449. Sanyal, B., *Organic compounds as corrosion inhibitors in different environments—a review.* Progress in Organic Coatings, 1981. **9**(2): p. 165-236.

450. Abdullah Dar, M., *A review: plant extracts and oils as corrosion inhibitors in aggressive media.* Industrial Lubrication and Tribology, 2011. **63**(4): p. 227-233.

451. Khamis, E. and N. Alandis, *Herbs as new type of green inhibitors for acidic corrosion of steel.* Materialwissenschaft und Werkstofftechnik: Entwicklung,

Fertigung, Prüfung, Eigenschaften und Anwendungen technischer Werkstoffe, 2002. **33**(9): p. 550-554.

452. Subhashini, S., et al., *Corrosion mitigating effect of Cyamopsis Tetragonaloba seed extract on mild steel in acid medium.* Journal of Chemistry, 2010. **7**(4): p. 1133-1137.

453. Sanghvi, M., et al., *Inhibition of hydrochloric acid corrosion of mild steel by aid extracts ofembilica officianalis, terminalia bellirica and terminalia chebula.* Bulletin of electrochemistry, 1997. **13**(8-9): p. 358-361.

454. Okafor, P., et al., *Combretum bracteosum extracts as eco-friendly corrosion inhibitor for mild steel in acidic medium.* Pigment & Resin Technology, 2009. **38**(4): p. 236-241.

455. Komorsky-Lovrić, Š. and I. Novak, *Determination of ellagic acid in strawberries, raspberries and blackberries by square-wave voltammetry.* Int. J. Electrochem. Sci, 2011. **6**(10): p. 4638-4647.

456. Simić, A.Z., et al., *Study of ellagic acid electro-oxidation mechanism.* Monatshefte für Chemie-Chemical Monthly, 2013. **144**(2): p. 121-128.

457. Akhter, S., et al., *Enhanced amperometric detection of paracetamol by immobilized cobalt ion on functionalized MWCNTs-Chitosan thin film.* Analytical biochemistry, 2018. **551**: p. 29-36.

458. Walgama, C., M. Gallman, and S. Krishnan, *Single Drop Electroanalysis and Interfacial Interactions: Sensitivity versus Limit of Detection.* Electroanalysis, 2016. **28**(11): p. 2791-2796.

459. Mundra, R.V., et al., *Nanotubes in biological applications.* Current opinion in biotechnology, 2014. **28**: p. 25-32.

460. Brett, C. and A. Oliveira-Brett, *Cyclic voltammetry and linear sweep techniques.* Electrochemistry. Principles, Methods and Applications, Oxford University Press, UK, 1993: p. 174-198.

461. Ameer, M. and A. Fekry, *Corrosion inhibition of mild steel by natural product compound.* Progress in organic coatings, 2011. **71**(4): p. 343-349.

462. de Souza, F.S. and A. Spinelli, *Caffeic acid as a green corrosion inhibitor for mild steel.* Corrosion science, 2009. **51**(3): p. 642-649.

463. Abdel-Hamid, R. and E.F. Newair, *Electrochemical behavior of antioxidants: I. Mechanistic study on electrochemical oxidation of gallic acid in aqueous solutions at glassy-carbon electrode.* Journal of electroanalytical chemistry, 2011. **657**(1-2): p. 107-112.

464. Su, Y.-L. and S.-H. Cheng, *Sensitive and selective determination of gallic acid in green tea samples based on an electrochemical platform of poly (melamine) film.* Analytica chimica acta, 2015. **901**: p. 41-50.

465. Ostovari, A., et al., *Corrosion inhibition of mild steel in 1 M HCl solution by henna extract: A comparative study of the inhibition by henna and its constituents (Lawsone, Gallic acid, α-d-Glucose and Tannic acid).* Corrosion Science, 2009. **51**(9): p. 1935-1949.

466. Chethana, B., S. Basavanna, and Y.A. Naik, *Electrochemical studies on lawsone and its determination in henna (Lawsonia inermis) extract using glassy carbon electrode.* Journal of analytical chemistry, 2014. **69**(9): p. 887-891.

467. Bodini, M.E. and P.E. Bravo, *Voltammetric and spectroscopic study of the iron (II) complexes with the semiquinone of 2-hydroxy-1, 4-naphthoquinone (lawsone) in aprotic medium.* Polyhedron, 1994. **13**(3): p. 497-503.

468. Ferraz, P.A., et al., *Electrochemical aspects of the reduction of biologically active 2-hydroxy-3-alkyl-1, 4-naphthoquinones.* Journal of Electroanalytical Chemistry, 2001. **507**(1-2): p. 275-286.

469. Raoof, D.B. and S.M. Golabi, *Electrochemical properties of carbon-paste electrodes spiked with some 1, 4-naphthoquinone derivatives.* Bulletin of the Chemical Society of Japan, 1995. **68**(8): p. 2253-2261.

470. Guin, P.S., S. Das, and P. Mandal, *Electrochemical reduction of quinones in different media: a review.* International Journal of Electrochemistry, 2011. **2011**.

471. El-Etre, A., M. Abdallah, and Z. El-Tantawy, *Corrosion inhibition of some metals using lawsonia extract.* Corrosion Science, 2005. **47**(2): p. 385-395.

472. Červeň, J., et al., *Electrochemical activity of wedelolactone and probing its interaction with DNA using voltammetry at a carbon electrode.* Electroanalysis, 2015. **27**(10): p. 2268-2271.

473. Janeiro, P. and A.M.O. Brett, *Catechin electrochemical oxidation mechanisms.* Analytica chimica acta, 2004. **518**(1-2): p. 109-115.

474. Enache, T.A. and A.M. Oliveira-Brett, *Phenol and para-substituted phenols electrochemical oxidation pathways.* Journal of Electroanalytical Chemistry, 2011. **655**(1): p. 9-16.

475. Johnsirani, V., et al., *The Effect of Eclipta Alba Leaves Extract on the Corrosion Inhibition Process of Carbon Steel in Sea Water.* Portugaliae electrochimica acta, 2013. **31**(2): p. 95-106.

476. Zafrilla, P., F. Ferreres, and F.A. Tomás-Barberán, *Effect of processing and storage on the antioxidant ellagic acid derivatives and flavonoids of red raspberry (Rubus idaeus) jams.* Journal of Agricultural and Food Chemistry, 2001. **49**(8): p. 3651-3655.

477. da Silva Pinto, M., F.M. Lajolo, and M.I. Genovese, *Bioactive compounds and quantification of total ellagic acid in strawberries (Fragaria x ananassa Duch.).* Food Chemistry, 2008. **107**(4): p. 1629-1635.

478. Ashnagar, A. and A. Shiri, *Isolation and characterization of 2-hydroxy-1, 4-naphthoquinone (lawsone) from the powdered leaves of henna plant marketed in Ahwaz city of Iran.* Int J ChemTech Res, 2011. **3**(4): p. 1941-1944.

APPENDICES

APPENDIX A

PHOTO-BIOELECTROCHEMISTRY OF CYANOBACTERIA LACKING RESPIRATORY TERMINAL OXIDASES

This chapter contains text from the following publication:

B. Suganthan, N. Sekar, Y. Zhou, Y. Fang and R. P. Ramasamy

ECS Transactions, Volume 85, Number 13.

Abstract

In cyanobacteria, the excess electrons produced through the photosynthetic electron transport chain at light intensities are re-oxidized by respiratory terminal oxidases (RTOs) present in the respiratory electron transport chain to minimize photodamage. By knocking out the genes responsible for the RTOs, the organism's extracellular electron transfer (EET) ability towards the electrode could be further enhanced. In this study, the genes responsible for the RTOs in *Synechococcus elongatus* (*S. elongatus*) PCC7942, namely bd-type quinol oxidase, aa_3-type cytochrome oxidase, and cbb_3-type cytochrome oxidase were knocked out individually and in combination to construct single and double mutants. PCR was carried out to confirm the successful construction of mutants. EET and photocurrent generation ability of the cyanobacteria in a photo bioelectrochemical cell were investigated through the ferricyanide reduction assay and conventional electrochemical experiments, respectively.

Introduction

Cyanobacteria could be used as an anode catalyst in the photo-bioelectrochemical cells, by utilizing their photo-generated electrons. Cyanobacteria generate electrons through a photosynthetic electron transport chain (P-ETC) during the high light intensities that could be re-oxidized by terminal oxidases present in the respiratory electron transport chain R-ETC (dark reaction). This mechanism helps the cyanobacteria to survive from photobleaching effect. However, from an engineering perspective, this excess electron overflow mechanism from P-ETC is a valuable source for photocurrent generation, and the transfer of those electrons to R-ETC could be considered a loss of electron source. If these

electrons could be rerouted outside of the cell to an anode, we could increase the photocurrent-generating ability of cyanobacteria. This could be carried out by knocking out genes responsible for the respiratory terminal oxidases (RTO), which accept the excess electrons from P-ETC [60, 403]. The role of RTOs of cyanobacteria for extracellular electron transfer has not been studied so far. Previous studies have reported that *Synechococcus elongatus* PCC7942 contains three types of RTOs namely 'aa_3-type cytochrome oxidase' encoded by *coxBAC* and 'cbb_3-type cytochrome oxidase' encoded by *ccoNQ* and 'bd-type quinol oxidase' encoded by *cydBA* [404].

Earlier studies extensively studied on physiology of cyanobacterium called *Synechocystis* sp. PCC 6803 and revealed that there are two types of RTOs such as bd-type quinol oxidase (Cyd) and cytochrome c oxidase (COX), present in the thylakoid membrane and an alternative respiratory terminal oxidase (ARTO) present in the cytoplasmic membrane. In addition, they reported how these mutant cyanobacteria respond to excess light intensities and how terminal oxidase mutants of the cyanobacterium *Synechocystis sp* PCC 6803 show increased electrogenic activity in biological photo-voltaic systems [60, 403]. However, the above papers did not extensively study how these knockout genes affect their growth rate. Therefore, detailed studies are needed to understand how this strategy will affect their growth rate. Still, cyanobacteria cannot be used efficiently in the microbial fuel cells since they cannot transfer the electrons to the outside of the cell efficiently compared to exoelectrogens (microorganisms that are usually utilized in the microbial fuel cells) since they lack special features such as outer membrane cytochrome S (*OmcS*) on their outer membrane to carry out extracellular electron transfer. This problem was already addressed by our research group by developing a genetically engineered cyanobacterium called *S.*

elongatus PCC 7942 to express *OmcS*, was found to generate ~ nine-fold higher photocurrent compared to that of wild-type cyanobacterium[61]. We hypothesize that knocking out the genes responsible for the RTOs, could increase the electron flux from the over-reduced P-ETC towards the electrode via extracellular electron transport.

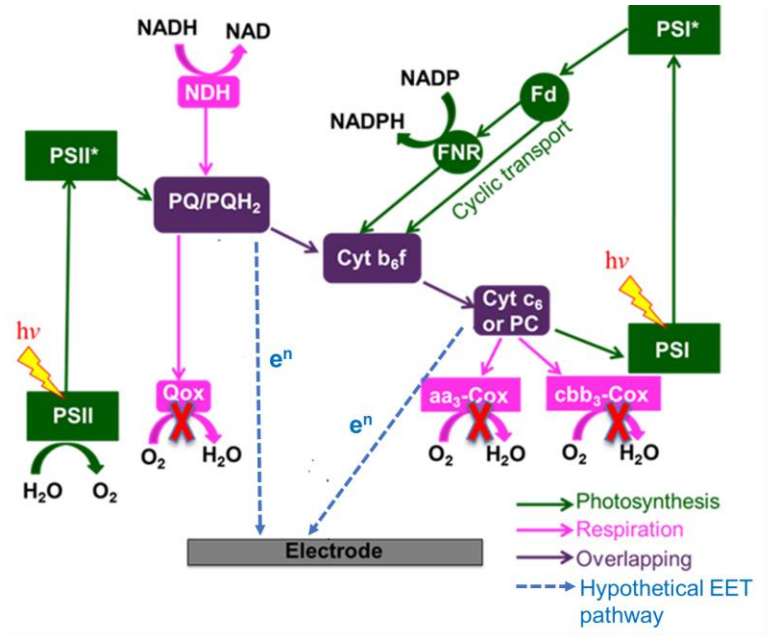

Figure 1: Schematic diagram representing the concept of enhancing the exoelectrogenic ability of cyanobacteria by genetic engineering them by knocking out the respiratory terminal oxidases.

Materials and Methods

Materials

Carbon paper (SpectraCarb 2050-L) was used as the electrode (3 mm diameter), where the carbon paper electrode (CP) was modified by adding a multi-walled carbon nanotube (10 nm diameter) (Dropsens, Spain) (MWCNT) solution (1 mg mL^{-1}). Cyanobacterial solution

(CB) was added on top of the MWCNT, and CP/MWCNT/CB was prepared as the working electrode. MWCNT was used as to increase the mechanical adsorption of the cyanobacteria on to the CP. Phosphate buffer (pH 7) was used as the electrolyte solution, and it was used to prepare the cyanobacterial solution. Nano pure distilled water (18 MΩ conductivity) was used to prepare all the chemicals. All the chemicals were purchased from Sigma-Aldrich, Acros Organics, EMD, and J. T. Baker. *S. elongatus* PCC 7942 strain and plasmids (pHBUV10 and UGS3-F2-P11) were used for genetic engineering and were obtained from Dr. Susan S. Golden (University of California, San Diego). Commercially available Quick-DNA TM Fungal/Bacterial Miniprep Kit (Zymo Research) was used for DNA extraction. All the PCR reagents were purchased from Promega. Go-Taq Polymerase (Promega) enzyme was used for PCR confirmation.

Construction of viable cyanobacterial knockouts

The cyanobacterial strain *S. elongatus* PCC 7942 was used for genetic manipulation. It undergoes natural transformation, where it can uptake the DNA from the environment and integrate it into its genome by homologous recombination. Single and double mutants were constructed by replacing the genes responsible for the respiratory terminal oxidases with the antibiotic resistance genes described in our previous work[405]. A detailed description of cyanobacterial mutants is shown in Table 1. Homologous recombination replaced the genes responsible for RTOs in the cyanobacterial genomic DNA with respective antibiotic resistance genes. The gene responsible for aa_3-type cytochrome oxidase (*coxBAC*) was replaced by an erythromycin antibiotic, the gene responsible for cbb_3-type cytochrome oxidase (c*coNQ*) was replaced with a chloramphenicol resistance gene, whereas the gene

responsible for bd-type quinol oxidase (*cydBA*) was replaced with kanamycin resistance gene responsible for bd-type quinol oxidase was replaced with a chloramphenicol resistance gene. Genetically engineered *S. elongatus* PCC 7942, which lack the RTOs, were grown in modified BG11 medium (10) with respective antibiotics. Plates were incubated under low light intensity (40 μmol m^{-2} s^{-1}) during the transformation process. Transformed colonies were inoculated in the autoclaved BG 11 medium, and cultures were incubated under continuous light intensity (80 μmol m^{-2} s^{-1}). All the cultures were maintained at 30 ± 2 ^{0}C, and all the liquid cultures were grown at 100 rpm. The genomic DNA of wild-type and mutant strains were isolated using Quick-DNA TM Fungal/Bacterial Miniprep Kit. Gene knocks out were confirmed with the respective gene-specific primers by PCR, as described in our previous work (5). To access the viability and life span of the mutants, growth analysis was carried out by measuring the absorbance value of the cultures at 750 nm using the UV-Vis spectrophotometer (Thermoscientific). Both wild-type and cyanobacterial mutant strains were incubated at 100 rpm with continuous light illumination (80 μmol m^{-2} s^{-1}). Absorbance measurement was taken every 24 hours.

Ferricyanide reduction assay

Ferricyanide reduction assay was used to study the extracellular electron transfer at the cellular outer envelope. All cyanobacterial strains were grown in 50 mL BG11 medium with appropriate antibiotics, harvested at an OD_{750} of 0.6, washed with fresh BG11 medium, and re-suspended in the same medium (50 mL). Potassium ferricyanide (1 mM) was added to the cultures after 24 hours, and the samples were collected every 12 hours to

monitor the reduction of potassium ferricyanide. Another 1 mL of the collected sample was centrifuged, and the absorbance of the supernatant was measured at 420 nm to calculate the concentration of potassium ferricyanide. In addition, chlorophyll content was measured at A_{665}. Cultures were incubated in continuous light conditions (80 μmol m^{-2} s^{-1}). The rate of ferricyanide reduction at 24 hours, normalized with the chlorophyll content, was calculated according to the calculation used in our group's previous work. (4). Wild type *S. elongatus* (wt) was used as control.

Table 1. Details of cyanobacterial strains used in this study1

Strain Name	**Parental strain**	**Plasmid present**	**Antibiotics used for screening purposes**	**Source**
Wt	*S. elongatus* PCC7942	None	None	Golden lab
cyd-	*wt*	pHBUV10	Kanamycin	[405]
cox-	*wt*	pNR2	Erythromycin	[405]
cco-	*wt*	UGS3- F2-P11	Chloramphenicol	[405]
cyd- cox-	*cyd-*	pNR2	Kanamycin and Erythromycin	This study
cox- cyd-	*cox-*	pHBUV10	Kanamycin and Erythromycin	This study
cox- cco-	*cox-*	UGS3- F2-P11	Erythromycin and Chloramphenicol	This study

cco- *cox-*	*cco-*	pNR2	Erythromycin and Chloramphenicol	This study

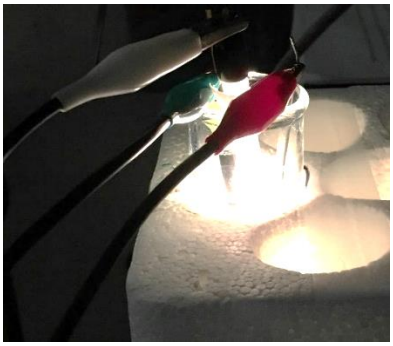

Figure 2: Photograph of the three-electrode electrochemical cell setup: CP/MWCNT/CB as working electrode (green), Ag/AgCl reference electrode (white), and Pt wire as a counter electrode (red) used in the present study.

Electrochemical experiments

The photocurrent-generating ability of all strains was measured using the chrono-amperometry technique in a three-electrode electrochemical cell setup [61] (Figure 2). The experiment was started in the dark and proceeded with an alternate light/dark cycle of 300 s. The cyanobacteria-immobilized MWCNT modified electrodes were used as the working electrode, along with a platinum wire counter electrode, and Ag/AgCl (Saturated KCl) was used as a reference electrode. Potassium phosphate buffer was used as an electrolyte. The MWCNT-modified working electrode was prepared as described by our previous group [405]. CH Instruments potentiostat (401a models, CH Instruments, Inc., Austin, TX) was used to measure the open circuit potential and photocurrent. The applied

potential was 100 mV higher than the open circuit potential. Wt *S. elongatus* was used as control.

Results and Discussion

Figure 3 shows the successful confirmation of double mutant (cox-cyd-) was verified by *cox* region-specific primer and *cyd* region-specific primers. The specific size band for the corresponding specific region (*cox* and *cyd*) was present in wt strains (Lane 2 and 8), whereas a truncated gene portion was observed in both cox- and cyd- (lane 3 and 9). The presence of a band in both lanes 4 and 10 (marked in a red rectangular shape) confirmed the successful construction of the double knockout. *S. elongatus* contain multiple copies of genomic DNA. The presence of only a single truncated band in lanes 3,4,9, and 10 confirms that the gene of interest was knocked out in all the copies present in *S. elongatus*. We could successfully construct all the single mutants (cox-, cyd- and cco-) and most double mutants (cox-cyd-, cyd-cox-, cox-cco-, and cco-cox-).

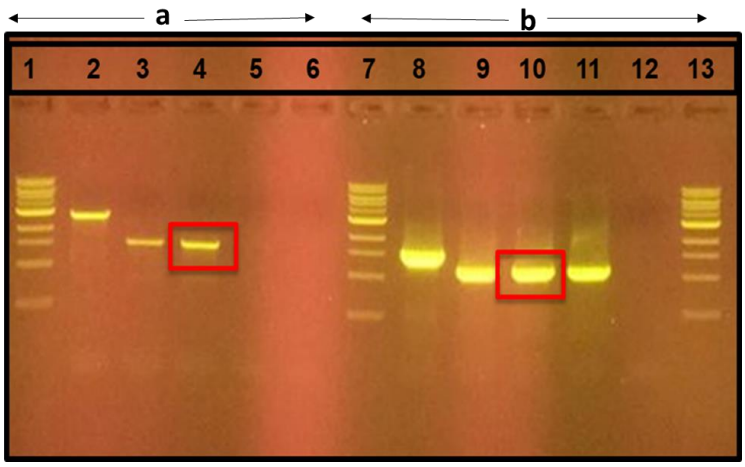

Figure 3: Verification of double knockout mutant (cox-cyd-) by PCR using (a) *cox* region-specific primers (b) *cyd* region-specific primers. Lane 1, 7 and 13: 1 Kb ladder; Lane 2 and

8: wt (control); Lane 3: cox- (control); Lane 9: cyd- (control); Lane 4 and 10: cox-cyd- Lane 6 and 12: Negative control.

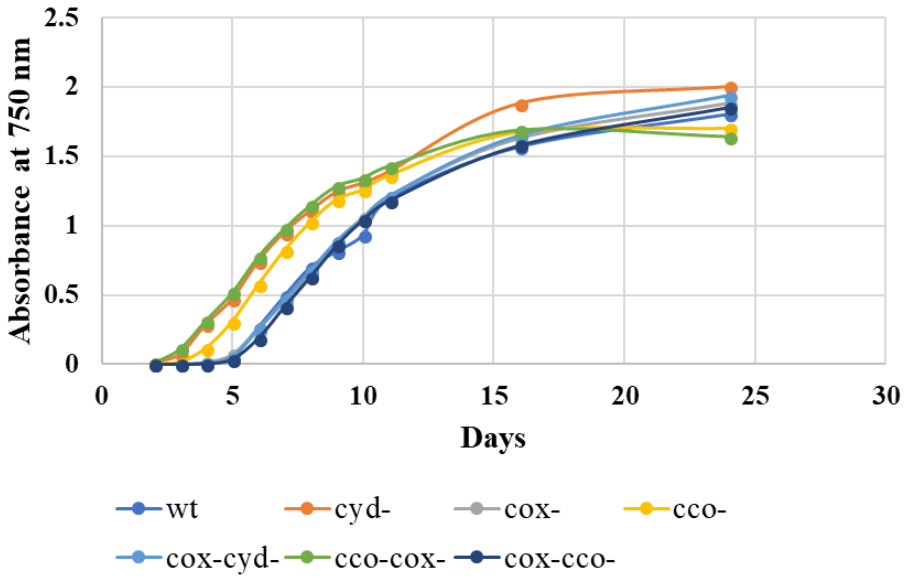

Figure 4: Growth analysis of wild-type, single and double mutant

Growth analysis for all the mutants was carried out to monitor their growth rate and to check whether they follow the same growth rate as wt *S. elongatus* or whether their growth rate will be retarded by mutating the RTOs. Figure 4 revealed that the growth rate was not affected by knocking out the genes responsible for respiratory terminal oxidases.

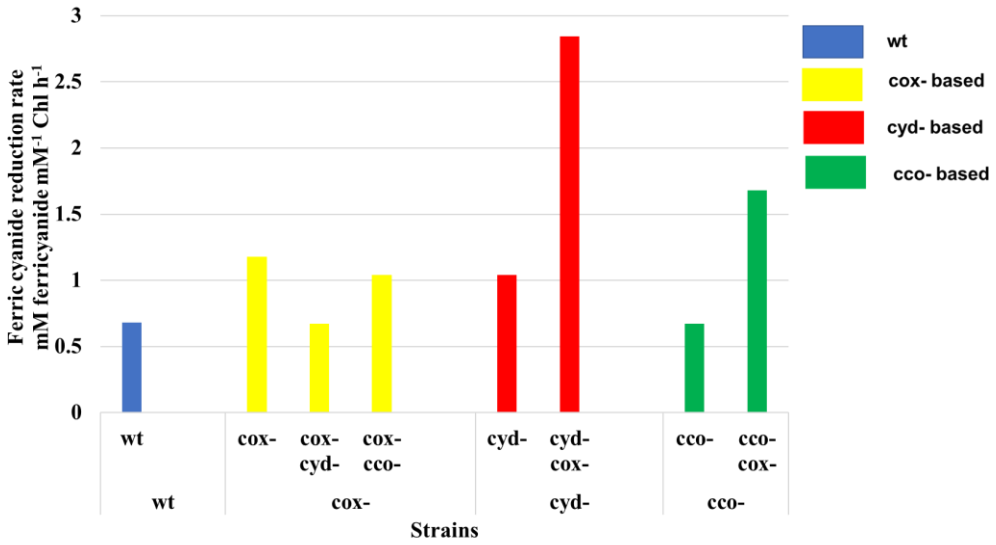

Figure 5: Comparison of ferricyanide reduction rate of single and double wild knockout mutants under light conditions. All the reduction rates were normalized with the chlorophyll content.

Ferricyanide reduction activity is considered one of the important parameters to access the EET ability since the bacterial outer membrane contains the terminal oxidases or reductases like NADH ferricyanide reductase, and they are associated with EET ability (6). As shown in Figure 5, ferricyanide reduction was comparatively higher in all the single and double mutants compared to wild type except the double mutant called cox-cyd- and cco-. In addition, cyd-cox- performed the highest ferricyanide reduction (4-fold than wild type) (Figure 5). When we consider the photocurrent generation ability of these strains, the double mutant cox-cyd- produced more current density than other mutants and wild type, shown in Figure 6. Figure 7 was derived from the results from Figure 6. In Figure 7, we calculated the difference between the current density when the condition changed from dark to light at 900 s. Here, we tried to understand how each strain responds when the

condition changes from dark to light. All the single and double mutants showed a higher difference in generating higher current density than wild type except cco- single mutant. A similar observation was made in the past literature with the cyanobacterial strain *Synechocystis* sp. PCC 6803[403]. The results revealed that cox-cyd- knockout strain produced more power density than single knockout strains. However, previous literature fails to compare the strains like cox-cyd- or cyd-cox-. Interestingly, although the cox-cyd- and cyd-cox strains are genetically similar, they do not similarly reduce the ferricyanide. In addition, the cox-cyd- and cyd-cox- strains did not exhibit similar performance when considering the photocurrent generating ability. Similar behavior was also observed for the other two look-alike double mutants, cco-cox- and cox-cco. The performance difference between the above look-alike strains needs further investigation.

The results for ferricyanide reduction and photocurrent density prove that knocking out the genes (*cox* and *cyd*) responsible for the respective terminal oxidases aids in generating high photocurrents. In addition, although knocking out of *cco* gene only (single mutant) could not result in higher power density than other mutants, the double mutants (cco-cox- and cox-cco-) can produce more current density than the wild type. The reasons for the above results could be since *cox* (aa3 type cytochrome oxidase) is present on the cytoplasmic membrane, *cco* (cbb3 type cytochrome oxidase) on the thylakoid membrane [404], and *cyd* (bd-quinol oxidase) on both thylakoid membrane and cytoplasmic membranes [406, 407]. Thylakoid membrane contains photosynthetic electron transport chain (P-ETC) and respiratory electron transport chain (R-ETC), whereas cytoplasmic membrane contains only the R-ETC. Therefore, knocking out both *cox* and *cyd* genes might decrease the

electron flux through R-ETC to reduce oxygen, and those electrons might increase the electron flux of the EET ability outside the cell. In addition, higher ferricyanide reduction and higher current density were observed in the double mutant strains, where both *cyd* and *cox* were knocked out compared to the double mutant where both *cox* and *cco* were knocked was since *cox* is only present in the cytoplasmic membrane.

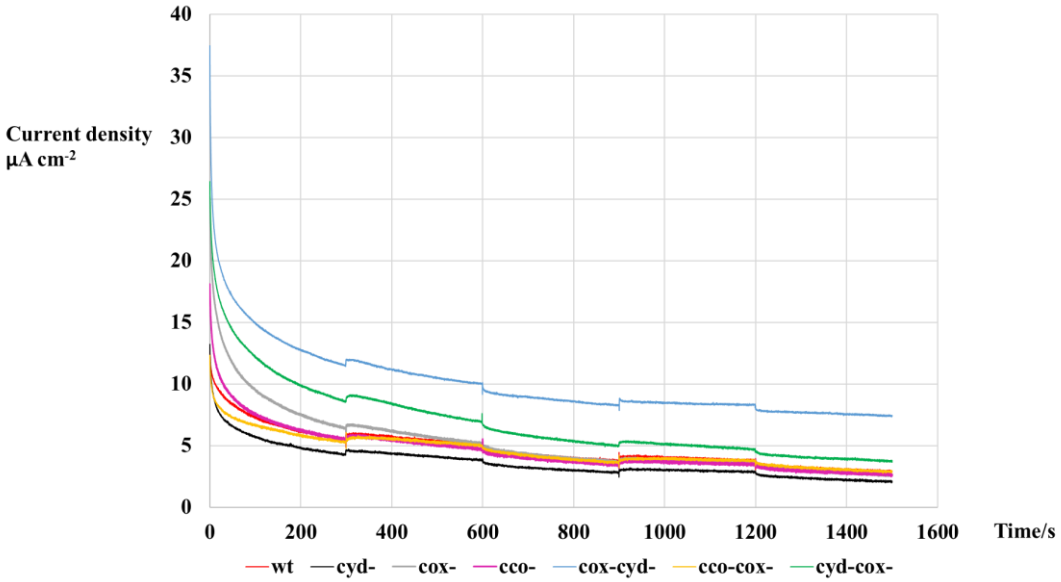

Figure 6: Photocurrent generation by wild-type and single knockout mutants by applying over-potential of 100 mV with respect to the respective OCP values. The experiment was started in the dark and proceeded with an alternate light/ dark cycle of 300 s.

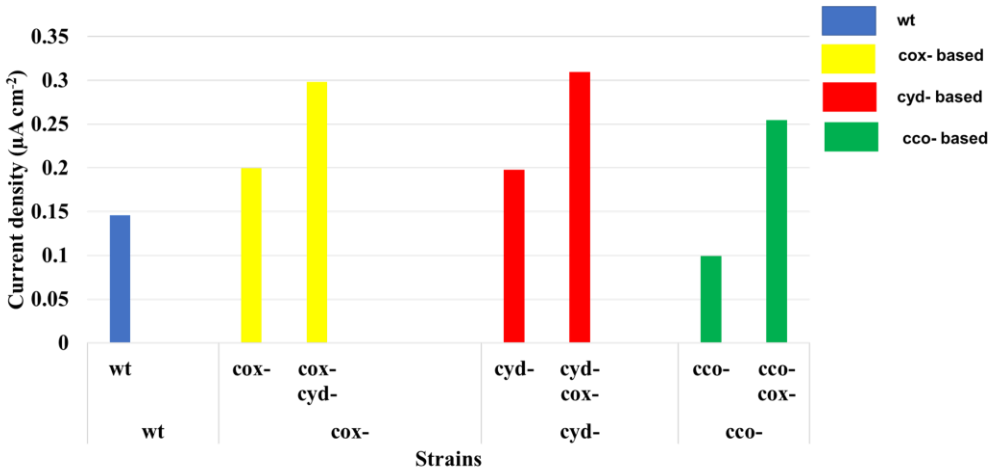

Figure 7: Difference between wild-type photocurrent density and single knockout mutants when the condition changed from dark to light at 900 s.

Conclusions

This work has demonstrated the construction of mutants of cyanobacterium *S. elongatus* PCC 7942, which lack the respiratory terminal oxidases (aa3-cytochrome oxidase, cbb3-cytochrome oxidase, and bd-quinol oxidase) to be used for photocurrent generation. We could successfully construct seven mutants, including three single mutants (cox-, cco- and cyd-) and four double mutants (cox-cyd-, cyd-cox-, cox-cco- and cco-cox-). All mutant and wild-type strains were evaluated for their EET ability with the ferricyanide reduction experiment by growing the cultures in the shake flasks with the addition of ferricyanide and photocurrent generation experiment using the Photo-bioelectrochemical cell. In addition, growth analysis was carried out to study the growth rate of the strains to understand whether mutating the respiratory terminal oxidases affected their growth rate. Results revealed that the double mutant cyd-cox- reduced the ferricyanide more than wild

type and other mutants. In addition, cox-cyd- and cyd-cox- produced more current density than wild-type and other mutants. Interestingly, although the double mutants (cox-cyd- and cyd-cox-; cox-cco- and cco-cox-) genetically look similar, their EET ability is different. This study clearly revealed that since the terminal oxidases (aa3-cytochrome oxidase and bd-quinol oxidase) in the cytoplasmic membrane were knocked out, they diverted the electrons produced during the photosynthesis to the outside of the cell, rather than using them for the oxygen reduction. They diverted the electrons produced during photosynthesis to the outside of the cell rather than using them for oxygen reduction. The results demonstrated in this work have significant implications for enhancing photocurrent and photo power density in cyanobacterial-based photo bioelectrochemical systems.

Acknowledgment

The authors wish to thank Dr. Susan S. Golden (University of California, San Diego) for donating *S. elongatus* PCC 7942 strain and the pHBUV10 and UGS3-F2-P11 plasmids.

APPENDICES

APPENDIX B

EXOELECTROGENICITY OF GENETICALLY MODIFIED *PYROCOCCUS FURIOSUS* AND ITS APPLICATION IN MICROBIAL FUEL CELLS

Baviththira Suganthan, Dominik K Haja, Chang-HaoWu, Yi Fang, Michael W. W. Adams, and Ramaraja P. Ramasamy. To be submitted to ECS Transctions.

Abstract

Pyrococcus furiosus (*Pf*), a hyperthermophilic microorganism, can act as anode biocatalyst for power generation in high temperature microbial fuel cells (MFC) using organic matter. The suitability of *Pf* as anode biocatalyst is dependent on its ability to transfer electrons extracellularly to a metallic electrode or terminal electron acceptor outside the cell. In *Pf*, the membrane bound hydrogenase (MBH) and cytoplasmic soluble hydrogenases (SHI and SHII) are believed to contribute to extracellular electron transport by serving as intermediate sites for catalysis in the electron transport pathways. In this study, we have genetically-manipulated *Pf* to determine the contributions of these enzymes to the extracellular electron transport by either over-expressing or knocking out the genes that encode them. Soluble ferric citrate and insoluble ferric oxide were used to investigate the ability of engineered *Pf* strains to reduce extracellular oxidants. In addition, *Pf* was used as the anode catalyst in a two-chamber microbial fuel cell that was used to study its exo-electrogenic ability towards electricity generation. The results revealed that exo-electrogenicity could be achieved in engineered strains, but likely at the expense of cell growth. This is the first report that compares the electricity-generating ability of different strains of genetically-engineered *Pf.*

Key words: Electricity, Hyperthermophile, iron reduction, *Pyrococcus furiosus*, microbial fuel cell.

1. Introduction

Microbial fuel cells (MFCs) are electrochemical devices that use microorganisms as catalysts to oxidize organic substrates to generate electricity. Microorganisms at the anode of MFC oxidize organic substrates and generate electrons, which then pass through the external circuit to the cathode where they are used for the reduction of a terminal electron acceptor. So far, exo-electrogenic microorganisms, such as *Geobacter* and *Shewanella*, have been extensively studied for use in MFC. These microorganisms are also known as dissimilatory metal respiring bacteria (DMRB), using their outer membrane cytochromes, pili or redox shuttling compounds to transfer the electrons to external electron acceptors such as mineral oxides of Fe, Mn, and U [408, 409]. In addition to DMRB, cyanobacteria such as *Synechocystis sp* PCC 6803 [403] and *Synechococcus elongatus* [405] have also been explored for their exo-electrogenic abilities in photo-bio MFC. However, thermophilic microorganisms that thrive at high temperatures have not been very well explored for use in MFC for electricity generation. Utilization of thermophiles for bio electrochemical energy conversion carries some advantages, such as faster chemical and electrochemical kinetics compared to that of mesophilic organisms. Previously, we reported that a hyperthermophilic microbe, *Pyrococcus furiosus* (*Pf*), could generate power in an MFC with a current density of 2 Am^{-2} and a power density of 225 mWm^{-2} in the absence of external redox mediators [410]. Nevertheless, there is a knowledge gap in the fundamental understanding of the underlying biological mechanisms of the respiratory electron transfer pathways and their impact on the exo-electrogenicity of *Pf*. Understanding the fundamentals of bio-electrochemical reactions could aid in the design and engineering of pathways to improve the extracellular electron transfer to an electron acceptor such as

an oxidant or a metal. To date, there have been no reports in the literature that investigate or even discuss the prospects of engineering pathways in hyperthermophiles for enhancing their exo-electrogenicity.

Pf is a strictly anaerobic hyperthermophilic organism that grows optimally near 100 ^{o}C [411] and uses a wide range of substrates as carbon sources, including various carbohydrates and proteins [412]. *Pf* is considered as a potential microbial catalyst for use in the anode of MFCs. *Pf* ferments carbohydrates to produce hydrogen gas (H_2) or hydrogen sulfide in the presence of elemental sulfur (S^0) [413]. It contains the enzyme termed membrane bound hydrogenase (MBH), which uses reducing equivalents from the oxidative fermentative pathway to produce H_2 [414]. It is predicted that extracellular H_2 can be used by soluble hydrogenases (SHI and SHII) for oxidized nicotinamide cofactor generation, although the conditions under which this occurs is not clear [415].

Additionally, a cytoplasmic enzyme called NADH-dependent ferredoxin $NADP^+$ oxidoreductase I (NfnI) thought to be the primary oxidoreductase that maintains redox balance in *Pf*, as it reversibly reduces ferredoxin and NAD^+ by using NADPH as the electron donor [416]. Reduced ferredoxin (Fd_{red}) can be generated by the modified Embden-Meyerhof pathway in *Pf* as shown in Figure 1. MBH uses the Fd_{red} that is generated as the electron donor for H_2 gas production, and simultaneously produces an ion (Na^+) gradient that can be used for ATP generation by an Na^+-dependent ATP synthase. We hypothesized that some uncharacterized proteins could be present in the cytoplasm and as well as in the membrane [410], shown as pink and red spheres in Figure 1, that could utilize Fd_{red} as the electron donor to reduce extracellular electron acceptors. Therefore, there might exist a competition between MBH and these hypothetical proteins (hp) to

access the pool of Fd_{red} in the cytoplasm for their respective reactions. Managing these competing pathways by manipulating the function of various enzymes or by varying the environmental conditions could determine the level of exo-electrogenicity exhibited by the organism. Figure 1a shows the hypothetical electron transfer pathway(s) when soluble ferric citrate is added to the growth medium. Since ferric citrate (Fe^{3+}) has the capability to permeate through the outer S-layer of the cell envelope, it could get reduced to ferrous citrate (Fe^{2+}) by the hypothetical proteins present in the cytoplasm (pink spheres in Figure 1) and as well as in the S-layer (red spheres in Figure 1). In contrast, insoluble ferric oxide should only be reduced by the hypothetical proteins present in the outer S-layer, as ferric oxide should not penetrate through the cell's S-layer [410] (Figure 1 b).

Redox enzymes such as MBH may play important roles in determining the electron flux both within the *Pf* cell as well as across the cell membrane. Any modification to this and related enzymes could impart redox functionalities to *Pf* that may help improve our understanding of the extracellular electron transfer mechanisms of the organism. The goal of this work was therefore to manipulate the production of membrane-bound MBH and of cytoplasmic hydrogenases SHI and SHII, enzymes thought to be involved in the respiratory electron transport pathway, in an effort to enhance extracellular electron transport towards an external electron acceptor (such as an electrode). This, in turn, could result in enhanced electricity generation in MFCs. This might be achieved by either knocking out or overexpressing the genes encoding for MBH and SHI/II.

2. Materials and Methods

2.1 Materials:

Ferric oxide, ferric citrate and ferrozine (3-(2-pyridyl)-5,6-diphenyl-1,2,4-triazine-p, p-disulfonic acid, monosodium salt hydrate) and hydrochloric acid were purchased from Sigma Aldrich. Potassium ferricyanide was purchased from Acros. Nafion membrane 115 and AvCarb G200 graphite felt were purchased from Fuel Cell Store. Titanium wire (0.25 mm diameter) was purchased from Alfa Aesar.

Strains: The *Pf* strains used in this study are summarized in Table 1.

2.2 Methods

2.2.1 Growth Conditions:

The composition of the medium used for growing *Pf* consisted of 1 × base salts, 1 × trace minerals, sodium tungstate (10 μM), nickel chloride (1 μM), yeast extract (0.5 % w/v), casein hydrolysate (enzymatic) (0.5 % w/v), maltose (0.5 % w/v), cysteine hydrochloride (0.17 g/L), sodium bicarbonate (1 g/L) and dipottasium phosphate (pH 6.8, 1 mM). The stock solutions of the base salts and trace minerals were prepared as described previously [417]. The media were prepared, filter sterilized using 0.22-micron filters and stored at 4 ^{o}C. About 0.01 % of the overnight culture was used as the inoculum to grow all the strains. Inoculated cultures were grown in anaerobic culture bottles which were degassed and purged with argon. The cultures were grown at 88 ^{o}C inside a conventional gravity oven.

2.2.2 Chemical Titration Experiments (Fe^{3+} Reduction):

Iron reduction experiments were carried out using either soluble ferric citrate (20 mM) and insoluble ferric oxide (15 mM) in the medium. All experiments were performed using biological triplicates. Overnight cultures were inoculated into a 50 mL culture bottle and maintained at 88 ^{o}C inside a shaking incubator. Samples were collected every 3 hours to monitor the cell growth and ferrous ion concentrations. Cell growth was measured using the Bradford assay and ferrous ion measured using the ferrozine assay [418].

2.2.3 Microbial Fuel Cell Setup:

A two-chamber microbial fuel cell setup as shown in Figure 2 was constructed using AvCarb G200 graphite battery felt as both the anode and cathode, in a similar manner to that previously reported [410]. Nafion 115^{TM}, treated with 5 % H_2O_2 and 8 % sulfuric acid in water at 80 ^{o}C for 1 hour, was used as the membrane separator between the anode and cathode chambers. 50 mM ferricyanide in 0.1 M phosphate buffer (pH 6.8) was used as the catholyte. An overnight culture of each *Pf* strain was harvested at 5,000 rpm for 20 minutes, and the cells were resuspended in 50 mL of the medium and used as the anolyte. The amount of anolyte was normalized based on the protein concentration in each sample, which was determined using the Bradford assay. Un-inoculated medium was used as an abiotic control. Air tight butyl rubber stoppers were used to seal both anode and cathode chambers. The headspaces of both anodic and cathodic chambers were filled with argon by purging for 15 minutes. MFC setup was maintained at 88 ^{o}C inside a gravity convection oven during the experiments.

2.2.4 Electrochemical Experiments:

Electrochemical experiments were conducted in an H-shaped two chamber MFC**.** The graphite felt containing the *Pf* biofilm was used for all electrochemical tests. Biofilm development on the MFC anode was induced by a 100 Ω resistance load across the MFC for 3.5 hours using an EXTECH Instruments 380400-decade resistance box. The voltage and current of the MFC were measured using the Arbin Instruments Electrochemical Cycler and analyses were done using MITS PRO software program. For fuel cell polarization experiments, the current was continuously measured by applying different voltages for a fixed duration of time at each voltage. Current density was calculated by normalizing the current based on the geometric surface area of the electrode (9 cm^2). Power density (mW m^{-2}) was calculated by multiplying the current density by the MFC voltage.

3. Results and Discussion

3.1 Growth Comparison Between the Strains COM1, OESHI, ΔSHI/II, OEMbhJ-N and ΔMbhL

3.1.1 Growth Analysis

The *P. furiosus* strains, COM1, OESHI, ΔSHI/II, OEMbhJ-N and ΔMbhL were grown at 88 ^oC in the presence of ferric citrate (a soluble electron acceptor) and ferric oxide (an insoluble electron acceptor) for 15 hours and growth was measured by the whole cell protein content. A medium without the inoculum was used as a control. The intent of this experiment was twofold: (1) to examine if the ferric citrate or ferric oxide have any

influence on the growth of these strains; and (2) to observe if the genetically-modified strains (OESHI, ΔSHI/II, OEMbhJ-N and ΔMbhL) exhibit any growth phenotype compared to the parent strain (COM1). A comparison of the growth of these strains in each of the three media is shown in Figure 3a-c and growth based on normalized cell protein concentrations is shown in Figure 3d. Some key observations drawn from these data include: (i) Genetic modification of the parent strain COM1 affected its growth, as none of the modified strains grew as fast as the parent strain in the absence of an iron-based acceptor (Figure 3a); (ii) With the exception of OEMbhJ-N in the presence of soluble ferric citrate (Figure 3b), the growth rate of the parent strain COM1 was higher than that of all engineered strains in any given medium (Figure 3a-c); (iii) The ΔMbhL strain did not exhibit any significant growth, except in the presence of citrate where it exhibited minimum growth, consistent with the published observation that the ΔMbhL strain requires elemental sulfur (S^0) for growth [413]; (iv) Normalized cell growth rates indicate that the insoluble electron acceptor (ferric oxide) did not result in any statistically significant variation in the growth of the strains studied (Figure 3d). Addition of ferric oxide, which is insoluble and cannot penetrate the S-layer of the cell membrane and therefore cannot act as an alternate terminal electron acceptor, did not result in the enhancement of cell growth; and (v) The presence of ferric citrate in the medium slowed the growth of all strains except for the ΔMbhL strain, which showed a dramatic growth enhancement (Figure 3d). This indicates that MBH normally diverts electrons to hydrogen gas rather than to soluble ferric iron, which could penetrate inside the cell through the cell membrane and act as a terminal electron acceptor in place of protons, as shown in Figure 1, thereby completing the metabolic pathway. Conversely, in the absence of a functional MBH, electrons can be

diverted to soluble ferric iron, although how this occurs is not clear. It is important to note that while the ΔMbhL did grow in the presence of soluble ferric iron, the absolute growth rate was still much lower than that observed for all other strains (Figure 3a-c). This would be expected since, in the absence of hydrogen gas production by *Pf,* ATP is generated only by fermentation and not by respiration.

3.1.2 Reduction of soluble Fe^{3+} (ferric citrate):

The exo-electrogenicity of the parent strain, COM1, in the presence of the soluble electron acceptor (ferric citrate) measured in terms of the production of soluble Fe^{2+} per unit cell protein was 141 nmol/mg (Figure 4). This was used as a reference value to determine if the genetic modifications of the parent strain COM1 resulted in a change in its exo-electrogenic ability.

3.1.2.1 Manipulation of SHI/II:

While both overexpression and deletion of the genes encoding the SHI/II enzymes resulted in marginally slower growth compared to parent strain, this did not result in a lower electrogenic ability. As shown in Figure 4, both OESHI and ΔSHI/II exhibited higher Fe^{2+} production than the parent strain by about 51 % and 16 %, respectively. This could be explained by overexpression of SHI (OESHI stain) resulting in increased uptake of H_2 by the cell, resulting in a higher concentration of Fd_{red} in the cytoplasm through the activity of NfnI. The increased availability of Fd_{red} then results in the enhancement of the reaction between hypothetical proteins that utilize the additional Fd_{red} to reduce Fe^{3+} to Fe^{2+}, as shown in Figure 1a. On the other hand, deletion of SHI/II (ΔSHI/II strain) should result in

the non-utilization of H_2 and therefore a lower intracellular concentration of NADPH (that would otherwise be generated by SHI/II). However, it is not clear how this leads to the increased conversion of Fe^{3+} to Fe^{2+} as Fd_{red} would be used for NADPH production via Nfn rather than for iron reduction (Figure 1).

3.1.2.2 Manipulation of MBH:

The growth yield results shown in Figure 3b demonstrate the importance of MBH for cell growth. Overexpression of MBH resulted in a roughly 45 % increase in cell yield while deleting MBH from the organism resulted in an 85 % reduction in the cell yield. These data can be explained by the metabolic pathways shown in Figure 1, which show that MBH is essential for the reduction of protons to H_2, a terminal redox reaction for metabolic oxidation or fermentation of sugar (in this case, the disaccharide maltose). Therefore, manipulation of cellular MBH activity will have the following implications for the exo-electrogenicity of the organism: (i) Overexpression of MBH (OEMbhJ-N strain) results in the reduction of exo-electrogenicity by about 49 %. This could be explained by the inability of the hypothetical proteins to compete with MBH for the Fd_{red} pool, simply because of higher activity of MBH in the OEMbhJ-N strain, thereby leading to less Fd_{red} available for Fe^{3+} reduction. (ii) Deleting the MBH from the organism (ΔMbhL strain) results in a 120 % increase in its exo-electrogenicity over the parent strain, which could be due to the lack of competing pathways for the reduction of $Fd_{red,}$ making Fe^{3+} reduction the only reaction (green block arrows) through which they could be utilized. However, it must be noted that this strain exhibits higher exo-electrogenicity than any of the other strains, even though it struggles to grow on maltose due to the absence of MBH.

A comparison of Fe^{3+} reduction data for ΔSHI/II and ΔMbhL show that when H_2 oxidation activity is absent due to a lack of the cytoplasmic enzymes, a 16 % increase in electrons going towards Fe^{3+} reduction was observed. However, when H_2 production activity was eliminated as in ΔMbhL strain, this resulted in a 120 % increase in electrons going towards Fe^{3+} reduction. This offers further evidence that any $Fd_{red,}$ not utilized by MBH is likely to be used by hypothetical proteins for Fe^{3+} reduction.

3.1.3 Reduction of insoluble Fe^{3+} (ferric oxide):

Insoluble ferric oxide cannot penetrate through the membrane S-layer into the cytoplasm and therefore is unable to receive electrons from the Fd_{red} pool in the cytoplasm directly. However, insoluble extracellular electron acceptors might still be reduced by hypothetical proteins present in the membrane (red spheres in Figure 1b). Figure 5 shows the Fe^{3+} reduction results for all strains in the presence of insoluble ferric oxide. It was observed that their exo-electrogenicity (measured in terms of the Fe^{2+} that was released) was about two orders of magnitude lower (on the basis of total cellular protein) than in the presence of the soluble electron acceptor ferric citrate (see Figure 4). The significantly lower Fe^{3+} reduction activity can be explained by the weak interaction between ferric oxide and the hypothetical proteins in the cell membrane, or by direct interaction between the insoluble iron and MBH as Fe^{2+} production could not be measured in the ΔMbhL mutant. In contrast, deletion of SHI (and SHII) and overexpression of either SHI or MBH led to an enhancement in the exo-electrogenicity of the organism as measured by Fe^{3+} reduction (Figure 5). However, the significance of these data is not clear, especially given the extremely low rates of iron solubilization. What is clear is that exo-electrogenicity is

absolutely dependent upon MBH, although whether this is mediated by a hypothetical membrane protein(s), as shown in Figure 1 (red spheres), or is the result of direct interaction is not known.

Mesophilic microorganisms belong to genera such as *Shewenella* [419-422], *Geobacter* [423, 424], *Desulfobulbus* [425] and *Desulfuromonas* [419, 426], as well as some hyperthermophilic microorganisms, such as *Ferroglobus placidus* and *Geoglobus ahangari* [427], are capable of reducing insoluble ferric oxide and have been extensively studied in microbial fuel cells. These microorganisms utilize direct contact with insoluble electron acceptor, electrically conductive pili, or redox shuttles to exhibit their electrogenicity. However, c-type cytochromes are involved in transporting the electrons to insoluble electron acceptors in all of these microorganisms. However, *Pf* does not contain the c-type cytochromes and therefore the results strongly suggest that its exoelectrogenicity is absolutely dependent upon the MBH enzyme.

3.2 Electrochemical Characterization

3.2.1 Short-term growth comparison:

Cultures of each *Pf* strain were grown for 16 hours and were used as inocula for electrochemical experiments. It is important to note that these cultures were grown without ferric citrate, ferric oxide or sulfur in the medium. The growth of each strain with the electrode was monitored over a period of 3.5 hours, the same time that it takes to carry out the polarization experiments, and the results are shown in Figure 6. The parent stain,

COM1, exhibits the fastest growth among all strains while the ΔMbhL strain showed little if any growth, as was observed in the absence of the electrode.

3.2.2 Electrochemical polarization study:

Figures 7 shows the polarization curve and the power density curves for the MFCs that use the different *Pf* strains on the anode. The polarization curve was plotted by measuring the steady state current density with the different applied cell voltages. The polarization results are in alignment with the cell growth data given in Figure 6. Hence, among the five strains, the strain exhibiting the best growth in the standard medium, COM1, generated the highest current density, while that showing the least growth, ΔMbhL, did not respond to electrochemical stimuli. Previous studies have proven that operating MFCs at high temperatures increases the reaction rates of both chemical and electrochemical reactions [428-430]. For example, marine sediment fuel cells operated at a temperature of 60 ^{0}C generated 10-times more current than that operated at 22 ^{0}C [429]. A number of other studies have reported utilizing both pure and mixed cultures of thermophiles and hyperthermophiles in MFCs and a comparative analysis of the current and power densities achieved is summarized in Table 2. It is important to note that comparing current densities of these earlier reports is more meaningful than comparing power densities, which vary based on MFC configuration and cathode type. In our study, a current density of 553 mA m^{-2} was measured with *Pf*, which was higher than the previously measured 450 mA m^{-2} [431] using a mixed culture of a petroleum reservoir, where a similar type of MFCs (same of the electrode) set up was utilized. The maximum current density reported so far is 1500 mA m^{-2} at 55 ^{O}C, by *Calditerrivibrio nitroducens* in a fed batch system. However, this

value includes the background current from the medium, which was excluded from our reported values. In summary, due to the lack of a unifying method for reporting MFC performances, a fair comparison of performance parameters is impossible at this time.

4. Conclusions

This work offers the first insight into the exo-electrogenic ability of parent and engineered *Pf* through both chemical and electrochemical tests using soluble/insoluble iron and the electrode as electron acceptors, respectively. Hydrogenases namely MBH and SHI/SHII appear to play important roles in both intracellular and extracellular electron transfer processes in *Pf*. The results offer a first-hand understanding of possible mechanisms that may prove useful for bio-electrochemical energy conversion using engineered *Pf* as biocatalysts in microbial fuel cells. More investigation is needed to further validate the suitability of *Pf* as catalyst in microbial fuel cells.

Acknowledgment

This work was supported in part by a grant (DE-FG05-95ER20175 to MWA) from the Division of Chemical Sciences, Geosciences and Biosciences, Office of Basic Energy Sciences of the Department of Energy. The authors wish to thank Dr. Narendran Sekar for helpful discussions and Thomas Sporer for experimental assistance.

Table 1: The *Pf* strains used in this study

Strain	**Description about the strain**	**Notation**	**References**
COM1	Naturally competent *P. furiosus*	COM1	(Lipscomb et al. 2011)
MW430	SHI overexpression in COM1	OESHI	(Chandrayan et al. 2015)
MW0015	SHI and SHII deletion mutant in COM1	ΔSHI/II	(Lipscomb et al. 2011)
MW0414	MbhJ-N overexpression in COM1	OEMbhJ-N	(McTernan et al. 2014)
MW0024	MbhL deletion in COM1	ΔMbhL	(Schut et al. 2012)

Table 2: Comparison of MFC current densities reported in the literature for thermophiles and hyperthermophiles with the results obtained in the present study

Anolyte culture	**MFC working temperature**	**Electrode materials**	**Current density (mA m^{-2})**	**Power density (mW m^{-2})**	**Comment**	**Reference**
Mixed culture	55 ^{0}C		100	37	*Full cell *Did not mention about type of electrode and surface area of the electrode. * Did not mention about the current produced by the medium	(Kelly C et al. 2008)
Mixed culture	95 ^{0}C	Carbon cloth (4*10 cm)	450	165	*Fed batch system * Did not mention about the current produced by the medium	(Fu et al. 2015)
Thermincola ferriacetica	60 ^{0}C	Graphite block (6.7 cm^2)	400	146	*Fed batch system *Mentioned as medium had no effect on current. However, did not show any data	(Marshall and May 2009)
Calditerrivibrio nitroreducens	55 ^{0}C	Carbon cloth (2*10 cm)	1500	272	*Fed batch system * Did not mention about the current produced by the medium	(Fu et al. 2013)

Ferroglobus placidus	85 ^{0}C	Graphite plate (92 m^2/m^3)	~680		*Single chamber * Fed -batch system	(Yilmazel et al. 2018)
Geoglobus ahangari	80 ^{0}C	Graphite plate (92 m^2/m^3)	~570		*Single chamber. * Fed -batch system	(Yilmazel et al. 2018)
Pyrococcus furiosus	90 ^{0}C	Graphite felt	2000 (1100) Current density produced by medium was subtracted and given inside the bracket	225 (50) Power density produced by medium was subtracted and given inside the bracket	*Batch system *Composition of the medium is different than the current study *Biofilm was grown for 8 hours	(Sekar et al. 2017)

Pyrococcus furiosus	88 ^{0}C	Graphite felt	1041 (553) Current density produced by medium was subtracted and given inside the bracket	152 (80) Power density produced by medium was subtracted and given inside the bracket	*Batch system * Biofilm was grown for 3.5 hours	This study

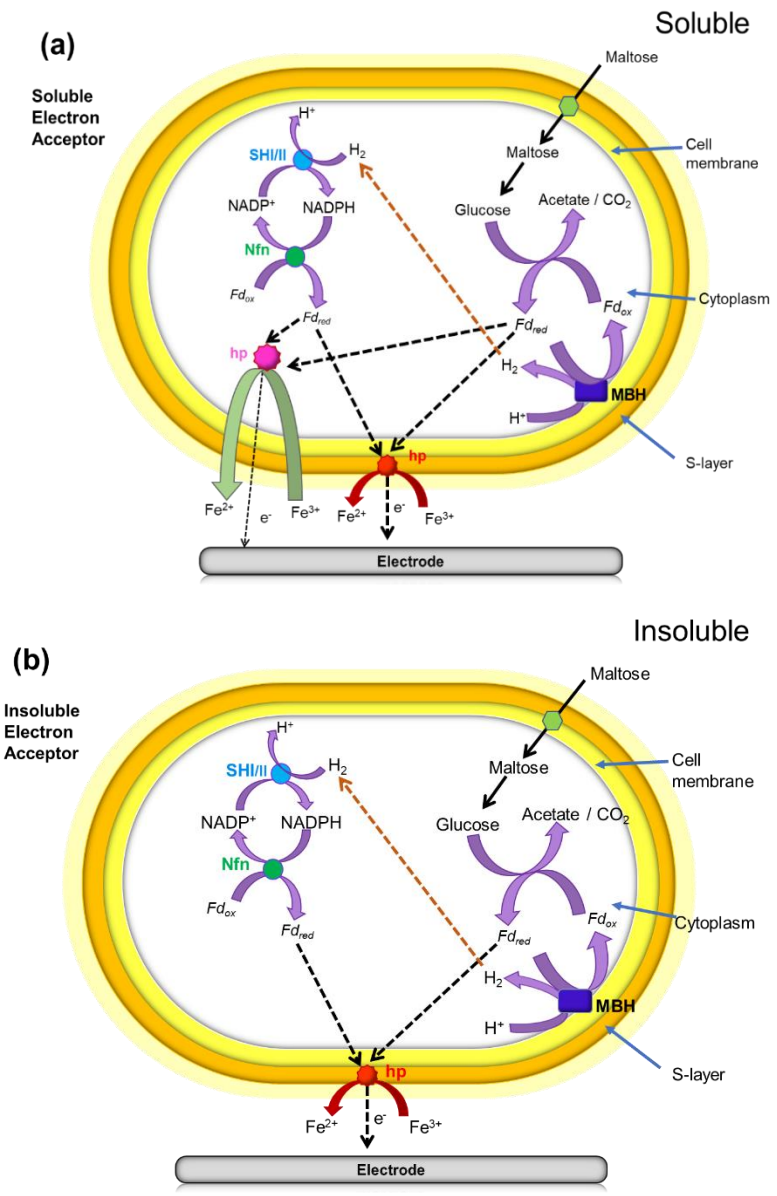

Figure 1: Schematic diagram of oxidative fermentative pathways and hypothetical extracellular electron transport pathway of *Pyrococcoccus furiosus* in the presence of: soluble ferric citrate (a) and insoluble ferric oxide (b).

MBH - membrane bound hydrogenase; SHI/II - soluble hydrogenase; hp - hypothetical proteins; fd_{ox} - oxidized form of ferredoxin; fd_{red} - reduced form of ferredoxin; M_{ox} -

oxidized form of mediators; M_{red} - reduced form of mediators; Nfn - NADH-dependent ferredoxin $NADP^+$ oxidoreductase; black solid and purple block arrows - physiological pathways of the metabolic processes; green block arrows – extracellular electron transfer to insoluble electron acceptor; red block arrows – extracellular electron transfer to insoluble electron acceptor; black broken arrows - hypothetical extracellular electron transport pathways showing possible routes for electron harvesting in the absence of MBH in microbial fuel cells.

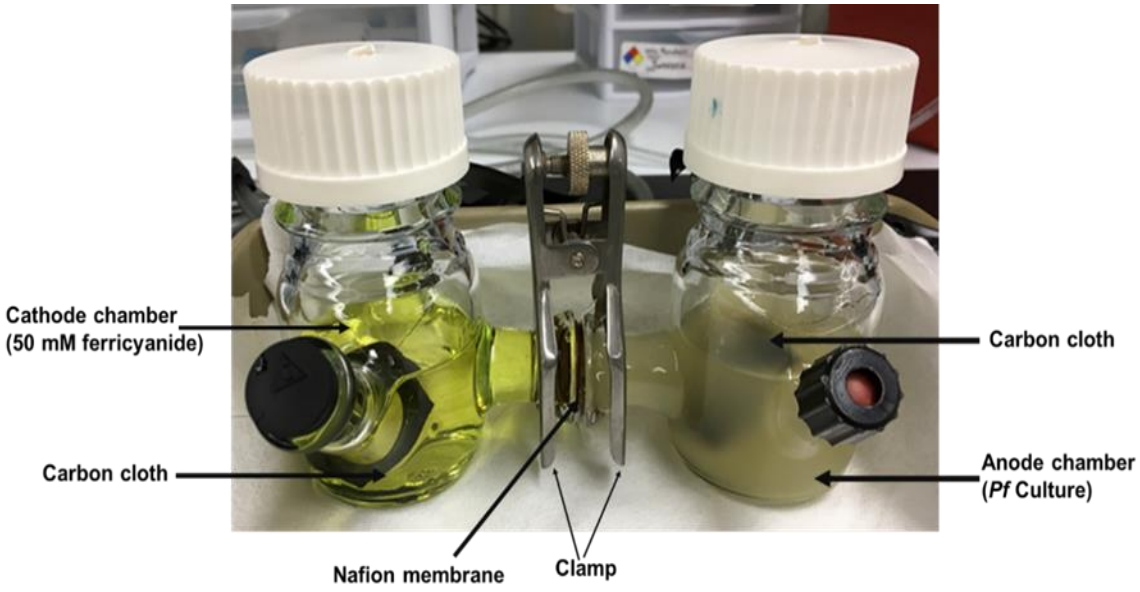

Figure 2: Picture of H-shaped microbial fuel cell (two chamber) used in the present study.

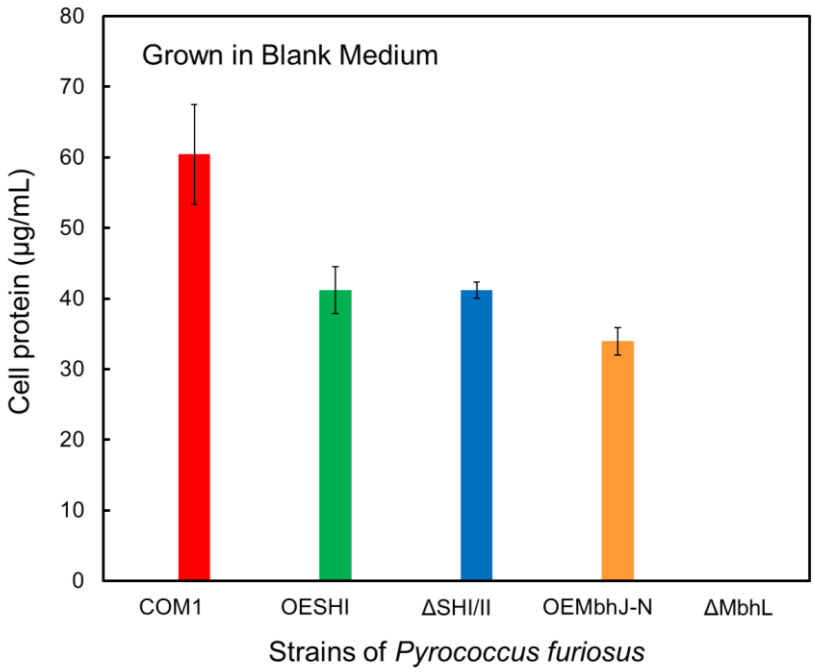
Grown in Blank Medium
Cell protein (µg/mL)
80
70
60
50
40
30
20
10
0
COM1
OESHI
ΔSHI/II
OEMbhJ-N
ΔMbhL
Strains of *Pyrococcus furiosus*

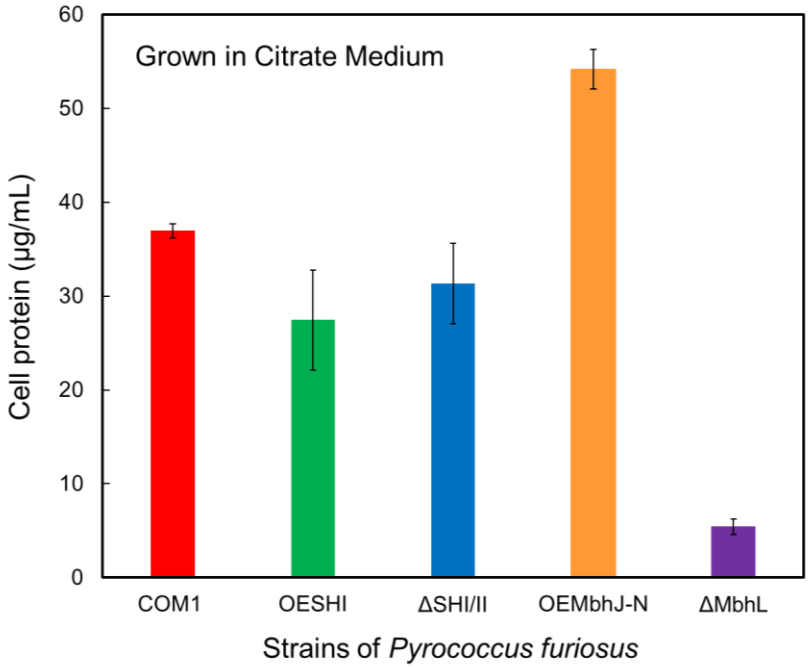
Grown in Citrate Medium
Cell protein (µg/mL)
60
50
40
30
20
10
0
COM1
OESHI
ΔSHI/II
OEMbhJ-N
ΔMbhL
Strains of *Pyrococcus furiosus*

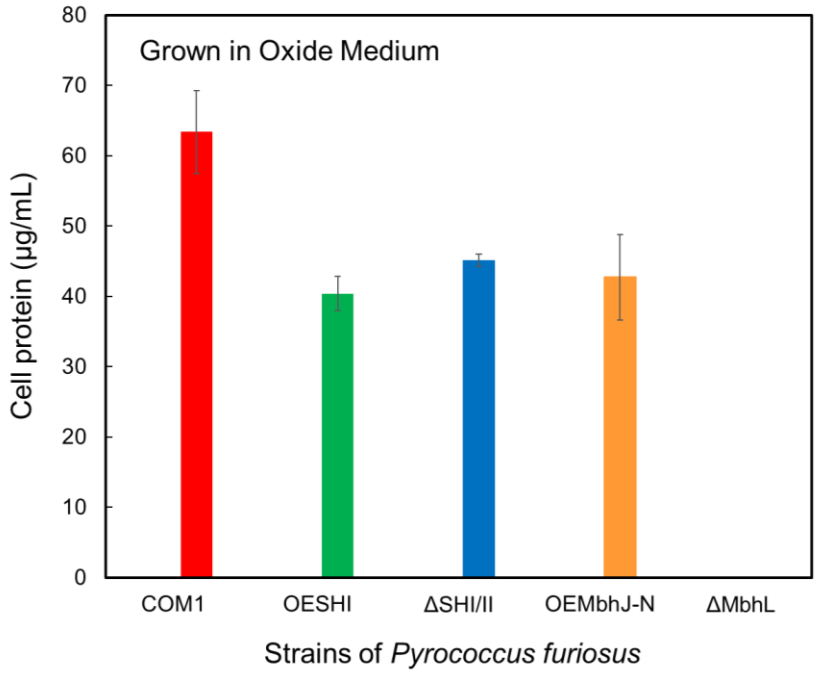
Grown in Oxide Medium
Cell protein (µg/mL)
80
70
60
50
40
30
20
10
0
COM1
OESHI
ΔSHI/II
OEMbhJ-N
ΔMbhL
Strains of Pyrococcus furiosus

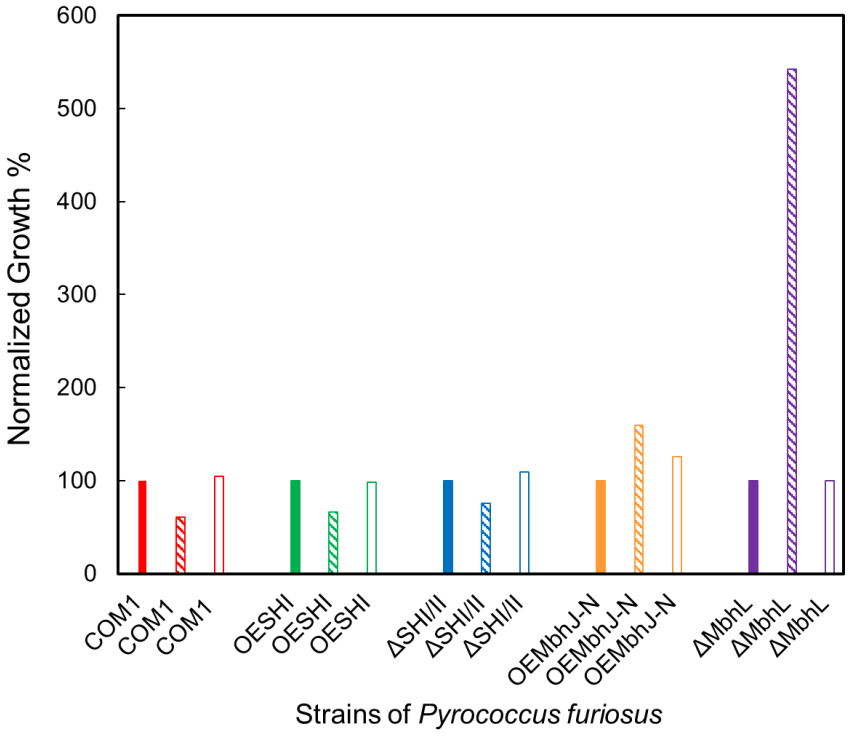
Normalized Growth %
600
500
400
300
200
100
0
COM1
COM1
COM1
OESHI
OESHI
OESHI
ΔSHI/II
ΔSHI/II
ΔSHI/II
OEMbhJ-N
OEMbhJ-N
OEMbhJ-N
ΔMbhL
ΔMbhL
ΔMbhL
Strains of Pyrococcus furiosus

Figure 3: Growth analysis of COM1, OESHI, ΔSHI/II, OEMbhJ-N and ΔMbhL in the presence of ferric citrate (b) and ferric oxide (c). Medium was used as a control (a). (Growth was carried out around at 15 hours). (d). Normalized growth of COM1, OESHI, ΔSHI/II, OEMbhJ-N and ΔMbhL in the presence of ferric citrate (stripes) and ferric oxide (open bars). The medium was used as a control (solid bars).

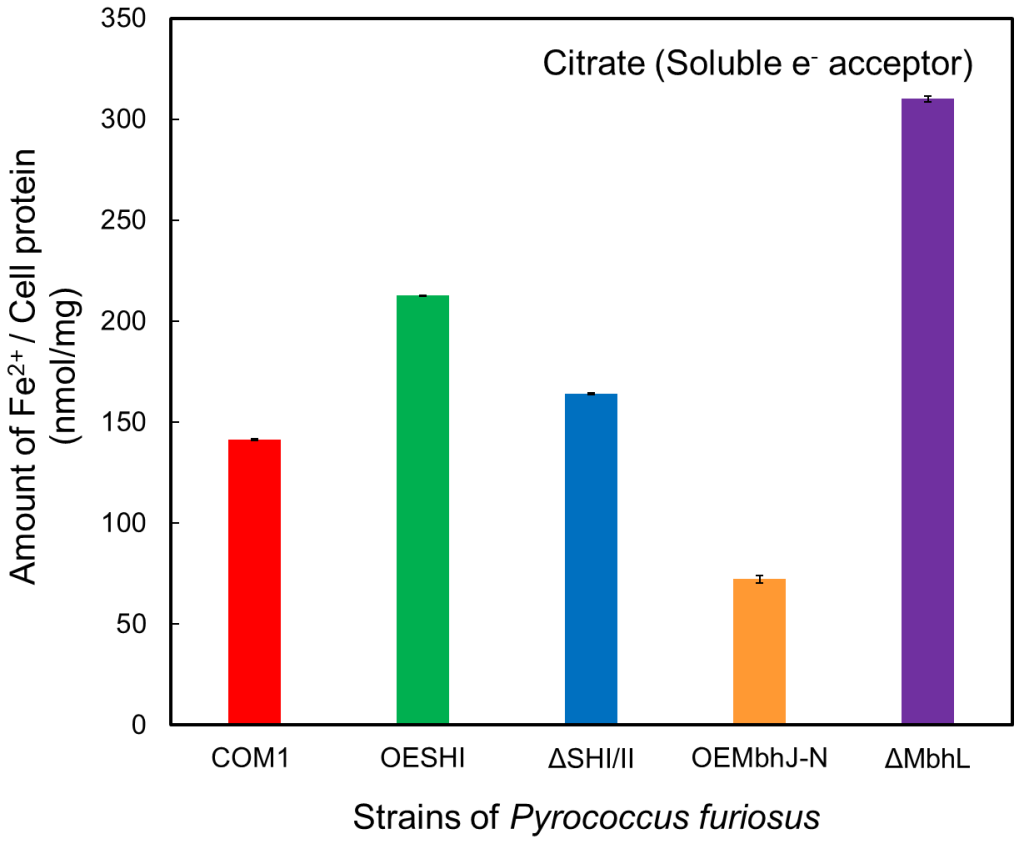

Figure 4: Comparison of the amount of soluble ferric iron (as ferric citrate) reduced to soluble ferrous iron by different strains of *Pf* with respect to the total cell protein after 15 hours of growth at 88 ^{o}C.

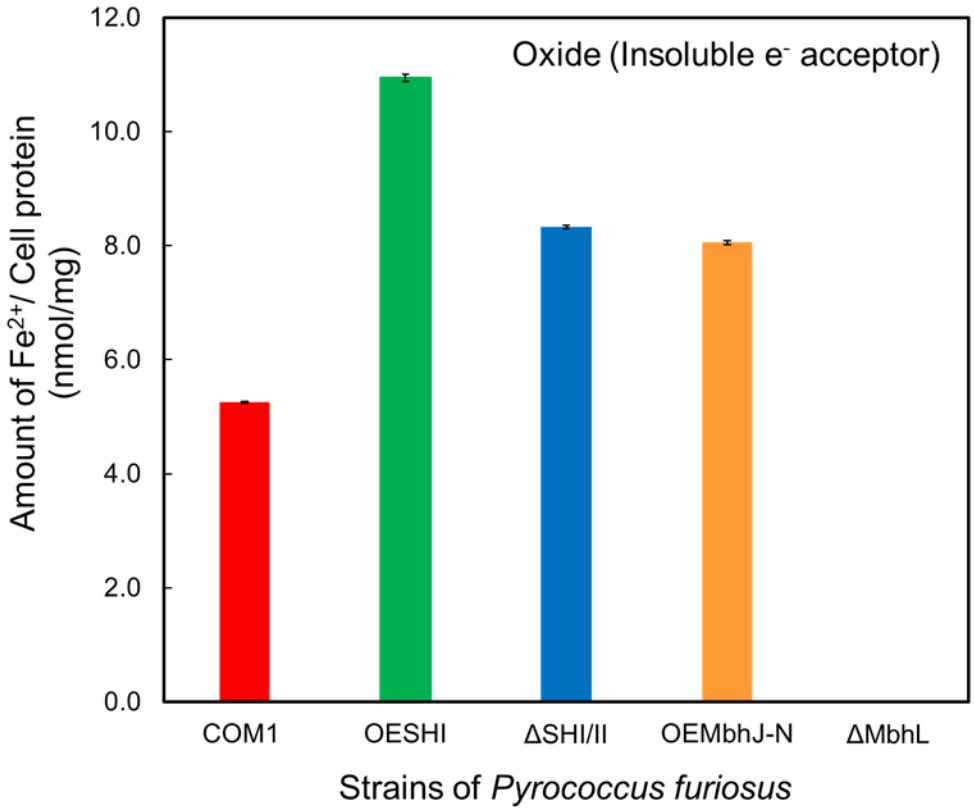

Figure 5: Comparison of the amount of insoluble ferric iron (as ferric oxide) reduced to soluble ferrous iron by different strains of *Pf* with respect to the total cell protein after 15 hours of growth at 88 ^{o}C.

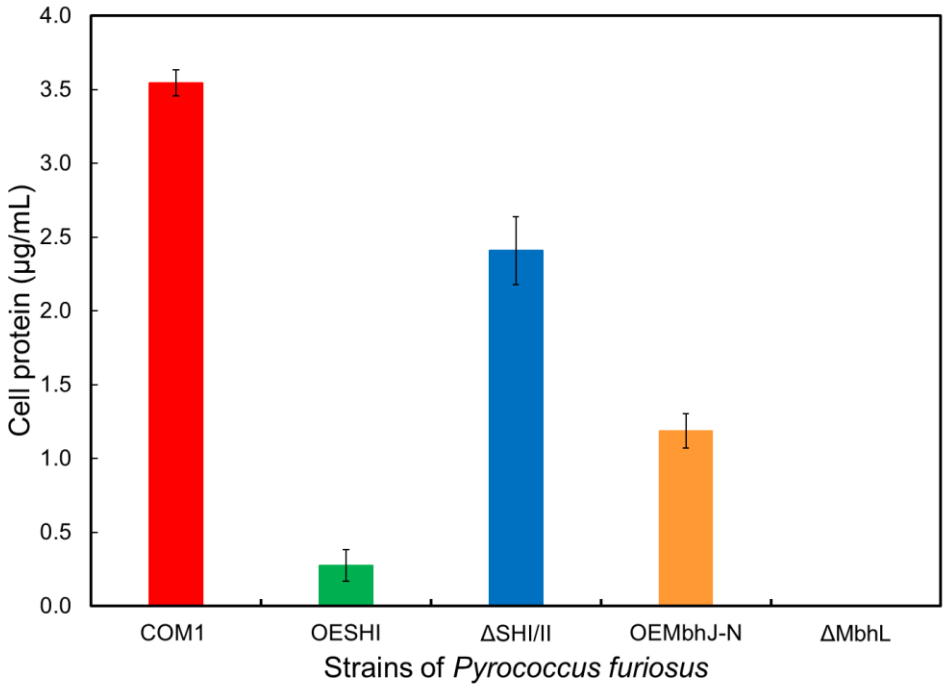

Figure 6: Growth comparison between COM1, OESHI, ΔSHI/II, OEMbhJ-N and ΔMbhL in the presence of the electrode measured after 3.5 hours

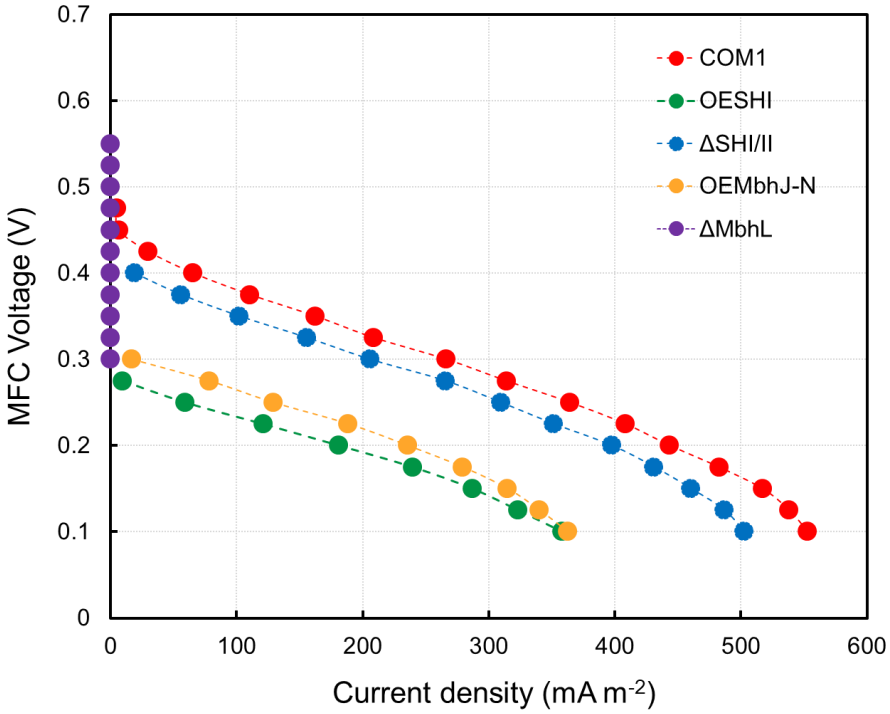
MFC Voltage (V)
Current density (mA m-2)
COM1
OESHI
ΔSHI/II
OEMbhJ-N
ΔMbhL
0
0.1
0.2
0.3
0.4
0.5
0.6
0.7
0
100
200
300
400
500
600

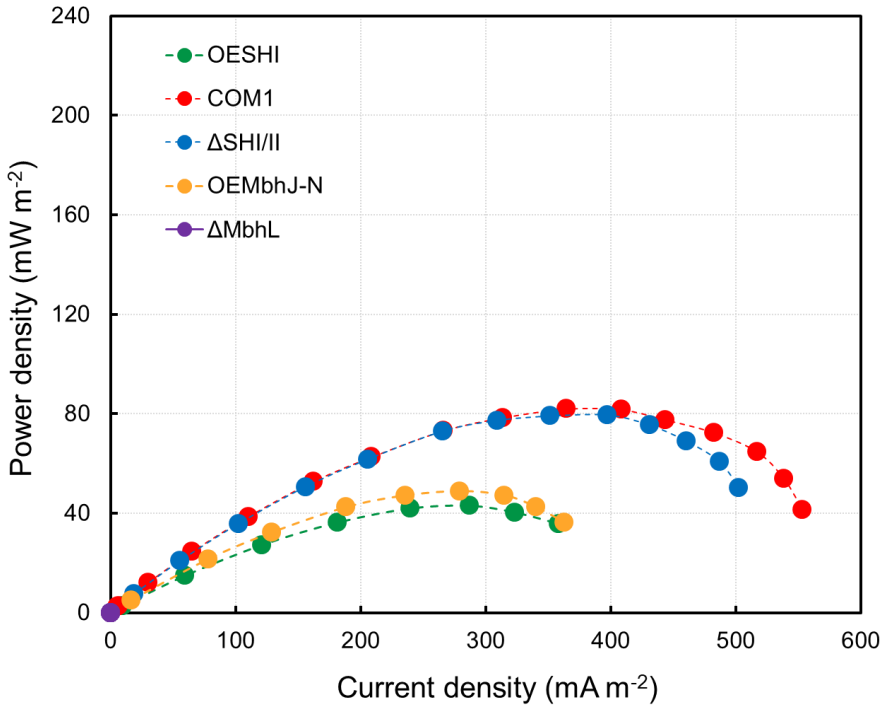
Power density (mW m-2)
Current density (mA m-2)
OESHI
COM1
ΔSHI/II
OEMbhJ-N
ΔMbhL
0
40
80
120
160
200
240
0
100
200
300
400
500
600

Figure 7: Polarization curves (a) and power density curves (b) for MFCs with different strains of *Pf* with respective control (medium-uninoculated abiotic control). The value of the medium is subtracted from respective samples. (a) The current was continuously at steady state by applying different voltages for a fixed duration of time at each voltage.

APPENDICES

APPENDIX C

ELECTROCHEMICAL CHARACTERIZATION OF AROMATIC CORROSION INHIBITORS FROM PLANT EXTRACTS

This chapter contains text from the following publication:

Yi Fang*, Baviththira Suganthan* and Ramaraja P. Ramasamy

*Equal Contribution

Journal of Electroanalytical Chemistry 840, 2019

Reprinted here with permission of the publisher.

Abstract

Plant extracts have been regarded as “green” alternatives as inhibitors for metal corrosion prevention and mitigation. Therefore, understanding the electrochemical properties and the reaction mechanisms of the electro-active compounds from the plant extracts is necessary to further explore the mechanism and application of the plant extract-based additives for corrosion prevention and mitigation. Among different plant derived chemicals, aromatic compounds are among the most effective for corrosion inhibition and mitigation. Thus, the electrochemical properties of seven aromatic active compounds from the plant extracts – caffeic acid, thymol (2-isopropyl-5-methylphenol, IPMP), gallic acid (3,4,5-trihydroxybenzoic acid) , tannic acid, lawsone (2-hydroxy-1,4-naphthoquinone), wedelolactone, and ellagic acid are studied using multiwalled carbon nanotube modified glassy-carbon electrode, and reported to enhance the fundamental understanding of their redox behavior at different environmental pH conditions.

Key words: plant extract, corrosion, inhibitor, carbon nanotube, aromatic, quinone.

Introduction

Metal corrosion, which results in its gradual destruction of its structural integrity, is caused by the electrochemical and chemical interaction between the metal surface and its surrounding environments [432]. Since corrosion cannot be completely eliminated, prevention and mitigation of corrosion are usually the primary focuses in industrial applications. The use of corrosion inhibitors is one of the most effective methods for metal protection against corrosion especially in acidic environments [433]. Different types of organic and inorganic compounds, such as heterocyclic compounds consisting of sulfur, oxygen and nitrogen atoms, have been discovered, synthesized, and applied on the metal surfaces as inhibitors to prevent corrosion [434-439]. Synthetic organic and inorganic inhibitors have also been proved to be effective towards corrosion mitigation, however their use has been limited due to their human and environmental toxicity [440]. Therefore, eco-friendly corrosion inhibitors also known popularly as 'green alternatives' to replace toxic and hazardous chemicals, have been studied extensively in recent years [441-443].

Among all the green alternatives, the use of corrosion inhibitors obtained from plant extracts has continued to attract interest due to their low human and environmental toxicity. Compared to the synthetic inhibitors, plant extract based corrosion inhibitors also cost less, and can easily be mass-produced if necessary [444]. The plant extract based additives have been used for rust mitigation in armors even during the medieval period [445, 446]. Many plant-derived chemicals reported in the literature have been characterized for their active constituents, their composition and their corrosion inhibition properties. For example, 95 % inhibition efficiency was reported from lawsone (2-hydroxy-1,4-naphthoquinone), the aqueous extract of the henna leaves (*lawsonia*) as the corrosion inhibitor for carbon steel

[445]. High inhibition efficiency of 99.6 % was reported from wedelolactone, the major active constituent from *Eclipta alba* [447]. Due to the enormous potential of the plant-derived chemicals as corrosion inhibitors, it is imperative to study the electrochemical properties of the active constituents present in plant-extracts in order to fully understand the mechanisms of corrosion and corrosion mitigation. Among the various classes of plant-derived compounds, aromatic compounds possess satisfactory corrosion mitigation properties and high electrochemical activity and therefore are the most studied group of compounds for this purpose. Understanding the electrochemical reaction mechanisms of the electro-active compounds derived from the plant extracts is important. These compounds function as corrosion inhibitors by adsorbing ions and molecules on the metal surfaces [448] or by decreasing the anodic / cathodic reaction or by increasing the electrical resistance of the metal surface. Sanyal and Abdullah Dar attributed the organic corrosion inhibitor functions to the donation of lone pair electrons to the metal [449, 450]. In this research, we report a comprehensive electrochemical study of seven different aromatic compounds as active constituents of plant extracts based corrosion inhibitors. The compounds are namely lawsone (2-hydroxy-1,4-naphthoquinone), thymol (2-isopropyl-5-methylphenol, IPMP), caffeic acid, gallic acid (3,4,5-trihydroxybenzoic acid), tannic acid, wedelolactone and ellagic acid. The structure of these active constituents and their corresponding inhibitors are tabulated in Table 1.

Table 1: Plant inhibitors, their active compounds and the corresponding structures

Active constituent	Inhibitor used	Structure	Reference

Lawsone (2-Hydroxy-1,4-naphthhoquinone)	*Lawsonia*	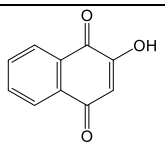	[445]
Thymol (2-isopropyl-5-methylphenol)	Thyme, Coriander, *Hibiscus,* Anis, Black Cumin and Garden Cress	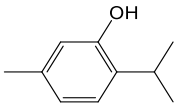	[451]
Caffeic acid	*Cyanopsis tetragonoloba*	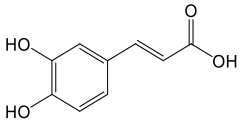	[452]
Gallic acid	*Embilica uflicianalis, Terminalia chebula* and *Terminalia bellirica*	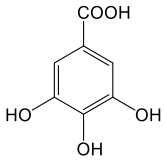	[453]
Tannic acid	*Combretum bracteosum, Embilica uflicianalis, Terminalia chebula* and *Terminalia bellirica*	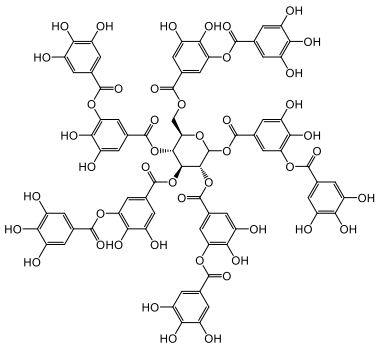	[453, 454]

Wedelolactone	*Eclipta alba*	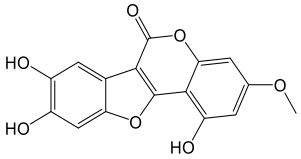	[447]
Ellagic acid	*Syzygium cumini*	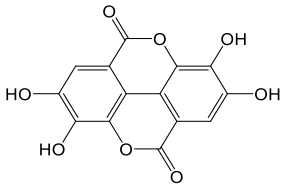	[455, 456]

In order to better understand the electrochemical reactions on the electrode, the electrodes used in this project was modified by carbon nanotubes (CNTs) to increase the sensitivity and observe the peaks that are not easily be observed from a plain electrode as reported previously for the detection of small organic compounds such as paracetamol, acetaminophen, nicotine, ascorbic acid, *etc* for pharmaceuticals [457, 458]. Compared to other nanomaterials, CNTs are more widely applied to modification of electrode due to their excellent electron transfer capability and high chemical stability [231, 232]. In addition, a high porosity feature can be created by CNT-modified electrode, leading to higher sensor activity [459].

Materials and Methods

Caffeic acid (> 98.0%, HPLC), thymol (> 98.5%), tannic acid, lawsone and ellagic acid (> 95%, HPLC) were purchased from Sigma-Aldrich and used without further treatment. Gallic acid (anhydrous) and wedelolactone were obtained from EMD Millipore Corporation and Cayman Chemical Company, respectively. Acetic acid, potassium phosphate dibasic (K_2HPO_4) and potassium phosphate monobasic (KH_2PO_4) were purchased from BDH. Sodium acetate (Trihydrate, crystal), sodium hydroxide (Pellets) and

sodium carbonate were obtained from J.T. Baker. Multiwalled carbon nanotubes (CNTs) and dimethylformamide (DMF) were purchased from DropSens and Acros, respectively. All the electrolytes and analyte solutions for electrochemical experiments were prepared using 18.2 MΩ nano pure water deionized (DI) water.

Glassy-carbon (GC) electrode purchased from CH Instrument was first polished on the electrode polishing pad with 0.05 μm alumina polishing slurry before each electrochemical experiment. The electrode was cleaned twice using ultrasonicator for 2 min to remove unattached polishing powder before modification. CNT suspension was prepared by ultrasonicating 1 mg CNT in 1 mL of DMF for an hour. The cleaned GC electrode was modified by drop-casting 8 μL (in 4 steps of 2 μL) CNT suspension followed by drying at 75 ºC in the oven after each addition of CNT suspension.

Cyclic voltammetry (CV) was performed using CHI 920 c potentiostat. The three-electrode system consisting of a 3 M Ag/AgCl as reference electrode, a platinum wire as counter electrode, and a CNT-modified GC electrode was used for all experiments. The electrolyte with different pH used for the experiments are listed in Table 2, and the electrochemical experiments were carried out in a conventional glass voltammetry cell. All experiments were conducted at 25 ± 2 ºC.

Table 2: Electrolyte with different pH used in this research

pH	**Concentration (mM)**	**Components**
3	0.1	Acetic acid (CH_3COOH) + Sodium acetate (CH_3COONa)
5	0.1	Acetic acid (CH_3COOH) + Sodium acetate (CH_3COONa)

7	0.1	Monopotassium phosphate (KH_2PO_4) + Dipotassium phosphate (K_2HPO_4)
9	0.1	Sodium hydroxide (NaOH) + sodium carbonate (Na_2CO_3)
11	0.1	Sodium hydroxide (NaOH) + sodium carbonate (Na_2CO_3)

Results and Discussion

The electrochemical oxidation and reduction experiments of the seven compounds – lawsone, thymol, caffeic acid, gallic acid, tannic acid, wedelolactone and ellagic acid were performed individually on the CNT-modified electrode, due to its outstanding conductivity and large surface area for electrochemical reactions.

Thymol

The cyclic voltammograms were collected from 0.5 mM of thymol in pH 7 electrolyte and the results are shown in Figure 1(A). At this pH, thymol undergoes a direct one-step oxidation, (peak a3) at E_{pa3} = + 0.48 V during the forward (positive) scan, which generates two quinone derivatives (*i.e. o*-quinone and *p*-quinone derivatives) from the mono-phenol group of thymol as shown in scheme 1. On the negative scan, two consecutive reduction peaks c2 and c1, at the E_{pc2} = + 0.35 V and E_{pc1} = - 0.054 V were observed, which correspond to the reduction of *o*-quinone and *p*-quinone to *o*-hydroquinone and *p*-hydroquinone, respectively as shown in scheme 1. On the second positive scan, two consecutive oxidation peaks a1 and a2, at the E_{pa1} = - 0.04 V and E_{pa2} = + 0.36 V (not observed during the first scan) were observed as shown in scheme 1, which can be explained by the oxidation of *p*-hydroquinone and *o*-hydroquinone (produced through the

negative scan during first scan) to *p*-quinone and *o*-quinone. The relative peak positions for both *ortho*- and *para*- positions of phenolic compounds are also confirmed (Supplementary Information Figure S1). The proximity of peaks a1 and c1, and peaks a2 and c2 further indicate the reversibility of electrochemical reaction between hydroquinone and quinone [460]. On the other hand, the lack of a reduction peak for the reduction of *o*-quinone and *p*-quinone derivatives to thymol (mono-phenol derivative) demonstrates that the first step of the reaction is irreversible as shown in scheme 1.

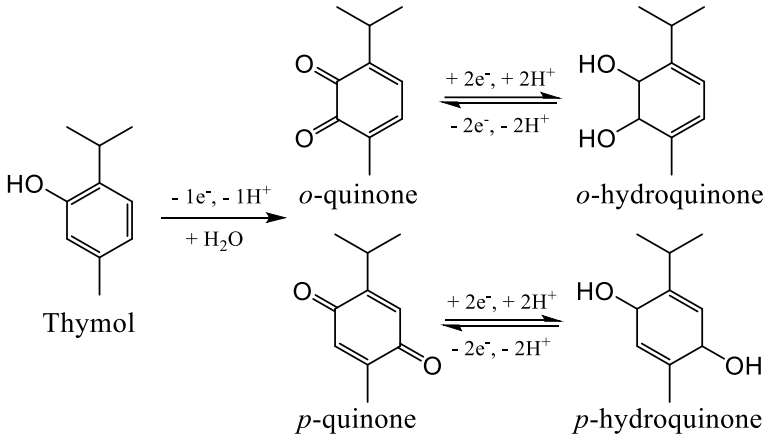

Scheme 1: Electrochemical reaction of thymol to quinone and secondary derivatives.

The relationship between proton and electron transfers during the electrochemical reaction can be studied by performing the electrochemical experiments in the electrolyte in different pH values, and the second scan of the cyclic voltammograms are shown in Figure 1(B). The results indicate that all five peaks (*i.e.* a1, a2, a3, c2 and c1) shift to the negative at high pH. In Figure 1(B) inset, peak potential of three major peaks a1, a3 and c1 decreased as pH increased. The slope of potential shift per pH unit, which is close to 59.2 mV / pH, demonstrates that the number of protons transferred during the electrochemical reaction is equal to the number of electrons [460]. Based on the electrochemical behavior observed here, the corrosion inhibition property of thymol could be attributed to the substitution of

terminal hydrogen of the phenyl ring and the formation of insoluble compound during the oxidation reaction. Previous reports also suggest that the insoluble Fe-thymol complexes dominate the composition of adsorbed intermediates and help prevent further corrosion of iron [461].

Caffeic acid

Cyclic voltammograms of 0.5 mM of caffeic acid obtained using the electrolytes at different pH of 3, 5, 7, 9, and 11, respectively on the CNT electrode are shown in Figure 2. In Figure 2, a clear oxidation peak and a corresponding reduction peak are observed for each pH, which can be explained by the oxidation of *o*-hydroquinone derivatives to *o*-quinone derivatives as shown in the scheme 2.

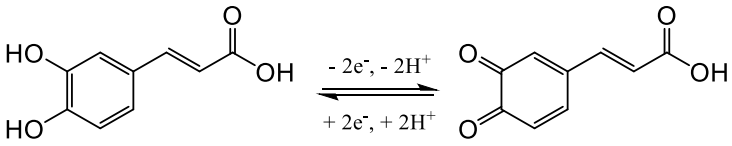

Caffeic acid *o*-quinone

Scheme 2: Reversible electrochemical oxidation of caffeic acid to *o*-quinone.

The peak potentials for both oxidation and reduction decreased with increasing electrolyte pH and the slope of both peak potential shifts per pH unit, was close to the theoretical value of 59.2 mV / pH, which suggests an equal number of proton and electron transfer during the electrochemical reaction [460]. The experimental results show that the potential shifts for anodeic and cathodic scans resulted in 66.9 mV/pH and 50.1 mV/pH, which is slightly different from the theoretical values because of possible mixed potential effects and variation in electrode preparation, or substrate/product accumulation at the electrode. Caffeic acid acts as an oxidation inhibitor by decreasing the available cathodic reaction

area and possible modifying the activation energy of the anodic reaction through the formation of Fe-caffeic acid complex in which iron is bound to the 1,2- phenol sites during oxidation as scheme 3 [462].

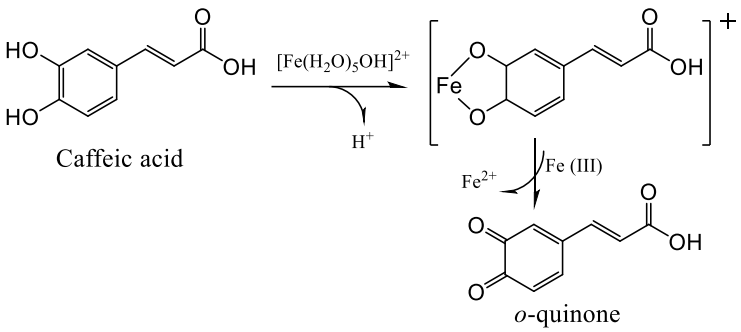

Scheme 3: Fe-caffeic acid complex formation during oxidation of caffeic acid.

Gallic acid

0.5 mM of gallic acid solutions in electrolyte with pH of 3, 5, 7, 9 and 11 were used to explore the electrochemical reversibility of gallic acid by cyclic voltammetry. The CV results are shown in Figure 3. As shown in Figure 3, it is obvious that under acidic conditions, a significant peak that corresponds to oxidation of gallic acid is observed at E_{pa} = + 0.58 V (pH = 3) and + 0.32 V (pH = 5). It is worthy to note that in neutral and basic solutions, the two oxidation peaks (*i.e.* a1 and a2) were observed which has not been reported previously [463]. The two oxidation peaks correspond to the two steps of oxidation respectively as introduced in scheme 4.

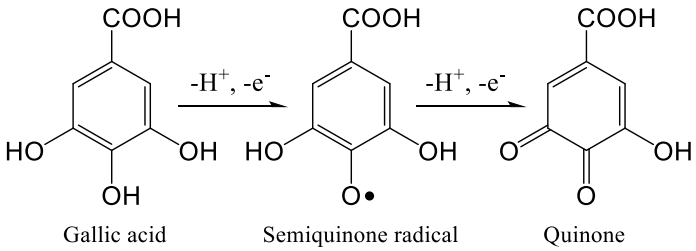

Scheme 4: Irreversible electrochemical oxidation of gallic acid.

The gallic acid first undergoes a one proton-one electron transfer reaction and forms semiquinone radical, which then can be further oxidized to form the final product – quinone. The data shown in Figure 3 inset can further validate the reaction assumptions by potential shift of E_{pa1} and E_{pa2} per pH, which are close to 59.2 mV / pH, demonstrating the same number of proton and electron was transferred during the reaction [460]. It is also clear that the anodic currents decreased sharply as the pH of solution was increased from 7 to 11 which is consistent with other previous reports [464]. Additionally, corresponding reduction peaks c, c1 and c2 (as appeared in Figure 3) were also detected using CV technique, and the asymmetry of the oxidation and reduction peaks demonstrate the irreversibility of the electrochemical reaction of gallic acid, which is advantageous to drive the reaction to form tannin complexes. The formation of the semiquinone radicals as shown in scheme 4 can be correlated with the formation of gallic acid-metal complexes, which may be responsible for the inhibition of metal corrosion [465].

Tannic acid

Tannic acid, which also called decagalloyl glucose, is a condensed form of 10 gallic acid molecules and a glucose molecule as shown in Table 1. Therefore, the electrochemical properties of tannic acid resemble those of gallic acid as found in Figure 4. Due to the similarity of tannic acid and gallic acid structures (tannic acid is formed through condensation of ten gallic acid molecules and one glucose molecule), tannic acid could yield similar anti-corrosion behavior on metals as that of gallic acid. [465]. The cyclic voltammograms of 0.5 mM gallic acid and tannic acid in electrolyte with pH 7 are shown in Figure 4(A) as below. The first two oxidation peaks a1 and a2 of tannic acid (E_{pa1} = +

0.15 V and E_{pa2} = + 0.24 V) fall in the same oxidation potential window of gallic acid, and the reaction can be explained by the two-step oxidation of secondary gallic acid moiety through formation of semiquinone as the intermediator (not shown) (the first step of reaction scheme (the molecule is partly shown) as introduced in below.

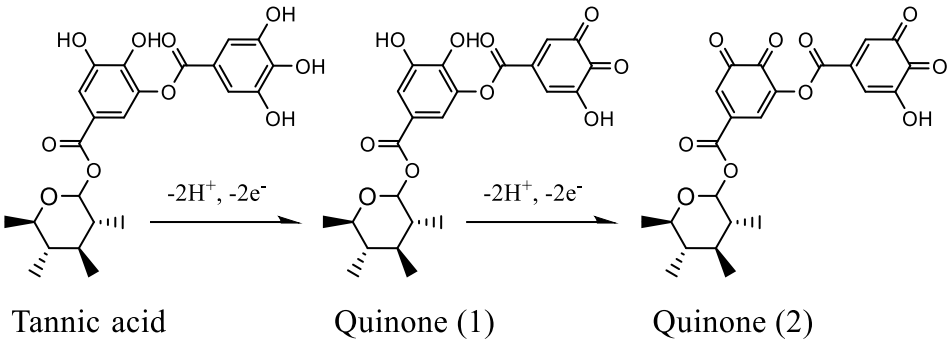

Scheme 5: Electrochemical reaction of tannic acid to quinone.

It is noteworthy to point out that at a higher potential (E_{pa3} = + 0.370 V), another oxidation peak was apparent, which could be attributed to the further oxidation of primary gallic acid moiety from the tannic acid as introduced in the second reaction arrow in the scheme 5.

The electrochemical study was also carried out by using cyclic voltammetry in electrolyte with various pH 3, 5, 7, 9 and 11, and the results are shown in Figure 4(B). Similar to the gallic acid, the two separate oxidation peaks a1 and a2 cannot be mutually identified, when the acidic electrolyte was used. However, as the pH increased from 7 to 11, both a1 and a2 can be clearly identified as they were shifted towards negative potential. In addition, the third oxidation peak a3 can be observed when pH is greater than 5, and a3 also shifted towards the negative potential as pH increased. The inset of the Figure 4(B) indicates the pH dependency of the three oxidation peaks (when they are be clearly observed and identified). The potential shift per pH for all three oxidation peaks a1, a2 and a3, which are close to 59.2 mV / pH, demonstrate the same amount of proton and electron transfer during

the electrochemical experiments. The results also proved the mechanism hypothesis as introduced in the scheme 5 above.

Lawsone

Lawsone (2-hydroxy-1,4-naphthoquinone) is the pigment discovered in the leaves of *Lawsonia alba*, commonly known as "Henna" [466]. Figure 5(A) shows the cyclic voltammograms of lawsone in electrolyte with pH 5. As lawsone was electrochemically scanned from -0.4 V to 1.0 V, a clear oxidation peak a1 was firstly found at -0.18 V, which is clearly paired with another reduction peak c1 found at -0.20 V during the backward scanning. These two peaks can be explained by the redox reaction of 1- and 4- hydroxyl groups on the naphthoquinone as introduced in the scheme 6.

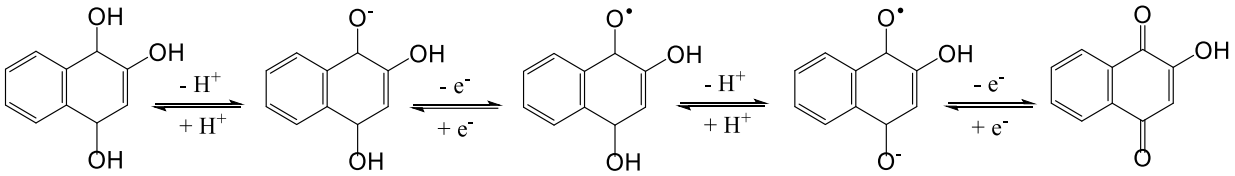

Scheme 6: Electrochemical reaction involving 1- and 4-hydroxyl groups of lawsone.

Lawsone (2-hydroxy-1,4-naphthoquinone) (NQOH as shown in the scheme) firstly undergoes electrochemical reduction to generate semi-naphthoquinone radical ($NQOH_2^{\bullet}$) via semi-naphthoquinone radical anion ($NQOH^{\bullet -}$) at the initial potential applied on the electrode (E = -0.4 V). The formed radical can be further oxidized during the positive scanning of the electrode to regenerate lawsone as depicted by peak a1 in Figure 5(A) [467-470]. The reversibility of this reaction is demonstrated from the symmetrical reduction peak c1 during the negative scan which corresponds to the reduction of lawsone to radical. Both reactions involve the same number of protons and electrons, which can be further

validated by the pH studies shown in Figure 5(B). In order to further identify the reactions represented by the redox peaks, a narrow potential window was used to avoid the interference from oxidation arising from peak a2 as in Figure 5(A), and the data are shown in Figure 5(B).In Figure 5(B), both peaks a1 and c1 undergo negative shift as pH increases and the slopes are determined to be 75.1 mV / pH and 67.0 mV / pH (close to theoretical 59.2 mV / pH for the transfer of same number of proton and electron). This observation also confirms that lawsone could be used for corrosion mitigation by enhancing the metal complex formation between metal ions and lawsone molecules after delocalization of the lone pair of electrons on hydroxyl group [471]. Additionally, another oxidation peak of 2-hydroxyl group (peak a2) was observed in Figure 5(A) to form a new radical (NQO**.**) as introduced in the scheme 7 when high potential was applied [467].

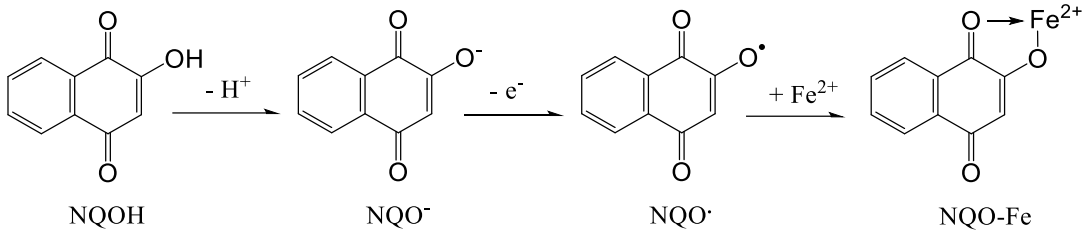

Scheme 7: Electrochemical reaction involving 2-hydroxyl group of lawsone.

However, this reaction is irreversible due to the lack of corresponding reduction peak. On the other hand, NQO**.** can still be reduced due to the presence of the reduction peak c2 which is absent in the control experiment when potential above 0.35 V was avoided as in Figure 5(A). During the second scan, the small peaks further suggest that NQO**.** can be reduced to form other compounds which can be further oxidized in the second scan. The formation of NQO**.** can be attributed to the formation of metal (Fe, Ni and Zn)-lawsonia complexes (NQO-Fe) as shown in scheme 7 that could prevent further corrosion of the metal [465, 471].

Wedelolactone

Wedelolactone (7-methoxy-5,11,12-trihydroxycoumestan) forms the major constituent of traditional medicinal plant *Eclipta alba.* The electrochemical response of wedelolactone was studied using cyclic voltammetry in various electrolytes with pH ranging from 3 to 11 as introduced above [447]. The cyclic voltammograms are shown in Figure 6 below. As in the Figure 6, two prominent peaks a1 and a2 are consistently observed at all pH, which could be attributed to the oxidation of catechol ring of wedelolactone molecule as shown in the scheme 8.

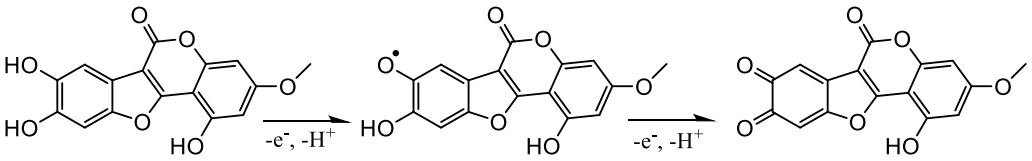

Scheme 8: Electrochemical reaction involving 8- and 9-hydroxyl groups of wedelolactone.

At high potentials, a semiquinone radical was formed (first step) from wedelolactone which corresponds to the peak a1 in Figure 6 [472]. The intermediate semiquinone radical can be further oxidized on the electrode (second step) to generate quinone which corresponds to the peak a2 in Figure 6 [472]. Figure 6 also shows that an increase of pH is associated with a decrease of the oxidation potential for both a1 and a2. The pH dependencies of both peak a1 and a2 are studied and shown in Figure 6 inset, demonstrating each step of the reaction occurred involved in the transfer of the same number of electron and proton, as hypothesized in the scheme below [473]. For the experiments conducted with pH > 5, another oxidation peak a3 was observed, which can be explained by the cascadic oxidation of wedelolactone as shown in the scheme 9.

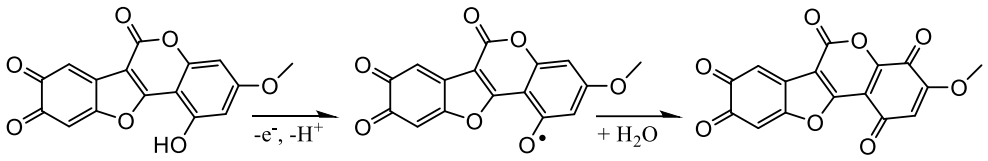

Scheme 9: Electrochemical reaction involving 3-hydroxyl group of wedelolactone.

In addition to the oxidation of the catechol ring, the phenolic ring with only one phenolic group was further oxidized after the oxidation of the catechol ring, giving the third peak a3 when pH > 5. Since the phenolic ring has only one hydroxyl group, it does not form a semiquinone, therefore, corresponds to only one peak [474]. The appearance of the fourth oxidation peak a4 when pH > 7 is not fully understood yet, which could be explained by other oxidation byproduct, or the oxidation of electrolyte at high potential. It is also noteworthy to indicate that the appearance of a3 coincides with the disappearance of the reduction peak c2 (which is corresponding to the a2 when pH = 3), therefore, demonstrating that the oxidation of the phenolic ring decreased the redox reversibility of the catechol ring. Due to the similarity of the electroactive moiety of this compound with other aromatic compounds explored in this study, the corrosion mitigation property of wedelolactone could be attributed to the formation of insoluble complex and hydroxide (*e.g.* Fe^{2+}-wedelolactone and $Zn(OH)_2$) [475].

Ellagic acid

Ellagic acid is a polyphenol dimeric derivative of gallic acid contained in the form of ellagitannins [476, 477]. The electrochemical studies of ellagic acid were performed in 1 mM solution in different pH. In pH 3 and 5, electrochemical signal was not observed due to poor solubility in acidic solution (data not shown). In pH 7, two consecutive oxidation peaks (*i.e.* a1 and a2) are observed at +0.37 V and +0.40 V, respectively, as shown in Figure

7, which resemble the oxidation peak pattern collected from gallic acid in Figure 3. The reaction can be explained as the scheme 10 shown below.

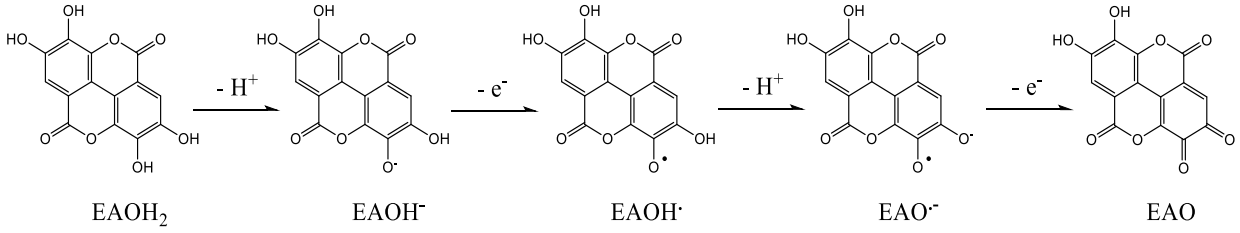

Scheme 10: Electrochemical reaction of ellagic acid.

Under neutral pH, ellagic acid ($EAOH_2$) first undergoes oxidation to generate semi-quinone radical (EAOH**.**) through the anion ($EAOH^-$), which generates the oxidation peak a1 [456]. Then the radical formed from the first step can be further oxidized to quinone (EAO) through the semi-quinone radical anion ($EAO^{\cdot -}$), which produces the oxidation peak a2 [456]. As pH increases, both peaks a1 and a2 shift to the negative and the potential shifts per pH were determined to be 80.9 mV / pH and 57.4 mV / pH, the proximity to 59.2 mV / pH demonstrate the both reactions involve in the transfer of the same number of proton and electron [456]. On the other hand, peak shifts for both a1 and a2 diminished from pH 9 to 11, this can be explained by the fact that ellagic acid ($EAOH_2$) dissociates to form anion ($EAOH^-$) due to the presence of alkaline before the being electrochemically oxidized to radical (EAOH**.**), therefore, only electron transfer was involved in the reaction. Furthermore, the formed radical (EAOH**.**) was further dissociated to radical anion ($EAO^{\cdot -}$) before oxidized to generate quinone (EAO), which only involves in electron transfer only. For all pH from 7 to 11, the formed quinone (EAO) may further undergo dimerization or polycondensation reactions, producing compound that can also be oxidized, which explains the existence of the third oxidation peak a3. Similar to other aromatic inhibitors such as

caffeic acid and lawsone, the electron relocation of ellagic acid results in the formation of insoluble compound from semiquinone radicals and metal ion, which could prevent metal corrosion as discussed in earlier paragraphs.

The electrochemical reactions derived from thymol, caffeic acid, gallic acid, tannic acid, wedelolactone, lawsone and ellagic acid are further tabulated in Table 3 with their reversibility and corresponding anodic and cathodic peak potentials.

Table 3: Summary of the electrochemical reaction in phosphate electrolyte with pH of 7, and its E_{pa} / E_{pc} from the plant extracts

Reactions in this project	E_{pa} / E_{pc}	**Reversibility**	**Reference from this project**
Mono-hydroxyl group substitution			
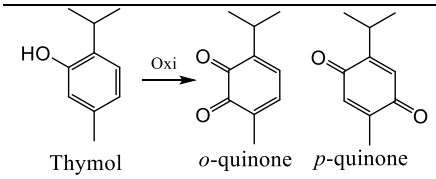	E_{pa} = 0.48 V	No	Thymol
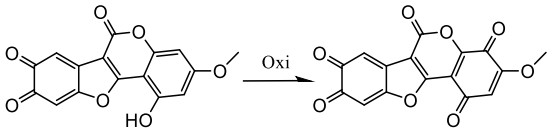	E_{pa} = 0.62 V	No	Wedelolactone
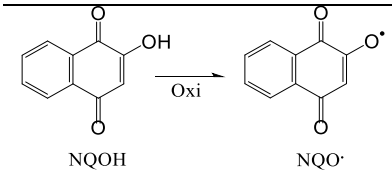	E_{pa} = 0.75 V	No	Lawsone
Ortho-hydroxyl groups substitution			

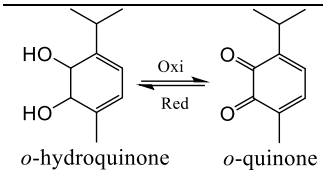	E_{pa} = 0.36 V E_{pc} = 0.35 V	Yes	Thymol
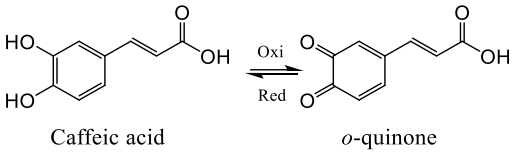	E_{pa} = 0.20 V E_{pc} = 0.16 V	Yes	Caffeic acid
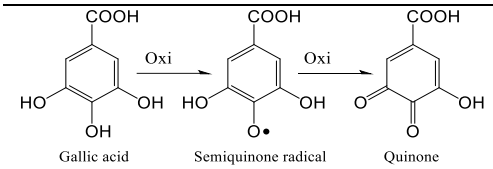	E_{pa1} = 0.14 V E_{pa2} = 0.24 V	No	Gallic acid
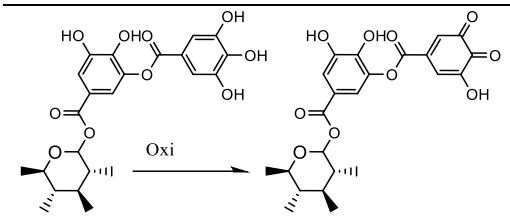	E_{pa1} = 0.15 V E_{pa2} = 0.24 V	No	Tannic acid
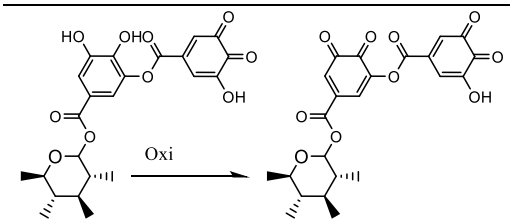	E_{pa3} = 0.35 V	No	Tannic acid
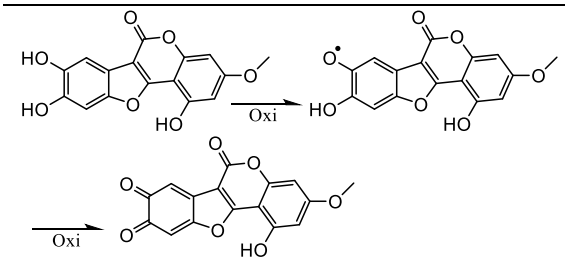	E_{pa1} = 0.14 V E_{pa2} = 0.28 V	No	Wedelolactone

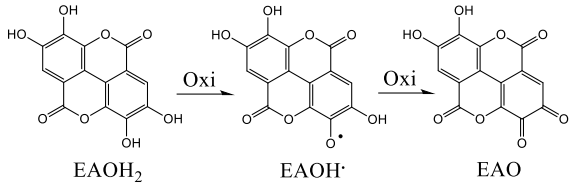	E_{pa1} = 0.37 V E_{pa2} = 0.40 V	No	Ellagic acid
Para-hydroxyl groups substitution			
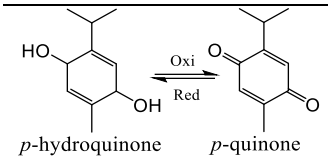	E_{pa} = -0.04 V E_{pc} = -0.05 V	Yes	Thymol
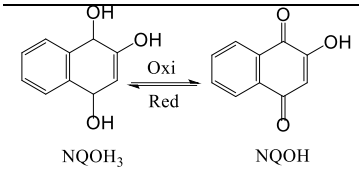	E_{pa} = -0.32 V E_{pc} = -0.35 V	Yes	Lawsone

Although the electrochemical reactions of the seven plant extracts studied here have been studied individually by various authors, in this work cyclic voltammetry experiments were performed using CNT-modified electrode in order to break down the reactions from the individual analyte of interest. The main difference of this work from previous reports is the investigation of electrochemical reaction mechanisms due to their structures and positions of the functional group. The previous studies demonstrated that the electrochemical activity from the plant extracts are mainly derived from the hydroxyl groups substituted on the aromatic and heterocyclic rings due to their corresponding formation of quinone or semiquinone during oxidation. According to the number of the hydroxyl group involved in the reaction, it can be categorized to mono-hydroxyl group reaction with only one hydroxyl group involved, and bi-hydroxyl group reaction with two hydroxyl groups involved. The bi-hydroxyl group reaction, based on the position of the two hydroxyl groups, can be further categorized to *ortho*-hydroxyl reaction and *para*-hydroxyl reaction. As the results

displayed in Table 3, the electrochemical oxidation occurs on mono-hydroxyl substituted compounds demonstrates higher potential from 0.48 V to 0.75 V for thymol (Figure 1A, peak a3) and lawsone (Figure 5A, peak a2) oxidation during the first scan, and second oxidation step from wedelolactone (Figure 6, peak a3). These reactions, as reported Table 3, are irreversible since the oxidation of mono-hydroxyl group results in the production of quinone, that can only be reduced to form bi-hydroxyl products. Compared to the oxidation of mono-hydroxyl group, electrochemical oxidation reaction for *ortho*-positioned bi-hydroxyl groups were found to possess lower redox potential with E_{pa} from 0.14 V to 0.40 V as shown in Table 3. It is also noteworthy to mentioned that most reactions with the detection of semiquinone formation (*i.e.* two different reaction steps and E_{pa}'s for quinone formation) are irreversible. This could be explained by the formation of more stable semiquinone from the bulky aromatic compounds (*e.g.* gallic acid and tannic acid) or the heterocyclic ring (*e.g.* wedelolactone and ellagic acid). On the other hand, the oxidation reaction reveals only one oxidation peak for *ortho*-bi-hydroxyl group substituted compounds with simple R chain, such as thymol and caffeic acid, while the reaction itself, is reversible. With different substitution position, *para*-positioned bi-hydroxyl groups display the reversibility of the redox reaction and the lowest oxidation peak potentials from -0.32 V to -0.04 V from thymol and lawsone as shown in Table 3. All three categories of reactions involving electroactive hydroxyl groups provide valuable information for mechanism interpretation and structure infer from redox potential and reversibility for future researches.

It is also noteworthy to mention that the acid dissociation constants (pK_a's) of the seven analytes of compounds are between 4.0 to 10.59 [478]. Therefore, the analytes are

considered weak acid, which makes them more dissociated under basic conditions (*i.e.* pH 9 and 11 in this research). On the other hand, the oxidation reaction of the electroactive hydroxyl group always involves in the dissociation of a proton, then followed by the electron donation as explained above. Under basic conditions, the first step (dissociation of proton) precedes the electrochemical reaction, which makes the oxidation less pH dependent. Thus, from the cyclic voltammograms, it is not surprising to find that the peak shift decreases at higher pH.

Conclusions

Seven aromatic compounds derived from plants were characterized electrochemically at different pH electrolytes using multi-walled carbon-nanotube modified glassy-carbon electrode by cyclic voltammetry. The compounds namely caffeic acid, thymol, gallic acid, tannic acid, lawsone, wedelolactone and ellagic acid were of industrial significance due to their corrosion inhibition properties. Based on the voltammetry results, the mechanisms of the electrochemical redox reactions and the reaction products that may aid in corrosion mitigation are proposed and discussed. All the seven compounds share the similar electrochemical behavior which could be attributed to the chemical properties of the aromatic structures of these compounds. This fundamental characterization work has significant implications for corrosion mitigation studies of plant-based additives and their anti-corrosive properties.

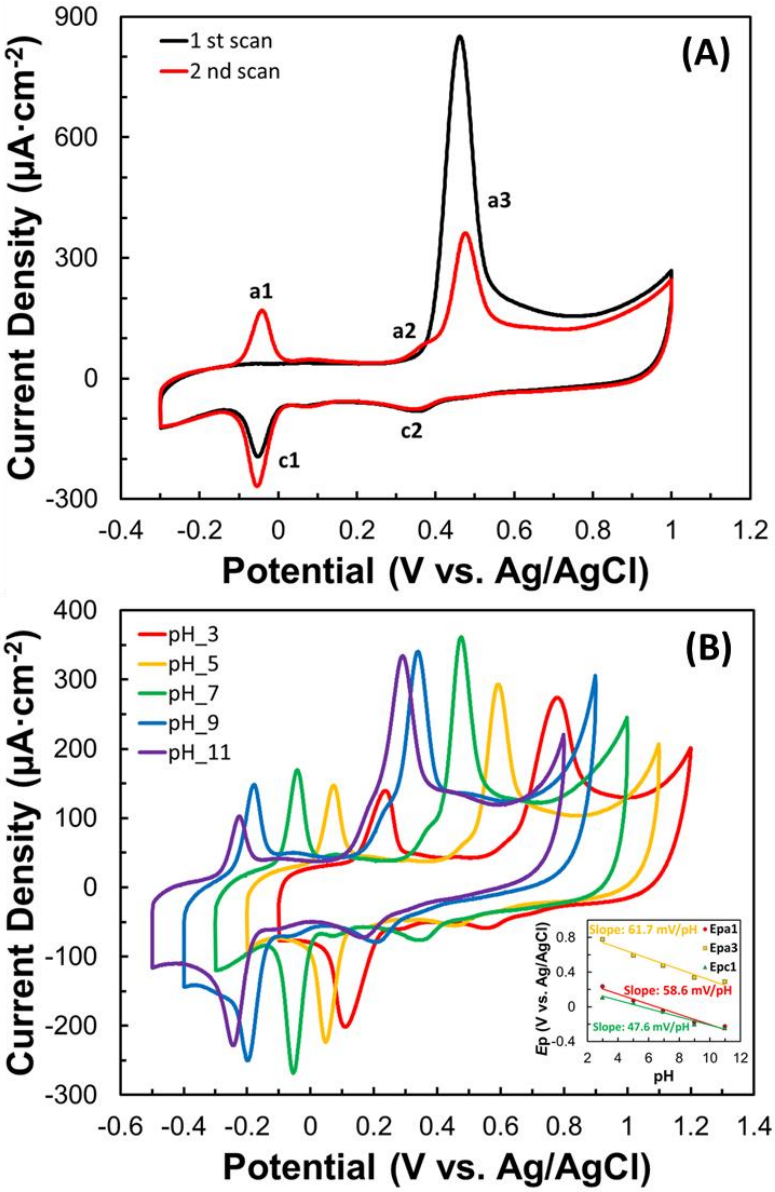

Figure 1: Cyclic voltammograms of 0.5 mM thymol from first and second scan in pH 7 (A) and from second scan in different pH (B) and the pH dependence of the redox peaks (Inset).

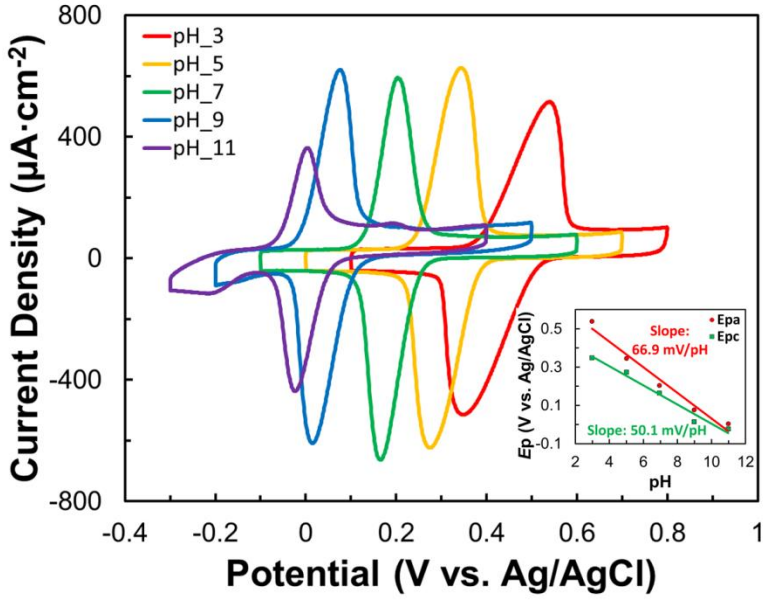

Figure 2: Cyclic voltammograms of 0.5 mM caffeic acid from the first scan in different pH, and the pH dependence of the redox peaks (Inset).

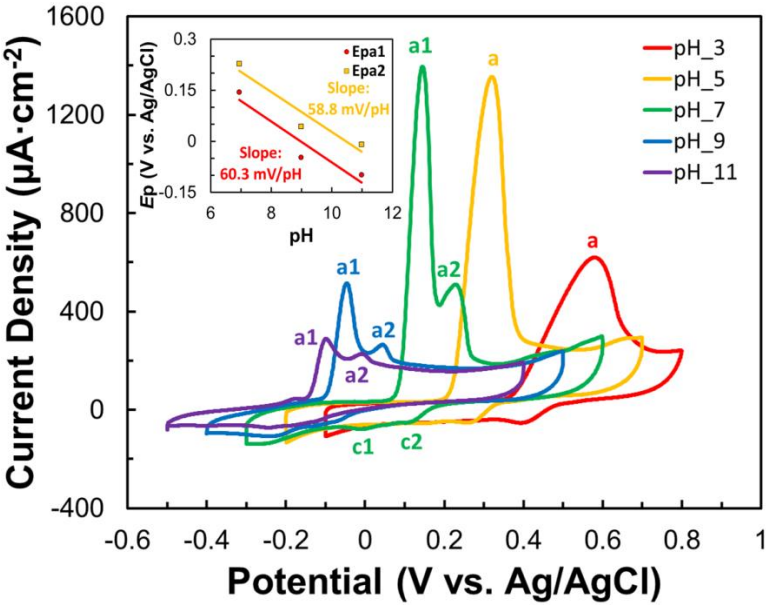

Figure 3: Cyclic voltammograms of 0.5 mM gallic acid from the first scan in different pH, and the pH dependence of the redox peaks (Inset).

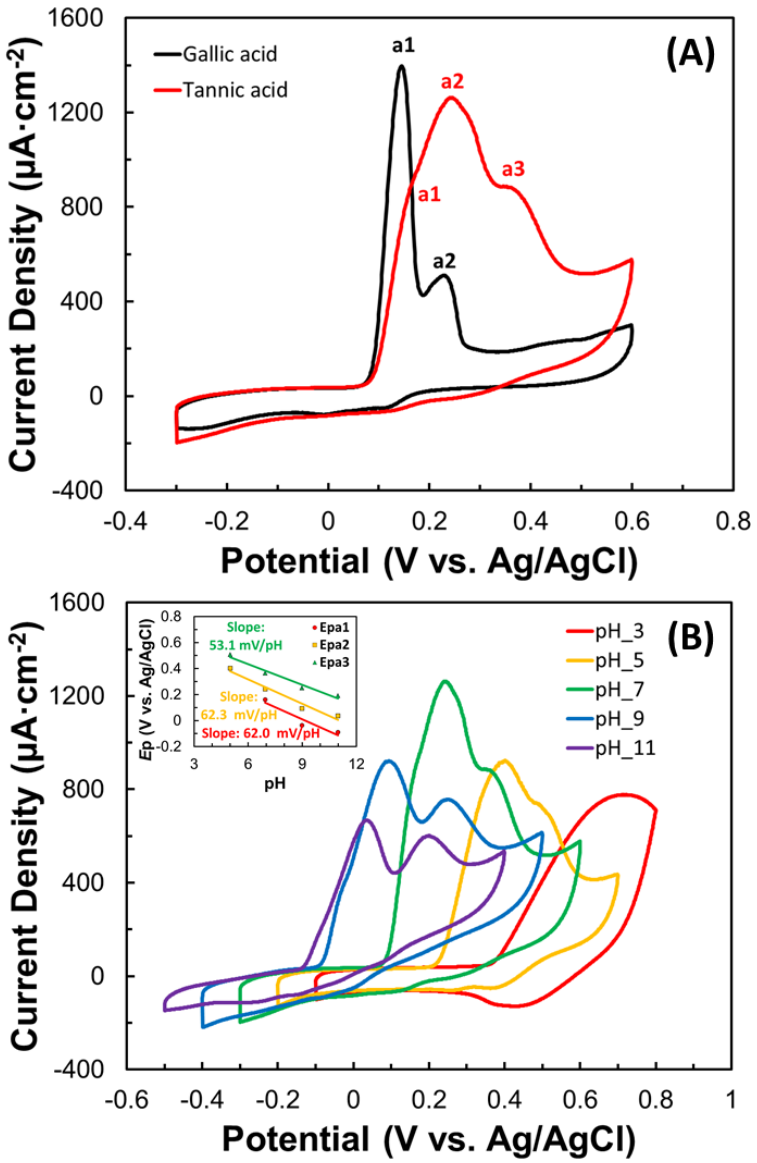

Figure 4: Cyclic voltammograms of 0.5 mM gallic acid and tannic acid in pH 7 electrolyte (A) and 0.5 mM tannic acid in different pH (B) and pH dependencies of the redox peaks (Inset).

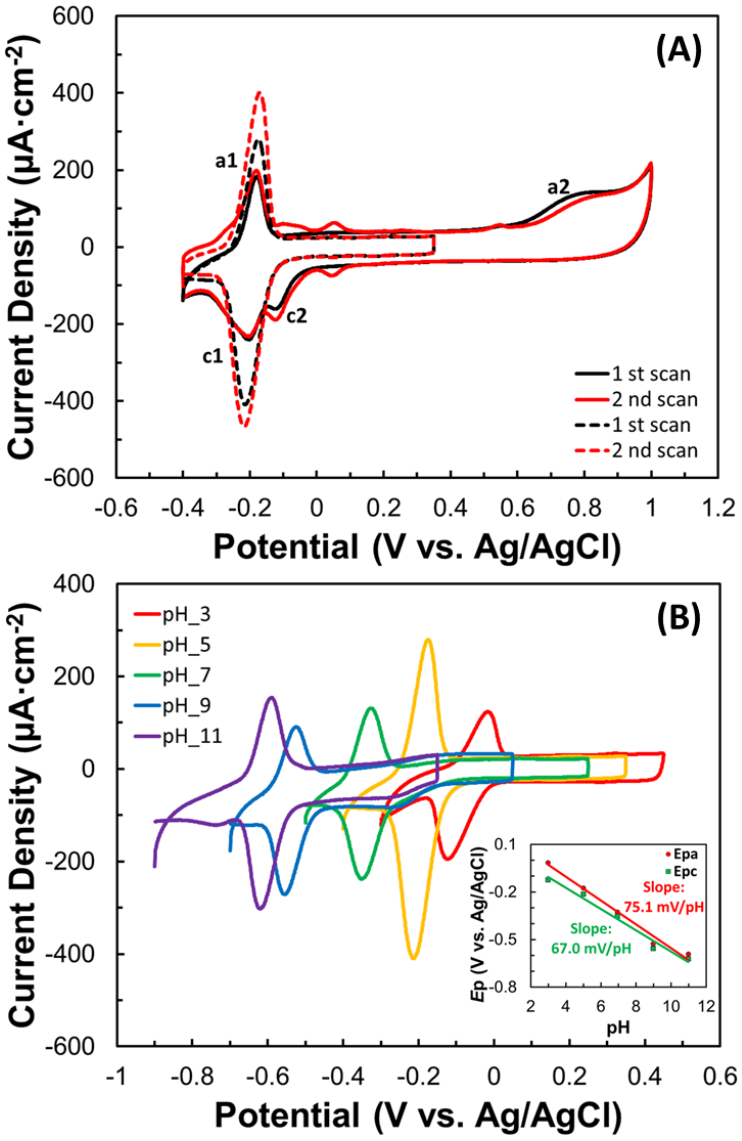

Figure 5: Cyclic voltammograms of 0.5 mM lawsone using different potential windows (A) and 0.5 mM lawsone in different pH (B) and pH dependencies of redox peaks (Inset).

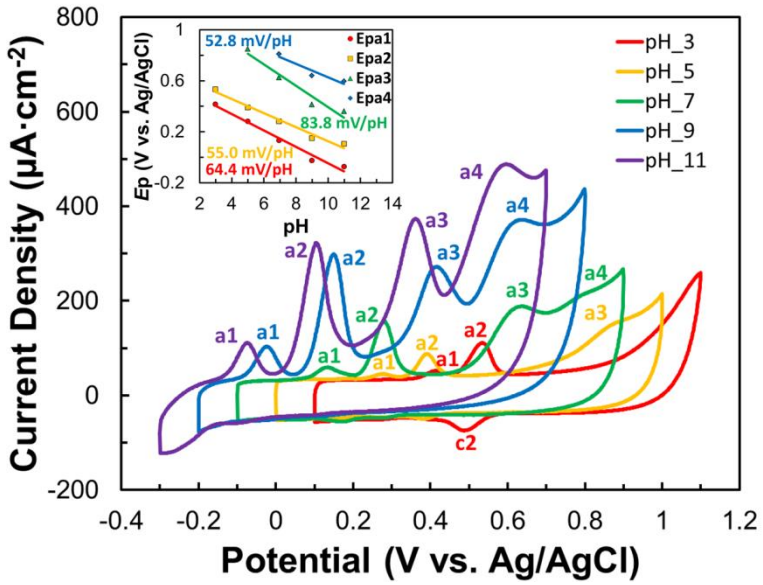

Figure 6: Cyclic voltammograms of 0.5 mM wedelolactone in different pH and pH dependencies of the redox peaks (Inset).

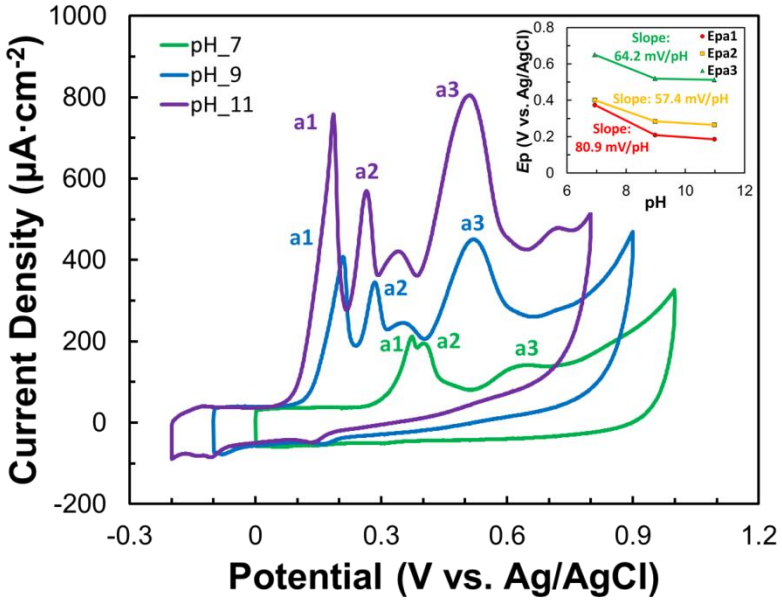

Figure 7: Cyclic voltammetry of 1 mM ellagic acid in different pH and pH dependencies of the redox peaks (Inset).